Search for Critical Fluctuations in the Quantum Chromodynamic Phase Diagram at High Baryon Densities

By

ZACHARY SWEGER
DISSERTATION

Submitted in partial satisfaction of the requirements for the degree of

DOCTOR OF PHILOSOPHY

in

Physics

in the

OFFICE OF GRADUATE STUDIES

of the

UNIVERSITY OF CALIFORNIA

DAVIS

Approved:

Daniel Cebra, Chair

Manuel Calderón de la Barca Sánchez

Ramona Vogt

Committee in Charge

2025

To my mom and dad for always believing in me. Also to my brother for never believing in me. That was pretty motivating too I guess.

Contents

List of Figures

List of Tables

Abstract

For over 20 years, the STAR experiment at Brookhaven National Laboratory's Relativistic Heavy-Ion Collider (RHIC) has worked to map the phase diagram of quantum chromodynamic (QCD) matter. Signatures of a deconfined phase of quarks and gluons have been observed in high energy Au+Au collisions. QCD matter is expected to undergo a continuous phase transition to this deconfined state at low baryon densities and a first-order phase transition at large baryon densities, with a critical point marking the endpoint in the phase diagram of the first-order phase transition curve. The experimental search for signatures of a QCD critical point is underway at RHIC in STAR's Beam Energy Scan (BES) program. Fluctuations in the number of protons detected in heavy-ion collisions is one such observable, as a critical point is expected to enhance fluctuations of conserved charges such as baryon number.

This dissertation presents measurements of proton-number fluctuations in STAR's fixed-target program at $\sqrt{s_{NN}} = 3.2$, 3.5, 3.9, and 4.5 GeV in order to search for signatures of a QCD critical point. These fluctuations are quantified by cumulant ratios and factorial cumulant ratios of event-by-event proton-number distributions. No evidence of a QCD critical point is observed in the fourth-order (factorial) cumulant ratios. However, large deviations from the non-critical baseline are reported in the second and third-order (factorial) cumulant ratios. Implications for the QCD critical-point search are discussed.

Acknowledgements

Getting through a PhD is challenging primarily because a lot of life happens in six years. There's politics, heartbreak, deaths, marriages, births, new friends, and every time you see your friends and family, they say something like "so you're still doing grad school?" I'd like to acknowledge everyone who made it easier for me to finish this.

To my parents, thank you for raising me with patience and for supporting me in all my endeavors. Thank you for putting up with all my science projects as a kid. Thank you for picking me up from the airport at 1 AM, for moving me all over northern California, for listening to me vent my frustrations, and for always keeping a bed for me to come home to. I couldn't have done this without you both. To my brother Wesley, I'm not sure that you've made my time in grad school "easier," but I'm lucky to have you as my brother and I can't wait to live closer to you in Los Angeles. To Lexi, you've been a constant in so much of my life and I'm so glad you're part of our family.

Thank you to my advisor, Daniel, for being the best mentor I could have asked for. You taught me how to be an excellent physicist, a good brewer, and an okay softball player. Also to Manuel, you've taught me so much, from the Glauber model to what a winning chili tastes like. Thank you to Spencer for always having my back at Berkeley Lab, and for teaching me how to write, question things, and follow the science. Thank you to Heather for always dishing back as much attitude as I give you. To Saeahram, thank you for always feeding me and having heartfelt conversations. And thank you to Frank and Matt for all the engaging

discussions from physics to politics. Thank you to Emma for always matching my energy and sweater choices. To the UC Davis Nuclear Physics Group as a whole, I could have done this with you all for a long time. As Heather likes to say, this was a little slice of heaven.

Thank you to my physics cohort for getting me through our first few years. I don't know what I would have done without you all. You all made me feel a little bit less like a pickle in a hurricane. Samantha, JB, Bobby, Alaina, Chris, Jamie, Rodrigo, Joe, Phurba, Erin, Ian, Spiegel, Spence, Bob, Finona, Hyun-Soo, and Jean, you made this so much fun.

Thank you also to Zack, for always being someone I can trust and count on at the Lab. I loved sharing an office with you. You've been there to listen whenever I needed a friend, and I appreciate that so much. Thank you also to Wyatt for keeping my time at the Lab interesting. I'm really going to miss our closed-door conversations, coffee time, and shopping outings.

To Matt and Priti, thank you for inviting me into your family. I'm so grateful to be part of your story and to have friends like you. You both were there to support me through my hardest days in Davis and I'll never forget that. To Chloe, if you're reading this, please don't. There's much better things to do with your time... go visit your guncle.

Thank you to all of my friends from before grad school that have put up with me these past few years. Thanks to Felix for being so patient with me ever since freshman year of college. Thanks to Roman, Ben, David, Eazy, Joey, and Katie for always being ready for a great time. Thanks to Alex, Sam, Carter, Kevin, Aaron, Cheuk, Taylor, Rachel, and Midori for being a constant in my life since undergrad. Thanks to Heather, Peter, Danh, Melos, Carlos, Kat, and Nina for tolerating me for over ten years, and still being willing to have the occasional poker night. Thanks also to Sameen, Guadalupe, Grabe, Emma, and Adrien for helping me get through physics at Cal. I wouldn't be here today without your support. Thank you to Bethany, Darren, James, Ninad, Gino, Chris, Joey, Adriana, and Lee for shaping me first into a nuclear physicist. And thank you to Ramona, Prithwish, Iris,

Yu, Greg, Minjung, Gene, Frank, Lijuan, Isaac, Emmy, Rita, Alex J., and Bassam for being a friend to me in this new (to me) field of heavy-ion physics.

To Mathias, you're a great physicist and roommate and I look forward to seeing everything you achieve... now skip to the end of this paragraph. To Austin, please take care of Mathias, he's a little unhinged. To Emma, please tell Austin that I think he's a super cool guy and that I've loved the time we've spent camping, dropping in, and going on road trips together. To Beatrice, let Emma know that I'm so grateful to have met you both as my first friends at the Lab, and I can't wait to dance at her wedding. To Anjali, tell Beatrice that she and Emma and the rest of our group made Berkeley feel like home again. To Mathias, make sure Anjali doesn't stargaze in the middle of the street, and comes down to LA to twirl with me instead. Now go back to the beginning again.

Chapter 1

Introduction

This dissertation investigates the ways in which nuclear matter may undergo phase transitions at extreme temperatures and pressures. Nuclear physics is an incredibly broad field. The nucleus is one of the only structures in nature in which quantum electrodynamics, quantum chromodynamics, and the weak interaction all play a role in describing its evolution in time. The interplay between these interactions results in the many topics we put under the umbrella of nuclear physics. These include nuclear structure, nuclear reactions, radioactive decay, fission, fusion, scattering theory, nucleosynthesis, and the nuclear phase diagram. Fission and fusion applications are the most familiar to the public and it is common to be asked whether our research is related to these applications. Unfortunately the response "no, we study *high energy* nuclear physics" is at best unhelpful, and at worst, frightening, because few people would describe a thermonuclear explosion as "low energy." I'll clarify by discussing some energy scales.

The core of a light-water nuclear reactor, for example, is cooled by water under high pressure to maintain a temperature of $\approx 300°\mathrm{C}$ [1]. The temperature at the core of the sun or a nuclear explosion is $10^7 - 10^8\ °\mathrm{C}$ or 10 to 100 million degrees Celsius [2]. The temperature of the matter we create in particle colliders like the Relativistic Heavy-Ion Collider is on the

scale of 10^{12} °C or 1 trillion degrees Celsius. These are temperatures which (aside from particle collisions) have not been seen in the universe since shortly after the Big Bang. However, unlike a reactor or nuclear explosion which both involve a macroscopic amount of matter, relativistic heavy-ion collisions create extremely hot matter that is approximately the size of two nuclei, or $\approx 10^{-14}$ meters across. This matter is so small and short lived that it is not comparable to the total energy in a nuclear reactor or weapon. Instead of these applications, the purpose of studying relativistic heavy-ion collisions is to learn how the universe came to be, and about one of nature's four fundamental forces: quantum chromodynamics.

Quantum chromodynamics (QCD) is the quantum field theory of the strong nuclear force. It describes interactions between quarks and gluons as well as composite hadrons and nuclei. Just as particles with electric charge are described by quantum electrodynamics (QED), certain particles are sensitive to a quantum charge called *color* charge which is described by QCD. Unlike the one dimensional electric charge, the color charge is three dimensional. The electric charge of each particle can be described as a multiple of the charge of the proton q_p. The antiproton has an electric charge of $-1q_p$, the electron has a charge of $-1q_p$, the antielectron (positron) has a charge of $+1q_p$, and the deuteron has a charge of $+2q_p$. To describe the color charge of a fundamental particle, there are three fundamental charges that are used, which we call red, green, and blue. In analogy to how the antiproton carries the opposite electric charge of the proton, an antiquark carries the opposite color charge of a quark. If we assign red, green, and blue as the quark color charges, then antiquarks carry antired, antigreen, or antiblue. Both quarks and gluons carry color charge. All other known fundamental particles have zero color charge. In typical nuclear matter, quarks and gluons remain confined within hadrons such as protons and neutrons. The analogy of the QCD charge to color was made when physicists observed that only particles with certain combinations of color charge may exist in the vacuum. That is, free particles are composed

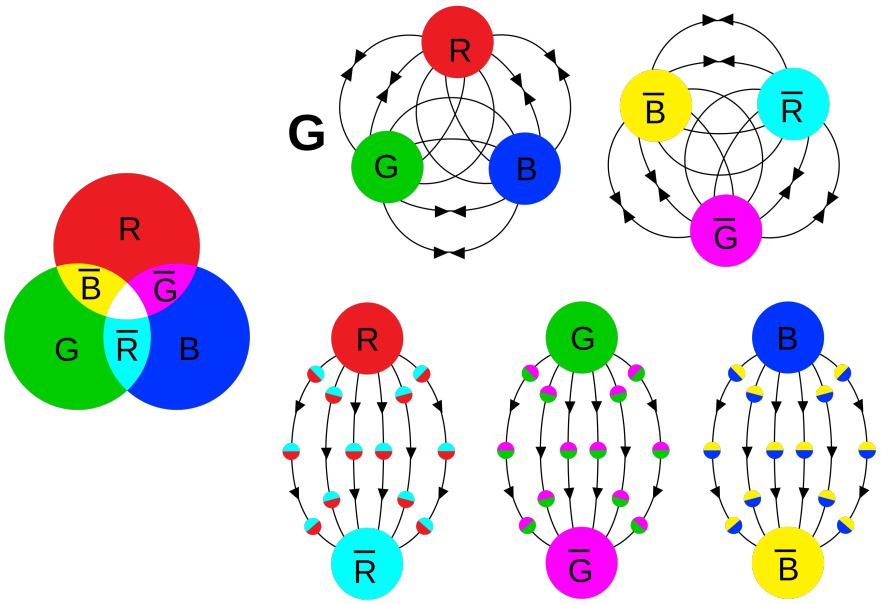

Figure 1.1: Color charges in QCD [3]. The fundamental charges of QCD are described in analogy to the additive color wheel shown at left. Baryons (top right) are colorless combinations of the three additive primaries red+green+blue, or their complements antired+antigreen+antiblue. Mesons (bottom right) are colorless combinations of color and anticolor.

of either three quarks (red+green+blue), three antiquarks, (antired+antigreen+antiblue) or one quark and one antiquark (red+antired, blue+antiblue, green+antigreen). These color charge combinations for free hadrons are shown in Fig. 1.1. Following the analogy, only colorless combinations of quarks may exist in the vacuum. This phenomenon is referred to as confinement because quarks are said to be confined within hadrons.

In 1975 Nicola Cabibbo and Giorgio Parisi used QCD to predict the existence of a state of matter consisting of deconfined quarks and gluons at high temperatures and at high densities [4]. By 1983 the Nuclear Science Advisory Committee was urging the construction of a relativistic heavy-ion collider in its Long Range Plan in order to discover and study this new state of matter [5]. In the early 2000s, experiments at CERN's Super Proton Synchrotron (SPS)

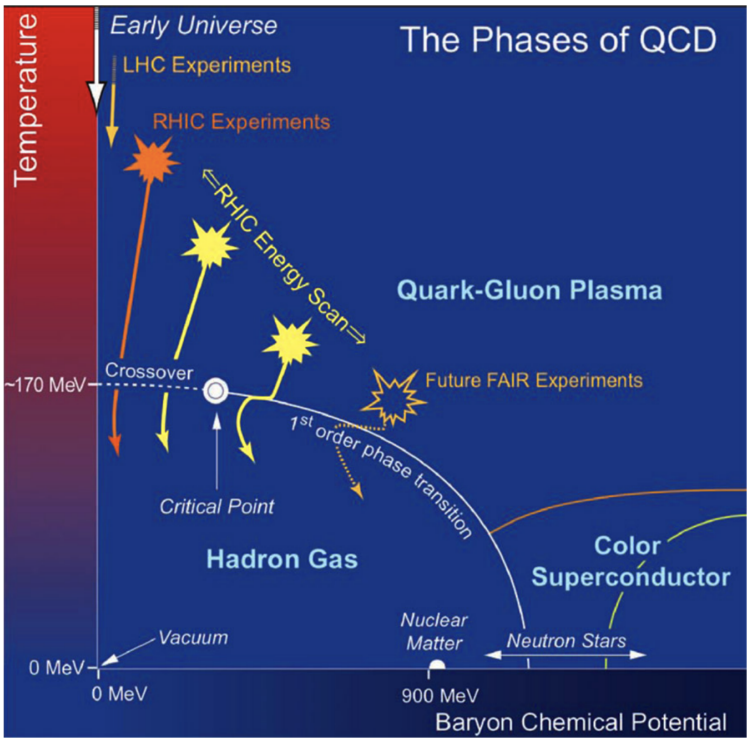

Figure 1.2: The conjectured QCD phase diagram as a function of temperature and baryon chemical potential (μ_B) [8].

and Brookhaven National Lab's Relativistic Heavy-Ion Collider (RHIC) reported evidence of the creation of a quark-gluon plasma and began studying its properties [6, 7].

What Cabibbo and Parisi proposed in 1975 was a change in the phase of QCD matter. A phase diagram for QCD matter is shown in Fig. 1.2 with experimental coverages superimposed. The phases of nuclear matter are described by two state variables: temperature and baryon chemical potential (μ_B), a measure of baryon density. Experiments have observed a quark-gluon plasma at high temperatures and a hadron-gas phase at lower temperatures. However, the nature of the transition between these phases is not well understood. In the figure, a dashed white line marks the location of a crossover phase transition between the quark-gluon plasma phase and the hadronic phase which is expected at low μ_B. The solid

orange curve marks the location of a proposed first-order phase transition between these phases which is expected at high baryon chemical potentials.

The Beam Energy Scan I (BES-I) program at the Relativistic Heavy-Ion Collider collected data in 2010 and 2011 across a range of collision energies which span much of the QCD phase diagram. One feature of the phase diagram that eluded experimental confirmation in BES-I was the existence of a critical point at the boundary between the QGP and hadron gas phases, although experimental results were suggestive of critical behavior [9]. A second program (Beam Energy Scan II) was proposed, in part, to refine measurements of critical behavior observed in BES-I. BES-II included a fixed-target program which extended the range of energies accessible at RHIC and has already collected high-statistics data in the vicinity of an expected critical point. The search for this critical point using fixed-target Au+Au collisions at RHIC is the subject of this dissertation.

1.1 QCD Critical Point

1.1.1 What is a Critical Point?

A critical point on a phase diagram marks the endpoint of a phase coexistence curve. On one side of a critical point there is a distinct boundary in phase space along which two phases of a substance can coexist. A familiar example is liquid water and steam coexisting at the boiling temperature of water as a function of pressure. On the other side of a critical point there ceases to be a distinct boundary between phases. For water, this critical point occurs at 374°C and 218 atmospheres of pressure. Above this temperature and pressure, the transition from the liquid to the gas phase occurs continuously as a function of pressure and temperature.

A phase transition in which phases coexist is known as a first-order transition. First-

order transitions are characterized by a discontinuity in the energy density of the substance across the phase boundary. This discontinuity manifests as latent heat, which is an energy exchange at constant temperature that is associated with the phase transition. Most familiar phase transitions are first-order transitions. As energy is added to liquid water at atmospheric pressure, the temperature of the water rises to the boiling temperature. At this temperature, additional energy is required in order to cause the liquid to vaporize, and the system will remain at the boiling temperature until enough energy has been added to completely vaporize the water. It is this latent heat that allows the phase coexistence in first-order phase transitions. Transitions with a continuous energy density across a phase boundary are known as continuous transitions and do not have an associated latent heat. Thus there is no phase coexistence in continuous phase transitions.

1.1.2 A Critical Point in Quantum Chromodynamics

It is currently unknown whether there is a critical point in the QCD phase diagram along the boundary between the QGP and hadron gas phases. Experiments at the Large Hadron Collider and at the Relativistic Heavy-Ion Collider have attempted to map the phase diagram, but experimentally characterizing the phase transition has remained elusive. Widely accepted lattice QCD calculations at $\mu_B = 0$ predict a continuous transition. However, the order of the transition depends on approximations of the quark masses, with some approximation schemes predicting a first-order transition [10]. Lattice QCD calculations at $T = 0$ predict a first-order phase transition, but uncertainties persist due to theoretical considerations and computational constraints [11].

If there is a first-order transition at low temperatures and high baryon densities and a continuous transition at high temperatures and low baryon densities, then there must be a critical point along the phase boundary. Yet, neither region of phase space is sufficiently well

understood to make definitive claims either way. There is no experimental confirmation of a first-order phase transition at high baryon densities. Therefore, discovering a critical point along this phase transition boundary is of theoretical interest because its existence would confirm the nature of the phase transitions to either side of the point and would improve theoretical understandings of quantum chromodynamics.

1.1.3 Cumulants and Moments

Several models predict fluctuations in certain observables of QCD matter in the vicinity of a critical point. In order to quantify fluctuations, it is useful to define statistical quantities such as the moments, central moments, cumulants, and factorial cumulants. These can all be used to describe probability distribution functions, so we should first make the distinction between them.

The n^{th}-order moment (μ'_n) of a distribution of a random quantity N is given by the expectation value of N^n,

$$\mu'_n = \langle N^n \rangle. \tag{1.1}$$

The first four of these are written

$$\begin{aligned} \mu'_1 &= \langle N \rangle \equiv \mu \text{ [mean]} \\ \mu'_2 &= \langle N^2 \rangle \\ \mu'_3 &= \langle N^3 \rangle \\ \mu'_4 &= \langle N^4 \rangle. \end{aligned} \tag{1.2}$$

These moments describe n^{th}-order fluctuations. However, it is often more useful to discuss the central moments (μ_n) in which the mean (μ) of the distribution is subtracted from each N,

$$\mu_n = \langle (N - \langle N \rangle)^n \rangle = \langle (N - \mu)^n \rangle. \tag{1.3}$$

The first four orders are

$$\begin{aligned}
\mu_1 &= \langle N - \mu \rangle = 0 \\
\mu_2 &= \langle (N - \mu)^2 \rangle \equiv \sigma^2 \text{ [variance]} \\
\mu_3 &= \langle (N - \mu)^3 \rangle \\
\mu_4 &= \langle (N - \mu)^4 \rangle .
\end{aligned} \tag{1.4}$$

The central moments describe n^{th}-order deviations from the mean value. The subtraction of the mean from each N eliminates the scaling with the mean that the moments are vulnerable to. A probability distribution $P(N)$ will have identical central moments if it is shifted uniformly by an amount N_0 to construct $P(N - N_0)$. For example, the second-order central moment (the variance) of a normal distribution is unchanged if the distribution is centered at 0 or 100, whereas the second-order moment is not.

The n^{th}-order cumulants are represented by the symbol C_n. These are constructed from the central moments. The first six cumulants are

$$\begin{aligned}
C_1 &= \langle N \rangle \equiv \mu \text{ [mean]} \\
C_2 &= \mu_2 \equiv \sigma^2 \text{ [variance]} \\
C_3 &= \mu_3 \\
C_4 &= \mu_4 - 3\mu_2^2 \\
C_5 &= \mu_5 - 10\mu_2\mu_3 \\
C_6 &= \mu_6 + 30\mu_2^3 - 15\mu_2\mu_4 - 10\mu_3^2 .
\end{aligned} \tag{1.5}$$

From these cumulants, some standardized moments of a distribution can be defined as

$$\begin{aligned}
s &\equiv C_3/(\sigma C_2) \text{ [skewness]} \\
\kappa &\equiv C_4/(\sigma^2 C_2) \text{ [kurtosis]}.
\end{aligned} \tag{1.6}$$

Critical-point analyses in heavy-ion physics often refer to the following related quantities,

which are simply ratios of cumulants:

$$\begin{aligned} s\sigma &= C_3/C_2 \\ \kappa\sigma^2 &= C_4/C_2. \end{aligned} \tag{1.7}$$

High-order cumulants and their ratios are useful because they describe behavior of the tails of probability distributions where the probability is low. For example, if the tails of a probability distribution are asymmetric, one will obtain a non-zero C_3/C_2. If a distribution has tails that are enhanced relative to a normal distribution with the same width, then it will have an enchanced C_4/C_2. These cumulants describe the behavior of outlier events and characterize large fluctuations from the mean in a dataset.

In addition to the cumulants, factorial cumulants, or correlation functions, are also of interest in heavy-ion collisions [12–14]. These n^{th}-order factorial cumulants, written κ_n, describe multi-particle correlations in the system of interest. The fourth-order factorial cumulants describe four-particle correlations, and can be used to investigate how multiple particles are correlated across rapidity and transverse momentum. These factorial cumulants are written up to fourth order in terms of the cumulants as

$$\begin{aligned} \kappa_1 &= C_1 \equiv \mu \text{ [mean]} \\ \kappa_2 &= C_2 - C_1 \\ \kappa_3 &= C_3 - 3C_2 + 2C_1 \\ \kappa_4 &= C_4 - 6C_3 + 11C_2 - 6C_1. \end{aligned} \tag{1.8}$$

1.1.4 Net-Proton Fluctuations

Critical points on phase diagrams often cause "critical fluctuations" in thermodynamic variables [15–18]. This behavior is observed in many thermodynamic systems and is attributable to a divergence of the correlation length (ξ). The correlation length of a thermodynamic system is a measure of the distance at which particle states are correlated. At the critical point, ξ approaches the size of the system. As the correlation length grows, fluctuations in the system can grow as well. Far from a critical point, small fluctuations away from thermodynamic averages occur but do not propagate through the system. Near a critical point however, the large correlation length allows small fluctuations to grow and become observable.

One such fluctuating observable in heavy-ion collisions is the net-baryon number. Each composite particle composed of quarks also has an antiparticle counterpart with the same mass, but opposite charge and baryon number. A proton has a baryon number of 1 and is made up of two up quarks and one down quark. An antiproton has a baryon number of -1, and is made up of two antiup quarks and one antidown quark. The net-baryon number is the difference between the number of baryons and antibaryons. In an experimental environment, it is impractical to attempt to measure all baryons. Neutrons, for example, are neutral and are not detected in charged-particle detectors. For this reason, we take the net-proton number as a proxy for net-baryon number. The net-proton number is the difference between the number of protons and the number of antiprotons detected in an event. Limiting the experimental analysis to net-proton number instead of net-baryon number will decrease the statistical significance of the measurement. However, the cumulants of net-proton number distributions have been shown to be related to net-baryon number cumulants and can be used to extract these cumulants [19]. For each dataset at a given collision energy, one can construct net-proton distributions as shown in Fig. 1.3. Fluctuations in the net-proton

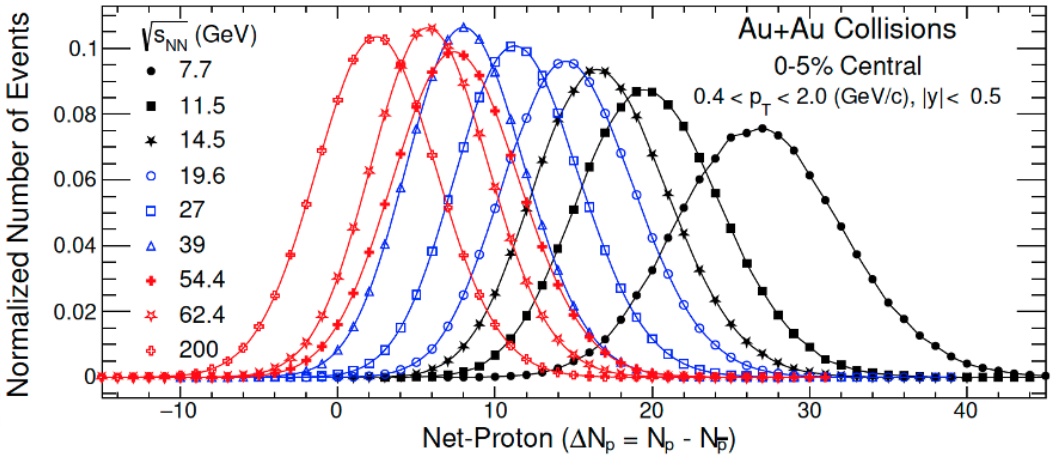

Figure 1.3: The red, blue, and black distributions are the net-proton number observed by the STAR detector at several collision energies [9].

number are observable in the cumulants of these distributions. QCD-based models provide predictions of how these behave near a critical point. It has been shown that higher-order cumulants of the net-proton distributions are expected to have increased sensitivity to the correlation length [20],

$$\begin{aligned} s\sigma &\sim \xi^{2.5} \\ \kappa\sigma^2 &\sim \xi^5. \end{aligned} \tag{1.9}$$

These sensitivities can thus be regarded as the sensitivity to a potential critical point.

Several QCD-based models are used to predict the behavior of proton number cumulants around a critical point [9, 20–22]. The most striking prediction by these models is the behavior of the fourth moment as a function of energy. If the chemical freeze-out curve is close to the critical point, fluctuations in the net-proton number become frozen and are observable in the final state particle distributions. These models predict a nonmonotonic variation in the fourth-order cumulants of the net-proton distribution as a function of collision energy in the vicinity of a critical point if the chemical freeze-out curve is sufficiently close

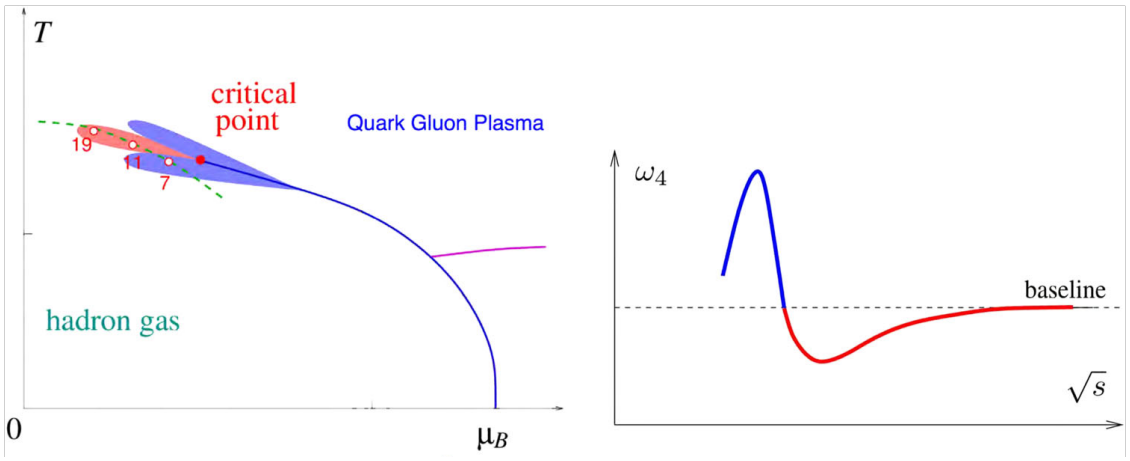

Figure 1.4: (Left) QCD phase diagram with the chemical freeze-out curve represented by the green dashed line. The points labeled with numbers represent the μ_B and T at freezeout for Au+Au collisions at $\sqrt{s_{NN}}$ = 19.6, 11.5, and 7.7 GeV. Areas where the fourth moment is greater than the baseline (non-critical) behavior are colored blue. The area where the fourth moment is less than the baseline is shaded red. Locations are imprecise and demonstrate how changing the collision energy can probe varying proximities to the critical point [21]. The magenta curve on the right side of the phase diagram represents the boundary between the QGP phase and a predicted phase of color-superconducting matter. (Right) Expected behavior of fourth moment ($\omega_4 = \kappa\sigma^2$) as a function of the collision energy in the proximity of a critical point [9].

to the critical point. Similar to the cumulants, high-order factorial cumulants are expected to experience enhancement and suppression in the vicinity of a critical point [13] as shown in Fig. 1.4.

Measurements of the net-proton kurtosis as a function of collision energy were made by the STAR collaboration over a range of collision energies from $\sqrt{s_{NN}}$ = 7.7 GeV up to 200 GeV, where $\sqrt{s_{NN}}$ refers to the center-of-mass energy per pair of colliding nucleons, as shown in Fig. 1.5. This center-of-mass energy is discussed further in Sec. 2.2. A recent analysis has added a point at $\sqrt{s_{NN}}$ = 3.0 GeV [23]. These previous kurtosis measurements deviate from the expected baseline behavior in the region from 7.7 GeV to 27 GeV, although the large uncertainties limit the significance of these deviations. The recent point at 3.0 GeV

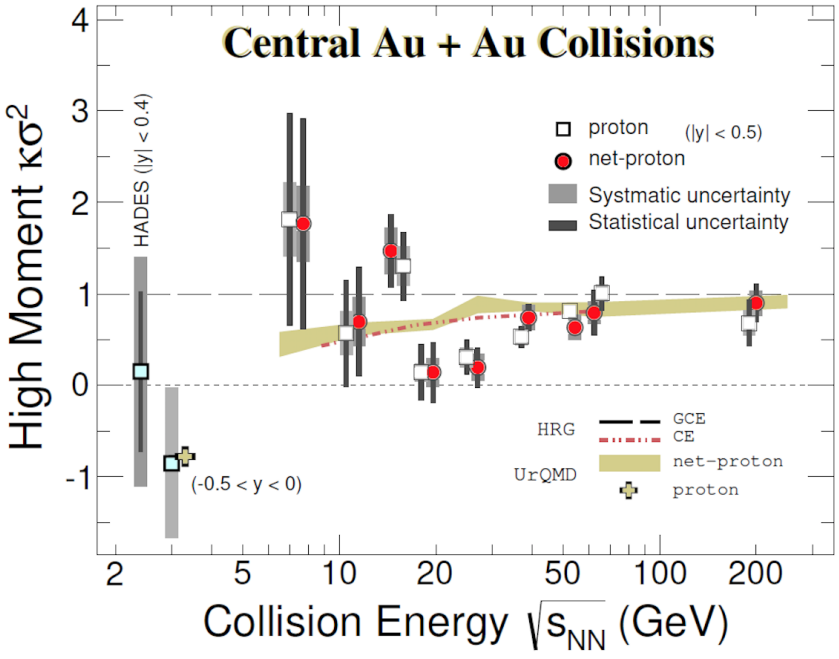

Figure 1.5: C_4/C_2 of net-proton distributions as a function of the collision energy from Beam Energy Scan I and fixed-target collisions at $\sqrt{s_{NN}} = 3.0$ GeV. The UrQMD baseline (non-critical) behavior is shown in beige [23]. A similar measurement by the HADES experiment is shown at $\sqrt{s_{NN}} = 2.4$ GeV [24].

demonstrates a return to the non-critical baseline behavior and is consistent with a measurement made by the HADES experiment at the GSI facility in Germany [24]. One might ask whether antiprotons are even created at energies as low as 3.0 GeV. Baryon number is always conserved, so for any proton that is created in a collision, and antiproton must also be created. This means that the minimum threshold center-of-mass energy for creating proton/antiproton pairs must be enough to account for the rest masses of the initial colliding nucleons, and the final-state proton/antiproton pair. The threshold center-of-mass energy for creating protons and antiprotons is thus $\sqrt{s_{NN}} \approx 4m_p = 3.75$ GeV. At 3.0 GeV, and other fixed-target energies, the number of antiprotons created in any event is negligible, so the net-proton number is taken to be equal to the proton number.

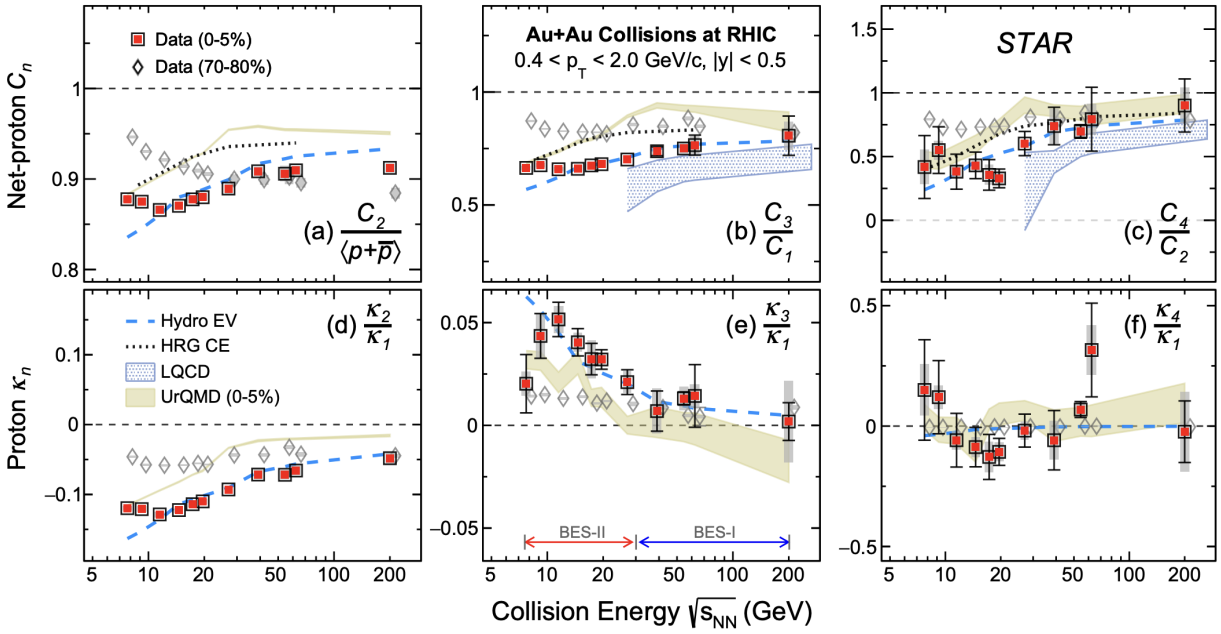

Figure 1.6: Cumulant (C_n) ratios and factorial cumulant (κ_n) ratios up to fourth order in STAR's Beam Energy Scan II [25].

A preprint [25] of the net-proton cumulants and factorial cumulants up to fourth order from STAR's Beam Energy Scan II was released in April of 2025 with new high statistics data at $\sqrt{s_{NN}} = 7.7$, 9.2, 11.5, 14.6, 17.3, 19.6, and 27 GeV. These results are shown in Fig. 1.6. The plots include comparisons with theoretical hydrodynamic excluded volume [26], and hadron-resonance gas canonical-ensemble [27] predictions. They also include predictions from lattice QCD [28] and from UrQMD simulations. None of these models include a critical point, so each serves as a non-critical baseline. The hydrodynamic excluded volume calculation describes the data well at all orders except at the lowest energies at second and third orders. There is no evidence of critical behavior in C_4/C_2 and κ_4/κ_1. The question remains whether C_4/C_2 will deviate from the baseline in the range from 3.0 GeV to 7.7 GeV.

1.2 This Work: Fixed-Target Proton Number Fluctuations at $\sqrt{s_{NN}}$ = 3.2, 3.5, 3.9, and 4.5 GeV

Beam-quality considerations place a lower limit on the energies accessible at the Relativistic Heavy-Ion Collider. RHIC cannot effectively run in collider mode below $\sqrt{s_{NN}} = 7.7$ GeV. The tantalizing hint of critical behavior around this energy motivated Beam Energy Scan II. In addition to collecting additional high-statistics data between 7.7 GeV and 27 GeV, the STAR fixed-target program (FXT) was developed to achieve energies below $\sqrt{s_{NN}} =$ 7.7 GeV. A gold target was placed inside the beam pipe on the west end of the STAR detector. This experimental configuration has allowed STAR to extend its energy range at the low end down to $\sqrt{s_{NN}} = 3.0$ GeV. As discussed in the prior section, data from 3.0 GeV has already been analyzed. There is now additional data at center-of-mass energies of 3.2, 3.5, 3.9, 4.5, 5.2, 6.2, 7.2, and 7.7 GeV.

This dissertation characterizes the behavior of the proton number kurtosis and other cumulants as a function of energy from Au+Au collisions at $\sqrt{s_{NN}} = 3.2$, 3.5, 3.9, and 4.5 GeV. This data collected from the STAR fixed-target program allows us to search for critical behavior in the high baryon density region of the QCD phase diagram. Significant deviations of the high-order cumulants from the non-critical baseline may indicate the existence of a critical point on the QCD phase diagram.

Chapter 2

The STAR Experiment at RHIC

2.1 The RHIC Facility

RHIC is located in Brookhaven National Laboratory (BNL) on Long Island, New York. The collider began operations in the year 2000, and is composed of two independent intersecting storage rings 2.4 miles in circumference with 6 intersection points. RHIC can collide many ion species such as protons, oxygen, zirconium, ruthenium, gold, and uranium. Because the beams are independent of each other, the ion species and the energy of the beam can be different in the two rings, allowing for asymmetric collisions in mass and energy.

A schematic of the RHIC complex from 2003 is shown in Fig. 2.1. When viewed from above as the face of a clock, the intersection points are located at 12, 2, 4, 6, 8, and 10 o'clock. The STAR detector is located at the 6 o'clock position. There are 1740 superconducting magnets that steer and focus the beams between the intersection regions. The schematic labels the PHOBOS and BRAHMS experiments which have since ceased operation. The PHENIX experiment located at the 8 o'clock position has been replaced by the sPHENIX experiment.

Beams at the RHIC complex start out with ions produced in a high charge state at the

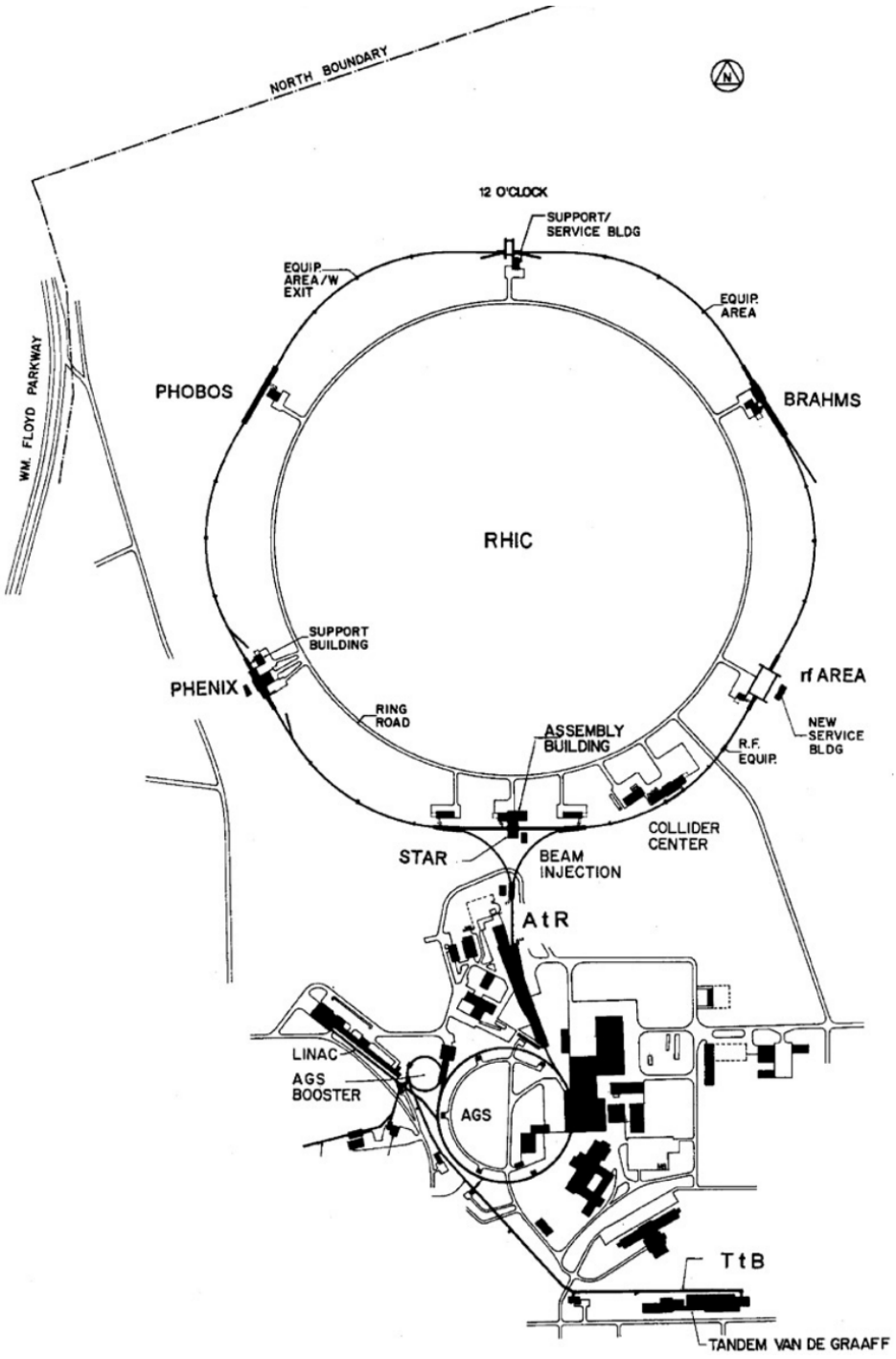

Figure 2.1: Layout of RHIC and its injection facilities [29].

Electron Beam Ion Source (EBIS) [30]. These ions are injected into the LINAC in the lower left corner of Fig. 2.1. They undergo an initial acceleration stage and are passed through stripping foils which serve to partially strip the ions of their electrons prior to injection into the Booster. The Booster stores and accelerates six bunches of gold ions up to a kinetic energy of 95 MeV per nucleon [29] before passing them through another stripping foil and into the Alternating Gradient Synchrotron (AGS). The AGS further accelerates these ions up to a total energy of 9.75 GeV per nucleon. Ions are fully stripped on exiting the AGS for injection into RHIC. A final stripping foil located in the transfer line between the AGS and RHIC removes the two remaining K-shell electrons [31].

The RHIC beam is composed of 111 bunches of $\approx 10^9$ ions each. The beam is established by injecting one bunch of ions at a time from the AGS into the RHIC ring and, once all 111 bunches are in the ring, the beam is complete. Then the magnets in the RHIC ring are gradually ramped in strength as the radio frequency cavities accelerate the bunches. When the beam has been accelerated to the desired energy, the magnets stop ramping, and the beam is circulated continuously with RHIC acting as a storage ring. The accelerator operators then focus the beams within the interaction region to induce collisions. This is the procedure when RHIC is operating as a collider. Fixed-target collisions at RHIC are also possible by circulating a single beam such that it grazes a target in the beam pipe. This fixed-target configuration is described in Sec. 2.4.

2.2 Background on Relativistic Kinematics

In order to describe the detector and experimental program in more detail, it is useful to briefly define several quantities that will be used often. The first of these is $\sqrt{s_{NN}}$ which is the center-of-mass energy per nuclear pair, and is defined using the four-momentum of the

average nucleon in each beam (p_1 and p_2) as

$$\sqrt{s_{NN}} = \sqrt{(p_1 + p_2)^2}. \tag{2.1}$$

Colliding two symmetric Au ion beams each with 100 GeV/nucleon yields $\sqrt{s_{NN}} = 200$ GeV. In a fixed-target configuration, one beam has zero momentum, and the $\sqrt{s_{NN}}$ is given by $\sqrt{s_{NN}} = \sqrt{2m_N^2 + 2m_N E_{\rm b}}$, where m_N is the mass of the average nucleon, and $E_{\rm b}$ is the energy per nucleon of the beam in the lab frame. A ^{197}Au nucleus has a mass of 183.4 GeV, resulting in an average nucleon mass of $m_N = 0.931$ GeV. With a 100 GeV/nucleon beam impinging on a fixed target, the center-of-mass energy is approximately 13.8 GeV.

Another quantity used often in this dissertation is the rapidity, y, given by

$$y = \frac{1}{2} \ln \left(\frac{E + p_z}{E - p_z} \right). \tag{2.2}$$

We often refer to the center-of-mass rapidity, $y_{\rm cm}$, to describe the rapidity of particles that have the same longitudinal velocity as the center-of-mass frame of the colliding nuclei. For symmetric colliding beams, the net momentum in the beam direction, p_z, is zero. In this case, the center-of-mass rapidity is $y_{\rm cm,\ sym} = \ln(1)/2 = 0$. In fixed-target collisions, the center-of-mass rapidity is non-zero. The total energy per nucleon pair is $E = E_{\rm b} + m_N$, and the total momentum in the z direction is $p_z = p_{\rm b} = \pm\sqrt{E_{\rm b}^2 - m_N^2}$. Defining the positive z direction to be that of the beam, the center-of-mass rapidity for fixed-target collisions is given by

$$y_{\rm cm,\ fxt} = \frac{1}{2} \ln \left(\frac{E_{\rm b} + m_N + \sqrt{E_{\rm b}^2 - m_N^2}}{E_{\rm b} + m_N - \sqrt{E_{\rm b}^2 - m_N^2}} \right). \tag{2.3}$$

This simplifies further to the following expression, which states that the center-of-mass rapidity is the average of the target rapidity (0) and beam rapidity ($y_{\rm b}$),

$$y_{\rm cm,\ fxt} = \frac{1}{4} \ln \left(\frac{E_{\rm b} + \sqrt{E_{\rm b}^2 - m_N^2}}{E_{\rm b} - \sqrt{E_{\rm b}^2 - m_N^2}} \right) = \frac{1}{2} y_{\rm b}. \tag{2.4}$$

The term midrapidity refers to particles with rapidities close to the center-of-mass rapidity. Midrapidity is often taken to range from $y_{\rm cm} - 0.5$ to $y_{\rm cm} + 0.5$. Rapidity is a useful quantity

because it is additive under Lorentz boosts, so if one wanted to calculate the rapidity of a particle in the center-of-mass frame, given a lab-frame rapidity y_{lab}, one would just need to boost to the center-of-mass frame using

$$y_{\text{boosted}} = y_{\text{lab}} - y_{\text{cm}}. \tag{2.5}$$

Rapidity is most useful when particle identification is available. Even if all momenta are known precisely, one still needs the particle mass in order to calculate the rapidity. When particle mass is not available it is more useful to discuss the pseudorapidity η, which is constructed by taking the ultrarelativistic limit of rapidity in which a particle's momentum is much greater than its mass ($|\vec{p}| \gg m$). In this limit, $E \approx |\vec{p}|$, and the equation for rapidity simplifies to the equation for pseudorapidity,

$$\eta = \frac{1}{2} \ln \left(\frac{|\vec{p}| + p_z}{|\vec{p}| - p_z} \right) = - \ln \left(\tan \left(\frac{\theta}{2} \right) \right), \tag{2.6}$$

where $|\vec{p}|$ is the magnitude of the three momentum of the particle, and θ is its angle with respect to the beam axis. In order to calculate the pseudorapidity of a particle, only θ is needed. This makes pseudorapidity a useful quantity for describing not only ultrarelativistic particles, but detector geometry as well. A pseudorapidity of 0 corresponds to particles traveling exactly perpendicular to the beam axis. Particles traveling along the beam axis have infinite pseudorapidity. As an example, in Sec. 2.4, the geometry of the fixed-target configuration in STAR is described. In that section, pseudorapidity is used to describe the angular coverage of the time projection chamber, which covers $0 < \eta < 2.2$. This means that, in fixed-target collisions, the time projection chamber provides tracking directly above the target and forward until about 221 milliradians from the beam axis.

2.3 The Solenoidal Tracker at RHIC (STAR)

The STAR detector is composed of many subsystems, but the two for which it is named are the time projection chamber (TPC) which enables charged particle tracking, and the large solenoidal magnet surrounding the TPC which maintains a nearly uniform 0.5 Tesla magnetic field within the TPC. The time projection chamber is described in more detail in Sec. 2.3.1. Charged particles traveling through the TPC are curved by the magnetic field, and the ionization that these particles cause enables tracking. In addition to tracking, the TPC enables particle identification by measuring the energy loss of charged particles as they travel through its gas filled volume. This is described in Sec. 5.2.2. At high momenta, it becomes difficult to distinguish particles by their energy loss alone. Time-of-flight (TOF) detectors are thus used to supplement the particle identification capabilities of the TPC for high-momentum particles. These TOF detectors are described in more detail in Sec. 2.3.2. This section describes how a subset of the STAR detector works. We focus here on the TPC and TOF detectors, and how the fixed-target configuration was implemented in STAR.

2.3.1 The STAR TPC

The STAR time projection chamber is a large charged particle tracker. The design of the TPC is detailed in Ref. [32]. A diagram of the TPC is shown in Fig. 2.2. The z direction is taken to be along the beam axis. The TPC extends from 50 cm to 200 cm radially from the beam axis. It is 4.2 m in length, and covers $|z| < 210$ cm from the center of the interaction region. In collider mode the TPC covers a pseudorapidity range of $-1.5 < \eta < 1.5$. In the fixed-target configuration discussed in Sec. 2.4, the TPC covers a pseudorapidity range of $0 < \eta < 2.2$ A high voltage central membrane is located at $z = 0$. When powered, the membrane is a cathode held at -28 kV. The endcap anodes are grounded. This configuration results in an electric field strength of ≈ 140 V/cm.

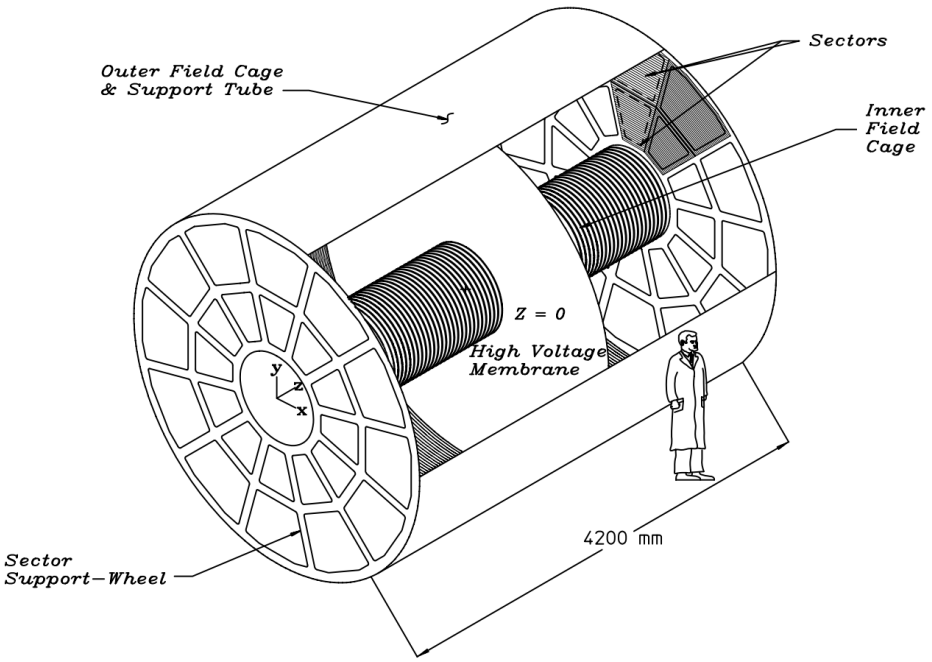

Figure 2.2: Diagram of the STAR TPC [32].

The volume of the TPC is filled with a gas called P10 maintained at 2 millibar above atmospheric pressure. P10 is made up of 90% argon and 10% methane. Argon is used because it is noble gas with a weak affinity for free electrons, so ionization electrons drifting toward the endcaps are not easily stopped by the gas. The methane quenches high-energy photons propagating within the TPC [33]. Under the electric field strength of ≈ 140 V/cm, the ion drift velocity is 5.5 cm/μs. These ionization electrons drift at a uniform velocity toward the endcap where they avalanche in the multi-wire proportional chambers in the readout pads. An electron avalanche happens when a few electrons, subject to a very strong electric field, accelerate and collide with other atoms, freeing additional electrons. These additional electrons are also accelerated and continue the cascade, causing a large amplified signal. The signals from these avalanches are digitized and recorded as a hit [32]. Hits

in several readout boards are used to reconstruct the ionization trail left by a high energy charged particle. The reconstructed tracks in the TPC from a central Au+Au collision are shown in Fig. 2.3. This event is from collider mode. An event display from the fixed-target program is shown in Sec. 2.4.

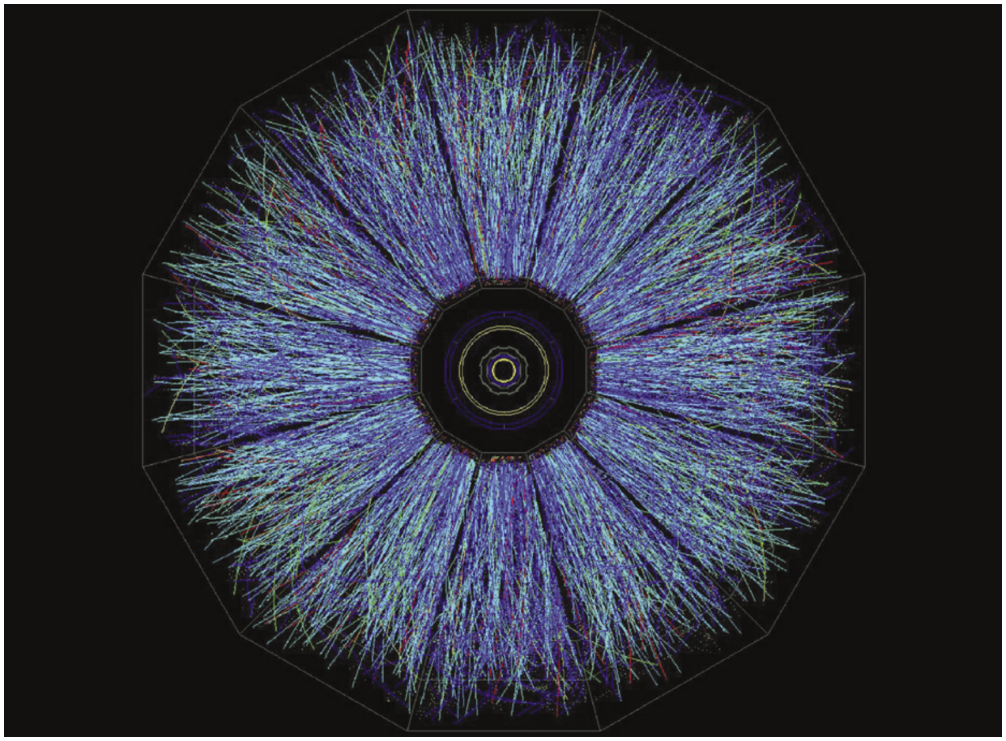

Figure 2.3: Event display of a central and symmetric Au+Au collision in the STAR time projection chamber [34].

2.3.2 Time-of-Flight Detectors

By combining the momentum information from reconstructed tracks in the TPC with precision timed hits in the TOF, high-momentum particles can be identified by their mass to charge ratios. There are two main time-of-flight detector systems in STAR. These are the barrel time-of-flight (BTOF) and the endcap time-of-flight (ETOF) detectors. The BTOF

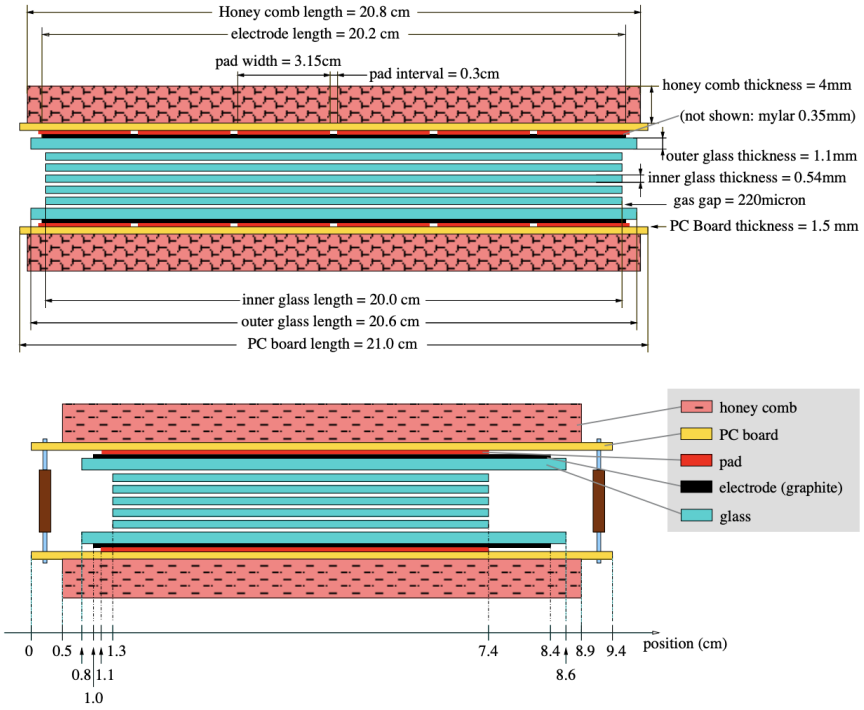

Figure 2.4: Crosssectional view of MRPC boards used in the STAR barrel time-of-flight detector [35].

is at the outer radius of the TPC and, in fixed-target collisions, it covers an approximate pseudorapidity range of $0 < \eta < 1.5$. The BTOF uses multi-gap resistive plate chambers (MRPCs) to detect charged particles with a timing resolution of < 100 ps [35]. A crosssectional view of these MRPCs is shown in Fig. 2.4. The electrodes, shown as black strips in the figure, apply a large electric field across the stack of glass plates. When a high energy charged particle passes through, it causes an avalanche in the gas between the glass plates. This signal is read out by copper pads shown in red.

The endcap time-of-flight was provided by the TOF group in the Compressed Baryonic Matter (CBM) collaboration and is a relatively new addition to STAR, installed for Beam Energy Scan II. The ETOF is planned for use at the future CBM experiment at GSI in

Germany. STAR's fixed-target program provided an ideal case for testing the detector at an active experiment with a complementary physics program. The ETOF was installed on the east endcap of the TPC to catch the spray of tracks originating from fixed-target collisions on the west end. In fixed-target collisions, the ETOF covers an approximate pseudorapidity range of $1.5 < \eta < 2.2$. It uses a similar MRPC technology, but was able to achieve a timing resolution of < 80 ps [36]. The ETOF, prior to installation, is pictured in Fig. 2.5. More details regarding the use of the ETOF in this analysis are provided in Sec. 5.2.6.

Figure 2.5: Endcap time-of-flight detector prior to installation. Photograph courtesy of Daniel Cebra.

The TPC has a relatively low timing resolution due to the long drift time of the ions in the TPC gas. The TOF does not have a similar limitation, allowing for much better timing resolution. The STAR BTOF and ETOF rely on a startless time-of-flight calculation in which a "t_0 algorithm" determines the start time of the event. In this algorithm, low momentum TPC tracks that are matched with TOF hits are used if they are positively

identified as pions or protons by their energy loss in the TPC. If a track is identified as a pion or proton, then the TOF hit associated with that track is used to identify the time the particle reached the outer edge of the TPC. The track is then reconstructed back to the collision vertex, and the time it would have originated from the vertex is calculated. Several of these well defined tracks are used to determine the start time (t_0) of the event.

Once a start time is calculated, it can be used to determine the time of flight ($\Delta t = t_{\text{hit}} - t_0$) for all other tracks [35]. The velocity of a particle with a reconstructed track length L is $v = L/\Delta t$. The inverse $\beta = v/c$ of the particle is then given by

$$1/\beta = c\Delta t/L. \tag{2.7}$$

The particle mass can be calculated from $1/\beta$ as

$$m = p\sqrt{(1/\beta)^2 - 1}. \tag{2.8}$$

This is useful primarily for high-momentum particles that cannot be distinguished by energy loss alone.

2.4 STAR's Fixed-Target Program

The STAR fixed-target program was implemented in order to lower the center-of-mass energy of Au+Au collisions possible at RHIC. When operating in collider mode, the luminosity drops with beam energy as the beam focusing weakens. The lowest center-of-mass energy that is feasible in collider mode is $\sqrt{s_{NN}} = 7.7$ GeV. However hints of critical behavior near this lower limit motivated STAR to explore other ways to reach center-of-mass energies lower than 7.7 GeV.

Students at the University of California, Davis had been analyzing gold collisions with the aluminum beam pipe in order to demonstrate the feasibility of analyzing fixed-target

collisions with STAR. In 2015, STAR had its first test run with a gold target inserted into the beam pipe. Following that test run, the target was replaced with that shown in Fig. 2.6. The first physics runs with this new target were performed in 2018 at $\sqrt{s_{NN}} = 3.0$ GeV, and 7.2 GeV. In 2019 and 2020, STAR additionally collected data at $\sqrt{s_{NN}} = 3.2$, 3.5, 3.9, and 4.5 GeV. Data were also collected at higher energies, but data from these four energies are the focus of this dissertation.

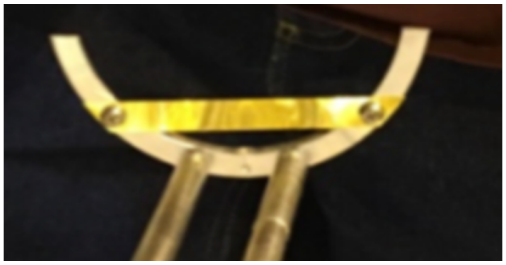

Figure 2.6: Photograph of the gold target and support structure.

The gold target sits 2 cm below the center of the beam pipe and 200 cm from the center of the STAR TPC, as shown in Fig. 2.7. When operating in fixed-target mode, only the yellow beam was injected and only every 10th bunch was filled. This fill structure was chosen to limit pileup from adjacent filled buckets. Pileup from adjacent filled buckets is discussed in more detail in Sec. 3.6.1. The beam operators lowered the beam center toward the target and monitored the luminosity until the interaction probability for any given bunch crossing was between approximately 0.001 and 0.005. Pseudorapidities in the fixed-target configuration are shown in Fig. 2.7. The center-of-mass frame boost increases with the yellow beam energy. This means that the center-of-mass rapidity approaches the edge of the TPC at the high fixed-target energies. An event display from STAR's fixed-target program is shown in Fig. 2.8. The yellow beam energies, center-of-mass rapidities (y_{cm}), and corresponding baryon chemical potentials for the $\sqrt{s_{NN}} = 3.2$, 3.5, 3.9, and 4.5 GeV datasets are tabulated in Table 2.1.

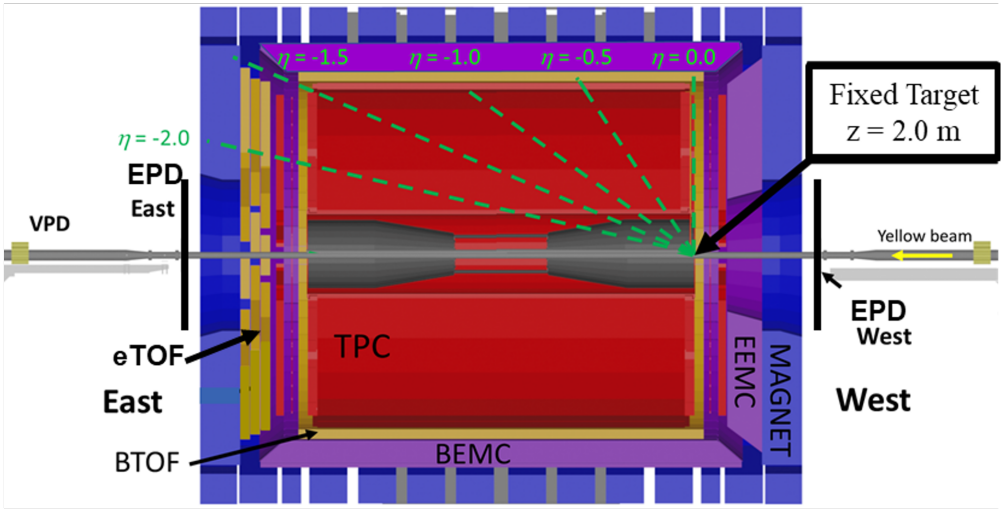

Figure 2.7: Cross-sectional view of STAR in fixed-target mode

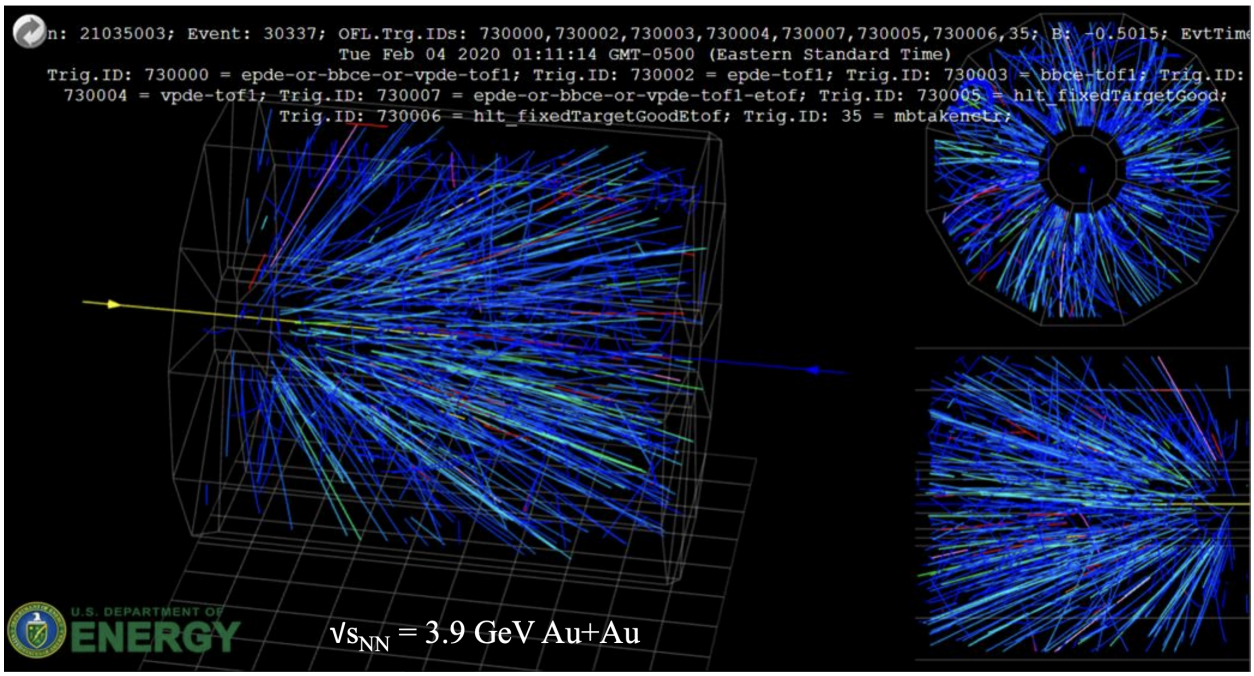

Figure 2.8: Event display of a fixed-target Au+Au collision in the STAR time projection chamber [37].

Table 2.1: Details of the fixed-target datasets.

Nominal $\sqrt{s_{NN}}$ (GeV)	Exact $\sqrt{s_{NN}}$ (GeV)	single beam energy (GeV)	y_{cm}	chemical potential (MeV)
3.2	3.208	4.593	1.139	697
3.5	3.531	5.761	1.254	666
3.9	3.918	7.309	1.375	632
4.5	4.470	9.752	1.522	589

The chemical potentials were determined from a parametrization of μ_B as a function of the collision energy [38]. This parametrization is

$$\mu_B(\sqrt{s_{NN}}) = \frac{d}{1 + e\sqrt{s_{NN}}}, \tag{2.9}$$

where $d = 1.308 \pm 0.028$ GeV and $e = 0.273 \pm 0.008$ GeV^{-1}. The parametrization is based on a fit to measurements of μ_B from experiments at SIS, AGS, SPS, and RHIC. The parametrization of these measurements is described in Ref. [38], and the resulting curve is shown in Fig. 2.9.

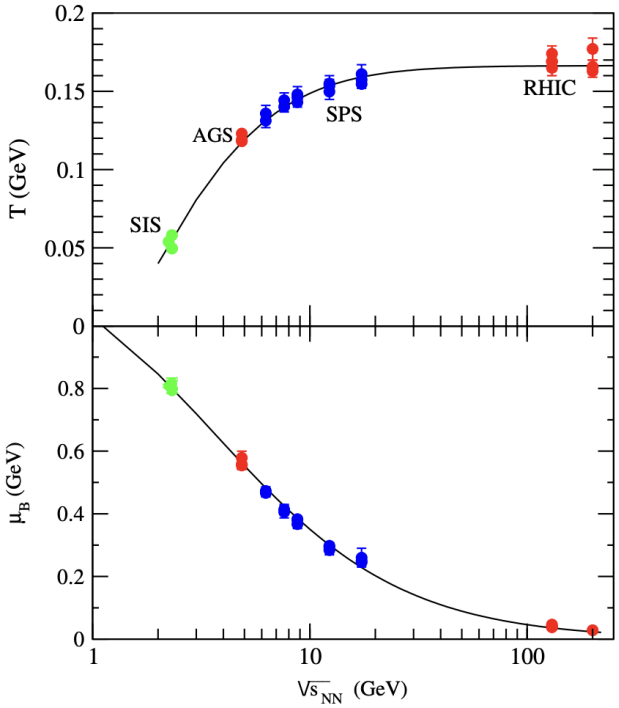

Figure 2.9: Measurements and parameterizations of μ_B and T as a function of $\sqrt{s_{NN}}$ [38].

Chapter 3

How Not to Measure a False Critical Signature

It is common to use different detectors to measure multiplicity and identify particles of interest. In STAR analyses, event-by-event multiplicity was determined from the number of tracks in a Time-Projection Chamber (TPC), excluding protons. Once the event has been classified by centrality, particles used in the analysis were determined by a combination of TPC and time-of-flight (TOF) detections. HADES measured net-charge in a hodoscope to determine centrality, and coincident TOF and energy-loss measurements to identify protons. ALICE used scintillators to measure centrality and energy-loss in a TPC to identify particles. In all of these measurements, a different detector was used for measuring multiplicity and for identifying particles of interest; a process we refer to as a mixed-detector approach.

High-order cumulants are measured as a function of multiplicity and are interpreted in terms of centrality. For simplicity, we focus on the measurement of the cumulants of proton number, n. Rather than measuring cumulants of the probability distribution of raw proton number, $P(n)$, we instead measure cumulants of the probability distribution of proton number given a multiplicity M: $P(n|M)$. The moments of one-dimensional slices in

the correlation between proton number and multiplicity shown in Fig. 3.1 is thus the entire measurement.

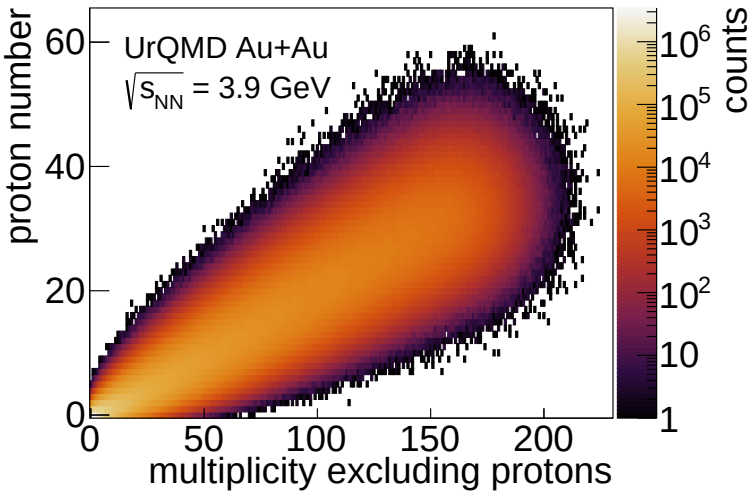

Figure 3.1: Proton number and multiplicity (excluding protons) in UrQMD simulations of $\sqrt{s_{NN}} = 3.9$ GeV Au+Au collisions.

Rare events, in which the correlation between proton number and multiplicity changes, can create large distortions in the proton number distribution at each measured multiplicity. These distortions can cause enhanced high-order cumulants. Figure 3.2 shows two simulated samples of proton-number distributions for a given multiplicity M. In both samples the proton number n is generated from normalized Gaussians with mean μ, and standard deviation σ:

$$G(n, \mu, \sigma) = \frac{1}{\sigma\sqrt{2\pi}} \exp\left[-\frac{1}{2}\left(\frac{n-\mu}{\sigma}\right)^2\right]. \tag{3.1}$$

The black distribution is sampled from $P(n|M) = G(n, \mu = 50, \sigma = 5)$. Any distribution with the same kurtosis as a normal distribution is known as mesokurtic. A perfect normal distribution has $C_4/C_2 = 0$. The magenta distribution is sampled from

$$P(n|M) = (1-\alpha)G(n, \mu, \sigma_1) + \alpha G(n, \mu, \sigma_2), \tag{3.2}$$

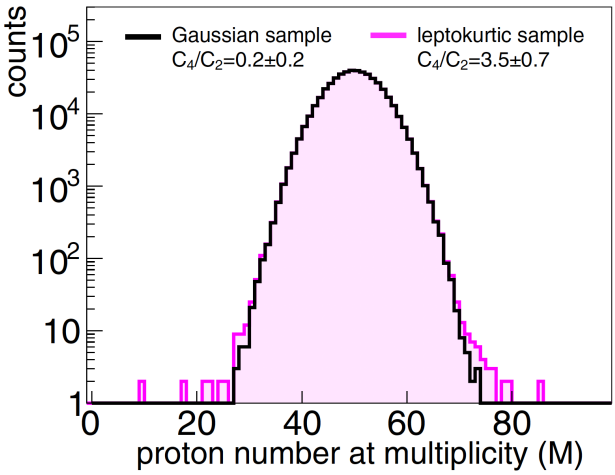

Figure 3.2: Two example distributions and respective C_4/C_2 values. The mesokurtic (C_4/C_2 consistent with 0) sample follows a normal (Gaussian) distribution. The leptokurtic ($C_4/C_2 > 0$) distribution is sampled from the same normal distribution, but also samples from a much broader normal distribution in 0.1% of events.

with $\alpha = 0.001$, $\mu = 50$, $\sigma_1 = 5$, and $\sigma_2 = 14$. In 0.1% of events, the proton number was sampled from a Gaussian distribution with a much broader width. In other words, in 0.1% of events, the correlation between multiplicity and proton number was much weaker. This rare and spontaneous decorrelation is enough to raise C_4/C_2 from being consistent with 0, to 3.5 ± 0.7. Any distribution with $C_4/C_2 > 0$ is known as leptokurtic. This enhancement is at a level and significance that would constitute a signal in the search for the QCD critical point.

The key to any measurement of high-order cumulants is distinguishing low-statistics outliers from the bulk behavior of the data. We demonstrate that the mixed-detector approach can result in rare and spontaneous changes in the correlation between multiplicity and proton number, resulting in anomalously-large high-order cumulants. Anomalous events alone are not responsible for enhanced fluctuations. Instead, the expression of anomalous events in high-order cumulants depends on analysis choices, which can be engineered to suppress

these contributions.

There are other effects that distort high-order cumulants of particle-number distributions in relativistic collisions. Imperfect mapping between event multiplicity and impact parameter distorts these cumulants. Such distortions are referred to as volume fluctuations. The effect of volume fluctuations and how to correct for them are described in Refs. [39, 40]. Distortions due to detector inefficiencies are treated in Ref. [41]. Both of these are well-understood effects and are not explained further here.

In Sec. 3.1 we show how a different correlation between proton number and multiplicity in detector-induced fluctuations leads to enhanced high-order central moments. In Sec. 3.2 we explore how detector responses to various classes of events change the correlation between proton number and multiplicity. In Sec. 3.3 we introduce two toy models of detector responses to UrQMD Au+Au collisions at $\sqrt{s_{NN}} = 3.9$ GeV in order to demonstrate this change in correlation. The first toy model simulates out-of-time pileup in order to investigate how using fast and slow detectors in the presence of pileup can enhance or suppress detector-induced fluctuations. The second toy model simulates the effect of a detector undergoing fluctuations in acceptance. The results of these toy models are evaluated in Sec. 3.4. In Sec. 3.5, we summarize these findings in a short list of prescriptions for fluctuations analyses. These prescriptions describe how to avoid measuring enhanced high-order cumulants and thus a false QCD critical-point signature.

3.1 Anomalous Fluctuations and High-Order Moments

In this section we evaluate the impact of detector-induced fluctuations on central moments. We demonstrate that the effect of a fluctuation on high-order central moments is determined

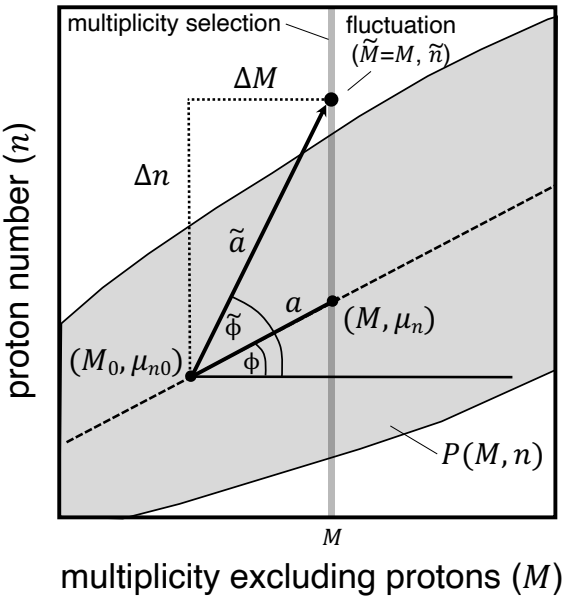

Figure 3.3: A zoomed-in view of a fluctuation embedded in the proton-number and multiplicity probability distribution used to clarify the variables in Sec. 3.1. The proton-number cumulants are calculated at multiplicity M, and a test fluctuation is shown at $(\widetilde{M} = M, \tilde{n})$.

by the correlation between proton number and multiplicity in the anomalous event.

Cumulants of a distribution are expressed in terms of the central moments up to sixth order as given in Eq. 1.5. The i^{th}-order central moment of the proton number n at some multiplicity M is given by

$$\mu_i(M) = \langle (\delta n|M)^i \rangle = \int (n - \mu_n)^i P(n|M) dn, \tag{3.3}$$

where μ_n is the mean proton number given M, $\delta n = n - \mu_n$ and $P(n|M) = P(M, n)/P(M)$. We can evaluate the impact of rare detector-induced fluctuations from the truth probability distribution by separating out the contributions to μ_i from such fluctuations. We first expand the measured probability distribution $P(M, n)$

$$P(M, n) = (1 - \alpha) P(M, n)_{\text{truth}} + \alpha P(M, n)_{\text{fluc.}}, \tag{3.4}$$

where α is the fraction of events with detector-induced fluctuations.

Separating the probability in this way allows us to separate contributions to the moments

$$\mu_i = (1-\alpha)\bar{\mu}_i + \alpha\tilde{\mu}_i, \tag{3.5}$$

where $\bar{\mu}_i$ is the i^{th}-order moment of the truth probability distribution, and $\tilde{\mu}_i$ is the contribution to the measured moment μ_i from detector-induced fluctuations.

We aim to quantify how a detector-induced fluctuation that changes the measured proton number and multiplicity can distort high-order moments of the multiplicity bin in which it is measured. For simplicity, we consider an event with multiplicity M_0 and proton number $n = \mu_{n0}$ where μ_{n0} is the mean proton number at M_0. We take a fluctuation that changes its proton number to $\tilde{n} = \mu_{n0} + \Delta n$ and its multiplicity to $\widetilde{M} = M_0 + \Delta M$. These selections result in a fluctuation in a single bin, located at $(\widetilde{M}, \tilde{n})$, as pictured in Fig. 3.3 and represented by the probability distribution

$$P(M,n)_{\text{fluc.}} = \delta(M - \widetilde{M}, n - \tilde{n}). \tag{3.6}$$

The deviation from (M_0,μ_{n0}) has magnitude $\tilde{a} = \sqrt{(\Delta n)^2 + (\Delta M)^2}$ and angle $\tilde{\phi}$, such that $\tilde{n} = \mu_{n0} + \tilde{a}\sin\tilde{\phi}$. We refer to $\tilde{\phi}$ as the fluctuation angle. In these coordinates, the fluctuation is expressed as

$$P(M,n)_{\text{fluc.}} = \delta(M - \widetilde{M}, n - \mu_{n0} - \tilde{a}\sin\tilde{\phi}). \tag{3.7}$$

The contribution of this fluctuation to the i^{th} moment in the multiplicity bin $M = \widetilde{M}$ is then

$$\tilde{\mu}_i(M) = (\mu_{n0} + \tilde{a}\sin\tilde{\phi} - \mu_n)^i. \tag{3.8}$$

The mean of the proton-number distribution at multiplicity M occurs at (M, μ_n). Relative to (M_0, μ_{n0}), μ_n can be expressed as $\mu_n = \mu_{n0} + a\sin\phi$, where a is the distance between (μ_{M0}, μ_{n0}) and (M, μ_n), and ϕ is the angle between them. This angle between the mean

proton number at M_0 and the mean proton number at M is referred to as the mean angle. Now Eq. 3.8 becomes

$$\tilde{\mu}_i(M) = (\tilde{a}\sin\tilde{\phi} - a\sin\phi)^i. \tag{3.9}$$

Expressing a in terms of the other quantities, we arrive at

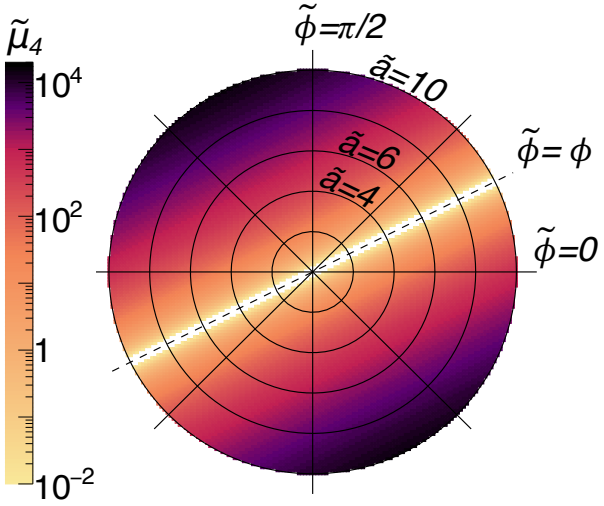

Figure 3.4: $\tilde{\mu}_4$ for a fluctuation with magnitude $\tilde{a}$ and angle $\tilde{\phi}$ embedded in a distribution of proton number as a function of multiplicity with mean angle ϕ.

$$\tilde{\mu}_i(M) \sim (\tilde{a}\sin\tilde{\phi} - \tilde{a}\cos\tilde{\phi}\tan\phi)^i. \tag{3.10}$$

When $\tilde{\phi} = 0$ the fluctuation is entirely in the multiplicity direction and $\tilde{\mu}_i(M) \sim (-a\sin\phi)^i = (-\tilde{a}\tan\phi)^i$. When $\tilde{\phi} = \pi/2$ then $a = 0$, and the fluctuation is entirely in the proton-number direction such that $\tilde{\mu}_i(M) \sim \tilde{a}^i$. When the fluctuation angle is equal to the mean angle, $\tilde{\phi} = \phi$, then $\tilde{a} = a$, and the contribution of the fluctuation to each moment vanishes. Thus, contributions from detector-induced fluctuations vanish when the correlation between proton number and multiplicity in the fluctuation matches the global correlation.

To visualize the effect on μ_4 of a fluctuation with magnitude $\tilde{a}$ and angle $\tilde{\phi}$, we plot, in Fig. 3.4, $\tilde{\mu}_4$ versus these two variables for some mean angle ϕ. Enhancements to high-order moments are minimized when the modification of proton number and multiplicity in an anomalous event maintains the same ratio of proton number to multiplicity as unmodified events. A detector-induced fluctuation can have a large effect on high-order moments if the ratio of proton number to multiplicity deviates from that of good events.

3.2 Detector Effects on Multiplicity Correlations

The detectors used for multiplicity and PID measurements define the fluctuation angle $\tilde{\phi}$. The nontrivial impact of detector efficiency on cumulants was treated in Ref. [41]. These efficiency considerations as well as the natural multiplicity and proton number define the mean angle ϕ. In addition to efficiency considerations, different detectors respond to certain classes of events in different ways. These discrepant responses to various event classes have the potential to cause cumulants of event-wise distributions to have large values that can be mistaken as a signal. To illustrate this point, we introduce two toy models of the measurement of proton-number cumulants:

1. fast and slow detectors in the presence of out-of-time pileup;

2. two detectors, one with stable and one with unstable acceptance.

These examples are illustrative of the problems that can arise from using different detectors for multiplicity and PID. Both of these examples use proton-number cumulants as a case study, but the conclusions are broadly applicable to measurements of other cumulants. These examples illustrate that enhanced fluctuations occur not simply due to the existence of pileup, acceptance fluctuations, or other anomalous events. These fluctuations are caused specifically by anomalous events detected with a mixed-detector approach. The

differing response of detectors to anomalous events changes the fluctuation angle and enhances high-order central moments and cumulants in datasets that would otherwise not show any anomalies.

3.2.1 Example 1: Pileup with fast and slow detectors

In Beam-Energy-Scan I, the STAR experiment used a Time-Projection Chamber for measuring the event-by-event multiplicity. TPCs are relatively slow detectors, as the measurable event rate is limited by the drift time of charged tracks. The STAR TPC has a drift time of 40 μs [34]. Time-of-flight detectors, on the other hand, use hundred-picosecond-scale timing resolution to identify particles. The resolution may be ≈ 100 ps, and TOF detectors typically remain live after a trigger for ≈ 10 ns.

With the slow drift time of TPCs, it is common for a second collision to occur while ionization from the first collision is still being collected. If tracks from this second collision are not separated from tracks from the first collision, the second collision is referred to as pileup. In accelerators such as RHIC and the LHC, radio-frequency (RF) oscillations in the electromagnetic field define discrete buckets in which ions can maintain closed orbits around the ring. Each of these buckets can be independently filled with ions or left empty. A filled bucket is referred to as a bunch.

Pileup can be categorized broadly as either in-time or out-of-time. In-time pileup occurs when there are multiple collisions within the same bunch crossing. The time elapsed between the two collisions is small. If we take a bunch length of roughly 1-10 m [42] traveling at close to c, then the time between collisions is on the order of 10 ns, so fast detectors like TOF and silicon trackers may measure particles from each collision. However hits from in-time pileup in a TOF detector will often have time-of-flight values that are skewed such that these hits are not identified with any particle. Out-of-time pileup happens when a collision from one

bunch crossing triggers the detectors, followed by a collision in a subsequent bunch crossing, while information from the first collision is still being collected. In a slow detector like a TPC, out-of-time pileup tracks may be counted as part of the triggered event. Fast detectors typically have short collection-time windows ($\approx$ 10 ns) following a trigger and do not detect out-of-time tracks. In the 3 GeV (2018) analysis, only every tenth bucket of the RHIC ring was filled. The RHIC clock in this dataset was 9 MHz [43], so each filled bucket arrived at the target every 1.1 μs. This left the TPC vulnerable to out-of-time pileup, whereas time-of-flight detectors were not.

In STAR's recent publication of proton cumulants at $\sqrt{s_{NN}} = 3$ GeV in the fixed-target program, the total pileup rate was 0.46% [44, 45]. Rather than reject pileup, an unfolding method was applied in order to correct for the effect of pileup on the cumulants [46, 47].

The unfolding method assumes that the detector has the same efficiency for pileup tracks, so that a pileup event is a simple sum of two individual events. This assumption starts to break down in the mixed-detector approach. When a fast detector like TOF is used for PID, much of the in-time and out-of-time pileup is sufficiently out-of-time that those pileup protons are not identified. However a slow detector like a TPC will include pileup tracks in the multiplicity. In the mixed-detector approach, many pileup events are seen as a single collision by a fast detector, and as a double collision by a slow detector.

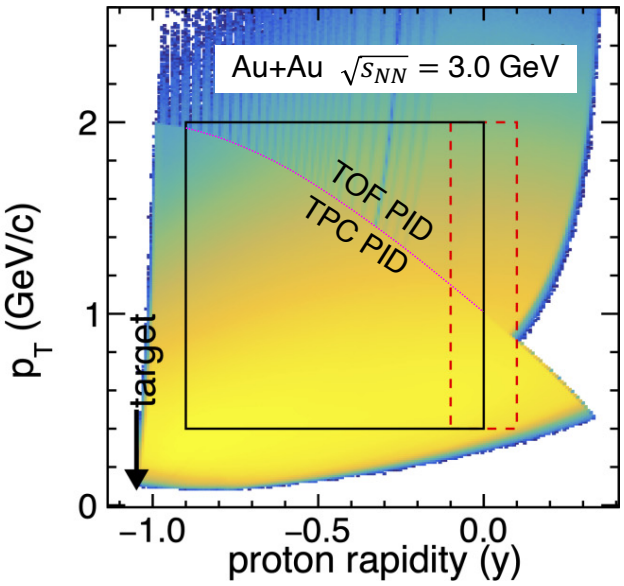

Figure 3.5: Analysis window used at $\sqrt{s_{NN}} = 3$ GeV from the STAR fixed-target program [44, 45].

In STAR's previous analyses of proton-number cumulants, protons are measured using both the TPC and TOF. Energy loss in the TPC is used to identify protons up to a given threshold momentum, above which TOF is used in order to maintain proton purity. The analysis window used at $\sqrt{s_{NN}} = 3$ GeV is shown in Fig. 3.5. For particles with momenta greater than 2 GeV, a hit in the TOF with a mass cut was required. When there is out-of-time pileup, the TPC measures the multiplicity as the sum of charged tracks from both collisions. Since both the TPC and TOF are used to identify protons, the proton number is made up of tracks above the momentum threshold from a single collision, and tracks below the momentum threshold from both collisions. These out-of-time pileup events will thus have an abnormally small number of protons, given their centrality as measured by the TPC.

If proton number and multiplicity measurements are both performed by a slow detector, then pileup tracks are counted in both. In this case, contributions to the cumulants from

pileup are suppressed due to the correlation between n and M. When pileup is observed in both numbers, the fluctuation angle matches the mean angle. Moreover, when n and M both contain pileup, the remaining contributions to the cumulants from pileup can be corrected by the unfolding method introduced in Refs. [46, 47].

If proton number is measured using a fast detector and multiplicity is measured by a slow detector, then out-of-time pileup will contribute to a long low-proton-number tail, which skews the high-order cumulants. Finally, if proton number is measured using a slow detector and multiplicity is measured by a fast detector, then out-of-time pileup will contribute to a long high-proton-number tail, which also skews high-order cumulants.

3.2.2 Example 2: Unstable acceptance

Another way to see the impact of the mixed-detector approach is to examine events in which one detector has an unstable acceptance and the other does not. For example, this can happen if one of the detectors is segmented into several active areas that independently reboot during a run. In a second example, acceptance can fluctuate if the algorithms used by a detector are prone to failure. Many time-of-flight detectors rely on a start-time algorithm to calculate exactly when each collision occurred. When that algorithm fails for some subset of events, then the efficiency for correct proton identification might fall or drop to zero within the TOF acceptance.

If an unstable detector is used to measure both PID and multiplicity, then events when the detector is partially or fully inactive have both reduced multiplicity, and fewer identifiable protons. In this case, the proton number scales with the reduced apparent centrality and the outlier events "blend in" with the bulk. If an unstable detector is used to identify protons while a separate stable detector measures centrality, then bad events can result in very central collisions with few identified protons. Finally if the stable detector identifies

protons but the unstable detector measures centrality, then central events will be sorted into more peripheral bins, resulting in high proton-number tails.

3.3 Numerical Analysis of Simulated Toy Models

In this section we introduce two toy models of detector response to UrQMD events in order to demonstrate the risks of a mixed-detector approach. Both toy models use 6.4×10^7 Au+Au collisions at $\sqrt{s_{NN}} = 3.9$ GeV from UrQMD in cascade mode. This energy was chosen because it corresponds to one of the datasets collected by the STAR experiment's fixed-target program. We use the same analysis window that was used in the analysis of the $\sqrt{s_{NN}} = 3$ GeV data: $0.4 < p_T < 2$ GeV/c and $-0.5 < y - y_{\rm cm} < 0$.

Multiplicity distributions from these simulated events are integrated to define centrality bins. The multiplicity was constructed to exclude protons in order to avoid autocorrelations. We simulate a realistic fixed-target acceptance by defining the multiplicity as all charged pions and kaons with $p_T > 0.06$ GeV/c, which, after boosting to the lab frame, have pseudorapidities of $0 < \eta < 2.15$.

The centrality bins used here are 0-5%, 5-10%, 10-20%, 20-30%, 30-40%, 40-50%, and 50-60%. The multiplicity distributions with and without pileup are shown in Fig. 3.6 along with the centrality cuts. Toy model 1 simulates the effects of pileup on the proton-number cumulants. In order to replicate experimental conditions, the pileup cut on multiplicity shown in Fig. 3.6, is used to reduce pileup contributions. Centrality cuts defined by integrating the red and black distributions (with and without pileup) were equivalent.

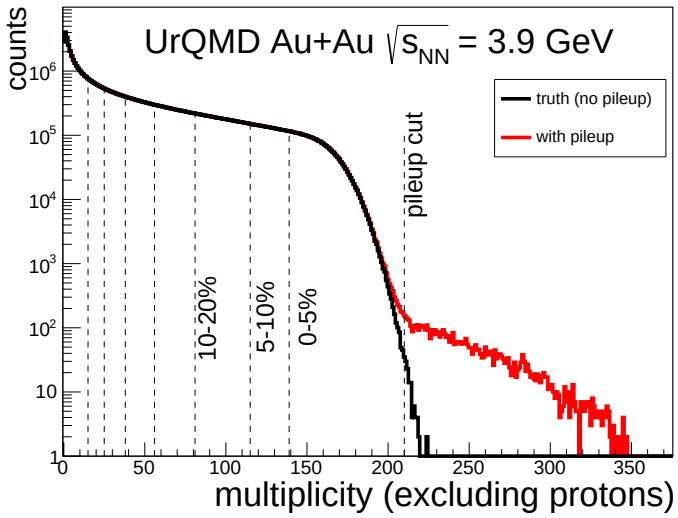

Figure 3.6: Multiplicity distributions excluding protons with and without pileup tracks. Centrality cuts are shown as dashed lines up to 60% centrality, including a pileup cut at the upper edge of the 0-5% bin.

In the coming sections we label plots with AA, AB, BA, and BB. The A label represents a truth measurement, and the B label represents an anomalous measurement. When two of these are used together to label a plot, the first letter represents whether the centrality measurement was anomalous, and the second letter represents whether the proton measurement was anomalous. So AA indicates that the measurement was free of anomalies. AB represents a true centrality measurement, but a proton measurement with anomalies. BA represents a centrality measurement with anomalies and a true proton measurement. BB indicates that both measurements had anomalies.

3.3.1 Toy model 1: out-of-time pileup

In the first toy model, out-of-time pileup was simulated by sampling two collisions in 0.2% of events. We simulate the responses of a fast and a slow detector to this pileup. Fast and

slow toy detectors have 100% efficiency for in-time collisions. For out-of-time pileup, the slow detector has 100% efficiency, while the fast detector has 0% efficiency.

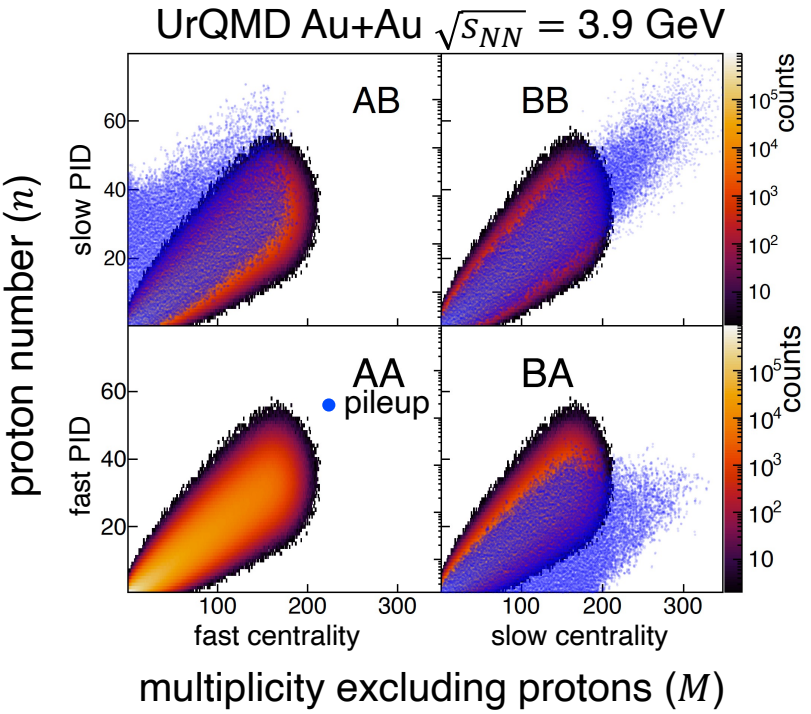

Figure 3.7: Distribution of detected proton number (n) versus multiplicity (M) for the four fast-slow detector combinations where the pileup events are shown in blue. The pileup rate is 0.2%.

The correlation between proton number and multiplicity in UrQMD events is shown in Fig. 3.7. In panel AA, the fast detector is used to measure both protons and multiplicity so no pileup tracks are included in the track sums. In panel BB, the slow detector is used to measure everything, so that pileup events have both a high proton number and a high multiplicity. Panel AB relies on the fast detector to measure multiplicity and the slow detector to measure protons, leading to many events with an abnormally large proton number given their multiplicity. Panel BA shows the use of the slow detector to measure multiplicity and

the fast detector to measure protons, so the pileup events often have too few identified protons for their multiplicity. The decorrelation between proton number and multiplicity in panels AB and BA contributes to large signals in the proton-number cumulants in these mixed-detector approaches. The correlation in panel BB suppresses the impact of pileup on the cumulants. This is quantified in Sec. 3.4.

3.3.2 Toy model 2: Unstable acceptance

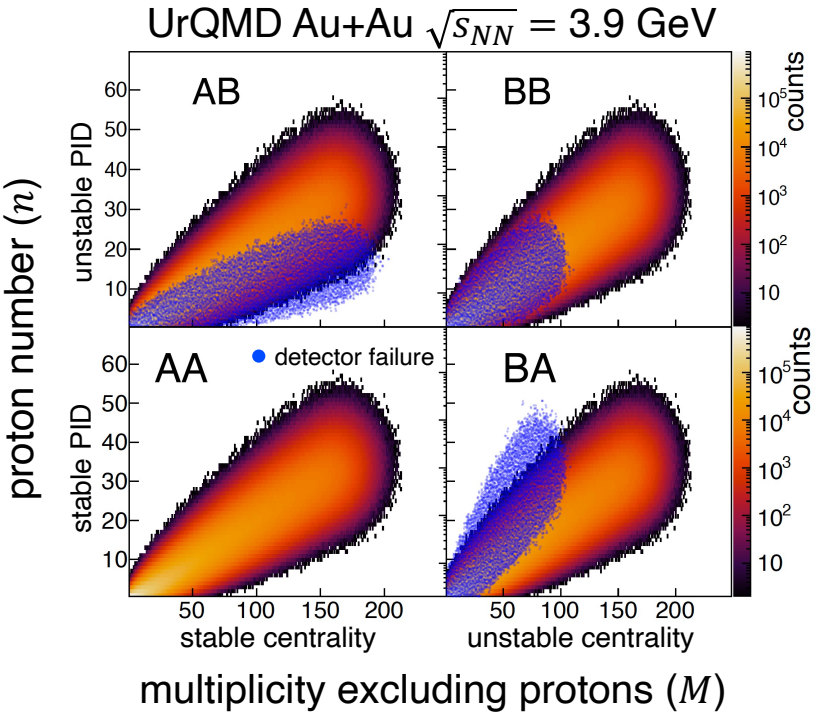

Figure 3.8: Distribution of detected proton number versus multiplicity for the four unstable-stable detector combinations. The 1% of events in which the unstable detector was half-dead are shown in blue.

The second model demonstrates the effect of a detector with unstable acceptance. In this scenario two detectors are again used in tandem to measure the proton number and multi-

plicity, however one of the detectors is unstable. For 1% of events, in half of the azimuthal acceptance, the unstable detector does not detect anything, while the other half is always active. The stable detector is always 100% active.

The correlation between proton number and multiplicity in this second toy model is shown in Fig. 3.8. In panel AA, the stable detector is used to measure both protons and multiplicity so we measure the true proton number versus multiplicity. In panel BB, the unstable detector is used to measure both, so that in the 1% of events in which the unstable detector fails, both proton number and multiplicity are reduced by half. The fluctuation angle matches the mean angle; thus the unstable events do not stand out from the true distribution.

In panels AB and BA, only one of the two measurements is susceptible to the acceptance fluctuations. When taking vertical slices at a given multiplicity, this results in proton-number tails on either side of the true distributions. The impact of these tails on the cumulants is quantified in Sec. 3.4.

3.4 Results of Simulations

In this section, we evaluate the cumulants of the proton-number distributions produced in the toy models described above.

3.4.1 Toy model 1: out-of-time pileup

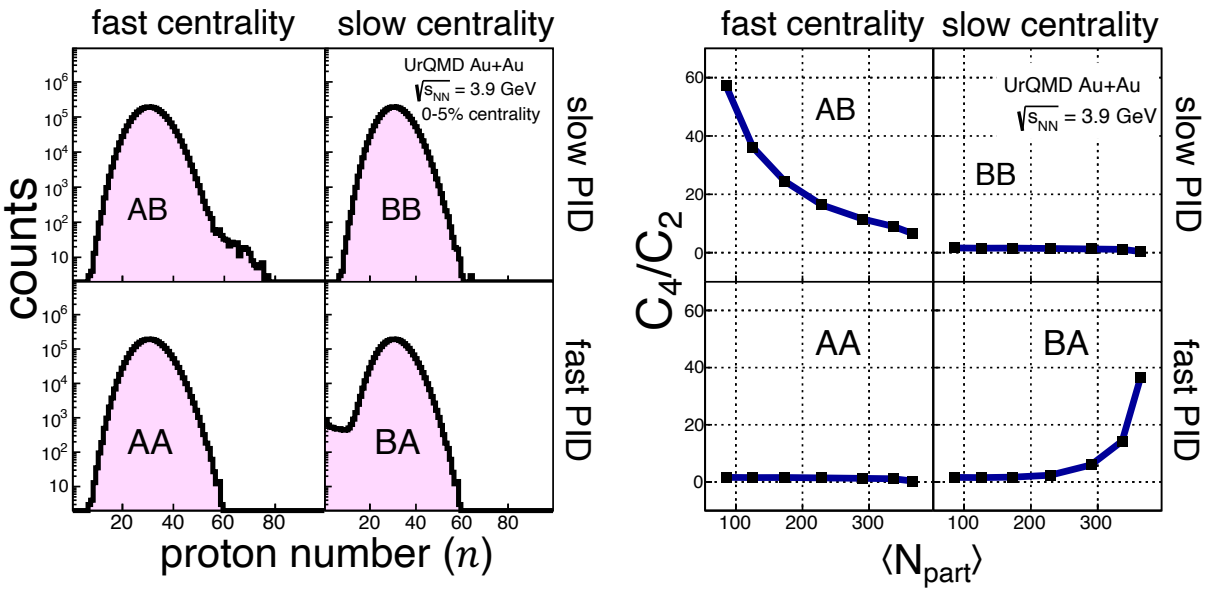

Figure 3.9: (left) Distribution of proton number in the 0-5% centrality bin with a 0.2% out-of-time pileup rate for all four combinations of fast-slow detector combinations. (right) C_4/C_2 as a function of centrality (plotted as $\langle N_{\rm part} \rangle$) for each fast-slow detection method.

The left-hand side of Fig. 3.9 shows proton-number distributions in the toy model in the 0-5% centrality bin as defined by cuts in multiplicity. The right-hand side shows the resulting C_4/C_2 from 0% to 60% centrality. Both are plotted as a function of the average number of participants $\langle N_{\rm part} \rangle$.

Figure 3.9, left sub-figure, lower-left panel, shows the proton-number distribution for the AA event class, those with no out-of-time pileup effect in the 0-5% centrality bin. In the toy model, this is identical to the true (single collision) distribution and results in values of C_4/C_2 as a function of centrality near 0 (right sub-figure, lower-left panel AA). Left sub-figure, upper-right panel BB shows the proton-number distribution when both the multiplicity and the proton number are enhanced by pileup. Tails on the proton-number distribution are

suppressed because the fluctuation angle is identical to the mean angle. High-order cumulants in panel BB are distorted by pileup, but these effects are minimal and can be corrected using the unfolding approach introduced in Ref. [46, 47]. These corrections assume that pileup events can be expressed as a superposition of two events, an assumption that is often invalid in the mixed-detector approach.

Figure 3.9, left sub-figure, lower-right panel BA shows the distribution when events with pileup-enhanced multiplicity do not have similarly enhanced proton numbers. In this case, pileup of two-midcentral collisions may be classified as a single central collision, but the fast detector identifies protons from only one of these collisions. This leads to a long low-proton-number tail.

Panels BB and BA are two extremes of the options for PID. It is often the case that PID is performed using several detectors. In previous STAR analyses, PID was performed with a TPC for low momenta particles, and additionally required TOF for high-momenta particles [44, 45, 48]. A more representative distribution would be intermediate between panels BB and BA (left). In the past, pileup was then corrected, assuming the distribution in panel BB (left). This is problematic due to potentially large contributions to the proton-number tails caused by TOF identification. Pileup events are no longer a simple sum of two single collisions, and the standard pileup correction [46, 47] should not be used.

It is tempting to suggest that enhanced multiplicity from pileup could be rectified by using a fast detector to measure multiplicity, shown in panels AA and AB (left). However, if a slow detector is used to measure proton number, as in panel AB, the result can be pileup events registering a low multiplicity and a high proton-number tail. It is often the case that both a fast and slow detector are used to identify protons. In this case, measuring multiplicity with a fast detector will result in something between AA and AB (Fig. 3.9, left sub-figure, leftmost two panels).

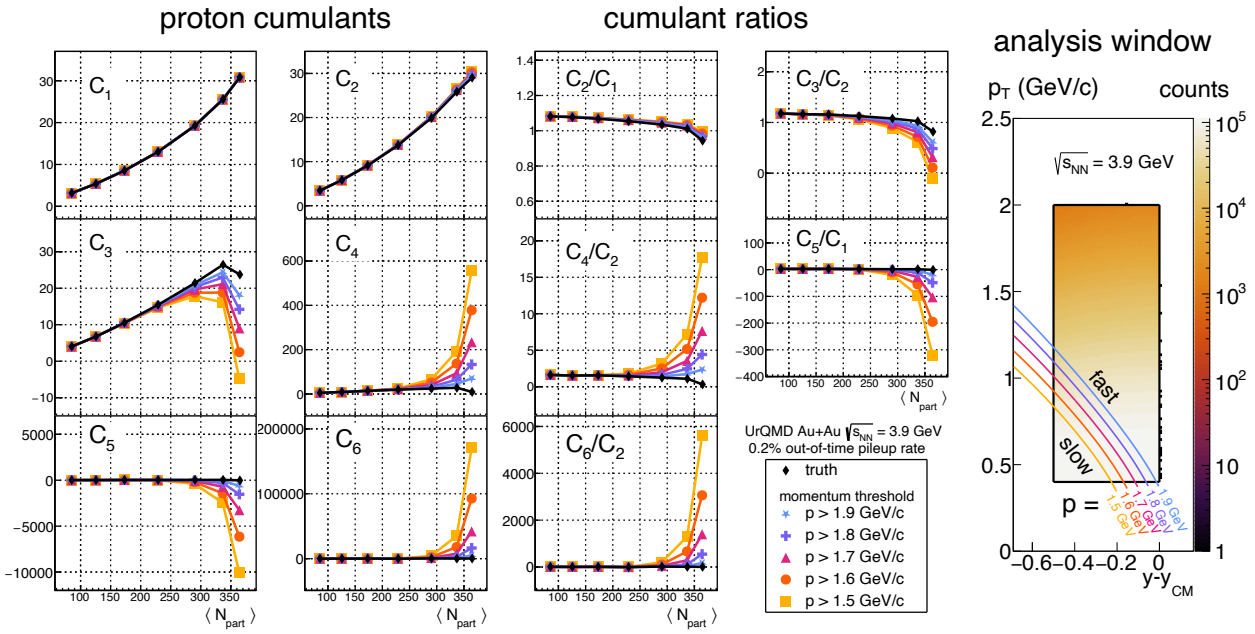

Figure 3.10: (left) Proton-number cumulants and cumulant ratios at $\sqrt{s_{NN}} = 3.9$ GeV with varying momentum thresholds for requiring a fast detector for PID, and using a 0.2% out-of-time pileup rate. High-order cumulants experience instability as the momentum threshold changes. (right) Analysis window with the various momentum thresholds.

To simulate a more realistic detector environment we next examined the effect of using a slow detector to measure low-momentum protons, and a fast detector for high-momentum protons. In this model, a slow detector measures the multiplicity. We choose five different momentum thresholds above which we require a fast detector for PID. The thresholds, p =1.5, 1.6, 1.7, 1.8, and 1.9 GeV/c, are shown on the right side of Fig. 3.10. The cumulants and cumulant ratios for each of these momentum thresholds are displayed on the left side of Fig. 3.10. For C_3 and above, the cumulants are unstable and have strong dependence on the chosen momentum threshold. Counter to conventional wisdom, the cumulants approach their true values (shown in black) when more pileup is allowed in the proton analysis window. This is because increasing pileup in the analysis window corresponds to the fluctuation angle

approaching the mean angle (as in Fig. 3.7, from panel BA to BB).

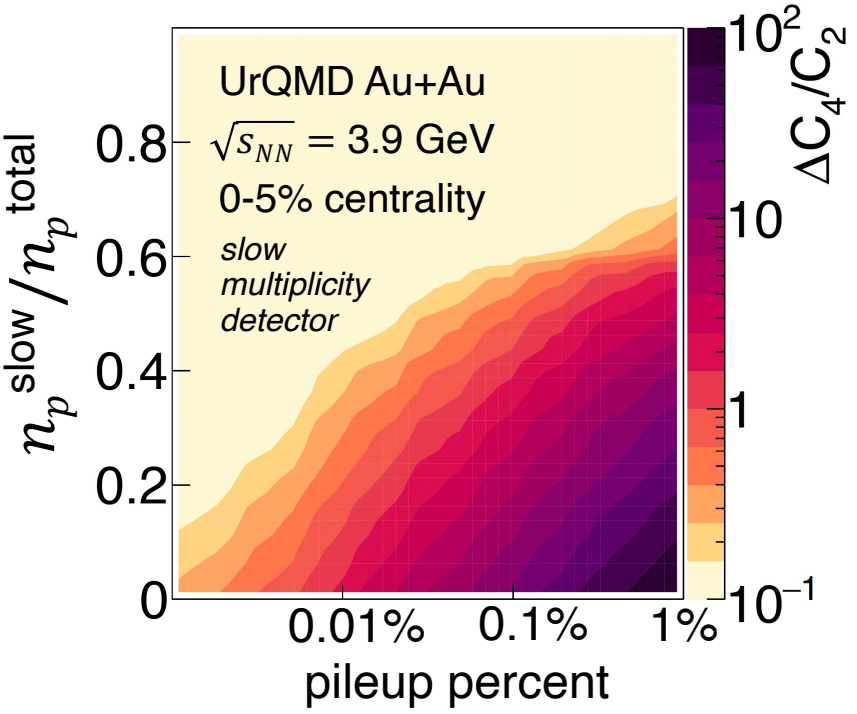

Figure 3.11: Difference between true and measured C_4/C_2 with several pileup rates and slow-detector acceptance fractions when using a slow detector to measure the multiplicity. The axis $n_p^{\text{slow}}/n_p^{\text{total}}$ indicates the fraction of protons identified by the slow detector.

We also investigated the pileup-rate dependence of the measured kurtosis. Scanning pileup rates from 0.001% to 1%, we simulated various momentum thresholds above which a fast detector was used for proton identification. For each momentum threshold we calculated the fraction of protons identified by the slow detector. The enhancement of C_4/C_2 for each slow-acceptance fraction and each pileup rate is plotted in Fig. 3.11. We find that up to a 1% pileup fraction, using the slow-detector to identify 70% of protons results in no significant enhancement of C_4/C_2. When the slow detector is not used for PID, the enhancement in the measured C_4/C_2 reaches $\approx 10^2$.

3.4.2 Toy model 2: Unstable acceptance

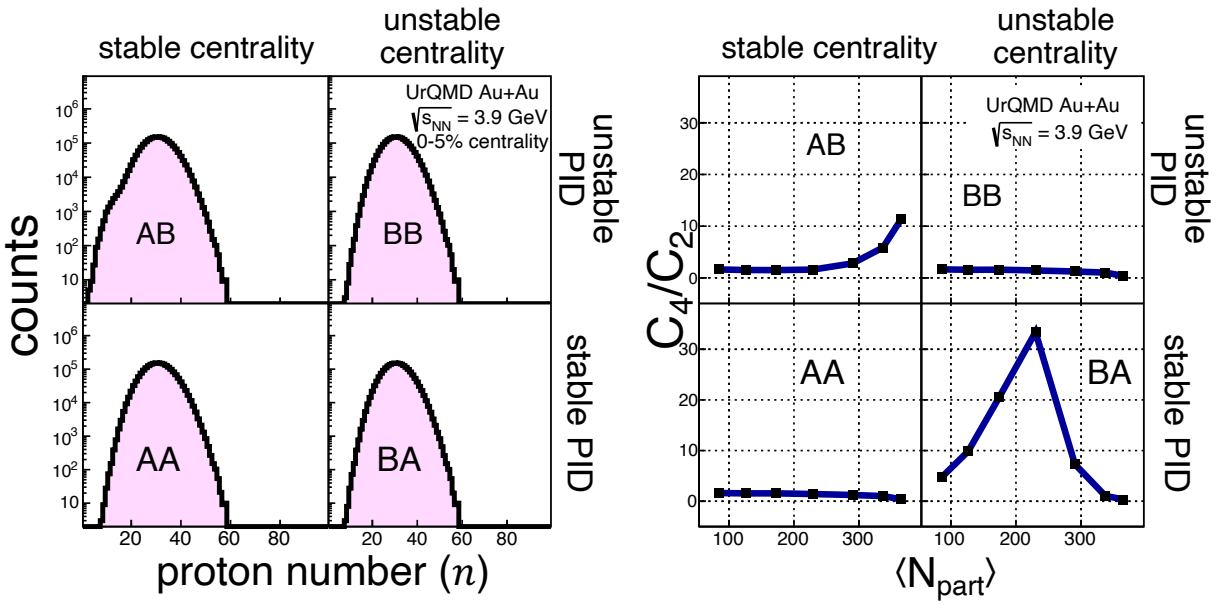

Figure 3.12: (left) Distribution of proton number in the 0-5% centrality bin when the stable and unstable detectors each were used to measure proton number and centrality. (right) C_4/C_2 in each centrality bin plotted as a function of $\langle N_{\rm part} \rangle$ for each stable-unstable detector combination.

The left-hand side of Fig. 3.12 shows the distribution of protons for 0-5% centrality when the stable and unstable detectors are used to measure centrality and proton number. Panel AA is the true distribution and BB exhibits no obvious modification. Panel BA is not modified because the events in which the centrality detector was unstable were shifted out of the 0-5% centrality bin and into more peripheral bins (see Fig. 3.8). Panel AB has a tail from the spontaneous failure of the proton-number measurement. Although panel BA (left) for the 0-5% centrality is unmodified, we can see from the right-hand side of Fig. 3.12 that there is significant modification of C_4/C_2 for 10-60%.

On the right-hand side of Fig. 3.12, panel BB does not exhibit strong deviations from AA

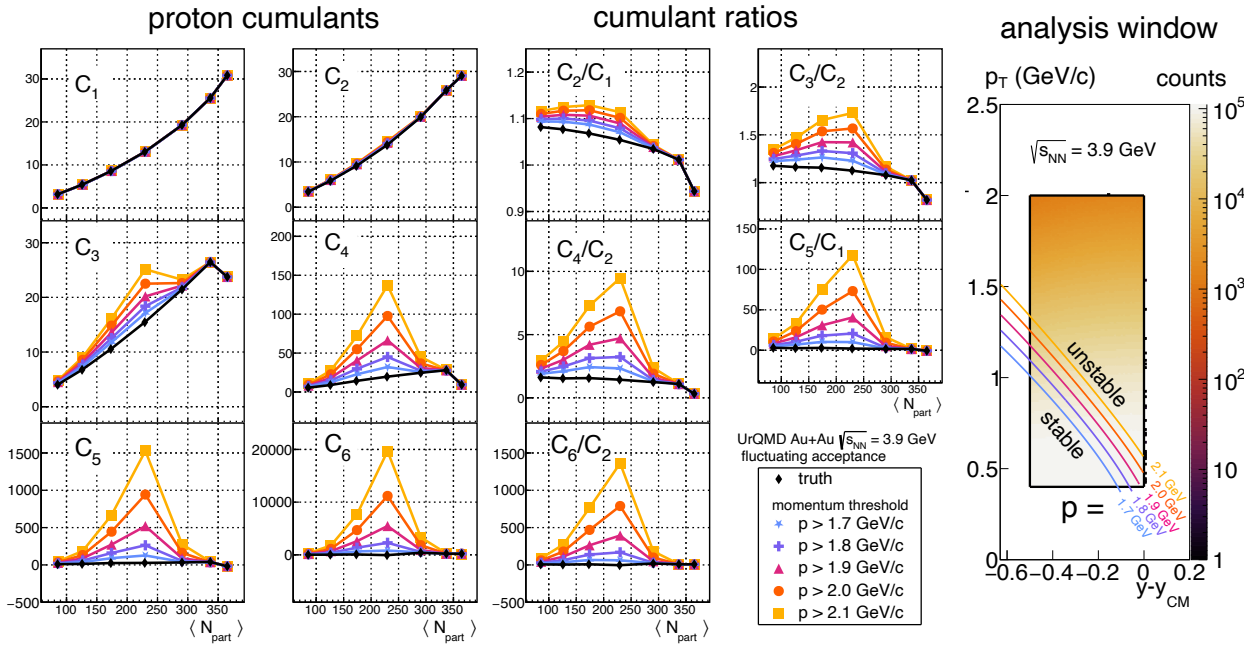

Figure 3.13: (left) Proton-number cumulants and cumulant ratios at $\sqrt{s_{NN}} = 3.9$ GeV with varying momentum thresholds for requiring an unstable detector for PID. High-order cumulants are unstable as the momentum threshold changes. (right) Proton analysis window with momentum thresholds superimposed.

at any centrality. Panel AB has a centrality dependence similar to Panel BA of Fig. 3.9 from model 1. This is because the low-proton-number tail is more pronounced at large centralities in both models. Panel BA on the right of Fig. 3.12 has very different behavior. The C_4/C_2 is unchanged for central collisions, but it exhibits a steep rise with falling centrality until it reaches a maximum deviation in the 20-30% centrality bin, and then drops again. This can be understood from panel BA in Fig. 3.8 because all the anomalous events are shifted away from the most central multiplicities. The sudden drop in efficiency for the multiplicity detection results in the categorization of many central events as mid-central, and yet they have too many protons. This leads to a long high-proton-number tail for mid-central collisions and a correspondingly-large C_4/C_2.

We now examine a more realistic detector scenario in which one detector is used for proton measurements below a certain momentum threshold and another is used above the threshold. For our proton measurements, we use the unstable detector above the momentum threshold, and the stable detector below the momentum threshold.

The analysis window with various momentum thresholds is shown on the right side of Fig. 3.13. We choose in this example to use the unstable detector for the multiplicity measurement. The cumulants and cumulant ratios are on the left side of the figure. As the momentum threshold increases, the cumulants experience greater and greater enhancement. In other words, the more the unstable detector is used, the better our measurement gets. This result again underscores a counter-intuitive conclusion: acceptance fluctuations have the greatest impact on the measured cumulants when not reflected equally in the proton-number and multiplicity.

Figure 3.14 plots the enhancement of C_4/C_2 as a function of the detector failure rate and the fraction of protons measured by the unstable detector. The enhancement in C_4/C_2 in Fig. 3.13 is greatest in the 20-30% centrality bin, so Fig. 3.14 is chosen to plot the C_4/C_2 at this centrality. In these simulations, the unstable detector is used to define centrality. We observe in this model that when an unstable detector measures multiplicity, it is beneficial to also maximize the amount of protons identified by the same unstable detector. The enhancement of C_4/C_2 in Fig. 3.14 with various rates of detector failure is model dependent. This simulation describes a detector which spontaneously loses half of its acceptance in azimuth. The map in Fig. 3.14 is specific to this model of detector failure and does not broadly describe fluctuations in detector acceptance. This is not reflective of actual detector failure patterns, and is used for illustrative purposes because it is a large-scale fluctuation that affects all rapidities equally.

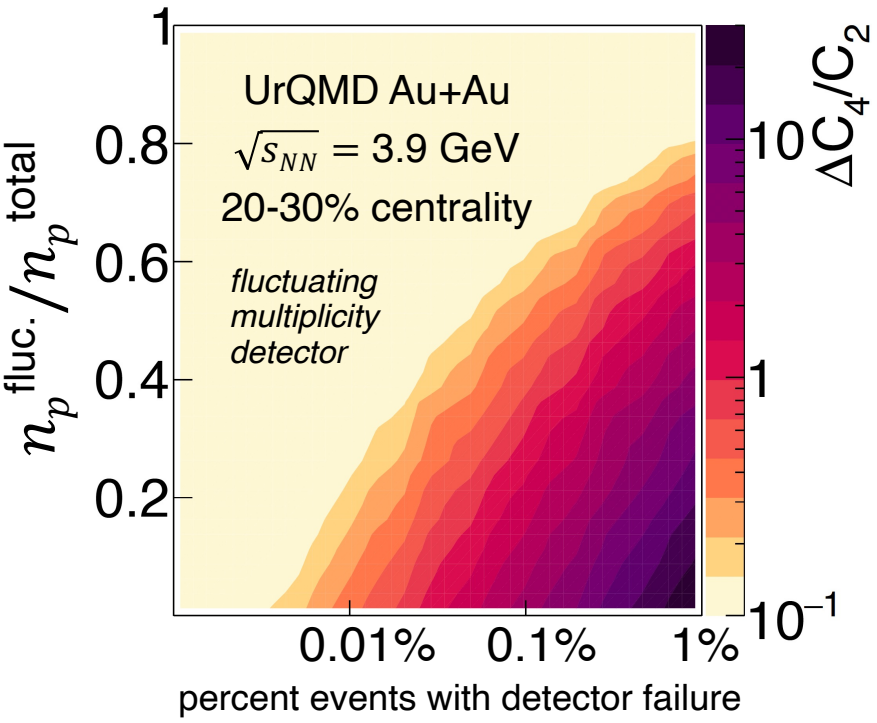

Figure 3.14: Difference between true and measured C_4/C_2 for 20-30% central collisions with several detector failure rates when using a fluctuating detector for centrality. The axis $n_p^{\text{fluc.}}/n_p^{\text{total}}$ indicates the fraction of protons identified by the fluctuating detector.

3.5 Conclusions from Simulation Studies

In previous measurements of cumulants, mixed-detector approaches were used to identify particles and multiplicity [44, 45, 48–55]. We demonstrated the risks associated with using different detectors to measure PID and centrality. Issues with the mixed-detector approach can be used to explain why the recent errata [56–58] correcting the proton cumulants at $\sqrt{s_{NN}} = 54.4$ GeV were necessary, and likely affect Refs. [44, 45] as well, because pileup was not rejected in these analyses. The mixed-detector approach enhances the vulnerability of analyses to detector effects, because spontaneous decorrelation between detector responses can cause large high-order cumulants. Pileup corrections to high-order cumulants, which

assume that pileup is a superposition of two events, are often invalid in the mixed-detector approach. Attempting to correct for pileup instead of removing it may allow enhanced cumulants to masquerade as a signal, even for moderate out-of-time pileup rates.

Spontaneous failure of one detector in a mixed-detector approach, if not carefully removed, will cause fluctuations. The same is true for spontaneous reductions in acceptance, as occurs when detector subsystems reboot during data-taking. This risk is minimized by using the same detector for centrality and PID.

We do not suggest that the mixed-detector approach should never be used. It is often necessary to use multiple detectors in fluctuations analyses in order to maintain a high proton purity. We emphasize that the mixed-detector approach enhances the vulnerability of analyses to detector effects. Rigorous quality assurance of data is necessary when using multiple detectors to measure high-order cumulants, including aggressive removal of out-of-time pileup. Rare detector failures should be understood and minimized when they do not affect both the multiplicity and PID measurements equally. When detector performance depends on event-by-event algorithms, it is necessary to check, event-by-event, that the detector is performing as expected.

Particle identification using multiple detectors is often necessary. When multiple detectors overlap in phase space, one can check the stability of cumulants with respect to how much of each detector is used. When TOF is used for PID for particles above a certain momentum, as in Refs. [44, 45, 48], analyzers may vary the momentum threshold in order to verify the stability of results, as was simulated in the toy models and shown in Figs. 3.10 and 3.13. The instability of higher-order cumulants can signal that detector-induced fluctuations are present.

How not to measure a false QCD critical point

The striking realization from the models shown here is that it is fairly easy to measure a false critical point signature. To be vulnerable to a false signature, an analyzer just needs two ingredients:

1. Multiplicity and proton number measurements with different detectors;

2. Uncorrelated responses of the two detectors to a small subset of events.

As long as these two things are present, an analysis has a high risk of measuring enhanced high-order moments. A large spike in kurtosis at $\sqrt{s_{NN}}$=3.9 GeV, as seen in Fig. 3.10, would be interpreted as an exciting confirmation of the predicted behavior of the fourth-order moment near a critical point [59] and of the predicted location of a critical point [60–65].

The other striking conclusion from these studies is that it is also fairly easy to make a signal that is robust against detector-induced fluctuations. In order to measure a robust signal, an analyzer just needs to follow one guideline:

1. Make the multiplicity and proton-number measurements as similar as possible.

Analyzers should maximize the degree to which both measurements are performed by the same detector. They should understand any effects which may cause the correlation between proton number and multiplicity to change. Analyzers should aim for anomalous events to have the same effect on the measured proton number as they do on multiplicity. Otherwise, those rare and spontaneous changes in the correlation between proton number and multiplicity will become the entire measurement.

3.6 What Happened at 3 GeV?

The $\sqrt{s_{NN}} = 3$ GeV (2018) proton high-moments results were the first to be published from the fixed-target program. The value of C_4/C_2 at 3 GeV is compared with collider datasets in Fig. 1.5. The 3 GeV point has a much larger systematic uncertainty than every other point in that figure. Despite this large uncertainty, the value is remarkably close to the value predicted by UrQMD, shown as a tan cross. This combination of a huge uncertainty and excellent agreement with the model is enough to raise eyebrows about the systematics. It seems plausible that the systematic uncertainty could have been overestimated. If every subsequent fixed-target measurement had similarly large systematic uncertainties, it could be difficult to make any significant statement about the results. I explain in this section the likely cause of the large systematic uncertainty at $\sqrt{s_{NN}} = 3$ GeV, and how to reduce these uncertainties in the other datasets.

3.6.1 Out-of-bucket Pileup

In the 3 GeV (2018) analysis, a DCA cut of 3 cm was applied in order to reject pileup tracks from out-of-time vertices. Standard operation while collecting data for the fixed-target program was for RHIC to only fill every tenth bucket. The RHIC clock in this dataset was 9 MHz [43], so each filled bucket comes every 1.1 μs. The drift velocity of STAR's Time-Projection Chamber is 5.5 cm/μs. This means that tracks from out-of-time vertices will appear shifted in the TPC by 5 cm. One might expect then that pileup tracks from out-of-time vertices are rejected by the DCA<3 cm cut. The problem with this is shown in Fig. 3.15. High-rapidity tracks that appear to originate 5 cm away from the primary vertex will nevertheless approach the primary vertex at a distance of less than 3 cm.

These high-rapidity tracks are not expected to cause a large distortion of the high moments because both the multiplicity measurement and the proton-number measurement re-

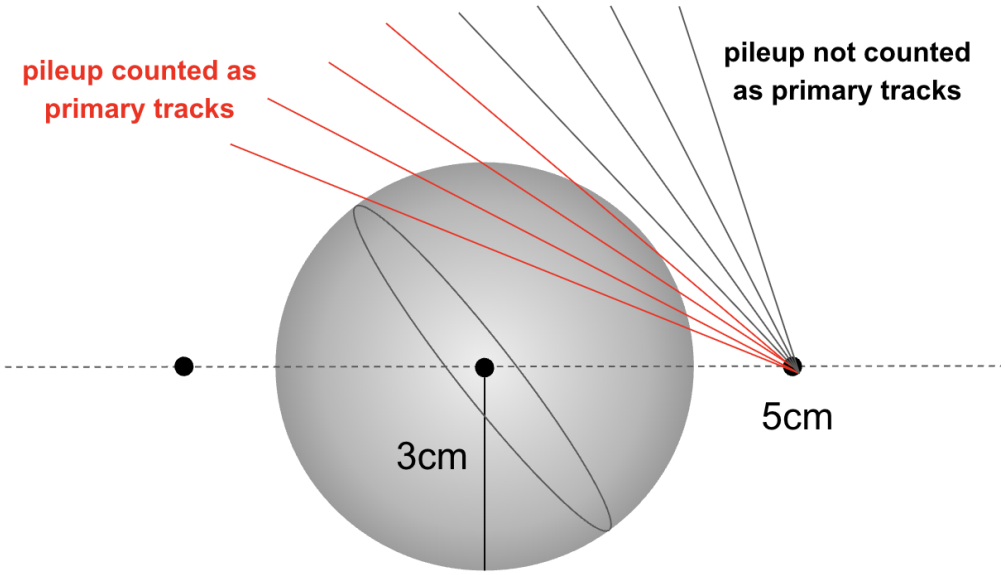

Figure 3.15: Sphere showing a DCA cut of 3 cm, as well as the apparent location of pileup tracks from an out-of-time vertex. High-rapidity out-of-time pileup tracks will satisfy a DCA<3 cm cut.

quire DCA<3 cm. The problem comes when an analyzer performs the calculation of systematic uncertainties. In the study of systematics in the 3 GeV (2018) analysis, the DCA cut was varied to check the stability of the high moments, but it was varied only in the proton-number measurement, not simultaneously the multiplicity measurement. So with a tighter DCA cut on protons, pileup from the next filled bucket would tend to cause rare and spontaneous enhancements of multiplicity. These rare events would be sorted into abnormally large multiplicity bins, and not have a similar enhancement in proton number.

Chapter 4

How to Quantify Nonmonotonicity

In Beam Energy Scan I, STAR measured the net-proton high-order cumulants as a function of the collision energy. In a 2021 analysis of the data, STAR claimed evidence of a nonmonotonic energy dependence of C_4/C_2, at a significance of 3.1σ [50]. During the analysis of STAR's Beam Energy Scan II results, it became clear that the methods used to determine significance in that 2021 analysis were flawed. This chapter discusses the issues with that analysis and how to correctly quantify the significance of nonmonotonicity.

4.1 Evidence of nonmonotonicity

Nonmonotonic energy dependence of high-order proton-number cumulant ratios was proposed as a critical point signature [66, 67]. In a 2021 analysis of STAR's Beam Energy Scan I net-proton high moments [50], the skewness and kurtosis at 8 Au+Au collision energies were fit with high-order polynomials. The results of these fits are shown in Fig. 4.1. Then each of the 8 data points was varied 1 million times according to a normal distribution centered on the point location with width equal to the uncertainty. For each of these 1 million resamplings of the data, fourth and fifth-order polynomials were again used to fit the data.

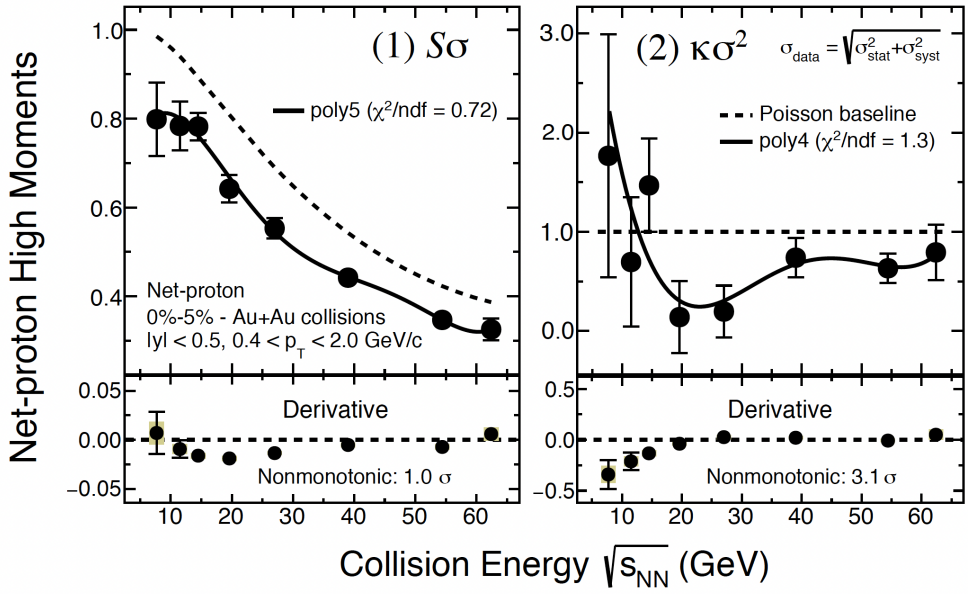

Figure 4.1: Polynomial fits to cumulant ratios from Beam Energy Scan I [50]. These fits were used to quantify the significance of nonmonotonicity.

A single sampling was determined to be monotonic if, at each data point, the slope of the polynomial fit had the same sign as at every other point. The ratio of monotonic fits to all fits was calculated. Then the significance of nonmonotonicity was determined by calculating the norm quantile corresponding to that probability of a monotonic fit.

4.2 Testing the BES-I Methodology

The use of fourth and fifth-order polynomials to fit 8 data points appeared to me to not be well motivated; there is no physical motivation to use a polynomial for these fits. More importantly, the methodology is concerning because fourth and fifth-order polynomials are almost always nonmonotonic and are thus not good benchmarks for determining whether data are monotonic or not. If the data one is fitting with these polynomials have large

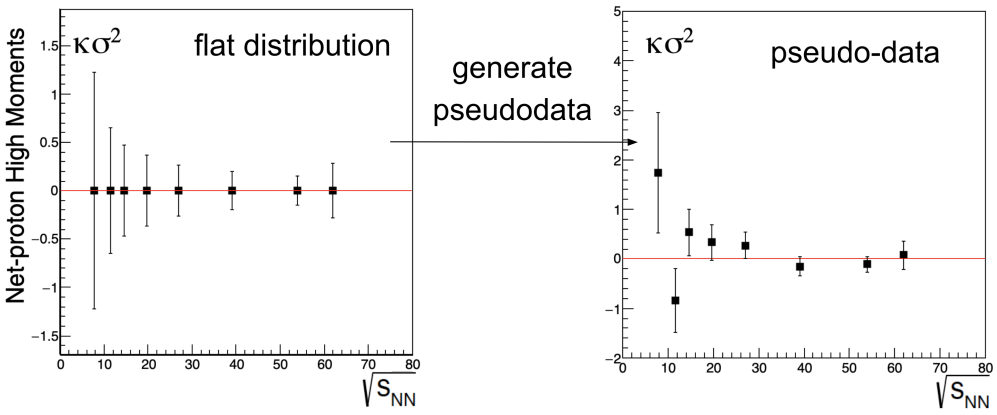

Figure 4.2: Example of generating pseudodata from a flat distribution.

uncertainties and a weak energy dependence, then the method could result in polynomials over-fitting random fluctuations and inflating the significance.

In order to test this hypothesis that the high-order polynomial fitting method inflates the significance, I applied the method to pseudodata generated from a flat distribution. I took 8 data points with the same error bars and spacing along the x axis as the $\kappa\sigma^2$ results from BES-I, and I set the y values each to 0. I then resampled each of the points according to normal probability distributions centered on 0 with standard deviations equal to the uncertainties on each point. This is shown in Fig. 4.2, where the right side of the figure shows one example of the 8 pseudodata points that can be generated from the flat distribution.

I generated several thousand pseudodata sets and for each of these samples, I ran the significance determination procedure on the sample. As a cross-check, I also determined the significance with a null-hypothesis test. In this test, I fit the pseudodata with a constant to generate a χ^2/ndf, then calculated the probability value (p value) from the χ^2 and degrees of freedom. For each p value, the norm quantile was calculated, and this value was taken as the significance that the pseudodata is not well described by a flat distribution. This is not the

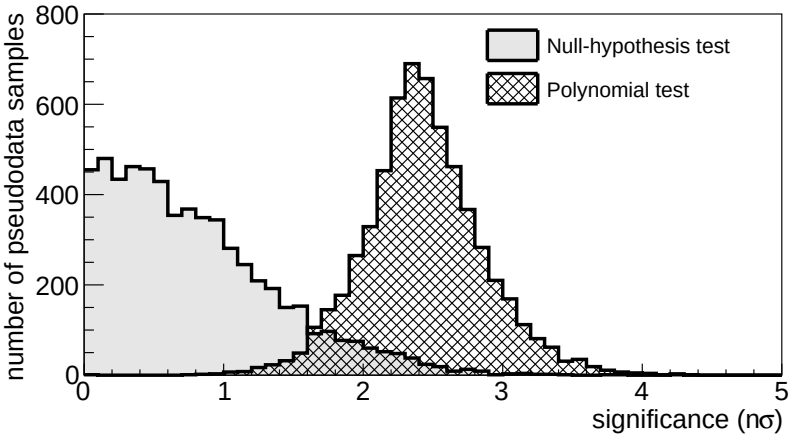

Figure 4.3: Comparison of nonmonotonicity significance estimation on flatly-distributed pseudodata. The method used in the BES-I analysis [50] inflates the most likely significance by $\approx 2.4\sigma$.

same as the significance of nonmonotonicity, but it is an upper limit on it. If the data only deviates from a constant at a significance of 2σ, then it cannot be said that the significance that the data is nonmonotonic is greater than 2σ. The results of these two methods are shown in Fig. 4.3. While the null-hypothesis testing gives a normally-distributed significance, the fourth-order polynomial method inflates the significance of this flatly-distributed pseudodata by $\approx 2.4\sigma$. This polynomial method over-fits random fluctuations and is not reflective of the nonmonotonicity of the data.

4.3 Null-Hypothesis Testing

Instead of using high-order polynomials to over-fit the data, it is standard in analyses like these to use the kind of null-hypothesis testing described above. In this method, the significance of nonmonotonicity means "the significance with which the data cannot be described by a monotonic function." In this approach, it is the analyzer's job to see if the data are well

described by any monotonic functions. The significance with which the data deviates from any one of these can be taken as an upper bound on the significance of nonmonotonicity. So the analyzer should attempt to find the fit with the smallest significance in order to place the tightest upper bound. For the case of the BES-I kurtosis result, the data are well-fit by a constant (or poly0). The fit result yields $y = 0.63 \pm 0.09$ with $\chi^2 = 9.3$ and ndf $= 7$. This gives a $\chi^2/\text{ndf} = 1.3$ and a significance of 1.2σ. This fit is shown in Fig. 4.4. The BES-I $\kappa\sigma^2$ result [50] is well-fit with a constant. The data are statistically indistinguishable from a flat distribution. This suggests that fitting these 8 data points with a five-parameter function is not necessary. The significance of nonmonotonicity of $\kappa\sigma^2$ from BES-I is no greater than 1.2σ, far from the evidence of nonmonotonicity that was claimed in Ref. [50]. The demonstration discussed here convinced STAR not to repeat this method in the Beam Energy Scan II analysis. To date, no action has been taken by STAR to correct the published significance from BES-I.

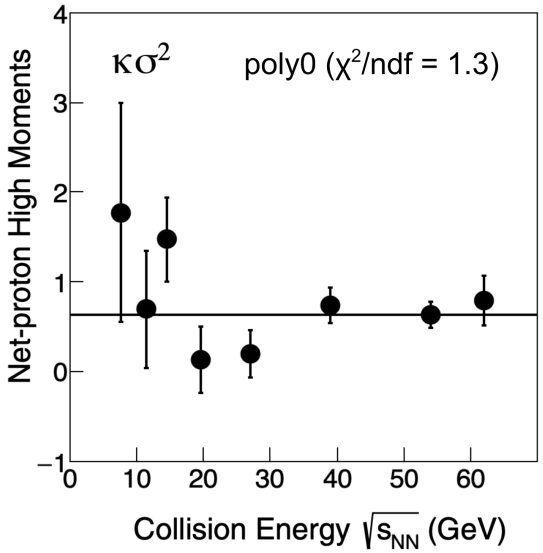

Figure 4.4: Fit of BES-I $\kappa\sigma^2$ energy dependence [50] with a constant.

Chapter 5

Data Selection

This chapter describes how events were selected to be used in the analysis. Once the best events are selected, various track-quality cuts are implemented in order to ensure that only those well identified tracks are used in the analysis. Finally, events are sorted based on the multiplicity of charged tracks into centrality bins. That centrality selection procedure is described here as well. In 2019, 277 million Au+Au minimum-bias-triggered events triggered the data acquisition and were collected at $\sqrt{s_{NN}} = 3.2$ GeV. In 2020, 152 million Au+Au events were collected at $\sqrt{s_{NN}} = 3.5$ GeV, 159 million events were collected at $\sqrt{s_{NN}} = 3.9$ GeV, and 189 million Au+Au events were collected at $\sqrt{s_{NN}} = 4.5$ GeV.

Event-selection in the fixed-target proton high-moments analysis was done in two stages. In the primary event selection described in Sec. 5.1, events were chosen to satisfy STAR's minimum-bias triggers, and further selected to have reconstructed vertices close to the beam spot. Following this first round of event selection, track-level particle identification calibrations were performed based on energy loss in the time-projection chamber. These calibrations and track-level cuts are described in Sec. 5.2. Then a secondary stage of event-selection is performed as described in Sec. 5.3. This secondary stage involves centrality classification, in-bucket and out-of-bucket pileup removal, and TOF performance quality cuts.

5.1 Primary Event Selection

5.1.1 Trigger Selection

The first event-selection cut used is the trigger selection. Minimum-bias triggers were used at each energy in order to minimize the inefficiency associated with triggering the STAR data acquisition. At 3.2 GeV, the ETOF detector was not included in the analysis, so the minimum-bias trigger was not selected to require that the ETOF was active. At 3.5, 3.9, and 4.5 GeV, the minimum-bias trigger used in the analysis did include the active ETOF requirement. This results in fewer events being selected, but ensures that all necessary detectors are active. The trigger selection details are summarized in Table 5.1. The 680001 and 740007 triggers used at 3.2 and 4.5 GeV respectively had no requirement that the yellow beam was filled. Approximately a third of the way through the data collection at 4.5 GeV, this requirement was added, creating the 740017 trigger. Triggers 720007, 730007, and 740017 used at 3.5, 3.9, and 4.5 GeV respectively included a requirement that the yellow beam was filled. All triggers used here required five or more hits in the barrel time-of-flight detector in addition to hits in either the East EPD, the East BBC, or the East VPD detectors.

Table 5.1: Triggers used in the fixed-target proton fluctuations analysis. The requirements for these triggers are discussed in the text.

$\sqrt{s_{NN}}$ (GeV)	Trigger ID(s)	% of total events
3.2	680001	99.9%
3.5	720007	85.4%
3.9	730007	88.5%
4.5	740007, 740017	70.2%

5.1.2 Bad-run Rejection

The identification of bad runs in the fixed-target data was performed by the STAR quality assurance (QA) group and the analysis is summarized at Ref. [68]. A run was marked as bad if it had greater than a 5 RMS deviation from the mean in any one of 6 observables. These are $\langle dE/dx \rangle$, $\langle \phi \rangle$, $\langle \eta \rangle$, $\langle$RMS(sDCAxy)$\rangle$, $\langle$charged-particle multiplicity$\rangle$, and $\langle$sDCAxy$\rangle$. dE/dx is the energy loss per unit length of tracks in the TPC. ϕ is the azimuthal angle of tracks. sDCAxy is the signed distance of closest approach of each track to the event vertex in the xy plane, and RMS(sDCAxy) is the root mean square of this quantity in each event. The fixed-target QA webpage lists no bad runs for 3.2 GeV but the detailed slides linked in Ref. [68] mention 10 junk runs in this dataset, so they were included in our bad-runs list to clarify that these have been excluded in this analysis. The bad runs are summarized in Tab. 5.2.

Dataset	Bad runs
3.2 GeV (2019)	20180005, 20180006, 20180019, 20180025, 20181016, 20182034, 20183001, 20183013, 20183014, 20183019
3.5 GeV (2020)	20355020, 20355021, 21044023, 21045024, 21045025, 21044027, 21044035, 21045004
3.9 GeV (2020)	21035011, 21036012
4.5 GeV (2020)	21032001

Table 5.2: Bad runs for 3.2 GeV (2019), 3.5, 3.9, and 4.5 GeV (2020).

5.1.3 Vertex Cuts

Following trigger selection, events are removed based on the quality of their reconstructed vertex. The gold target is fixed at a z-position of 200 cm, and 2 cm below the center of the beam-pipe. Event reconstruction locates most vertices within millimeters of these values, but the precise location can vary depending on the number of tracks available for reconstruction, as well as the quality of the TPC drift-velocity calibration. For this reason, we plot the distribution of vertices and select on the peak locations. The distributions of reconstructed vertices along the z-axis are shown in Fig. 5.1. Cuts on the z location of the reconstructed vertex (V_z) are shown as red dashed lines. Satellite peaks can be seen in the distributions. These come from changes to the TPC drift velocity calibration, and from jumped-bucket pileup. This type of pileup occurs because ions from the primary filled bucket can leak into the adjacent unfilled bucket, thereby contributing to tracks that appear shifted in z by 5 mm. The amount of this bucket jumping was dependent on accelerator conditions and changes from one dataset to another.

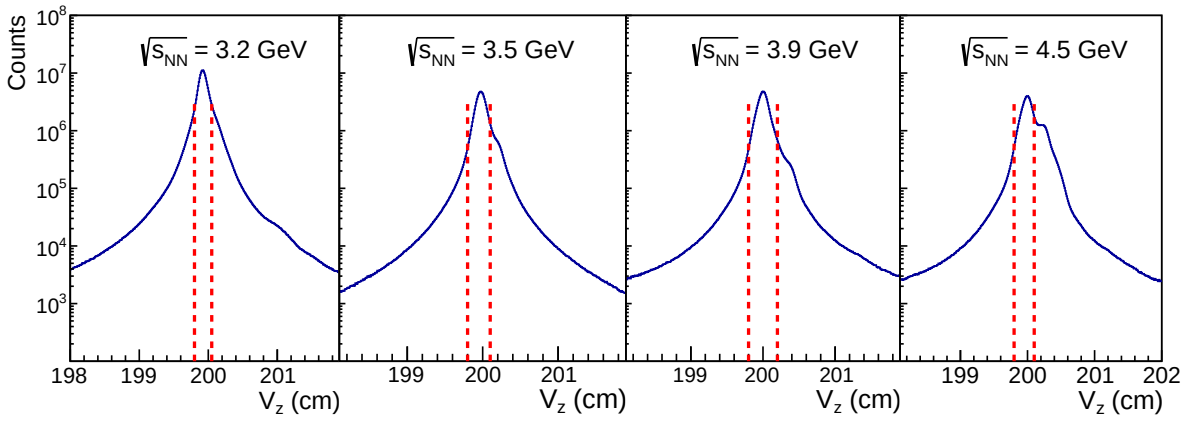

Figure 5.1: Distributions of reconstructed vertices along the z-axis. The V_z cuts are shown as red dashed lines.

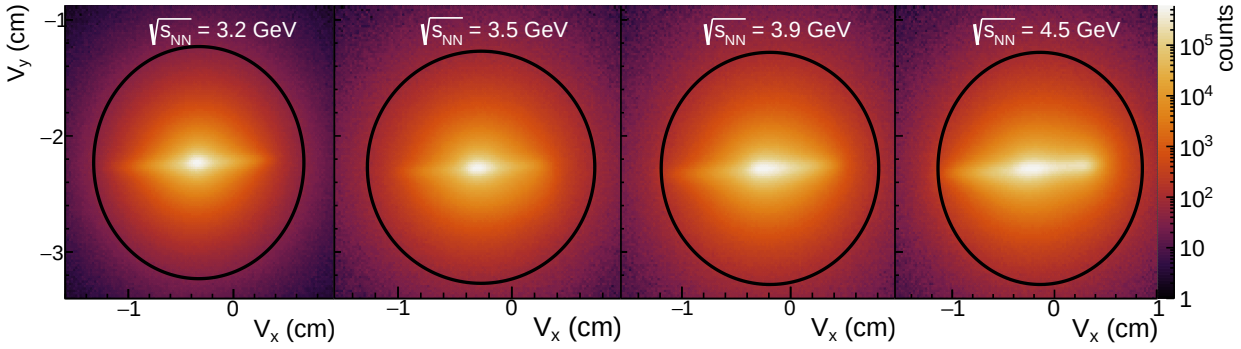

Figure 5.2: Distributions of reconstructed vertices in the xy-plane. The vertex cut in this plane is shown as a black circle.

To cut on vertices in the xy-plane, the average vertex position was calculated in x and y. Then a circular cut with a radius of 1 cm was drawn around that center. These circular cuts are shown in Fig. 5.2. A rectangular cut would be more appropriate due to the distribution of event vertices in Fig. 5.2, but radial cuts were used in previous STAR analyses. With a 99% efficiency, this cut was not one that that was prioritized for optimization. The vertex cuts in x, y, and z are tabulated in Table 5.3.

Table 5.3: Event-level vertex cuts and their associated selection efficiencies.

Vertex Selection				
$\sqrt{s_{NN}}$ (GeV)	V_z range (cm)	V_z cut efficiency	$V_r < 1$ cm centered on (V_x,V_y)	V_x, V_y cut efficiency
3.2	[199.8, 200.05]	74%	(-0.33,-2.23)	99%
3.5	[199.8, 200.1]	77%	(-0.27,-2.27)	99%
3.9	[199.8, 200.2]	84%	(-0.19,-2.28)	99%
4.5	[199.8, 200.1]	63%	(-0.14,-2.28)	99%

5.2 Track-Level Calibration and Selection

5.2.1 Initial Track Reduction

Track-quality cuts were implemented in order to ensure that all tracks included in the analysis originated from the primary vertex, and that the tracks were of a high-enough quality that their momenta could be faithfully reconstructed and energy loss within the TPC calculated. Primary tracks were selected using the isPrimary flag available is STAR's picoDst data format. For each reconstructed track a distance of closest approach (DCA) to the primary vertex is calculated. The isPrimary flag is set to true if the DCA was less than 3 cm. The DCA cut is frequently reduced to 1 cm in later stages of the analysis, but for initial data reduction a 3 cm cut is used. Next, the number of TPC hits used to reconstruct the track is compared to the maximum possible number of hits that a track with those kinematics might be expected to have. If the number of hits is less than 51% of that total, the track is thrown out. This is to reduce contamination from broken tracks. If hit points from a single track are reconstructed as two tracks, this cut ensures that only one of those tracks will have enough hit points associated with it to be included in the analysis.

It is common to also include quality cuts on hits in the time-of-flight detectors. For the barrel time-of-flight (BTOF) detector, hits are assigned y_{local} and z_{local} values which describe where in each counter the hit was located. Each hit was required to have $|y_{\text{local}}| < 1.6$ cm and $|z_{\text{local}}| < 3.0$ cm in order to ensure it was inside a counter. Hits in the endcap time-of-flight (ETOF) detector are assigned Δx and Δy values which quantify the distance between the hit location and the location pointed to by the reconstructed TPC track to which the hit was matched. We required in this analysis that each ETOF hit have $|\Delta x| < 5$ cm and $|\Delta y| < 10$ cm. In the local coordinates of each counter, the ETOF has a spatial resolution of 1.6 mm in x and 3.1 mm in y for identifying hit locations [69].

5.2.2 Proton Identification ($n\sigma_p$) Calibration

Proton identification involves isolating protons based on the amount of energy they lose per centimeter of distance they travel through the gas of the time-projection chamber. This energy loss, called dE/dx, is saved as an attribute of each reconstructed track and is described by the relativistic Bethe-Bloch equation [70],

$$\left\langle \frac{dE}{dx} \right\rangle = Kz^2 \frac{Z}{A\beta^2} \left[\frac{1}{2} \ln \frac{2m_e c^2 \beta^2 \gamma^2 W_{\max}}{I^2} - \beta^2 - \frac{\delta(\beta\gamma)}{2} \right], \tag{5.1}$$

where $K = 0.397$ MeV cm^2/mol, z is the charge of the particle, Z and A are the atomic number and atomic mass, respectively, of the absorber (the TPC gas in this case). The electron mass is m_e, $W_{\max}$ is the maximum possible energy transfer to an electron in the absorber in a single collision, I is the mean excitation energy, and $\delta(\beta\gamma)$ is a correction to the ionization energy loss that depends on the density of the absorber. The low-density environment of a TPC gas minimizes this last correction [70]. In 2006, Hans Bichsel published a seminal article with empirical improvements to the Bethe-Bloch formula for use with a time-projection chamber [71]. He developed what we refer to as Bichsel curves of the form

$$f(\beta\gamma) = \frac{P_1}{\beta^{P_4}} \left[P_2 - \beta^{P_4} - \ln \left(P_3 + \frac{1}{(\beta\gamma)^{P_5}} \right) \right]. \tag{5.2}$$

These Bichsel curves can well describe the energy loss observed in STAR's time-projection chamber and are used in the particle-identification calibration.

Reconstructed track energy loss follows characteristic curves as a function of momentum, as shown in Fig. 5.3. Different particle species fall into different bands in this plot. At a given momentum, these particle bands are approximately log-normal in energy loss. This means that at $p = 1$ GeV/c, the distribution of counts for each particle type follows a normal distribution in the variable $\ln(dE/dx)$. So if a track is reconstructed with momentum p_{obs} and energy loss dE/dx_{obs}, it can be compared against the distribution in energy loss of protons with that same momentum, and assigned a probability that that particle is also a

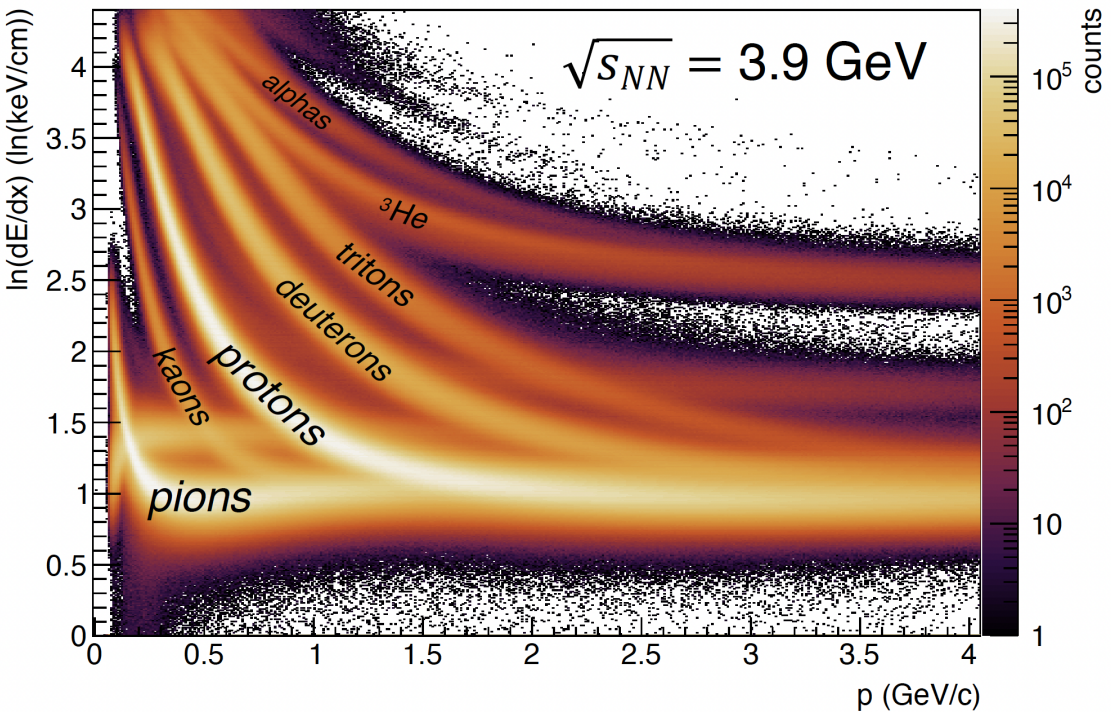

Figure 5.3: Energy loss in the TPC at $\sqrt{s_{NN}} = 3.9$ GeV as a function of momentum.

proton. In order to assist this process, we define a variable called $n\sigma_p$ which quantifies the number of standard deviations each track is away from the mean dE/dx for a proton with those same kinematics. For a given momentum and rapidity, 68% of protons will have an energy loss that corresponds to $|n\sigma_p| < 1$, and 95% of protons will have an energy loss that corresponds to $|n\sigma_p| < 2$. Thus $n\sigma_p$ is defined as

$$n\sigma_p(\ln(dE/dx)) = \frac{\ln(dE/dx) - \langle \ln(dE/dx) \rangle_p}{\sigma(\ln(dE/dx))_p}. \tag{5.3}$$

To calculate $n\sigma_p(\ln(dE/dx))$ for any given track, one first subtracts the average $\ln(dE/dx)$ for protons with those same kinematics, and then scales by the standard deviation of $\ln(dE/dx)$ for protons with those same kinematics.

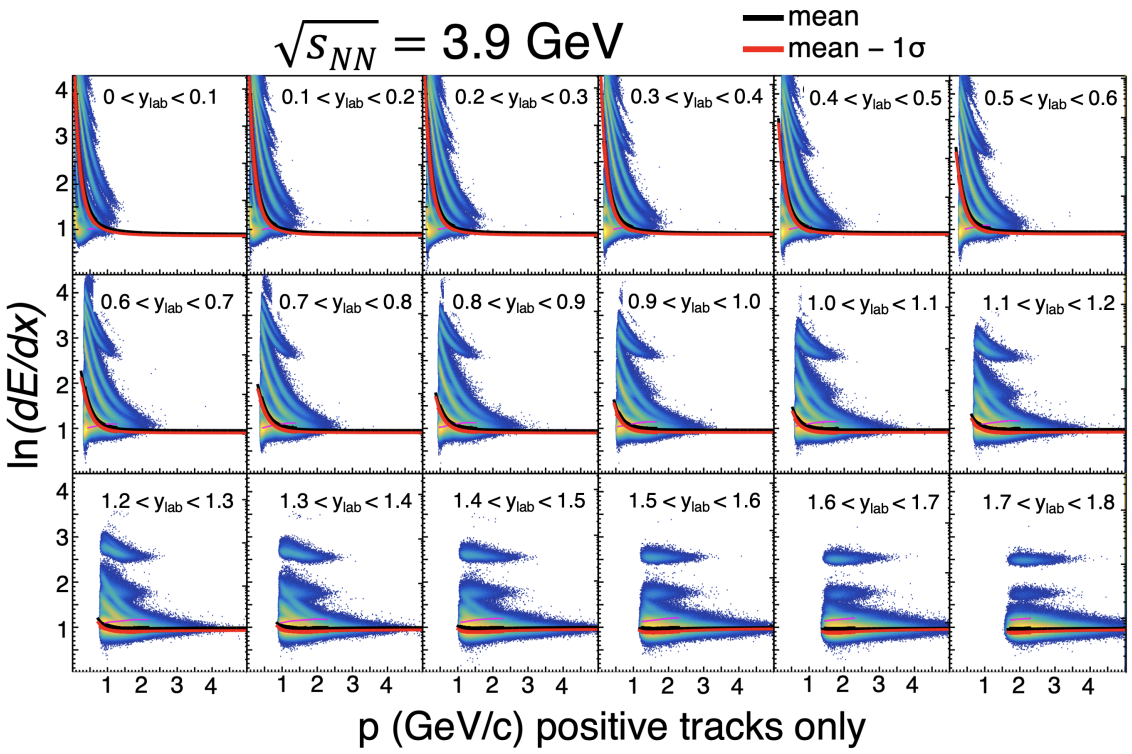

Figure 5.4: Energy loss curves in slices of 0.1 units of rapidity at $\sqrt{s_{NN}} = 3.9$ GeV as a function of momentum.

In order to make an $n\sigma_p$ calibration for the data, $\ln(dE/dx)$ was plotted as a function of momentum for positively-charged tracks for lab-frame rapidity slices in rapidity steps of 0.1. This is shown in Fig. 5.4. Then for each momentum and rapidity, the proton peak in $\ln(dE/dx)$ was fit with a normal distribution, the mean of which was marked with a black dot. One standard deviation below the mean was marked with a red marker in Fig. 5.4. In each rapidity slice, once every momentum was fit, the means and widths as a function of momentum were then fit with Bichsel curves. These Bichsel curves are then used to parameterize the means and widths needed in Eq. (5.3) to define the $n\sigma_p$ variable.

After parameterizing the means and widths in Fig. 5.4, the curves are shifted and stretched according to Eq. (5.3). The result of this is to cast the proton curves into normal

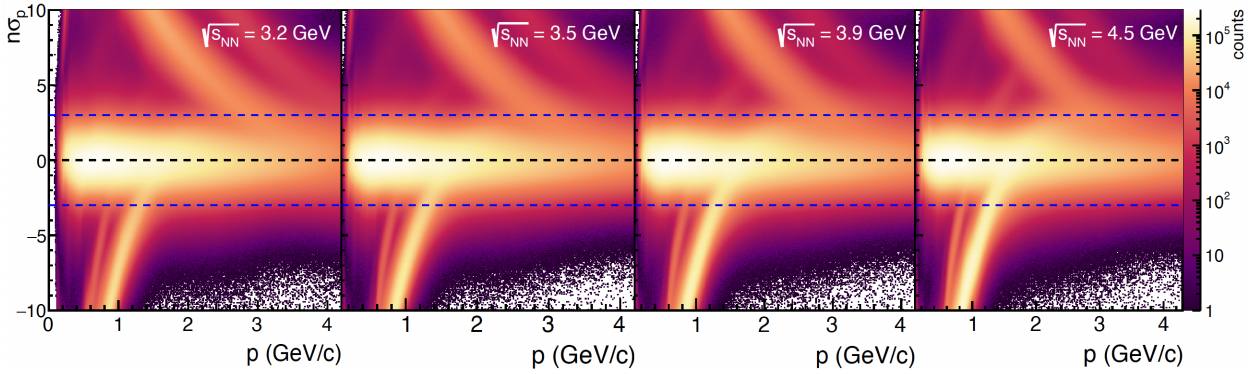

Figure 5.5: Results of $n\sigma_p$ calibration $\sqrt{s_{NN}} = 3.2$, 3.5, 3.9, and 4.5 GeV as a function of momentum for positively-charged tracks.

distributions centered on 0 with standard deviations equal to 1, as shown in Fig. 5.5. The default $|n\sigma_p| < 3$ cuts are shown as blue dashed lines.

5.2.3 Proton Purity using dE/dx

As shown in Fig. 5.5, the kaon and pion bands merge with the proton band first. The pion band is the bright band below the protons at low momentum. The kaons are the darker band to the left of the pions. As the center-of-mass energy rises, the ratio of pions to protons increases, and the pion band gets brighter toward $\sqrt{s_{NN}}$ =4.5 GeV. At a momentum of $\approx$ 2 GeV/c, the pion band passes through the proton band. The deuteron band is the brightest band at positive $n\sigma_p$. Near a momentum of 3 GeV/c, the deuteron band starts to merge with the protons.

In addition to this momentum dependence, the ratios of particles are rapidity dependent. When selecting on protons using a flat $|n\sigma| < 3$ cut, contamination from pions and deuterons becomes significant. This contamination can be calculated using rapidity and p_T-dependent multi-Gaussian fits to the proton, pion, and deuteron peaks. The proton purity is then the fraction of counts in any given p_T and rapidity window that are attributed to the proton

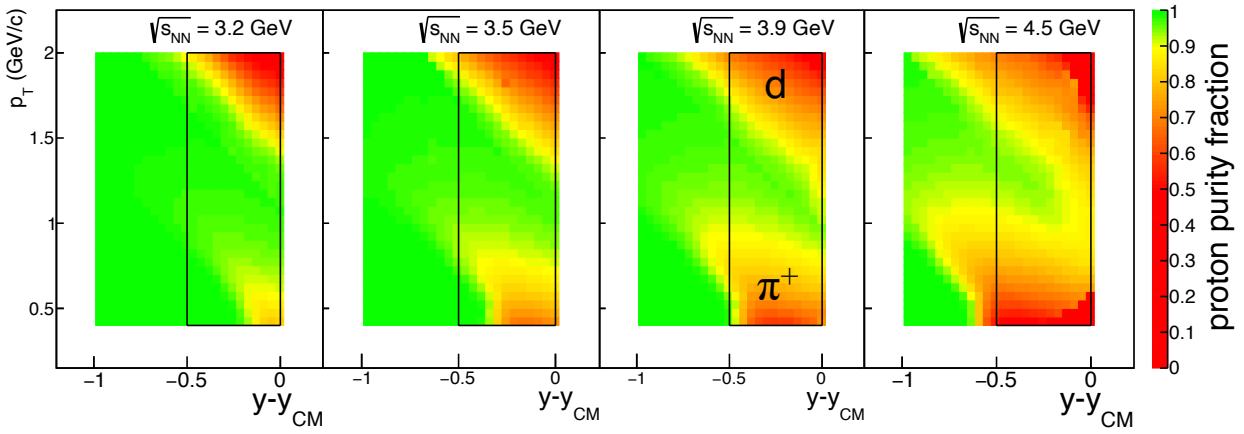

Figure 5.6: Proton purity using $|n\sigma| < 3$ at $\sqrt{s_{NN}} = 3.2$, 3.5, 3.9, and 4.5 GeV as a function of p_T and rapidity. The black rectangle highlights the analysis window from $-0.5 < y - y_{\rm cm} < 0$ and $0.4 < p_T < 2$ GeV/c.

peak. The purity maps at each energy are shown in Fig. 5.6. Regions of high contamination from positively-charged pions and deuterons are labeled on the $\sqrt{s_{NN}} = 3.9$ GeV panel. Pion contamination increases with momentum, but falls again as the pion band passes through the protons. At the highest momenta, the deuterons increasingly contaminate the protons.

In the proton high-moments analysis, we aim to achieve greater than 90% purity in each rapidity and p_T bin. The color palette in Fig. 5.6 marks the 90% threshold with pure yellow. There are two methods to increase the purity when it dips below 90%. The first is to dynamically shift the limits of the $n\sigma_p$ cut. When this is not sufficient to maintain 90% purity, PID based on the time-of-flight detectors can be used.

As seen in Fig. 5.5, the pion band moves into the proton band from negative $n\sigma_p$ values. At lower momenta, when the pions are first starting to contaminate the protons, a 90% purity can be maintained by increasing the lower limit of the $n\sigma_p$ cut from -3 up to -2.9, -2.8, and so on. At higher momenta, when the pion band is centered around more positive values of $n\sigma_p$, the proton purity can be increased by decreasing the upper limit of the $n\sigma_p$

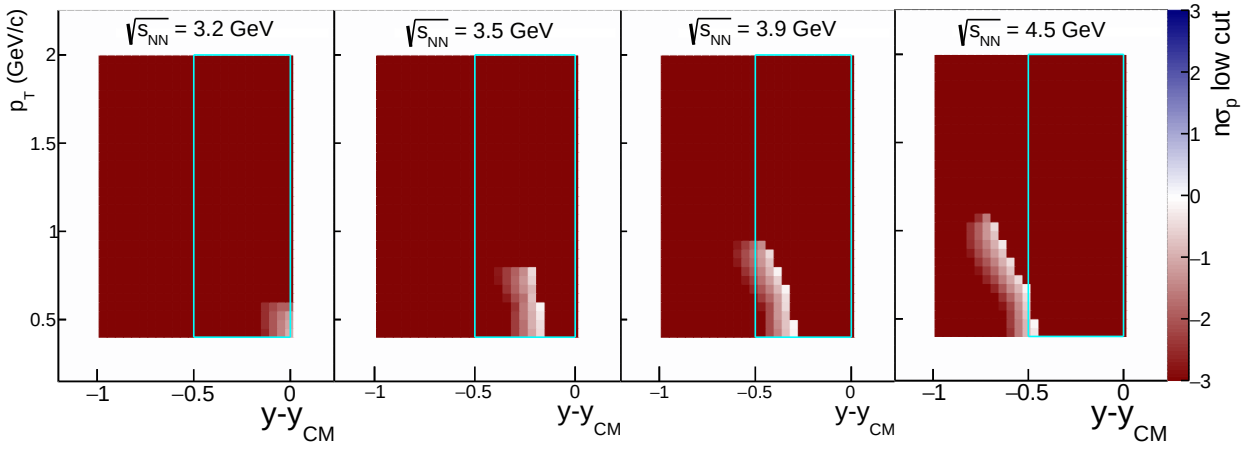

Figure 5.7: $n\sigma_p$ low cut at $\sqrt{s_{NN}} = 3.2$, 3.5, 3.9, and 4.5 GeV as a function of p_T and rapidity. The cyan rectangle highlights the analysis window from $-0.5 < y - y_{\rm cm} < 0$ and $0.4 < p_T < 2$ GeV/c.

cut down from 3. At momenta close to 3 GeV/c, the deuteron band moves in from positive values of $n\sigma_p$, so the purity can again be maintained by decreasing the upper limit of the $n\sigma_p$ cut. In this analysis, the upper and lower limits of the $n\sigma_p$ cut were allowed to shift with a limiting value of 0 in each case. If a tighter cut than this is not sufficient to maintain 90% purity, then PID using the time-of-flight was required. The upper and lower limits of the $n\sigma_p$-low$< n\sigma_p <$ $n\sigma_p$-high cut are shown in Fig. 5.7 and Fig. 5.8 respectively.

The resulting purity maps after dynamically shifting the $n\sigma_p$ cuts are shown in Fig. 5.9. At 3.2 GeV, a 90% purity is maintained across the entire phase space, and no time-of-flight PID is necessary. At 3.5, 3.9, and 4.5 GeV, the purity dips below 90% in some of the phase space, so TOF will be required. As discussed in Ref. [72], if tracks in the TPC are being used to define multiplicity, then it is beneficial to maximize the amount of phase space over which the proton number is also identified using tracks in the TPC exclusively. This is the reason for using these $n\sigma_p$ cuts to maximize the purity instead of immediately switching to

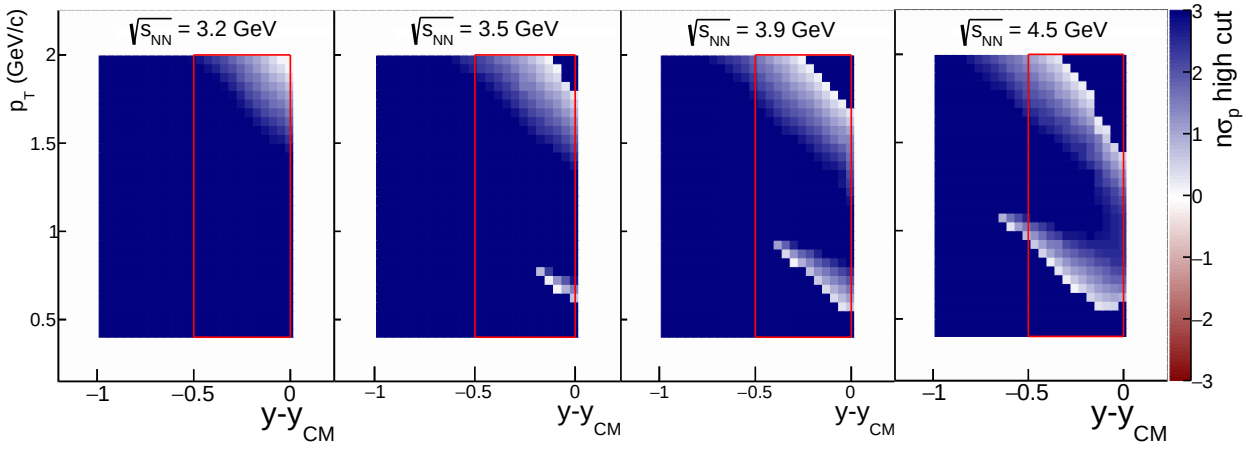

Figure 5.8: $n\sigma_p$ high cut at $\sqrt{s_{NN}} = 3.2$, 3.5, 3.9, and 4.5 GeV as a function of p_T and rapidity. The red rectangle highlights the analysis window from $-0.5 < y - y_{\rm cm} < 0$ and $0.4 < p_T < 2$ GeV/c.

using the time-of-flight for particle identification.

The maps of where to require a TOF-match after dynamically shifting the $n\sigma_p$ cuts are shown in Fig. 5.10. At 3.5, 3.9, and 4.5 GeV, the purity dips below 90% due to pion contamination in the lower-left corner and deuteron contamination in the upper-right corner, so a TOF-match is required in these regions. No TOF-matching is required at 3.2 GeV.

The traditional $|n\sigma_p| < 3$ cut introduces a negligible inefficiency. However, once dynamic $n\sigma_p$ cuts are used, the inefficiency can become significant. For the cases in which the upper or lower-limit of the $n\sigma_p$ cut approaches 0, the additional inefficiency introduced by this cut can reach 50%. This must be accounted for in the track-by-track efficiency correction used. In each rapidity and p_T bin, the additional inefficiency introduced by these dynamic $n\sigma_p$ cuts are mapped in Fig. 5.11. The acceptance maps after using dynamic $n\sigma_p$ cuts and requiring TOF hits are shown in Fig. 5.12.

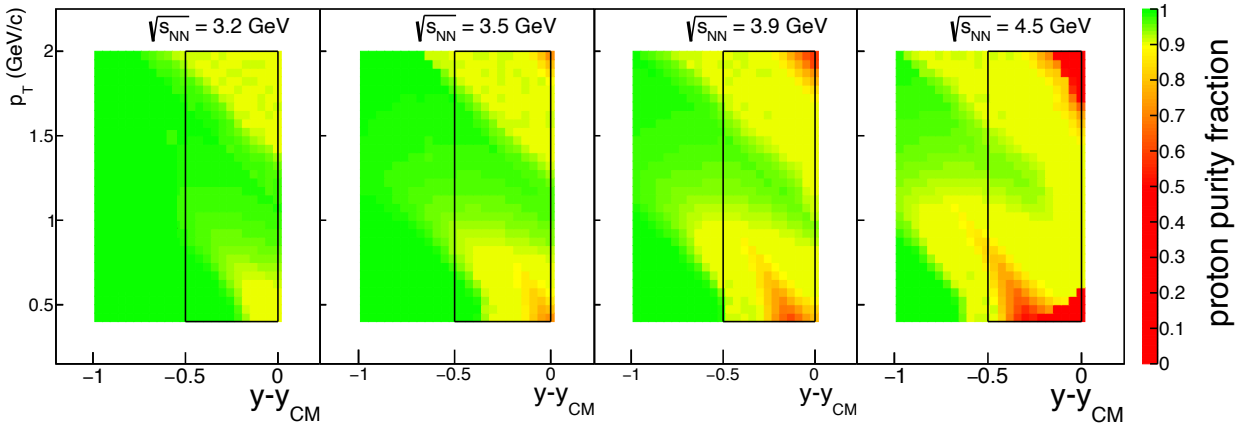

Figure 5.9: Proton purity after dynamically shifting the $n\sigma_p$ cuts at $\sqrt{s_{NN}} = 3.2$, 3.5, 3.9, and 4.5 GeV as a function of p_T and rapidity. The black rectangle highlights the analysis window from $-0.5 < y - y_{\rm cm} < 0$ and $0.4 < p_T < 2$ GeV/c.

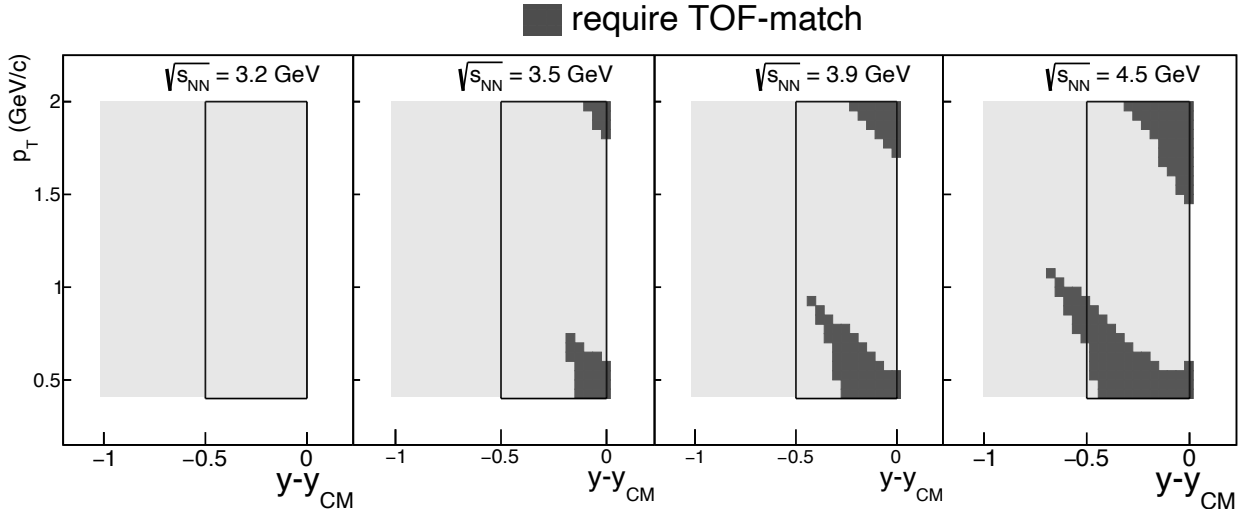

Figure 5.10: Map of where to require a TOF-match for proton identification at $\sqrt{s_{NN}} = 3.2$, 3.5, 3.9, and 4.5 GeV as a function of p_T and rapidity. The black rectangle highlights the analysis window from $-0.5 < y - y_{\rm cm} < 0$ and $0.4 < p_T < 2$ GeV/c.

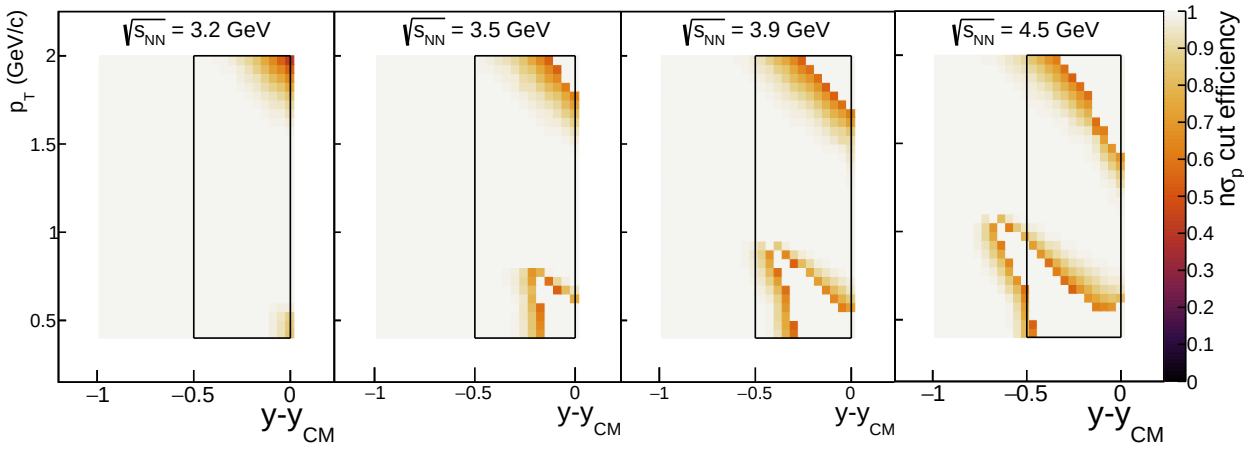

Figure 5.11: Map of additional efficiency introduced by using tighter $n\sigma_p$ cuts at $\sqrt{s_{NN}} =$ 3.2, 3.5, 3.9, and 4.5 GeV as a function of p_T and rapidity. The black rectangle highlights the analysis window from $-0.5 < y - y_{\rm cm} < 0$ and $0.4 < p_T < 2$ GeV/c.

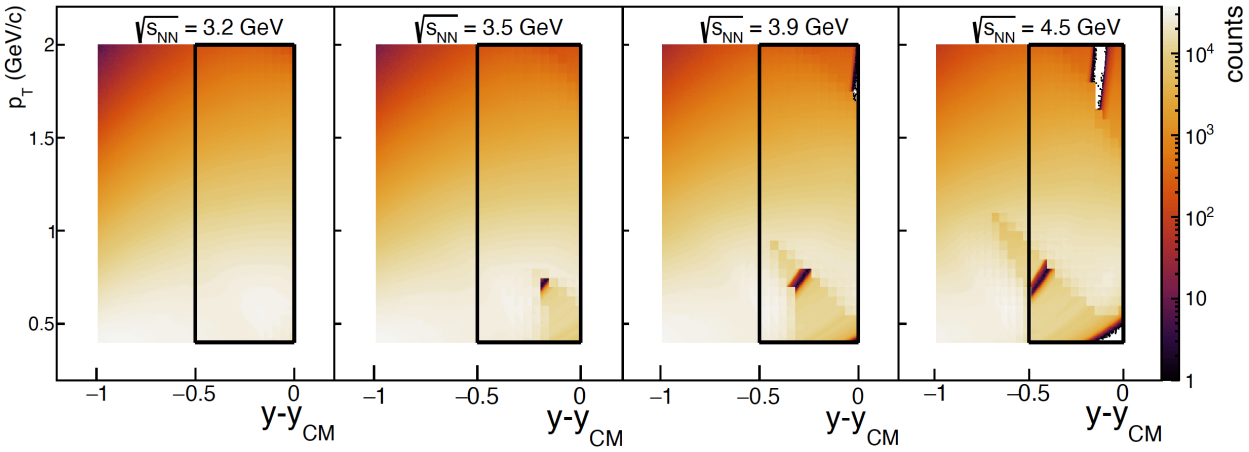

Figure 5.12: Midrapidity acceptance maps at $\sqrt{s_{NN}} = 3.2$, 3.5, 3.9, and 4.5 GeV as a function of p_T and rapidity. The black rectangle highlights the analysis window from $-0.5 < y - y_{\rm cm} < 0$ and $0.4 < p_T < 2$ GeV/c.

5.2.4 Distance of Closest Approach

Each track reconstructed by the time-projection chamber is projected back as close to the initial vertex as it will go. The closest distance to the vertex that it achieves is called the distance of closest approach or DCA. As described in Subsection 3.6.1, a DCA cut of 3 cm was used in the $\sqrt{s_{NN}}$ =3 GeV (2018) analysis. That section also explains how a DCA cut of 3 cm allows tracks from out-of-bucket pileup to enter the analysis window at large rapidities. With a 3 cm DCA cut, the analysis is vulnerable to rapidity-dependent pileup. Following the iTPC upgrade, the 2019 and later datasets can reconstruct a tighter DCA. In order to avoid out-of-bucket pileup, we decrease the DCA cut in this analysis down to 1 cm. We do this for both the protons and the multiplicity used to define centrality, because allowing pileup in only one of these variables makes the analysis more vulnerable to enhanced high-order moments [72]. These cuts are shown in Fig. 5.13.

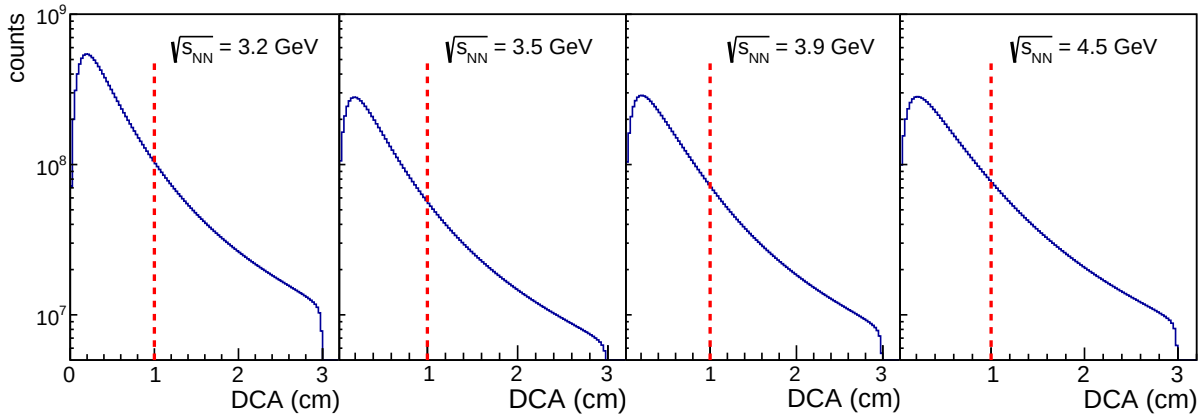

Figure 5.13: DCA distribution of primary tracks and 1 cm DCA cut at $\sqrt{s_{NN}}$ = 3.2, 3.5, 3.9, and 4.5 GeV.

5.2.5 Cuts on the Number of Hits

Included in STAR's picoDsts is track-level information on the number of hits points used to reconstruct the track, and the number of hits from the TPC used as space-points in the fitting algorithm used to extract track parameters such as energy loss. These are called nHitsFit and nHitsDedx respectively. In order to ensure that all tracks included in the analysis are high quality, we require that each track used toward the proton number have nHitsFit ≥ 20 and nHitsDedx ≥ 20. This is shown in Fig. 5.14. The nHitsFit ≥ 20 cut is not redundant because both nHitsFit and nHitsDedx are independently varied during the systematic uncertainty estimation.

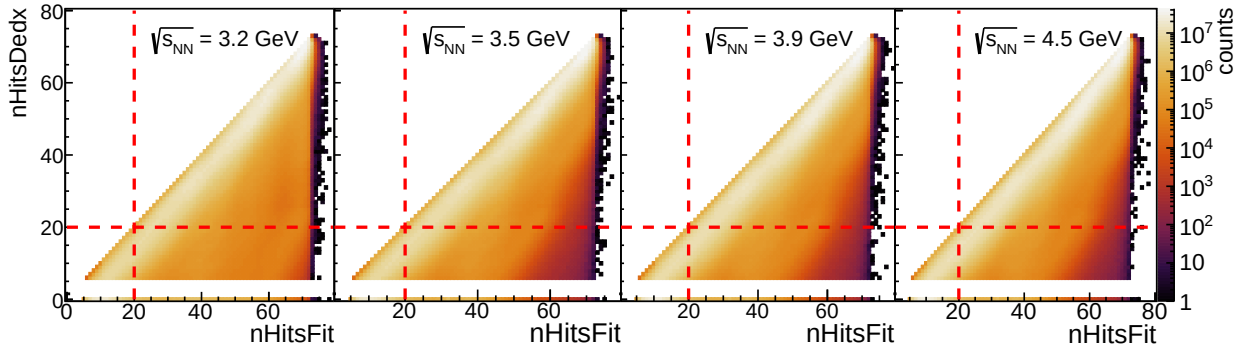

Figure 5.14: nHitsFit and nHitsDedx at $\sqrt{s_{NN}} = 3.2$, 3.5, 3.9, and 4.5 GeV with cuts superimposed in red.

5.2.6 Endcap Time-of-flight

The ETOF detector is made up of 12 sectors like the face of a clock. Each sector is composed of 3 modules consisting of 3 counters. Each counter is made of 32 strips. The strips are read out on each side for precise timing resolution, and are clustered in groups of four. One side of the counter has 8 readout points called a Get4. The other side of the counter has another 8 Get4s, each reading out the other side of the strips. Thus each counter contains 16 Get4s and 8 Get4 pairs which read out hits from 8 groups of 4 strips each. Each of these components are broken down in Fig. 5.15.

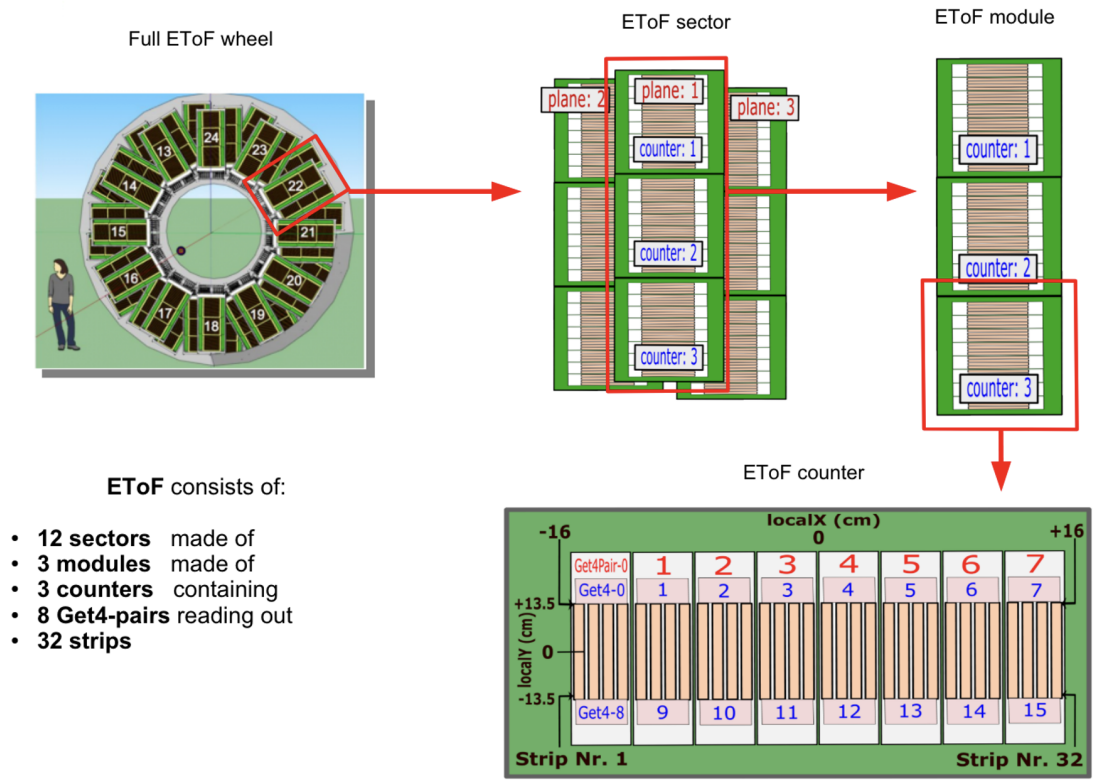

Figure 5.15: Schematic of composition of ETOF detector, presented by Yannick Söhngen [73].

At $\sqrt{s_{NN}} = 3.0$ and 3.2 GeV, the ETOF detector is not necessary when using the half midrapidity analysis window $-0.5 < y - y_{\rm cm} < 0$ and $0.4 < p_T < 2$ GeV/c. Particle identification using energy loss in the TPC is sufficient at these energies. However, in order to maintain greater than 90% proton purity at higher energies, high-momentum tracks need to also be accompanied with a hit in either the barrel time-of-flight or the endcap time-of-flight. The ETOF is necessary at $\sqrt{s_{NN}} = 3.5$, 3.9, and 4.5 GeV.

As stated above, hits in ETOF strips are read out by what are called Get4s. During a run, the Get4s had to spontaneously reboot, and would do so independently of each another. While a Get4 was rebooting, the efficiency of reading a hit from that particular Get4 drops. In older productions of the fixed-target data, if any of the Get4s were rebooting in a given event, then the whole counter was flagged as bad. This posed a difficulty for the fluctuation analysis because the most straightforward remedy to fluctuating detector components is to mask those that fluctuate the most. However if only one Get4 out of 16 on a counter is particularly flaky, then it is overkill to mask the entire counter.

Starting from the P24ia production and later, Yannick Söhngen implemented changes to the picoDst libraries that flag exactly which Get4s are fluctuating in any event. Additionally, Yannick created a single-sided matching routine wherein a hit on a given strip could still be matched to a TPC track even if a Get4 on one side of the strip is rebooting. This single-sided matching routine reduces fluctuations in acceptance and allows analyzers to mask flaky Get4s with higher granularity. With single-sided matching, an analyzer only needs to mask those Get4 pairs for which both sides of the strip are consistently rebooting.

An example code snippet of how the new eTofGoodEventFlag is used to check for bad Get4 pairs is shown below. There are 1728 Get4s in total in the ETOF, and for each event, each one has a status flag indicating whether it was on or rebooting. We loop through each Get4, and simultaneously check the Get4 on the other side of the strip. If both Get4s have a bad status flag for an event, then the pair is considered bad. This leaves 864 Get4 pairs

in total to keep track of.

```
int skipCounter = 0; //tracks when to skip Get4s already counted
int iPair = 0; //index of Get4-pair
for(int icount=0; icount<1720; icount++){
  skipCounter++;
  bool badPair = false;
  if( !(event->eTofGoodEventFlag(icount)) && !(event->eTofGoodEventFlag(
   icount+8)) ) {// both bad
    timeDeadPairs->Fill(iPair);
    badPair=true;
  }
  if(skipCounter==8){skipCounter=0; icount+=8;} //skip Get4s on downside
  iPair++;
}
```

We then make a chart of the fraction of events in which each Get4 pair was flagged as bad. This chart is shown at $\sqrt{s_{NN}} = 3.5$ GeV in Fig. 5.16, at $\sqrt{s_{NN}} = 3.9$ GeV in Fig. 5.17, at $\sqrt{s_{NN}} = 4.5$ GeV in Fig. 5.18. Some Get4 pairs are flagged as bad much more frequently than others. In order to reduce fluctuations in the data, we can mask these problematic Get4 pairs for the whole dataset in order to achieve a stable acceptance. The loss in efficiency is corrected for by calculating the matching after these bad Get4 pairs have been masked.

We then use these charts to list the 100 most unstable Get4 pairs. The 100 most unstable Get4 pairs from most to least unstable are given below for each dataset:

- 3.5 GeV: 770, 771, 769, 772, 773, 774, 768, 795, 192, 240, 199, 794, 775, 198, 194, 50, 247, 386, 528, 197, 241, 704, 534, 196, 535, 529, 550, 798, 531, 545, 551, 549, 242, 672, 193, 799, 543, 538, 548, 720, 385, 544, 688, 245, 537, 533, 532, 53, 793, 711, 384, 208, 339, 796, 379, 539, 735, 246, 7, 73, 144, 289, 79, 195, 291, 127, 151, 243, 792, 239, 679, 762, 763, 673, 576, 433, 168, 200, 676, 147, 150, 74, 677, 648, 145, 149, 695, 148, 674,

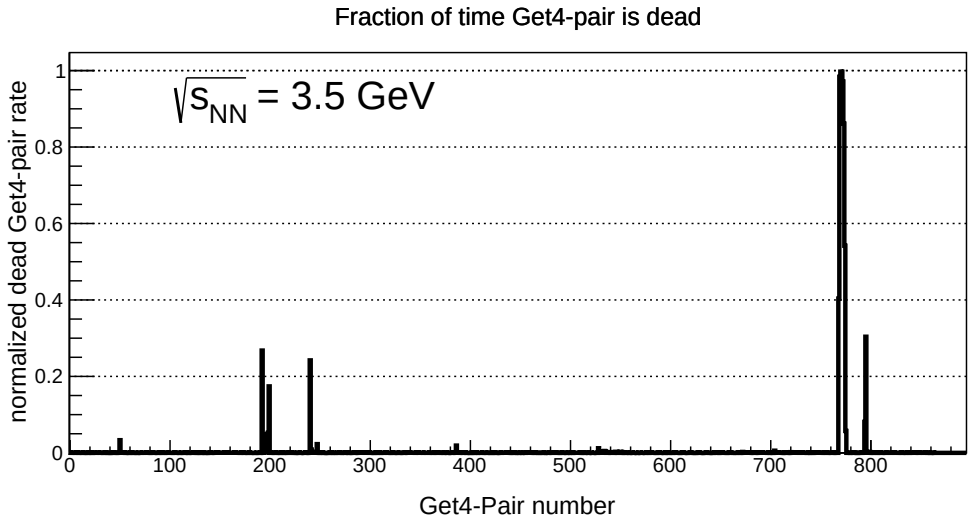

Figure 5.16: Fraction of events for which each ETOF Get4 pair was flagged as bad for $\sqrt{s_{NN}} = 3.5$ GeV.

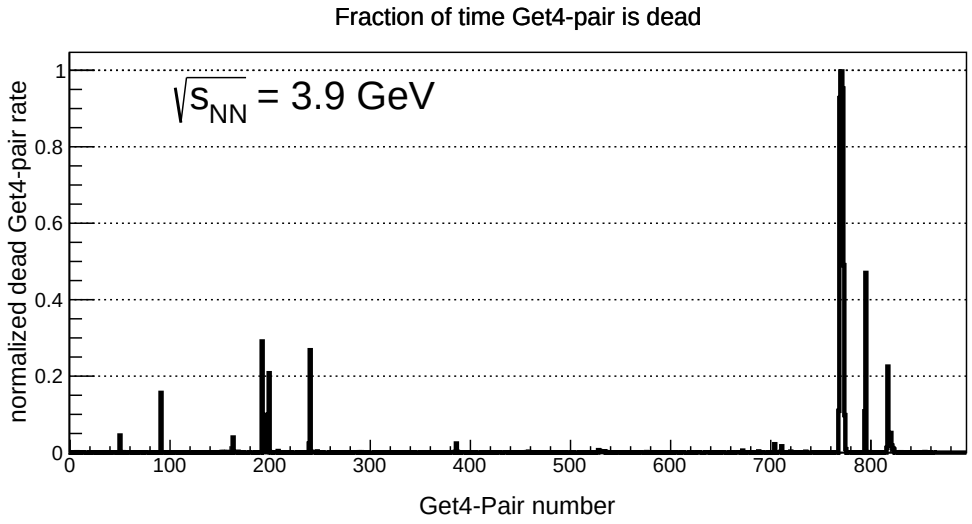

Figure 5.17: Fraction of events for which each ETOF Get4 pair was flagged as bad for $\sqrt{s_{NN}} = 3.9$ GeV.

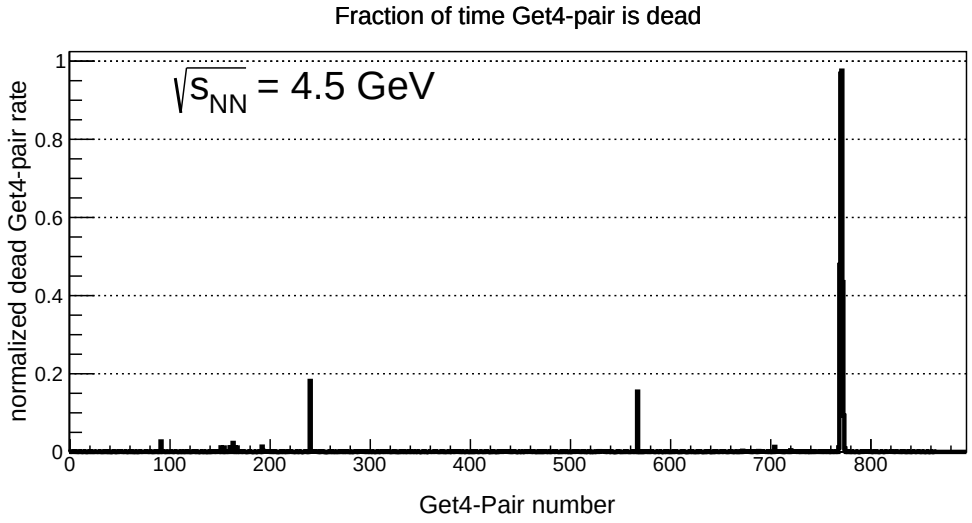

Figure 5.18: Fraction of events for which each ETOF Get4 pair was flagged as bad for $\sqrt{s_{NN}} = 4.5$ GeV.

678, 161, 705, 244, 690, 723, 290, 146, 160, 152, 675

- 3.9 GeV: 771, 770, 772, 769, 773, 795, 192, 240, 817, 199, 91, 768, 794, 198, 194, 774, 820, 819, 50, 163, 818, 197, 386, 239, 704, 821, 196, 711, 816, 822, 775, 823, 528, 672, 193, 529, 208, 531, 688, 247, 534, 720, 735, 458, 241, 168, 530, 535, 710, 387, 152, 157, 533, 385, 854, 576, 532, 154, 456, 384, 53, 200, 291, 799, 7, 289, 830, 797, 829, 584, 195, 827, 648, 290, 747, 680, 679, 763, 437, 673, 379, 160, 242, 432, 674, 433, 676, 74, 677, 292, 51, 144, 678, 436, 288, 434, 695, 793, 705, 315

- 4.5 GeV: 771, 770, 769, 772, 240, 567, 773, 91, 163, 192, 704, 160, 151, 768, 162, 154, 167, 165, 774, 720, 672, 193, 688, 529, 775, 528, 795, 247, 711, 576, 534, 794, 735, 530, 385, 194, 276, 734, 533, 387, 144, 458, 199, 196, 241, 197, 531, 168, 198, 532, 799, 200, 195, 535, 386, 792, 679, 456, 763, 289, 676, 673, 674, 242, 384, 705, 648, 161, 677, 504, 291, 678, 53, 793, 246, 817, 762, 690, 675, 721, 290, 724, 239, 436, 292, 823, 216, 706, 505, 434, 243, 433, 245, 818, 695, 435, 146, 600, 707, 819

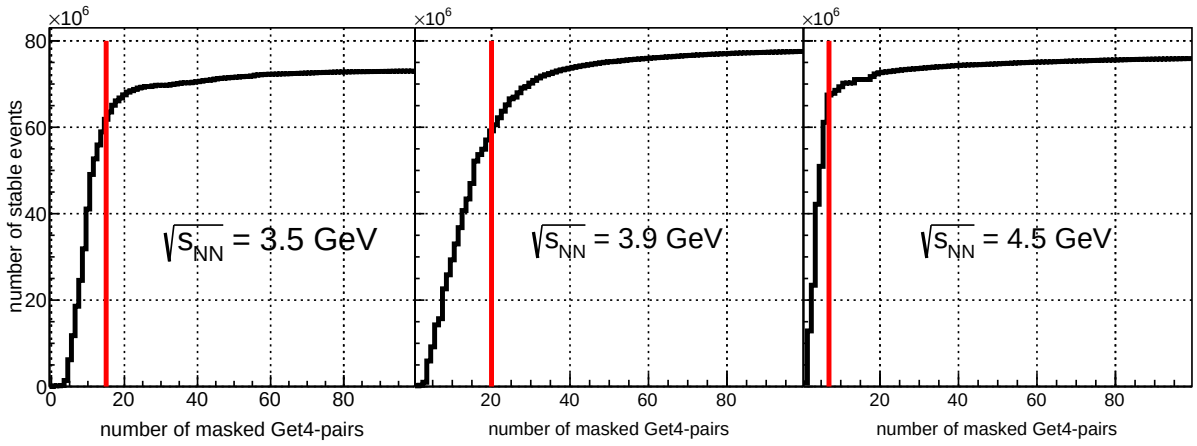

Figure 5.19: Number of good (stable acceptance) events left after masking N Get4 pairs. The cut is shown in red.

Using these lists, those Get4 pairs that were most frequently bad were then sequentially masked. After masking each additional Get4 pair, the number of events for which all unmasked Get4 pairs were active was tallied. The results of this are shown in Figure 5.19. At $\sqrt{s_{NN}} = 3.9$ GeV, when we mask only one Get4 pair (771), 160k events have all remaining Get4 pairs active. When we mask both 771 and 770, 300k events have all remaining Get4 pairs active. When we mask the 20 worst Get4 pairs (771, 770, 772, 769, 773, 795, 192, 240, 817, 199, 91, 768, 794, 198, 194, 774, 820, 819, 50, 163), we get 59 million events for which the remaining Get4s are stable.

As shown in Fig. 5.19, we see that masking 15 Get4 pairs at 3.5 GeV leaves 62 million events with stable ETOF acceptance; masking 20 Get4 pairs at 3.9 GeV leaves 59 million stable events; and masking 7 Get4 pairs at 4.5 GeV leaves 67 million stable events. Get4 pairs were masked until the number of stable events started to plateau. The Get4 pairs to mask at each energy are listed here:

- 3.5 GeV: 770, 771, 769, 772, 773, 774, 768, 795, 192, 240, 199, 794, 775, 198, 194
- 3.9 GeV: 771, 770, 772, 769, 773, 795, 192, 240, 817, 199, 91, 768, 794, 198, 194, 774, 820, 819, 50, 163
- 4.5 GeV: 771, 770, 769, 772, 240, 567, 773

5.3 Secondary Event Selection

This section describes a secondary stage of event selection. This stage is described separately from the primary event selection stage because it relies on the track selection and calibrations described in Sec. 5.2. For example, many of the following steps depend on the definition of multiplicity used in the analysis. We use a multiplicity variable that excludes protons in order to reduce autocorrelations between our cuts and the observed moments. Thus the $n\sigma_p$ variable must be defined prior to calculating the multiplicity and prior to implementing many of the following cuts. This multiplicity variable is called FXTMult3 and is rigorously defined in Sec. 5.3.4.

5.3.1 Out-of-Bucket Pileup Removal

Subsection 3.6.1 describes how tracks from out-of-bucket pileup can enter the analysis at high rapidities. These tracks are mostly removed by using a tight DCA < 1 cm cut. In addition to removing tracks, we can remove events with out-of-bucket pileup by additionally removing events that are outliers when plotting (DCA < 3 cm multiplicity) and (DCA < 1 cm multiplicity). A linear cut is used to remove out-of-bucket pileup at each energy. In this space, $x =$ FXTMult3 for DCA < 1 cm and $y =$ FXTMult3 for DCA < 3 cm. Events are flagged and removed for out-of-bucket pileup by requiring that all events fall below the line $y = a_0 + a_1 x$, where the parameters are tabulated in Table 5.5. The multiplicity distributions and out-of-bucket pileup cuts are shown in Fig. 5.20.

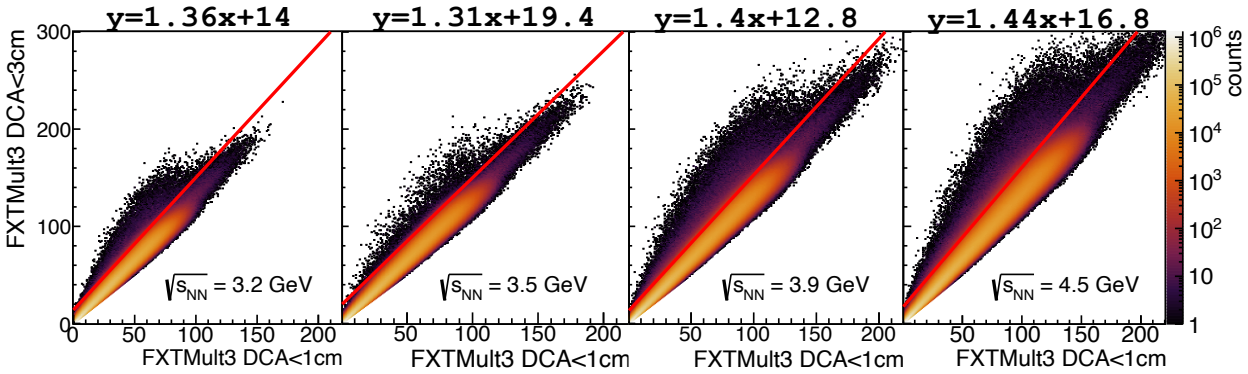

Figure 5.20: Multiplicity (excluding protons) of charged tracks with DCA < 3 cm and with DCA < 1 cm, and cuts (in red) used to remove out-of-bucket pileup.

Table 5.4: Event-level out-of-bucket pileup removal cuts, $y < a_0 + a_1 x$ with $x =$ FXTMult3 for DCA < 1 cm and $y =$ FXTMult3 for DCA < 3 cm.

$\sqrt{s_{NN}}$ (GeV)	a_0	a_1	% events kept
3.2	14.0	1.36	99.95
3.5	19.4	1.31	99.97
3.9	12.8	1.40	99.76
4.5	16.8	1.44	99.80

5.3.2 In-Bucket Pileup Removal

In addition to out-of-bucket pileup, there is much more in-bucket pileup than in the collider analyses. In fixed-target mode, the accelerator operators tried to maintain a luminosity corresponding to a collision probability per bunch crossing of $\approx 0.2\%$. This was done by lowering the beam in the interaction region until the desired rate was achieved. The $\approx 0.2\%$ collision rate means that the in-bucket pileup rate must also be $\approx 0.2\%$.

As discussed in Chapter 3, this in-bucket pileup can massively skew the cumulants if the TOF and TPC are being used to separately measure proton number and multiplicity. In each dataset for which we use any TOF information, we reject as much pileup as possible by rejecting outliers in the distribution of TPC multiplicity and TOF multiplicity (both excluding protons). This cut was included at 3.5, 3.9, and 4.5 GeV. It was defined also at 3.2 GeV in order to reject pileup prior to the Glauber fit. However, at 3.2 GeV, out-of-bucket pileup was left in and corrected for according to the procedure discussed in Sec. 6.3.

In order to reject pileup, 5th-order polynomials were defined at each energy to reject outliers. These polynomials are shown in red in Fig. 5.20. At the maximum value of the polynomial, the cut switches to a constant value, also shown in red. The parameters of these cuts, including their piecewise nature, are included in Table 5.5.

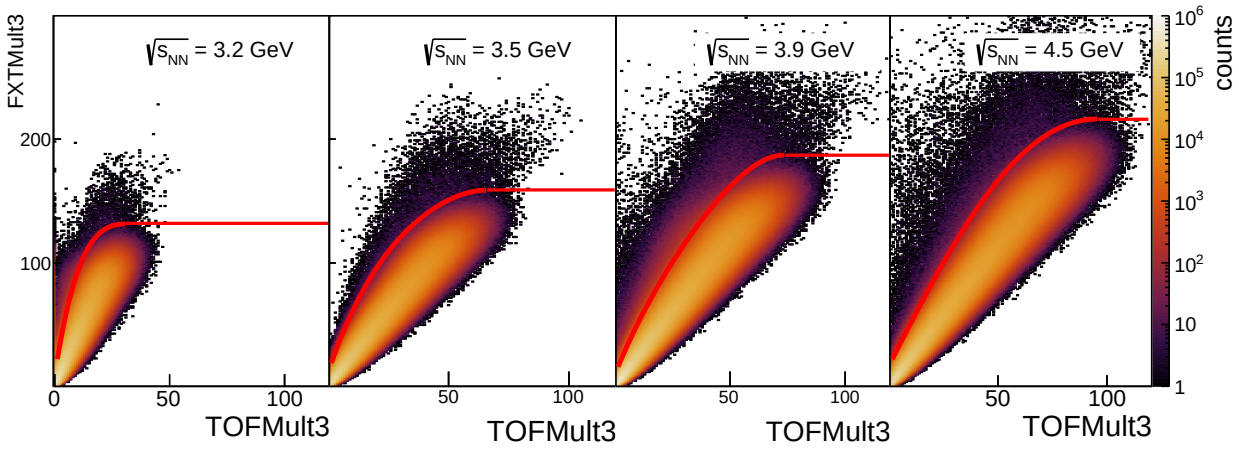

Figure 5.21: Multiplicity (excluding protons) of charged tracks with DCA < 3 cm and those tracks with a TOF-match with $0 < m^2 < 0.6$ GeV$^2/c^2$. Cuts (in red) used to remove out-of-bucket pileup.

Table 5.5: Event-level out-of-time pileup removal cuts, $x = \mathsf{TOFMult3}$ for DCA < 3 cm and $y = \mathsf{FXTMult3}$ for DCA < 3 cm.

$$\text{if } x \leq X_0\text{: } y < a_0 + a_1 x + a_2 x^2 + a_3 x^2 + a_4 x^4$$
$$\text{else: } y < Y_0$$

$\sqrt{s_{NN}}$ (GeV)	a_0	a_1	a_2	a_3	a_4	X_0	Y_0
3.2	9.0	12.197	-0.4460	0.00716	-4.360e-5	31	132
3.5	12.0	5.7340	-0.0948	0.000969	-5.137e-6	66	159
3.9	10.1	4.564	-0.0503	0.00062	-4.55e-6	74	187
4.5	17.5	3.441	-1.205e-6	-0.00022	7.476e-7	96	216

5.3.3 TOF Performance Cuts

It was found that some small fraction of events, the time-of-flight did not identify any tracks with $m^2 > 0$. While many of the tracks in these events had TOF matches, the time-of-flight for these was unrealistic. This was unexpectedly observed even for very central events, as shown in Fig. 5.22. In the fixed-target program, the time-of-flight relies on a startless t_0 algorithm which uses well identified protons and pions to determine the start time of the event. If this algorithm fails, then the timing of all tracks can be distorted resulting in no well identified hits. In order to control this, we required that each event have at least one hit in both the BTOF and ETOF with $0 < m^2 < 0.6$ GeV^2.

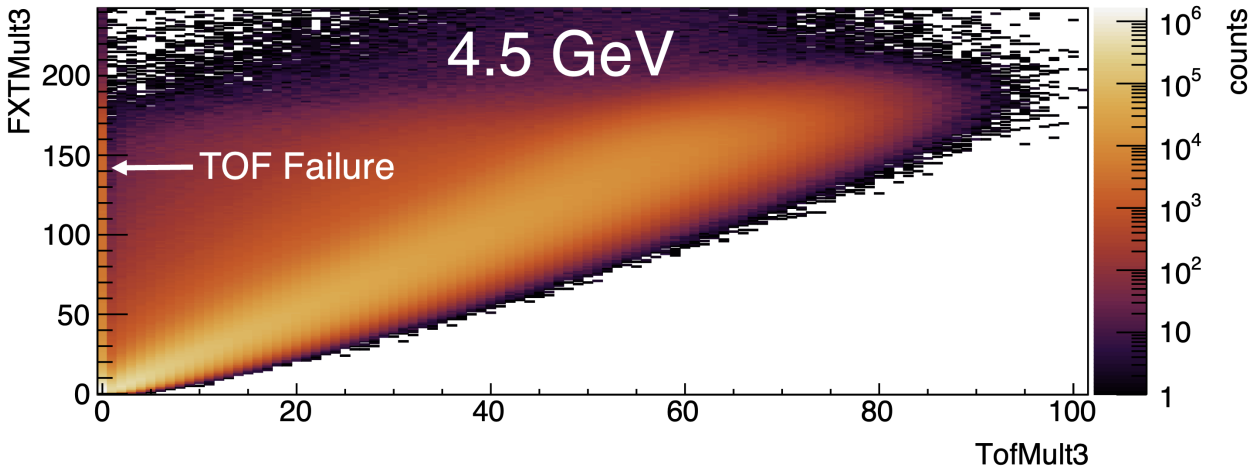

Figure 5.22: Multiplicity (excluding protons) of TPC tracks and multiplicity (excluding protons) of TOF tracks for DCA < 3 cm, used to illustrate the failure of the t_0 algorithm for some events, shown as the bright band at TOFMult3 $= 0$.

5.3.4 Centrality Determination

The multiplicity variable used for the proton moments analysis is referred to as RefMult3 for collider data sets and FXTMult3 for fixed-target data sets. This multiplicity variable is constructed to exclude protons and light nuclei so as to avoid autocorrelations which may arise from cutting on the variable we are attempting to measure. FXTMult3 is conceptualized as the number of primary pion and kaon tracks measured in the TPC.

There are nearly no antiprotons (or antibaryons) produced at the energies accessed in the fixed-target program. For this reason, we count all negatively charged tracks in our definition of FXTMult3. The TPC PID is based on dE/dx measurements of energy loss by charged particles traveling through the TPC gas. This energy loss PID provides sufficient separation of pions, kaons, and protons for low-momentum tracks. For tracks with momenta greater than 2 GeV/c, the pion, kaon, and proton bands are fully merged, and it is impossible to exclude baryons from the multiplicity definition above $p = 2$ GeV/c. We therefore define FXTMult3 as all primary tracks which are either negatively charged or have a momentum less than 2 GeV/c and are three standard deviations below the proton band as identified by dE/dx. The FXTMult3 definition is shown in Fig. 5.23.

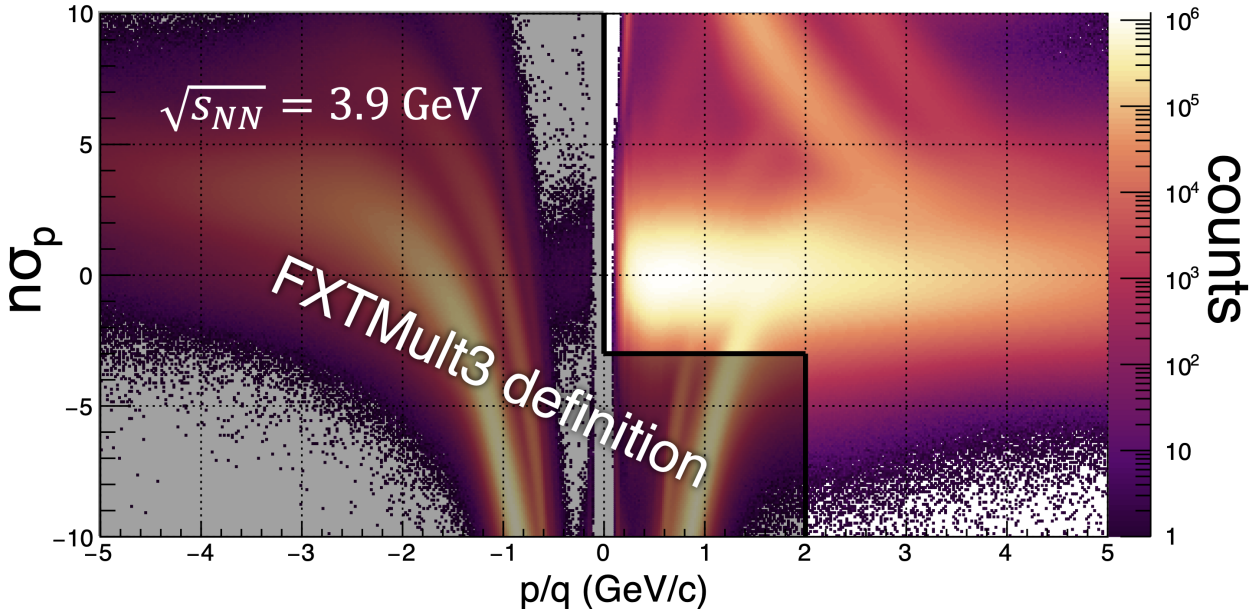

Figure 5.23: FXTMult3 definition (shaded region), constructed to exclude protons and light nuclei.

5.3.4.1 The Glauber Model

A Glauber model and two-component particle-production model were used to determine the centrality. The Glauber Monte Carlo (GMC)[74] randomly simulates two ^{197}Au ions, with nucleons distributed according to a Woods-Saxon density distribution,

$$\rho(r) \sim \frac{1}{1 - \exp(\frac{r-R}{a})}. \tag{5.4}$$

In this equation, r is the distance from the center of the nucleus, R is a size parameter describing the radius at which the nucleon density has dropped to half of its density at $r = 0$, and a, referred to as the skin depth, parametrizes how quickly the nucleon density drops at the edge of the nucleus. The nuclear radius parameter R for heavy ions is typically described well by $R = (1.07 \text{ fm}) * A^{1/3}$, where A is the number of nucleons in that nucleus. However, in the STAR Glauber model, the nuclear size and skin thickness are informed by Ref. [75] in

which elastic scattering of electrons off of the ^{197}Au nucleus yielded $R = 6.38 \pm 0.06$ fm, and $a = 0.535 \pm 0.027$ fm. Nucleon density profiles for ^{197}Au and ^{63}Cu are shown in Fig. 5.24.

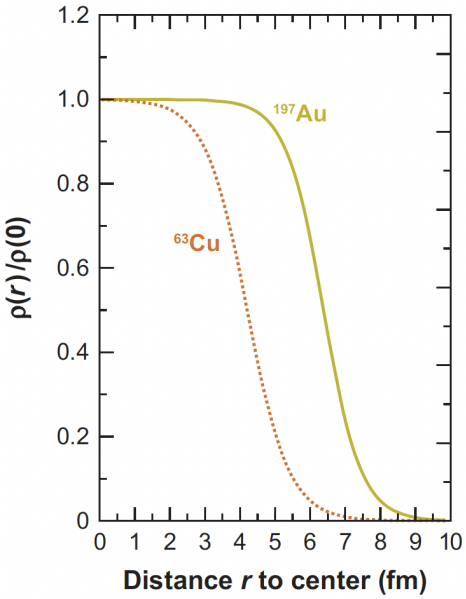

Figure 5.24: Density profiles of nucleons distributed within ^{197}Au and ^{63}Cu nuclei from Ref. [74].

After simulating two gold nuclei by sampling 197 nucleons each according to Eq. (5.4), a nuclear collision is simulated by sampling a random impact parameter. The nucleon+nucleon inelastic cross section is used to assign an effective size to each nucleon in the Glauber simulation. These inelastic scattering cross sections are informed by data from the Particle Data Group [76], shown in Fig. 5.25. These data were fit as described in Ref. [77]. In order to extract the nucleon+nucleon inelastic cross sections, the total and elastic cross sections were fit. The inelastic cross section was taken to be the difference between the total and elastic cross sections. The values for the inelastic cross sections at each fixed-target energy are in Table 5.6.

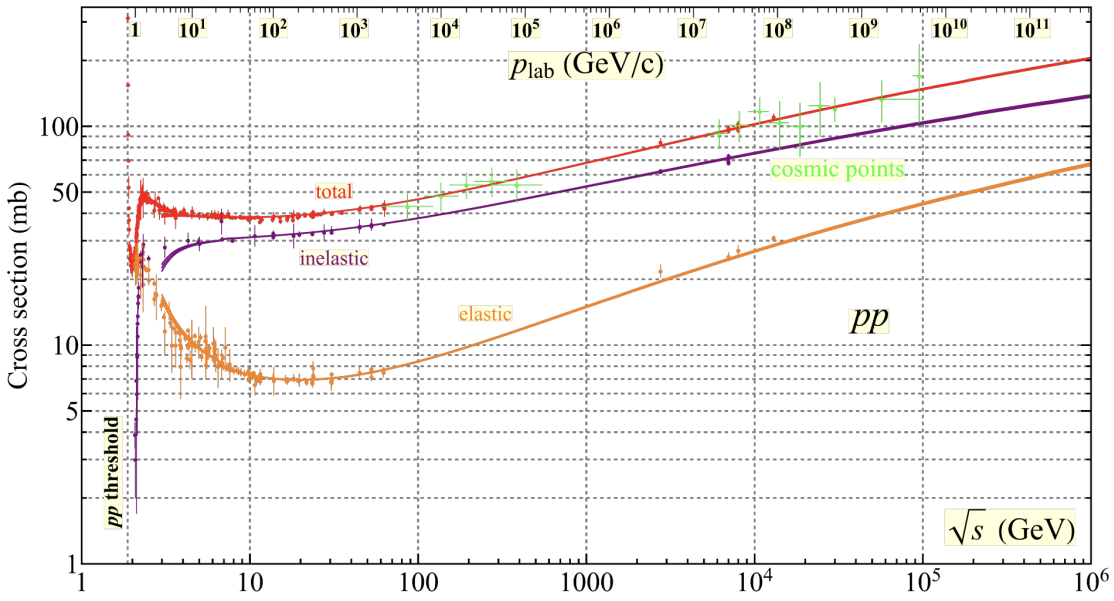

Figure 5.25: Elastic, inelastic, and total pp scattering cross sections from Ref. [76].

Table 5.6: Extracted values of the nucleon+nucleon inelastic cross sections at STAR fixed-target energies.

$\sqrt{s_{NN}}$ (GeV)	$\sigma_{\rm inel}$ (mb)
3.0	28.1 ± 0.2
3.2	28.0 ± 0.2
3.5	28.17 ± 0.15
3.9	28.50 ± 0.11
4.5	29.00 ± 0.08
5.2	29.50 ± 0.07
6.2	30.02 ± 0.06
7.2	30.39 ± 0.05

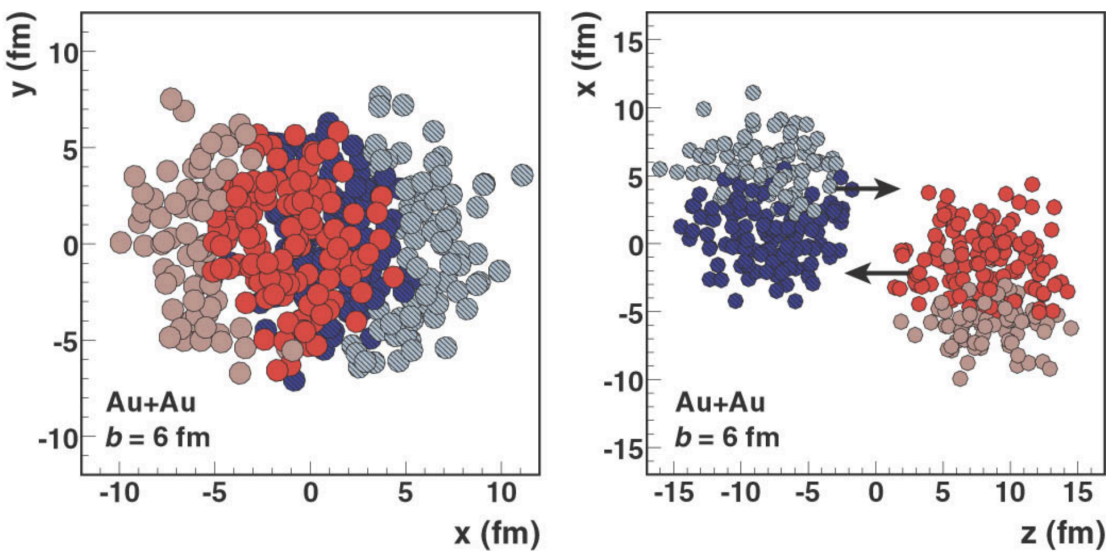

Figure 5.26: Glauber model overlap of two colliding gold nuclei in the plane transverse to the beam direction (left), and in the plane including the beam direction (right) from Ref. [74].

A Glauber model simulation of a nuclear collision is shown in Fig. 5.26. One nucleus is shown in red and the other in blue. After overlapping the nuclei according to a random impact parameter, each nucleon in one nucleus is compared with each nucleon in the other to determine if they overlap, and therefore undergo an inelastic collision. Those nucleons that undergo an inelastic collision are colored with a bright red and blue in Fig. 5.26. These nucleons that undergo inelastic collisions are referred to as "participants" in the collision. For each nuclear collision, we can count the number of participant nucleons, $N_{\rm part}$. However, a nucleon in one nucleus might undergo inelastic collisions with multiple nucleons in the other nucleus. Each subsequent collision can also contribute to particle production, so it is not only important to tabulate $N_{\rm part}$, but the number of binary nucleon+nucleon collisions as well, $N_{\rm coll}$.

5.3.4.2 Simulated Multiplicity Distributions Compared with Data

Distributions for the number of participating nucleons, $N_{\rm part}$, and number of binary collisions, $N_{\rm coll}$ are simulated in the Glauber model. The second part of the simulation is a particle production model which uses a Negative Binomial Distribution (NBD) to randomly produce particles. The probability of generating n particles for any given sampling is given by

$$P(\mu, k; n) = \frac{\Gamma(n+k)}{\Gamma(n+1)\Gamma(k)} \cdot \frac{(\mu/k)^n}{(1+\mu/k)^{n+k}}. \tag{5.5}$$

For each simulated Au+Au collision, the NBD is sampled m times, where

$$m = xN_{\rm coll} + (1-x)\frac{N_{\rm part}}{2}, \tag{5.6}$$

and x is the hardness parameter, which determines the contributions of hard collisions ($x \sim 1$) which scale with $N_{\rm coll}$ unlike the soft collisions ($x \sim 0$) which scale with $N_{\rm part}/2$.

This is a four-parameter problem with x; the two NBD parameters: μ, related to the mean, and k, related to the shape of the distribution; and one additional parameter d. The d parameter adds an additional multiplicity dependence by simulating a multiplicity-dependent efficiency: $\varepsilon = 0.98(1 - d * \text{mult}/540)$. This d parameter is standard in STAR's centrality code, and is generally left as a free parameter between 0 and ≈ 0.2. If $d = 0$ then the multiplicity is moderated by a uniform efficiency factor of 0.98. If $d = 0.1$ then the multiplicity distribution is moderated by an efficiency that drops linearly from 0.98 at 0 multiplicity to 0.88 at a multiplicity of 540.

The multiplicity distributions are fit by sampling these four parameters in a $10 \times 10 \times 10 \times 10$ uniform grid. The multiplicity distribution from the Glauber model is simulated for each sample. After simulating, the multiplicity distribution is normalized to the data, and the χ^2/ndf is calculated. The normalization and χ^2/ndf calculation exclude the low-multiplicity region where the trigger inefficiency drives the data lower than the Glauber distribution.

The fit ranges were determined at each energy. These fit ranges and the fits are shown in Fig. 5.27. The multiplicity distribution from the data is shown in black and the multiplicity from the Glauber simulation is in red. The centrality cuts for 0-5%, 5-10%, 10-20%, 20-30%, 30-40%, 40-50%, and 50-60% are displayed as vertical dashed lines. The resulting Glauber parameters and χ^2/ndf values are tabulated in Table 5.7.

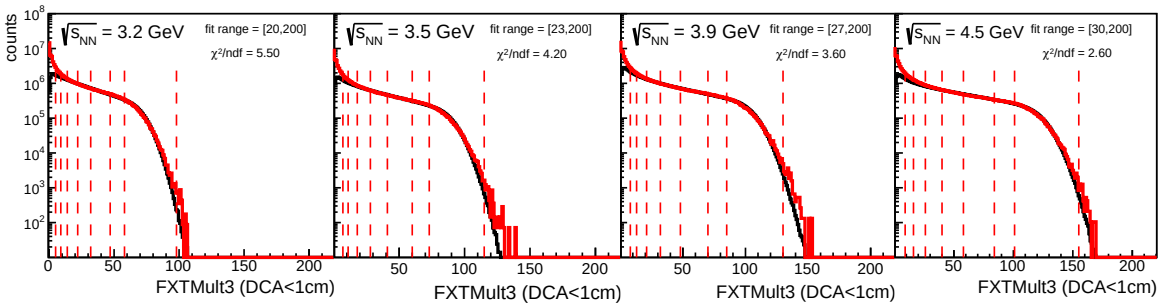

Figure 5.27: Multiplicity distributions (excluding protons) of charged tracks with DCA $<$ 1 cm, superimposed with the Glauber fit (in red). Centrality cuts are represented as vertical red bars.

Table 5.7: Glauber+negative-binomial fit parameters and χ^2/ndf for each fit.

Glauber fit parameters

$\sqrt{s_{NN}}$ (GeV)	μ	k	x	d	χ^2/ndf
3.2	0.272 ± 0.009	44.6 ± 4.5	0.12 ± 0.02	0.16 ± 0.02	5.5
3.5	0.361 ± 0.020	28.2 ± 4.5	0.10 ± 0.02	0.08 ± 0.02	4.2
3.9	0.400 ± 0.012	28.2 ± 4.5	0.12 ± 0.02	0.06 ± 0.02	3.6
4.5	0.511 ± 0.018	22.8 ± 4.5	0.10 ± 0.02	0.17 ± 0.02	2.6

5.3.4.3 Centrality Cuts

The centrality cuts for 3.2 GeV as well as the average N_{part} and N_{coll} values are in Table 5.8. The $\langle N_{\text{coll}} \rangle$ is not used in this analysis, but is included here for completeness. The $\langle N_{\text{part}} \rangle$ is only used when plotting the cumulants in centrality bins as a function of $\langle N_{\text{part}} \rangle$. The values of these do not affect the calculation of the cumulants in any way. The centrality classes for 3.5 GeV are shown in Table 5.9, those for 3.9 GeV in Table 5.10 and for 4.5 GeV in Table 5.11.

Centrality Classes for 3.2 GeV

Centrality	FXTMult3 Range	$\langle N_{\text{part}} \rangle$	$\langle N_{\text{coll}} \rangle$
0–5%	500–58	326.2±0.2	695±30
5–10%	57–47	285±5	581±21
10–20%	46–32	224±10	425±25
20–30%	31–22	160±10	275±22
30–40%	21–14	112±10	172±21
40–50%	13–9	76±10	104±19
50–60%	8–5	50±9	60±13

Table 5.8: Centrality cuts for 3.2 GeV with associated $\langle N_{\text{part}} \rangle$ and $\langle N_{\text{coll}} \rangle$.

Centrality Classes for 3.5 GeV

Centrality	FXTMult3 Range	$\langle N_{\text{part}} \rangle$	$\langle N_{\text{coll}} \rangle$
0–5%	500–73	327.8±2.1	703±30
5–10%	72–60	286±5	587±22
10–20%	59–41	224±8	428±21
20–30%	40–28	159±11	274±25
30–40%	27–18	111±11	170±22
40–50%	17–11	74±10	100±18
50–60%	10–7	49±8	58±13

Table 5.9: Centrality cuts for 3.5 GeV with associated $\langle N_{\text{part}} \rangle$ and $\langle N_{\text{coll}} \rangle$.

Centrality Classes for 3.9 GeV

Centrality	FXTMult3 Range	$\langle N_{\text{part}} \rangle$	$\langle N_{\text{coll}} \rangle$
0–5%	500–85	329.7±1.9	715±29
5–10%	84–70	287±5	594±19
10–20%	69–48	226±8	435±21
20–30%	47–32	160±10	276±24
30–40%	31–21	111±11	171±22
40–50%	20–13	75±11	102±20
50–60%	12–8	49±10	59±16

Table 5.10: Centrality cuts for 3.9 GeV with associated $\langle N_{\text{part}} \rangle$ and $\langle N_{\text{coll}} \rangle$.

Centrality Classes for 4.5 GeV

Centrality	FXTMult3 Range	$\langle N_{\text{part}} \rangle$	$\langle N_{\text{coll}} \rangle$
0–5%	500–101	330.8±1.8	728±30
5–10%	100–84	287±6	603±21
10–20%	83–58	225±8	438±21
20–30%	57–40	160±10	280±24
30–40%	39–26	112±10	174±21
40–50%	25–16	74±9	101±17
50–60%	15–9	46±8	55±13

Table 5.11: Centrality cuts for 4.5 GeV with associated $\langle N_{\text{part}} \rangle$ and $\langle N_{\text{coll}} \rangle$.

Chapter 6

Analysis Corrections

The high-order cumulants are corrected for efficiency, centrality-bin width, and pileup contamination (when TOF is not used in the analysis). Any correction to the high-order cumulants must be understood up to the sixth-order cumulant if we are to apply it here. The impact of many corrections might be trivial at first order, but cannot be used in high-moments analyses. For example, the impact of finite proton purity on C_1 is trivial if the purity is known. However, in order to understand how, for example, pion contamination affects the sixth-order cumulant of the proton-number distribution, one would need to understand pion-number cumulants up to sixth order. This is extremely nontrivial and could in principle be calculated using a model such as UrQMD. This makes the measurement model-dependent, and the assumption that models can reproduce pion-number high-order cumulants has not been confirmed. We therefore correct for efficiency, centrality bin width, and pileup contamination, because these corrections are well understood at high orders. Other effects like impurity and limited acceptance are unknown unknowns. The measurement should be understood, not simply as a measurement of the proton-number cumulants, but as a measurement of the proton-number cumulants given a $\sim 95\%$ purity and the acceptance gaps discussed in Chapter 5.

6.1 Efficiency Corrections

A track-by-track efficiency is used in the analysis of proton high-order moments. In this track-by-track efficiency, the efficiency is evaluated based on the proton lab-frame rapidity (or pseudorapidity) and its p_T. In the fixed-target configuration, it is important to specify that the efficiencies are determined in the lab frame because the center-of-mass frame shifts with the beam energy, so evaluating efficiencies in the lab frame makes these efficiencies relatively independent of the beam energy. In principle, the only dataset dependence of the lab frame efficiencies is due to changing detector configurations, or is part of a multiplicity dependence of the efficiency. For these reasons, the efficiencies were calculated for each dataset. Embedding simulations are used to calculate the TPC proton identification efficiency. To evaluate the efficiency of TOF PID, we use the rate at which TPC tracks have a TOF-match to determine the TOF-matching efficiency.

6.1.1 Efficiency Correction Methodology

The methodology for applying efficiency corrections to the proton cumulants is detailed in Ref. [41]. We use the track-by-track efficiency method discussed in the reference. We summarize the main points from the paper here. The method expresses the m-th order cumulants C_m in terms of their cumulant generating function $K(\theta) = \ln\langle e^{N\theta}\rangle$

$$C_m = \langle N^m \rangle_c = \frac{\partial^m}{\partial \theta^m} K(\theta)\Big|_{\theta=0}. \tag{6.1}$$

We may also express m-th order factorial cumulants FC_m in terms of their own generating function $K_f(s) = \ln\langle s^N\rangle$

$$FC_m = \langle N^m \rangle_{fc} = \frac{\partial^m}{\partial \theta^m} K_f(s)\Big|_{s=1}. \tag{6.2}$$

Cumulants can be expressed in terms of factorial cumulants,

$$\langle N\rangle_c = \langle N\rangle_{fc} \tag{6.3}$$

$$\langle N^2\rangle_c = \langle N^2\rangle_{fc} + \langle N\rangle_{fc} \tag{6.4}$$

$$\langle N^3\rangle_c = \langle N^3\rangle_{fc} + 3\langle N^2\rangle_{fc} + \langle N\rangle_{fc} \tag{6.5}$$

$$\langle N^4\rangle_c = \langle N^4\rangle_{fc} + 6\langle N^3\rangle_{fc} + 7\langle N^2\rangle_{fc} + \langle N\rangle_{fc} \tag{6.6}$$

$$\langle N^5\rangle_c = \langle N^5\rangle_{fc} + 10\langle N^4\rangle_{fc} + 25\langle N^3\rangle_{fc} + 15\langle N^2\rangle_{fc} + \langle N\rangle_{fc} \tag{6.7}$$

$$\langle N^6\rangle_c = \langle N^6\rangle_{fc} + 15\langle N^5\rangle_{fc} + 65\langle N^4\rangle_{fc} + 90\langle N^3\rangle_{fc} + 31\langle N^2\rangle_{fc} + \langle N\rangle_{fc}. \tag{6.8}$$

Likewise factorial cumulants can be expressed in terms of cumulants

$$\langle N\rangle_{fc} = \langle N\rangle_c \tag{6.9}$$

$$\langle N^2\rangle_{fc} = \langle N^2\rangle_c - \langle N\rangle_c \tag{6.10}$$

$$\langle N^3\rangle_{fc} = \langle N^3\rangle_c - 3\langle N^2\rangle_c + 2\langle N\rangle_c \tag{6.11}$$

$$\langle N^4\rangle_{fc} = \langle N^4\rangle_c - 6\langle N^3\rangle_c + 11\langle N^2\rangle_c - 6\langle N\rangle_c \tag{6.12}$$

$$\langle N^5\rangle_{fc} = \langle N^5\rangle_c - 10\langle N^4\rangle_c + 35\langle N^3\rangle_c - 50\langle N^2\rangle_c + 24\langle N\rangle_c \tag{6.13}$$

$$\langle N^6\rangle_{fc} = \langle N^6\rangle_c - 15\langle N^5\rangle_c + 85\langle N^4\rangle_c - 225\langle N^3\rangle_c + 274\langle N^2\rangle_c - 120\langle N\rangle_c. \tag{6.14}$$

Under the assumption of a binomial detector response with efficiency p, the binomial distribution relates the true number of particles, N, and the observed number of particles, n by

$$B_{p,N}(n) = \frac{N!}{n!(N-n)!}p^n(1-p)^{N-n}. \tag{6.15}$$

This is the probability of observing n particles when the true number is N, when the efficiency of detecting any given particle is given by p. This binomial response has a known cumulant generating function which can be used to correct the factorial cumulants in a predictable way. The binomial cumulant generating function can be used to demonstrate that the true

and observed factorial cumulants are related to the efficiency by

$$\langle n^m \rangle_{fc} = p^m \langle N^m \rangle_{fc}. \tag{6.16}$$

We can thus relate the true and measured cumulants by first expressing the true cumulants in terms of true factorial cumulants, then using the above equation to express the true cumulants in terms of the measured factorial cumulants and efficiencies, and finally expressing the true cumulants in terms of the measured cumulants and efficiencies.

When using a track-by-track efficiency, in which the efficiency is evaluated for each track according to its kinematics, the cumulant generating function for the detector response must involve the product over all tracks of binomial detector efficiency responses. The calculation involving this product is detailed in Ref. [41], and the result relates the true cumulants to observed particle numbers and track-by-track efficiencies. The relations up to fourth order are

$$\langle N \rangle_c = \langle q_{(1,1)} \rangle_c \tag{6.17}$$

$$\langle N^2 \rangle_c = \langle q^2_{(1,1)} \rangle_c + \langle q_{(2,1)} \rangle_c - \langle q_{(2,2)} \rangle_c \tag{6.18}$$

$$\begin{aligned} \langle N^3 \rangle_c = {} & \langle q^3_{(1,1)} \rangle_c + 3\langle q_{(1,1)} q_{(2,1)} \rangle_c - 3\langle q_{(1,1)} q_{(2,2)} \rangle_c \\ & + \langle q_{(3,1)} \rangle_c - 3\langle q_{(3,2)} \rangle_c + 2\langle q_{(3,3)} \rangle_c \end{aligned} \tag{6.19}$$

$$\begin{aligned} \langle N^4 \rangle_c = {} & \langle q^4_{(1,1)} \rangle_c + 6\langle q^2_{(1,1)} q_{(2,1)} \rangle_c - 6\langle q^2_{(1,1)} q_{(2,2)} \rangle_c \\ & + 4\langle q_{(1,1)} q_{(3,1)} \rangle_c + 3\langle q^2_{(2,1)} \rangle_c + 3\langle q^2_{(2,2)} \rangle_c \\ & - 12\langle q_{(1,1)} q_{(3,2)} \rangle_c + 8\langle q_{(1,1)} q_{(3,3)} \rangle_c - 6\langle q_{(2,1)} q_{(2,2)} \rangle_c \\ & + \langle q_{(4,1)} \rangle_c - 7\langle q_{(4,2)} \rangle_c + 12\langle q_{(4,3)} \rangle_c - 6\langle q_{(4,4)} \rangle_c, \end{aligned} \tag{6.20}$$

where

$$q_{(r,s)} = \sum_{i=1}^{M} (a_i^r / p_i^s) n_i. \tag{6.21}$$

This is a sum over M bins of phase space with distinct efficiencies. In each bin, the number of protons detected is n_i, and the detection efficiency is p_i. For protons, $a_i = 1$, and for antiprotons, $a_i = -1$. Only protons are used in this analysis, so this simplifies to

$$q_s = \sum_{i=1}^{M} (1/p_i^s) n_i. \tag{6.22}$$

Using this, the relations simplify to

$$\langle N \rangle_c = \langle q_1 \rangle_c \tag{6.23}$$

$$\langle N^2 \rangle_c = \langle q_1^2 \rangle_c + \langle q_1 \rangle_c - \langle q_2 \rangle_c \tag{6.24}$$

$$\langle N^3 \rangle_c = \langle q_1^3 \rangle_c + 3\langle q_1^2 \rangle_c - 3\langle q_1 q_2 \rangle_c + \langle q_1 \rangle_c - 3\langle q_2 \rangle_c + 2\langle q_3 \rangle_c \tag{6.25}$$

$$\begin{aligned} \langle N^4 \rangle_c = {} & \langle q_1^4 \rangle_c + 6\langle q_1^3 \rangle_c - 6\langle q_1^2 q_2 \rangle_c + 7\langle q_1^2 \rangle_c + 3\langle q_2^2 \rangle_c \\ & - 18\langle q_1 q_2 \rangle_c + 8\langle q_1 q_3 \rangle_c + \langle q_1 \rangle_c - 7\langle q_2 \rangle_c + 12\langle q_3 \rangle_c - 6\langle q_4 \rangle_c. \end{aligned} \tag{6.26}$$

6.1.2 TPC Proton-PID Efficiency

The track-by-track efficiency of TPC-identified protons is based on STAR's embedding procedure. In this procedure, Monte Carlo tracks of the particle of interest are embedded into real events and passed through the TPC simulation and reconstruction algorithm. This way, the tracks are embedded into events with vertices, multiplicities, and active readout configurations identical to those in the analysis. The efficiency is then calculated as the fraction of those tracks that are successfully reconstructed and pass track-level cuts. The TPC simulator and reconstruction include the same track-level variables on the Monte Carlo tracks as the data tracks. So if an nHitsFit cut of 20 is applied to the data, then this cut should also be included in the embedding efficiency calculation. It is known that the embedding procedure used by STAR does not perfectly reproduce the distributions of quantities like nHitsFit and DCA, so a systematic uncertainty on the efficiency correction was included. This is discussed in Sec. 7.2.

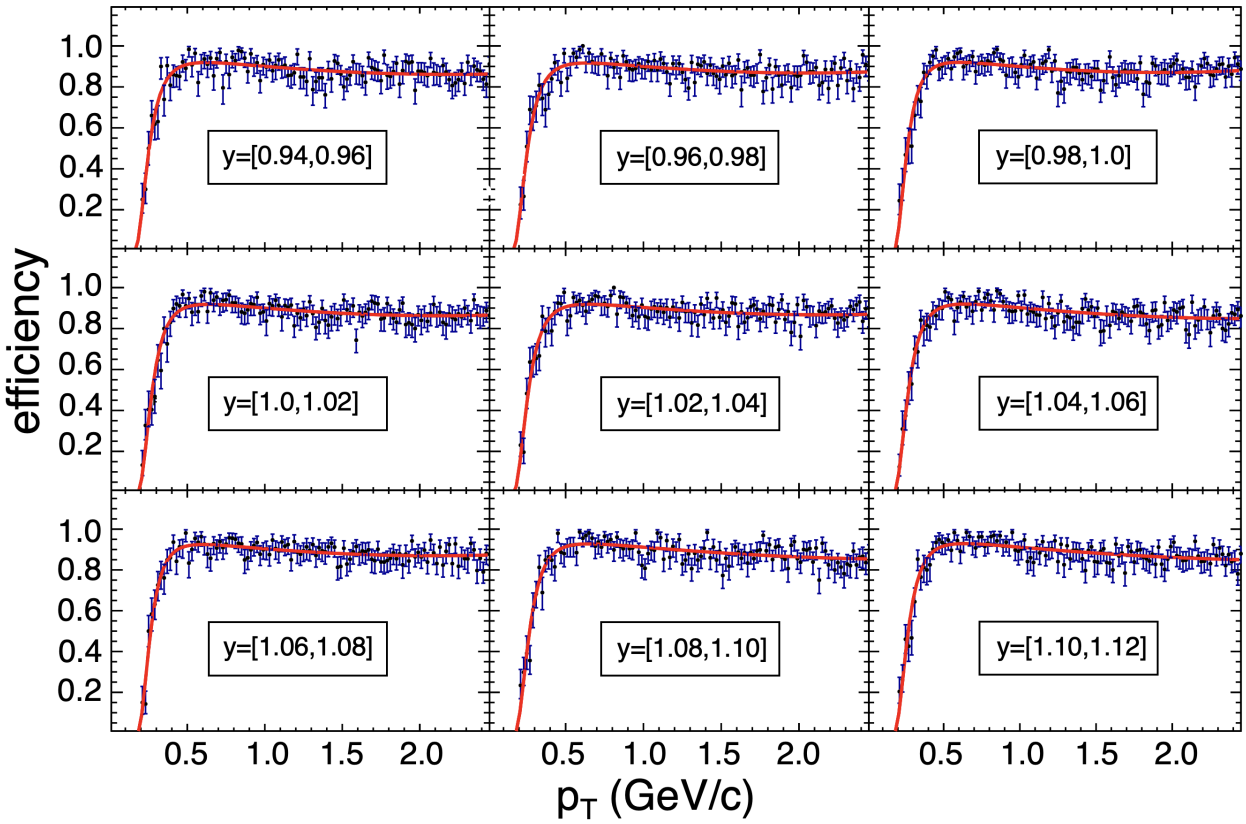

Figure 6.1: Tracking efficiencies as a function of p_T in steps of size 0.02 in lab rapidity at $\sqrt{s_{NN}} = 3.2$ GeV.

For this analysis, embedded protons were sampled uniformly over all azimuth, uniformly in p_T from 0 to 2.5 GeV, and uniformly in η from 0 to 2.4. Three protons were embedded per event, and these protons were embedded into one million events sampled from the lists of good runs. This embedding was done at 3.2, 3.5, 3.9, and 4.5 GeV each due to the different active readout configurations in each dataset. The fractions of embedded protons that were successfully reconstructed and passed the track-level cuts are shown in Fig. 6.1. This figure is from embedding at $\sqrt{s_{NN}} = 3.2$ GeV, but the efficiency was calculated independently at each energy. These efficiencies ϵ are calculated as a function of p_T and sampled in bins of width 0.02 in the lab-frame rapidity.

The efficiencies as a function of p_T are fit with the functional form

$$\epsilon = a_0 \exp(-a_1 p_T^{-a_2}) + a_3 p_T + a_4 p_T^2. \tag{6.27}$$

The resulting fits are shown as red curves in Fig. 6.1. These curves were stored for each rapidity window, at each energy, and for each set of track-level cuts. When nonstandard track-level cuts were used in the systematic uncertainty calculations, the efficiencies were recalculated with the corresponding cuts.

6.1.3 Time-of-flight Matching Efficiency

The TOF-matching efficiencies are calculated using a data-driven methodology. Tracks are first required to meet the DCA, nHitsFit, nHitsDedx, and nHitsRatio requirements used in the analysis. Then tracks that are identified as not being protons are rejected by ignoring those with $|n\sigma| > 3$. Importantly, this cut allows high momentum deuterons, kaons, and pions into the calculation. This means that the TOF-matching efficiencies must be expressed in terms of pseudorapidity instead of rapidity because a calculation in terms of rapidity would require an assumption of the particle mass.

From this point, the fraction of tracks with a TOF-match and positive m^2 was calculated. Cuts on BTOF y_{local}, z_{local}, and ETOF Δx and Δy were included in the calculation. The efficiency calculation was performed after masking the same ETOF counters that were masked in the analysis. The m^2 cut of $0.6 < m^2 < 1.2$ GeV^2 introduces an additional inefficiency but this cut cannot be included at this stage because when pion, kaon, and deuteron contamination become significant, their inclusion in the denominator of the TOF-matching ratio would appear to drive the matching efficiency artificially low. The resulting TOF-matching efficiencies at $\sqrt{s_{NN}} = 3.2$ GeV are shown in Fig. 6.2 as a function of p_T in various pseudorapidity windows. These efficiencies were calculated independently at each energy. The

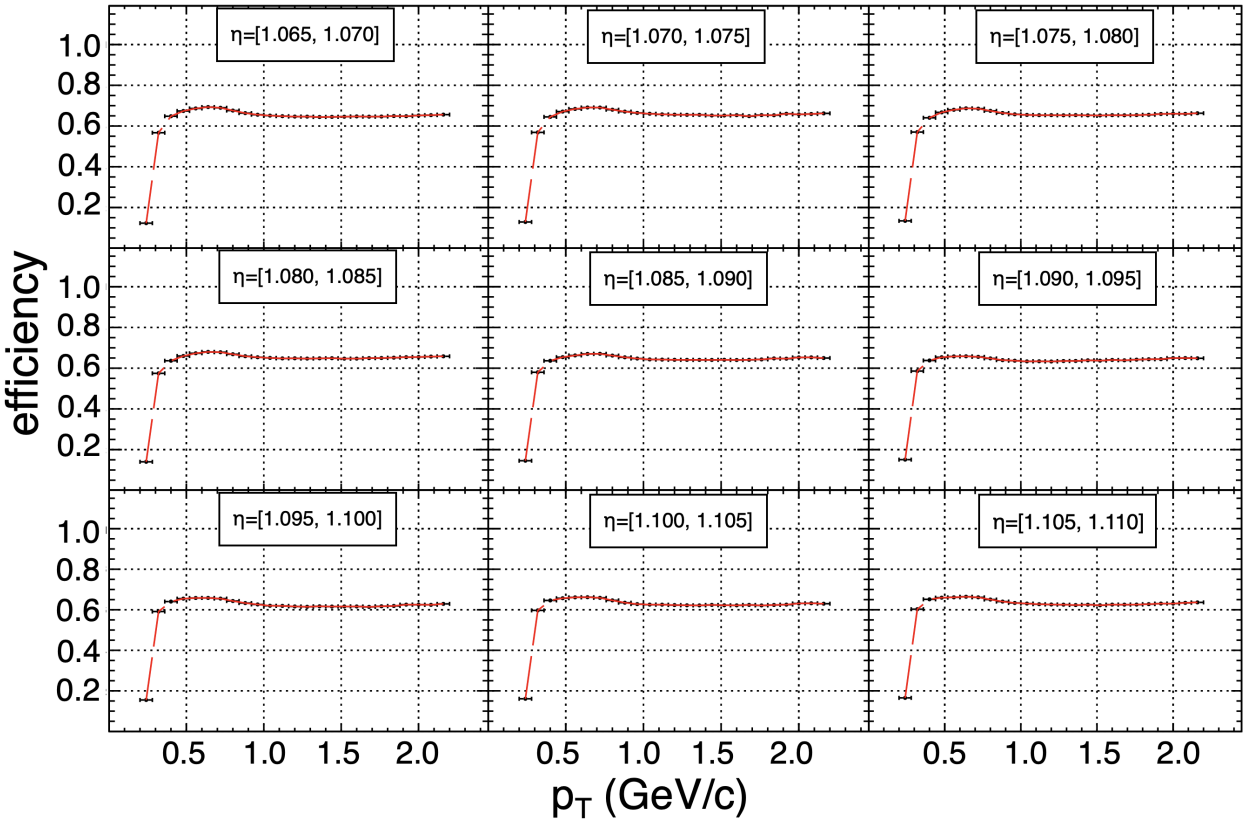

Figure 6.2: TOF-matching efficiencies at $\sqrt{s_{NN}} = 3.2$ GeV as a function of p_T in steps of size 0.005 in pseudorapidity.

points fluctuate much less than those efficiencies determined by the embedding procedure. Instead of a fit, a linear interpolation (shown in red) between points is used.

The inefficiency introduced by the m^2 cut is calculated separately. As shown in Fig. 6.3, the m^2 bands broaden with increasing momentum and protons increasingly fall outside the static $0.6 < m^2 < 1.2$ GeV^2 bands. This introduces an additional inefficiency for TOF-matched particles for both the ETOF and BTOF. Because the two detectors have slightly different timing resolutions, the impact of this effect was calculated independently for each detector.

The inefficiencies introduced by the m^2 cut are shown in Fig. 6.4. Efficiencies for BTOF

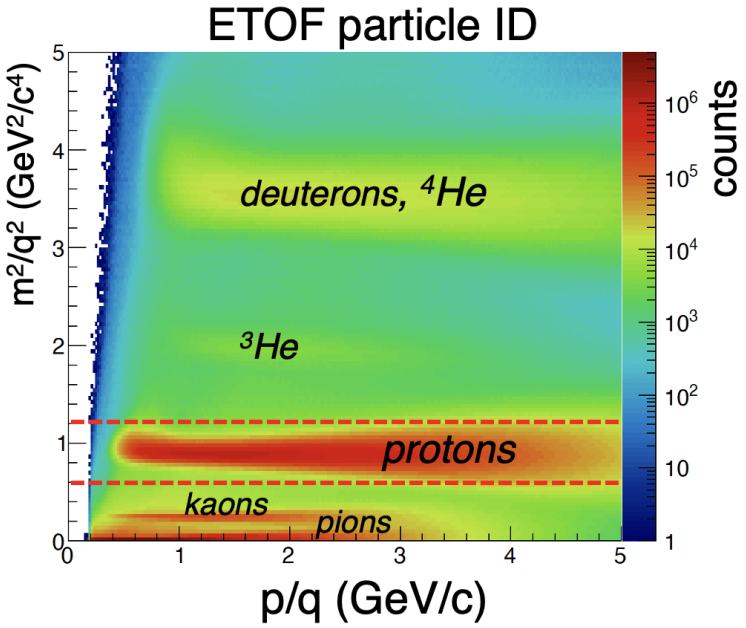

Figure 6.3: ETOF m^2/q^2 bands as a function of p/q and default cuts shown as red dashed lines. For protons, π^+, and k^+, the charge number q is 1 and the plot shows the m^2 as a function of momentum.

are shown as shades of red. Efficiencies for ETOF are shown as shades of blue. In addition to the default $0.6 < m^2 < 1.2$ GeV^2 cut, the cuts used in the systematic uncertainty calculation are also included. At low momenta, the efficiencies are near 100% because the m^2 peak is narrow. As the peak broadens at high momenta, the efficiency drops. The BTOF efficiency is slightly enhanced relative to the ETOF efficiency. The default m^2 cut has the highest efficiency compared to the variations on the cut introduced in the systematic uncertainties.

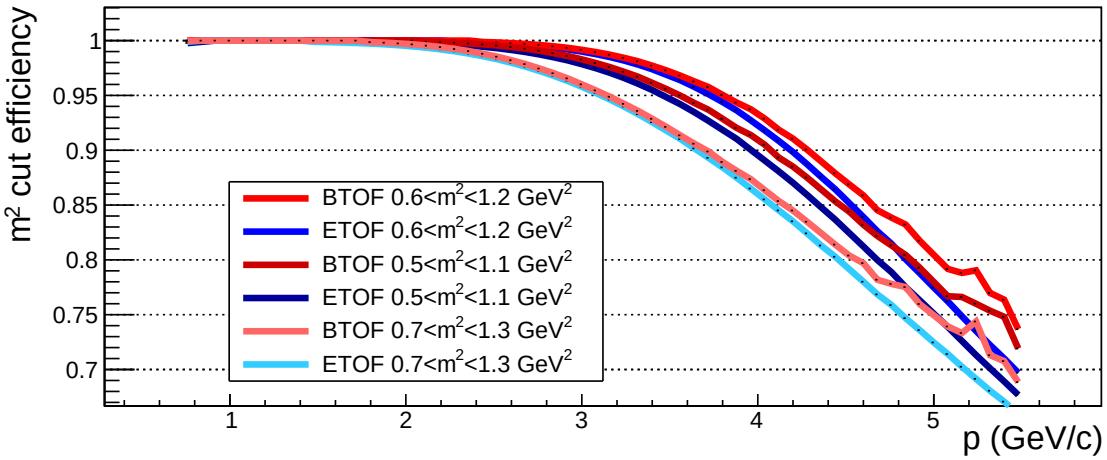

Figure 6.4: Additional inefficiency introduced by TOF m^2 cuts as a function of momentum. Efficiencies for BTOF are shown as shades of red. Efficiencies for ETOF are shown as shades of blue. In addition to the default $0.6 < m^2 < 1.2$ GeV^2 cut, the cuts used in the systematic uncertainty calculation are also included.

6.2 Centrality-Bin-Width Correction

The proton-number cumulants are often expressed in 5 to 10% centrality bins. This analysis groups the cumulants into centrality bins of 0-5%, 5-10%, 10-20%, 20-30%, 30-40%, 40-50%, and 50-60%. The centrality-bin-width correction (CBWC) outlined in Ref. [78] is applied. This correction accounts for the variation of cumulants from one multiplicity to the next within the same centrality bin. It expresses the cumulants in each centrality bin as a weighted average of the cumulants from each multiplicity within the centrality bin. The cumulants at each multiplicity are weighted by the number of events with that multiplicity. The cumulants in each centrality bin are then given by the expression

$$C_n = \frac{\sum_m N_m C_n^m}{\sum_m N_m} = \sum_m w_m C_n^m. \tag{6.28}$$

In the above expression, we sum over each multiplicity m within the given centrality bin. N_m is the number of events at each multiplicity, and C_n^m is the n^{th}-order cumulant of the proton-number distribution with multiplicity m. On the right-hand side, the division by the total number of events in the centrality bin is brought inside the summation, turning the multiplicative factor on the cumulants into a weight w_m applied to each multiplicity.

Initial-volume fluctuations (IVF) are fluctuations imprinted on the proton-number distributions by the imperfect mapping between the number of participant nucleons (N_{part}) and multiplicity. We are not able to make cuts on collisions by their N_{part}, so the best we can do is cut on event multiplicity with the hope that this is strongly correlated with N_{part}. The centrality-bin-width correction outlined here makes the cumulants less sensitive to multiplicity-binning effects, and reduces the impact of initial-volume fluctuations on the final result.

6.3 Pileup Correction

At 3.2 GeV, in-bucket pileup events were left in the analysis and corrected for. In STAR's previously-published $\sqrt{s_{NN}} = 3$ GeV analysis, the pileup rate was 0.46% [44, 45] and the cumulants were corrected for this. The correction was made using an unfolding method [46, 47] which assumes that a pileup event is a sum of two individual collisions, as seen by the detector. When a time-of-flight detector is used in the analysis, this assumption is invalid. At 3.2 GeV, we use only the TPC for both PID and multiplicity measurements, so the pileup correction may be applied.

The pileup correction detailed in Ref. [46] constructs the probability distribution of observing N protons given an event of multiplicity m

$$P_m(N) = (1 - \alpha_m)P_m^{\mathrm{t}}(N) + \alpha_m P_m^{\mathrm{pu}}(N), \tag{6.29}$$

where $P_m^{\mathrm{t}}(N)$ is the probability of observing N protons given a multiplicity m for a true single collision, $P_m^{\mathrm{pu}}(N)$ is the same probability for a pileup event, and $_m$ is the pileup fraction at multiplicity m. The pileup probability distribution $P_m^{\mathrm{pu}}(N)$ can be expressed in terms of the probability distributions of two single-collisions with multiplicities i and j, proton numbers N_i and N_j, that satisfy $m = i + j$ and $N = N_i + N_j$:

$$P_m^{\mathrm{pu}}(N) = \sum_{i,j} \left[\delta_{m,i+j} w_{i,j} \Big[\sum_{N_i,N_j} \delta_{N,N_i+N_j} P_i^{\mathrm{t}}(N_i) P_j^{\mathrm{t}}(N_j) \Big] \right], \tag{6.30}$$

where $w_{i,j}$ is the probability, given a pileup event, of observing subevent i in coincidence with subevent j.

It is shown in Ref. [46] that the r^{th}-order cumulants ($\langle N^r \rangle_c$) of these subevents can be straightforwardly expressed as a sum of the true cumulants of the constituent collisions

$$\langle N^r \rangle_{i,j,c}^{\mathrm{sub}} = \langle N^r \rangle_{i,c}^{\mathrm{t}} + \langle N^r \rangle_{j,c}^{\mathrm{t}}. \tag{6.31}$$

Therefore the cumulants of the measured proton number at multiplicity m are made up of a sum of the true cumulants of pileup events which have multiplicities summing to equal

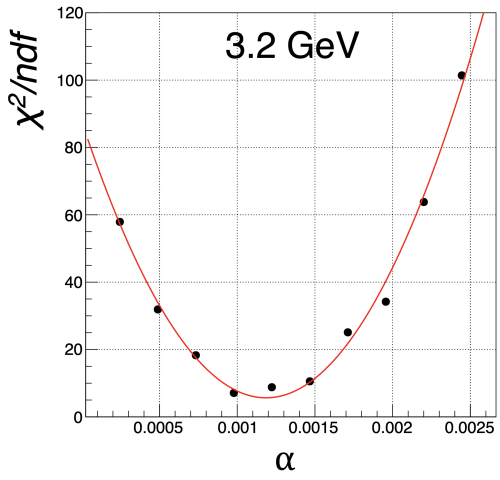

Figure 6.5: The χ^2/ndf after unfolding, for several values of the pileup rate α. The χ^2/ndf is fit with a parabola (red curve) to extract the best pileup rate.

m. The true cumulants can be extracted from the measured cumulants, after applying some additional relations detailed in Ref. [46] as

$$\langle N^r \rangle_m^{\mathrm{t}} = \frac{\langle N^r \rangle_m - \alpha_m C_m^{(r)}}{1 - \alpha_m + 2\alpha_m w_{m,0}}, \tag{6.32}$$

with

$$C_m^{(r)} = \mu_m^{(r)} + \sum_{i,j} \delta_{m,i+j} w_{i,j} \langle N_{i,j}^r \rangle. \tag{6.33}$$

The extraction of the true cumulants from the measured cumulants is a recursive process using these equations. First $\langle N \rangle_0^{\mathrm{t}}$ is calculated as $\langle N \rangle_0^{\mathrm{t}} = \langle N \rangle_0 / (1 + \alpha_0)$, because $m = 0$ has no pileup contribution. Then we move to $m = 1$ and construct $C_1^{(1)}$, as in Eq. (6.33), from subevents with moments $\langle N \rangle_0^{\mathrm{t}}$. After constructing $C_1^{(1)}$, we calculate $\langle N \rangle_1^{\mathrm{t}}$. We then move to $m = 2$ and construct $C_2^{(1)}$ with contributions from $\langle N \rangle_0^{\mathrm{t}}$ and $\langle N \rangle_1^{\mathrm{t}}$, weighted by $w_{i,j}$. This continues, reconstructing the true moments at multiplicity m from combinations of already-reconstructed moments at lower multiplicities. This is a mostly data-driven algorithm, but does depend on estimations of α_m and $w_{i,j}$.

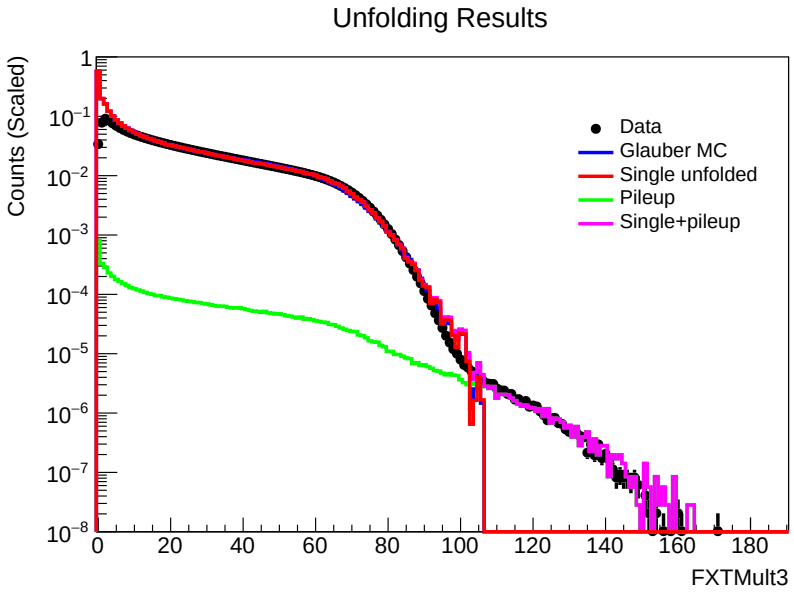

Figure 6.6: The data compared against the unfolded multiplicity distribution, and the estimated pileup multiplicity distribution.

The first step toward estimating α_m and $w_{i,j}$ is to fit the multiplicity distribution with a Glauber model. Next, the unfolding method detailed in Ref. [47] is applied. A total pileup rate α is sampled, for example, $\alpha = 0.2\%$. Then a summed (single+pileup) distribution is constructed by sampling a multiplicity at random from the Glauber simulation with probability $1-\alpha$. Pileup multiplicities are included by sampling twice at random from the Glauber simulation with probability α. The resulting multiplicity distribution resembles the data if the pileup rate was correctly estimated. The χ^2/ndf is calculated in the pileup region (very large multiplicities) in order to determine if the sampled α was a good estimate. These values of the χ^2/ndf for several α rates are shown in Fig. 6.5. The values are fit with a parabola in order to extract the best α and estimate the uncertainties on that value. In this case the pileup rate was determined to be $\alpha = 0.119\% \pm 0.013\%$.

The unfolding is used because the Glauber multiplicity was fit with a multiplicity dis-

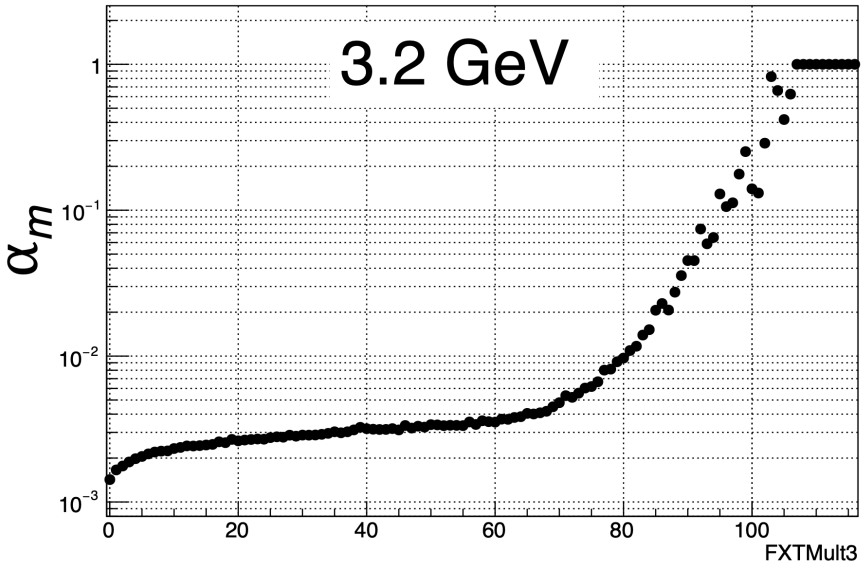

Figure 6.7: The pileup fraction, α_m, at each multiplicity, FXTMult3.

tribution that was contaminated by some low level of pileup, so the Glauber multiplicity is not always a perfect representation of the single-event multiplicity distribution. The effects of pileup on the multiplicity distribution can be reduced through unfolding, wherein, after constructing the summed multiplicity distribution for a given α, the summed simulated multiplicity is compared against the data and the differences between the two are calculated. These differences are used to reweight the single-multiplicity distribution such that, in the next iteration, the summed multiplicity is a closer match to the data. This is done iteratively 50 times. The resulting unfolded multiplicity distribution is shown in Fig. 6.6.

For each multiplicity bin, the pileup fraction, α_m, is shown in Fig. 6.7. The fraction is low at low multiplicities, and rises to 1 at the highest multiplicities. The response matrices resulting from the unfolding procedure are shown in Fig. 6.8. This includes the response matrix for the best pileup rate, as well as the pileup rates systematically high and low used for the systematic uncertainty calculation.

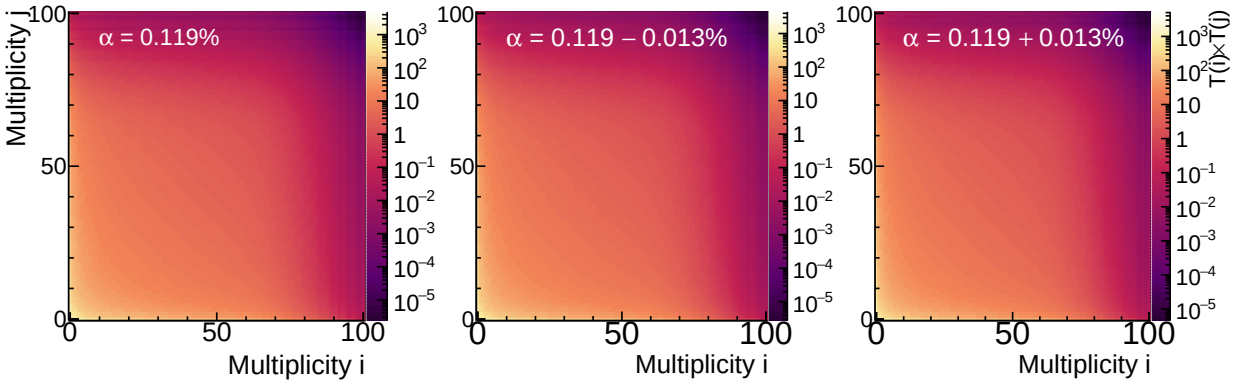

Figure 6.8: Response matrices $w_{i,j}$ for the default pileup rate, and the low and high pileup rates used in the systematic uncertainty calculation.

Chapter 7

Uncertainty Estimation

Statistical and systematic uncertainties were calculated on all orders of cumulants, factorial cumulants, and their ratios. Statistical uncertainties were estimated using a bootstrapping method discussed in Sec. 7.1. Systematic uncertainties were calculated by reasonably varying analysis cuts. This is described in Sec. 7.2. A Barlow check [79] is performed with each systematic variation in order to ensure that the systematic uncertainty is not being needlessly inflated.

7.1 Statistical Uncertainties

Statistical uncertainties on the cumulants and their ratios were determined using the bootstrap method discussed in Ref. [80]. The bootstrap method is performed by randomly sampling events (with replacement) from the entire distribution of events to create a bootstrap sample. The replacement of events means that an event taken for one bootstrap sample can also be used in another bootstrap sample. Take $\hat{e}$ to be the estimator of one of our quantities. For each bootstrap b of N total bootstraps, one recalculates the estimator, obtaining $\hat{e}^*_b$. Considering all of the N bootstraps, a distribution of the estimators is constructed. Then

the variance and uncertainty of the estimator can be constructed. This variance is calculated as:

$$Var(\hat{e}) = \frac{1}{N-1}\sum_{b=1}^{N}(\hat{e}_b^* - \langle\hat{e}^*\rangle)^2, \tag{7.1}$$

where

$$\langle\hat{e}^*\rangle = \frac{1}{N}\sum_{b=1}^{N}\hat{e}_b^*. \tag{7.2}$$

There are several other possible ways to estimate the statistical uncertainties. One of these is using the delta theorem to derive analytical forms for the uncertainties [81, 82]. In the delta theorem, the uncertainty on each cumulant is constructed from measured central moments. For example, the uncertainty on the mean of a proton number distribution constructed from N samples is given by

$$\sigma_{\text{stat}}(C_1) = \sqrt{\frac{\mu_2}{N}}. \tag{7.3}$$

In order to calculate the statistical uncertainty on C_1 using the delta theorem, one needs to calculate the higher-order central moment μ_2. The uncertainty on C_2 of the same distribution is given by

$$\sigma_{\text{stat}}(C_2) = \sqrt{\frac{\mu_4 - \mu_2^2}{N}}. \tag{7.4}$$

Now one needs to calculate the fourth-order central moment in order to determine the uncertainty on C_2. Likewise, in order to calculate the statistical uncertainty on C_6, one needs to measure central moments up to μ_{10}. Another method of estimating the statistical uncertainty is to use subsamples of the dataset to both evaluate the estimator and construct the variance on the estimator [80, 83, 84]. The statistical bootstrap method was chosen over the delta-theorem method because one does not need to measure higher-order central moments than those used in the analysis. The bootstrap method also converges more quickly than the subsample method. The subsample method suffers from larger uncertainties on each estimator because subsamples are formed by sampling from the dataset without replacement [80].

Estimators that require large statistics, such as C_6, may suffer if a 50 million event dataset is split into 50 1 million event subsamples. We therefore use the statistical bootstrap method with $N = 50$ bootstraps in this analysis.

7.2 Systematic Uncertainties

The systematic uncertainties were estimated by varying 8 variables, each in two different ways. The nHitsFit and nHitsDedx cuts were each varied from the default value of 20 up to values of 22 and 25. These were raised from the default value instead of varied in each direction in order to maintain the quality of reconstructed tracks in the systematic uncertainty estimation. The estimated tracking efficiency uncertainty in STAR is nominally 5%. The efficiency was adjusted by the nominal 5% uncertainty so that $\epsilon_{\rm sys} = \epsilon_{\rm norm}(1 \pm 0.05)$. This adjusted efficiency was used to obtain the systematic uncertainty on the efficiency. When the time-of-flight was used for particle identification, the m^2 cuts were adjusted up and down from the default $0.6 < m^2 < 1.2$ GeV^2 to $0.7 < m^2 < 1.3$ GeV^2 and $0.5 < m^2 < 1.1$ GeV^2. The DCA cut was varied by ± 0.1 cm from the default 1 cm cut. The default $|n\sigma_p|$ cut was decreased from 3 to 2.75 and 2.5. The pileup correction was performed using the low and high variations in the pileup rates given by the unfolding method described in Sec. 6.3. When pileup was rejected and not corrected at 3.5, 3.9, and 4.5 GeV, the pileup cuts described in Sec. 5.3.2 were scaled by 5% in FXTMult3. If the pileup cut at a given TOF multiplicity was FXTMult3 < 100, then the systematic variation was to scale this to 95 and 105. Finally the stability of the results with respect to the centrality definition was estimated by varying the centrality cuts by one unit in multiplicity in either direction. The 5-10% cuts at 3.2 GeV, for example were changed from the default 47-57 to 46-56 and 48-58. The use of more restrictive cuts in the systematic uncertainty analysis results in analyses of slightly different subsets of the data. Any variation observed in a systematic study might be attributable to sampling

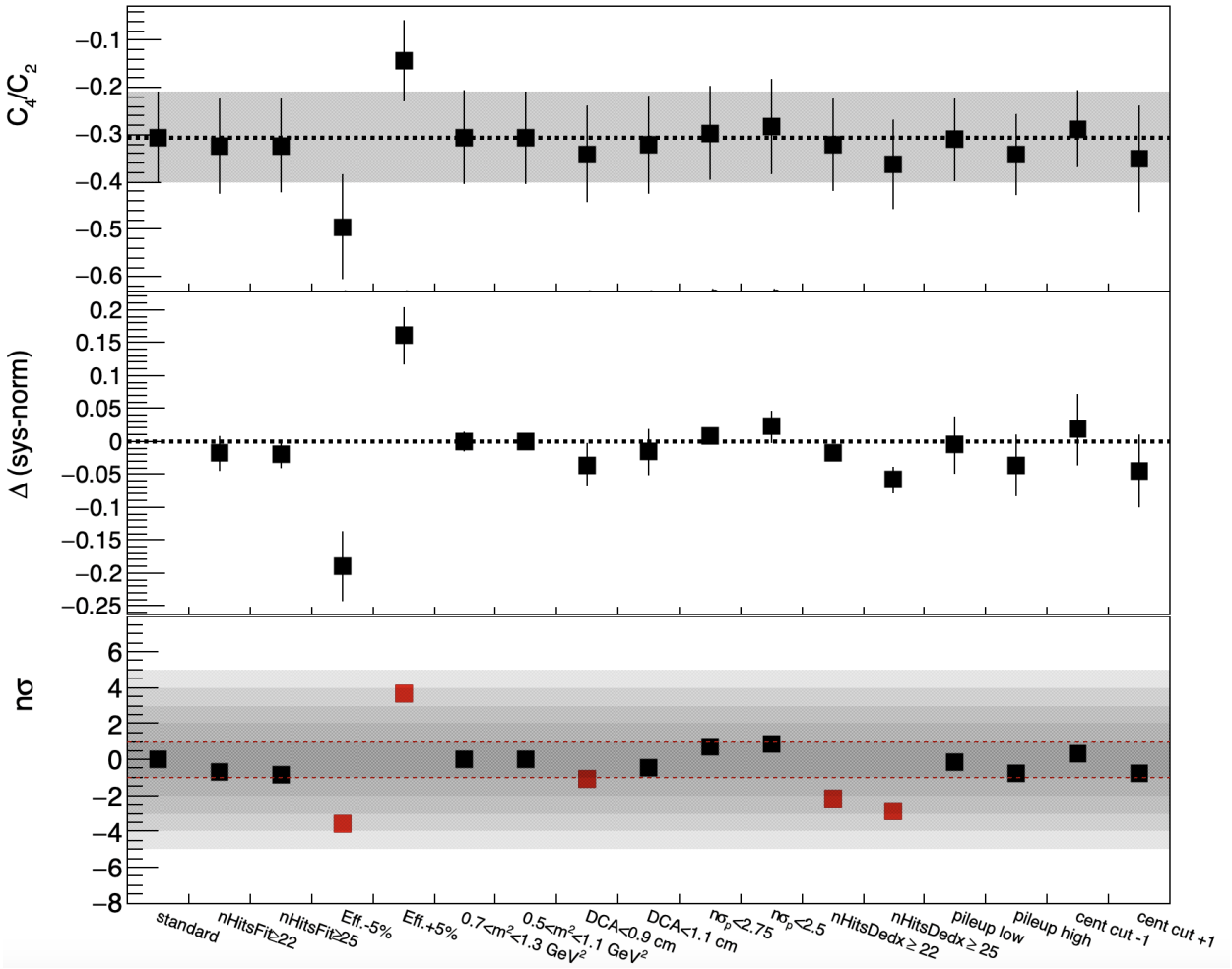

Figure 7.1: Barlow check for C_4/C_2 in 0-5% central collisions at 3.2 GeV. The top panel shows the value of C_4/C_2 for each systematic variation. The middle panel displays the difference between each value and the default value, with uncertainties. The bottom panel shows the significance of deviations for each systematic variation.

a different subsample of the data. In order to account for this, we introduce Barlow checks on each systematic variation.

7.2.1 Barlow Check

The Barlow check performed here is described in Ref. [79]. Barlow checks are designed to flag those systematic variations that are not statistically significant. Without a Barlow check, the size of an analyzer's systematic uncertainty increases with the number of systematics the analyzer varied, penalizing those analyzers with more comprehensive systematic variations. To make the Barlow check, the result is calculated for each systematic variation, along with the statistical uncertainty on that result. The results for each variation are shown for the central value of C_4/C_2 at 3.2 GeV in the top panel of Fig. 7.1.

The middle panel of Fig. 7.1 displays the difference between the default value of C_4/C_2 and the value obtained during a particular systematic variation, $\Delta(\text{sys} - \text{norm})$. The uncertainty on each difference is approximated assuming that the samples used in the default and systematic variation are correlated, giving $\sigma^2_\Delta = \sigma^2_{\text{norm}} - \sigma^2_{\text{sys}}$. These differences and their errors are converted into significances in the bottom panel of Fig. 7.1. Any systematic deviation greater than 1σ away from the default value is flagged as significant and is shown in red. In the example shown in the figure, the efficiency variations were significant, the DCA$<$ 1 cm variation was significant, and both of the nHitsDedx variations were significant. It is true that more restrictive cuts on some of these variables like nHitsDedx may lead to larger systematic uncertainties. By adjusting the efficiency map to match each cut, this effect can be minimized. It is worth investigating in future analyses whether performing restrictive cuts in this way is appropriate in measurements of proton high-order cumulants.

Those systematics flagged as significant by the Barlow check are summed in quadrature to calculate the total systematic uncertainty. If both variations of a single variable were flagged as significant, their magnitude was averaged. Therefore, if the low efficiency variation changed C_4/C_2 by -0.3, and the high efficiency variation changed the value by $+0.1$, the systematic uncertainty introduced by the efficiency was taken to be ± 0.2. The contri-

butions to the systematic uncertainties are tabulated for each energy and centrality bin in Appendix B.

In order to evaluate the contributions from each source of systematic uncertainty, it is useful to analyze the dominant systematic at each energy and for each cumulant. The systematic uncertainty is composed of a sum of squares of several sources of systematic uncertainties,

$$\sigma_{\text{sys}} = \sqrt{\sum_i \sigma^2_{\text{sys } i}}, \tag{7.5}$$

where $\sigma_{\text{sys } i}$ is the systematic uncertainty from the i^{th} contribution. The fraction that each systematic contributes to the total systematic uncertainty can be quantified by the fraction f given by

$$f_{\text{this sys}} = \frac{\sigma^2_{\text{this sys}}}{\sum_i \sigma^2_{\text{sys } i}}. \tag{7.6}$$

This fraction is plotted for $C_1 - C_6$ for each systematic uncertainty source and each energy in Fig. 7.2. The systematic uncertainties for C_1, C_1, and C_3 are dominated by the uncertainty on the efficiency. The efficiency is also a dominant source at C_4 for $\sqrt{s_{NN}} = 3.2$ and 3.5 GeV. However, at 3.5 GeV the nHitsDedx and centrality cuts dominate the uncertainty. At 4.5 GeV, the DCA cut dominates the C_4 uncertainty. At C_5 and C_6, the nHitsDedx cut is often the largest systematic uncertainty, but not uniformly. The same fractions are plotted for the cumulant ratios in Fig. 7.3. The dominant systematic changes for each order, and the centrality cut is much more dominant for the C_3/C_1 systematic uncertainty than for the C_3 systematic uncertainty. It makes sense that the efficiency systematic uncertainty is the largest contributor to the uncertainty for low-order cumulants, because a 5% systematic on efficiency leads to a 5% variation on C_1. The reason that the DCA, nHitsDedx, and centrality cuts dominate the systematic uncertainty at other orders is unknown.

The contributions to the systematic uncertainties are plotted for $\kappa_1 - \kappa_6$ for each systematic uncertainty source and each energy in Fig. 7.4. The systematic uncertainties are

again dominated by the uncertainty on the efficiency and the nHitsDedx cuts, but this is not the case at every energy. The same fractions are plotted for the factorial cumulant ratios in Fig. 7.5. The dominant systematic changes for each order, and the efficiency correction, DCA cut, nHitsDedx cut, and centrality cut all play a role in inflating the systematic uncertainty.

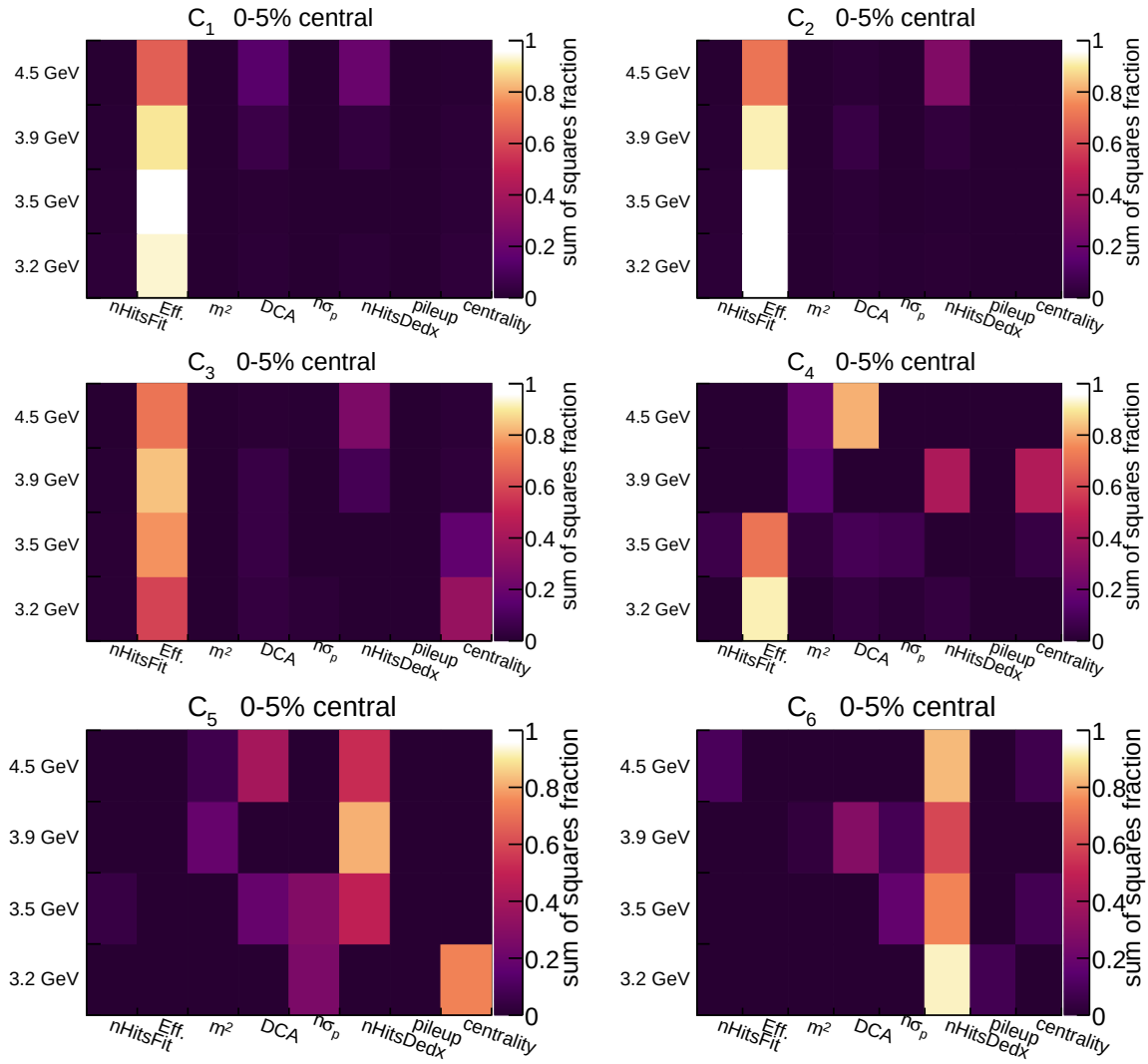

Figure 7.2: Contributions to the systematic uncertainties of the cumulants of 0-5% most central events. Each systematic is plotted on the x axis. The four energies are plotted on the y axis. The color axis encodes the fraction that each systematic contributes to the sum of squares that makes up the total systematic uncertainty, $\sigma^2_{\text{this sys}} / \sum_i \sigma^2_{\text{sys } i}$.

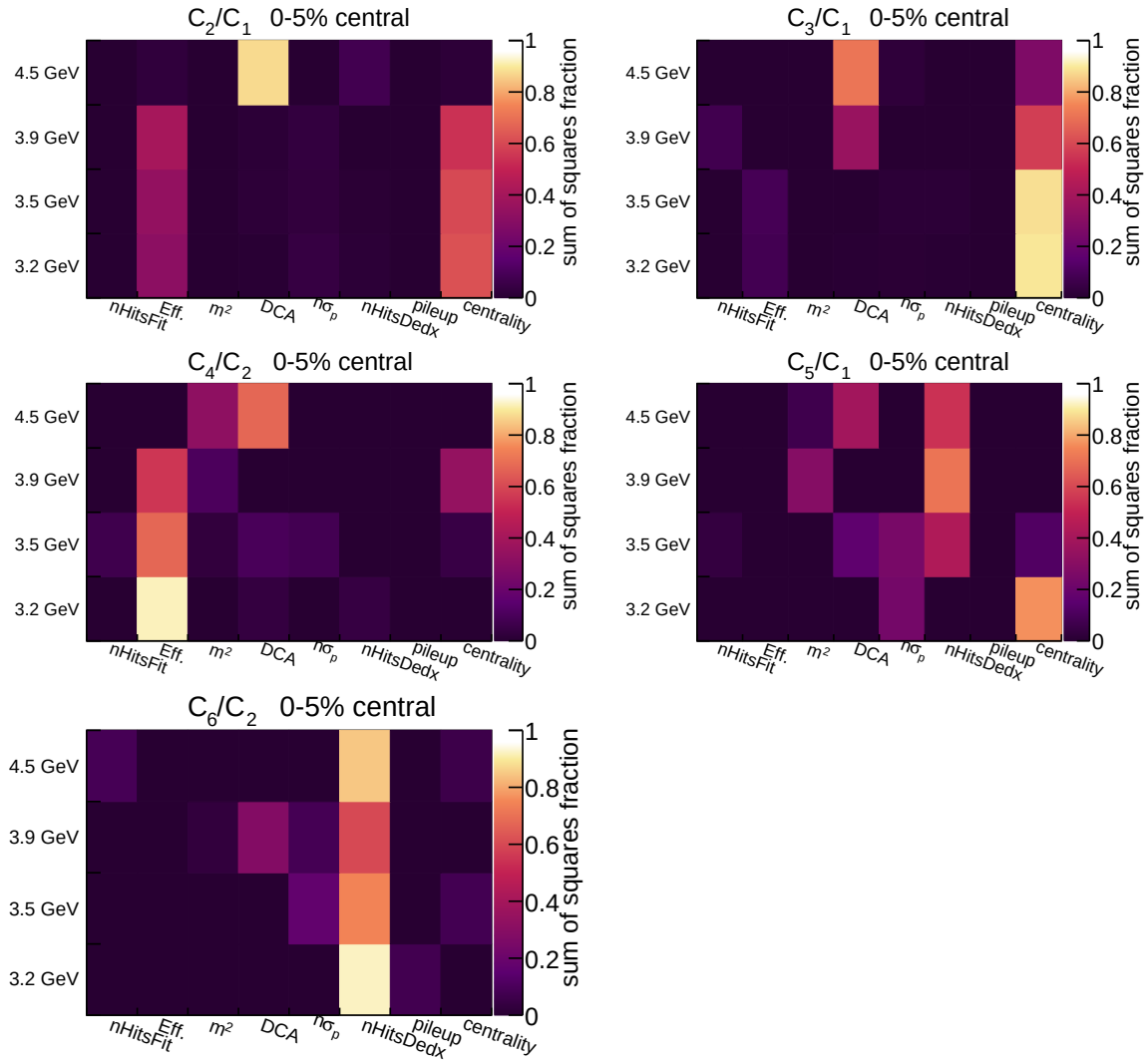

Figure 7.3: Contributions to the systematic uncertainties of the cumulant ratios of 0-5% most central events. Each systematic is plotted on the x axis. The four energies are plotted on the y axis. The color axis encodes the fraction that each systematic contributes to the sum of squares that makes up the total systematic uncertainty, $\sigma^2_{\text{this sys}} / \sum_i \sigma^2_{\text{sys } i}$.

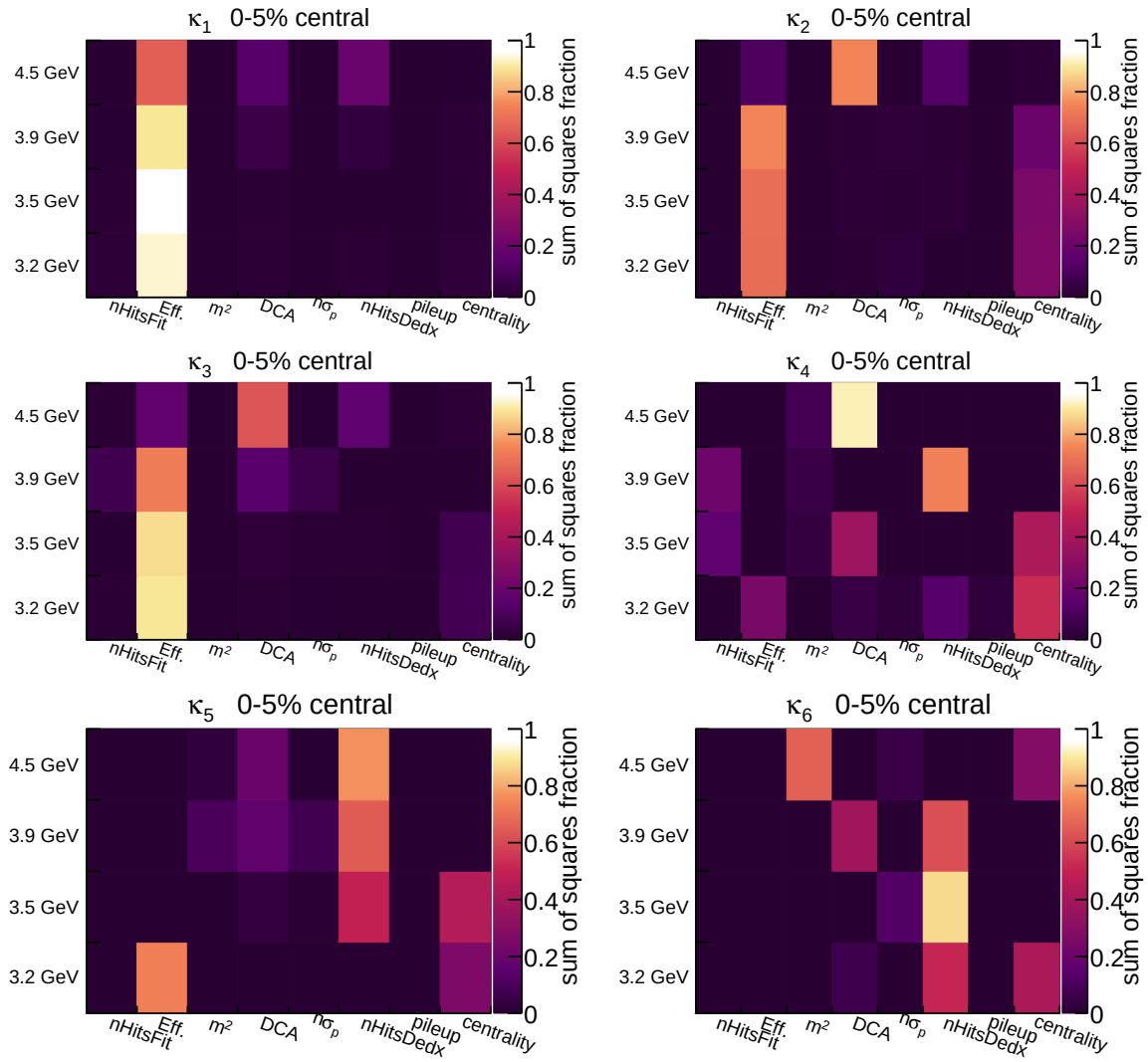

Figure 7.4: Contributions to the systematic uncertainties of the factorial cumulants of 0-5% most central events. Each systematic is plotted on the x axis. The four energies are plotted on the y axis. The color axis encodes the fraction that each systematic contributes to the sum of squares that makes up the total systematic uncertainty, $\sigma^2_{\text{this sys}} / \sum_i \sigma^2_{\text{sys } i}$.

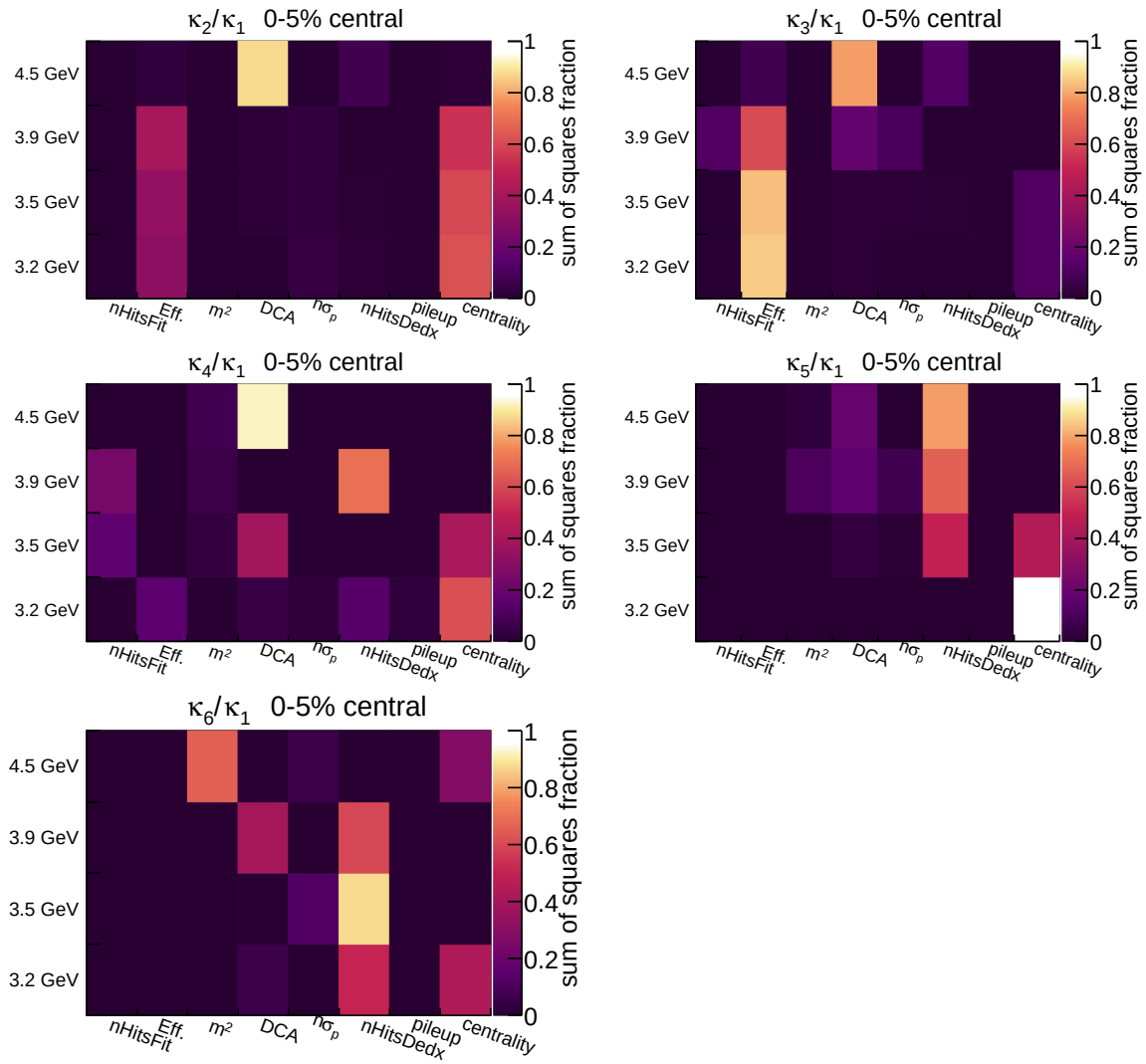

Figure 7.5: Contributions to the systematic uncertainties of the factorial cumulant ratios of 0-5% most central events. Each systematic is plotted on the x axis. The four energies are plotted on the y axis. The color axis encodes the fraction that each systematic contributes to the sum of squares that makes up the total systematic uncertainty, $\sigma^2_{\text{this sys}} / \sum_i \sigma^2_{\text{sys } i}$.

Chapter 8

The UrQMD Baseline

The measured cumulants and factorial cumulants are compared against non-critical baselines in order to identify evidence of critical behavior. Early on, it was thought that the C_4/C_2 calculated for a Skellam distribution would serve as an appropriate baseline. A Skellam distribution is the probability distribution of a quantity, Δn_p, describing the difference of two Poisson-distributed random variables, n_p and $n_{\bar{p}}$ with $\Delta n_p = n_p - n_{\bar{p}}$. Because $C_4/C_2 = 1$ for a pure Skellam distribution, the measured C_4/C_2 values were benchmarked against this beaseline. With the addition of STAR's $\sqrt{s_{NN}} = 3$ GeV measurement, it was found that C_4/C_2 was far below 1. This behavior was validated by UrQMD simulations, which allowed analyzers to realize that the suppression of C_4/C_2 was due to baryon-number conservation in the increasingly limited rapidity space available for the measured protons. In other words, as the beam rapidity decreases at low energies, the midrapidity analysis window occupies a larger and larger fraction of the rapidity range available to the measured protons. The magnitude of fluctuations in proton number is therefore suppressed, which suppresses high-order cumulants like C_4/C_2. It is important therefore to have a baseline that incorporates effects like baryon-number conservation.

At collider energies (> 7.7 GeV), various models including UrQMD, a hadron-resonance

gas (HRG) calculation, and a hydrodynamic excluded volume (Hydro EV) calculation are available as theoretical baselines. Because the hadron resonance gas and hydrodynamic excluded volume calculations have not been performed below 7.7 GeV, we compare our results to a UrQMD calculation only. The UrQMD baseline does not contain any critical dynamics. It was run in cascade mode, which means it simulates a cascade of hadrons scattering, rescattering, forming resonances, and producing particles through inelastic collisions.

UrQMD is used as a baseline is because it includes, or can be made to include, several effects which can distort the cumulants. One of these is the effect of baryon number conservation on suppressing high-order cumulants at low energies. At $\sqrt{s_{NN}} = 4.5$ GeV, the beam rapidity is $y_{\text{beam}} = 3.044$, and the target rapidity is $y_{\text{target}} = 0$, which means nearly every proton will have a rapidity between 0 and 3.044. If we use a midrapidity analysis window of $-0.5 < y - y_{\text{cm}} < 0$, this means that we are selecting protons within $\approx 16\%$ of the total available rapidity space. At $\sqrt{s_{NN}} = 3.0$ GeV, the beam rapidity is $y_{\text{beam}} = 2.096$, so we are selecting protons within $\approx 24\%$ of the total available rapidity space. As the energy decreases, the midrapidity analysis window becomes an increasingly large fraction of the total available phase space. This effect causes fluctuations from the mean to be suppressed, and high-order cumulants are likewise suppressed. Such a suppression was observed in C_4/C_2 at $\sqrt{s_{NN}} = 3.0$ GeV [23], and was reproduced by UrQMD.

Another advantage of UrQMD as a baseline is that analyzers can include the exact same acceptance in the UrQMD calculation as was used in the experiment. If there is a gap in the acceptance (as between the BTOF and ETOF), this can be incorporated into the UrQMD baseline by rejecting protons in the simulation that fall within that gap. This allows us to compare our result with a baseline using the same acceptance, and also to evaluate the effect of such a gap on the cumulants. Many studies have been performed using UrQMD to determine how acceptance gaps may change high-order cumulants. In addition to acceptance gaps, the flexibility of UrQMD allows us to measure the cumulants in a half

midrapidity analysis window ($-0.5 < y - y_{\rm cm} < 0$) in the fixed-target program, and compare to a baseline with that same half window. The bridging of results from fixed-target collisions with $-0.5 < y - y_{\rm cm} < 0$ to collider results with $-0.5 < y - y_{\rm cm} < 0.5$ would not be possible without a model that could simulate both of these configurations.

Imperfect mapping between event multiplicity and impact parameter also distorts cumulants and can be simulated in UrQMD. Such distortions are referred to as volume fluctuations and are described in Refs. [39, 40]. If analyzers were able to cut directly on impact parameter, then volume fluctuations would not be an issue. However, we sort events by their multiplicities into centrality bins. The classification of events by their multiplicities adds an additional distortion to the proton number distributions which results in altered cumulants. We can include this effect in the UrQMD model by simulating a multiplicity for each event, and sorting UrQMD events not by their impact parameter, but by multiplicity cuts.

To obtain the baseline, we performed UrQMD simulations of Au+Au collisions in cascade mode. In order to calculate the multiplicity (FXTMult3), the events were simulated in the center-of-mass frame and then boosted to the lab frame, where pions and kaons were tabulated over $0 < \eta < 2.4$. Both the half-midrapidity analysis window $-0.5 < y - y_{\rm cm} < 0$ and the gaps in acceptance were simulated. Between 90 and 120 million Au+Au collisions were simulated at each energy. In UrQMD, the cumulants could be calculated in terms of the impact parameter. However, in order to provide a reasonable baseline, the cumulants are calculated according to the multiplicities in UrQMD. These then undergo the same centrality-bin-width correction (CBWC) that is performed on the data. The final baseline thus includes the same acceptance effects as the data, and is also subject to initial volume fluctuations like the data. The statistical uncertainties are calculated and represented as shaded bands.

The resulting cumulants and their ratios are shown in Fig. 8.1 as a function of $\langle N_{\rm part} \rangle$ for $\sqrt{s_{NN}} = 3.2$, 3.5, 3.9, and 4.5 GeV. The $\langle N_{\rm part} \rangle$ is calculated in each of the seven centrality

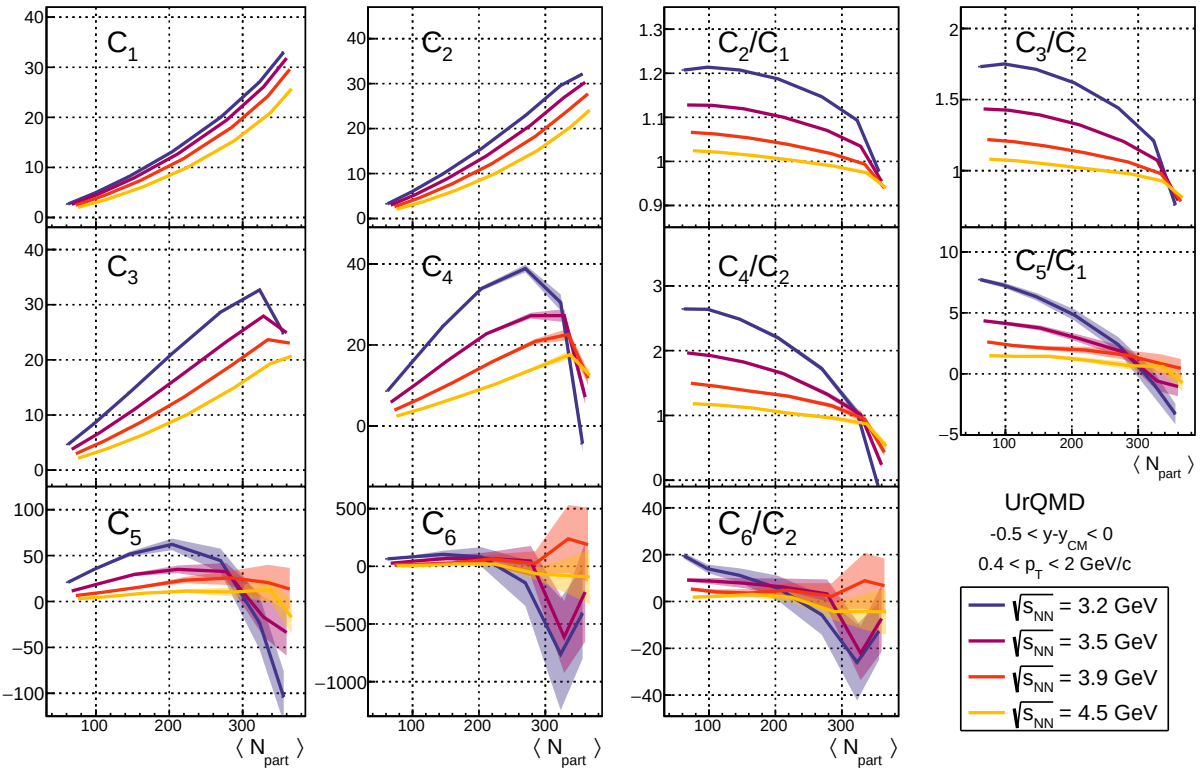

Figure 8.1: Cumulants and their ratios at $\sqrt{s_{NN}}$ = 3.2, 3.5, 3.9, and 4.5 GeV, as calculated in UrQMD with the same acceptance as used in the analysis.

bins. This is done by cutting on the simulated multiplicity to isolate the 0-5%, 5-10%, 10-20%, 20-30%, 30-40%, 40-50%, and 50-60% most central collisions. Each event is sorted into a centrality bin, and added to a histogram of the number of participant nucleons in each collision ($N_{\rm part}$). The average $N_{\rm part}$ value is then calculated in each centrality bin. The $N_{\rm part}$ quantity is discussed in more detail in Sec. 5.3.4.1.

As the center-of-mass energy decreases, C_1 rises up to a maximum at 3.2 GeV. This is because the midrapidity analysis window captures more of the total protons for the lowest energy used in this dissertation. In other words, more protons are stopped at midrapidity at lower energies. A similar trend is seen in C_2 and this is because the variance tends to

increase with increasing C_1. The Skellam baseline simplifies to a Poisson when the number of antiprotons vanishes at low energies. This Poisson behavior explains why the variance follows C_1, although centrality-bin-width effects and baryon-number conservation contribute to non-Poisson behavior. As discussed above, baryon-number conservation causes central C_4 and C_4/C_2 to fall with decreasing energy. In general, we can see in the cumulant ratios that, as the collision energy increases, we increasingly approach the Skellam baseline of 1 and the cumulants as a function of centrality tend to flatten. Importantly, Fig. 8.1 shows that for most of the analysis range in energy and centrality, the cumulant ratios in the baselines are not 1, so these simulations are crucial for providing realistic baselines.

The factorial cumulants and their ratios are shown in Fig. 8.2. The factorial cumulants and their ratios are different from the cumulants in interesting ways. The simulated values of κ_1, κ_2, and κ_3 show a strong energy dependence just like the cumulants. In the simulation of κ_4, the energy dependence nearly disappears, and all energies but 3.2 GeV seem to have little to no centrality dependence. In general, the factorial cumulant ratios exhibit less model dependence than the cumulant ratios. This is often why factorial cumulants are preferred over cumulants. It may be that the factorial cumulants are less sensitive to baryon-number conservation effects, but that these effects become prominent enough at low energies to introduce centrality dependence to κ_4/κ_1.

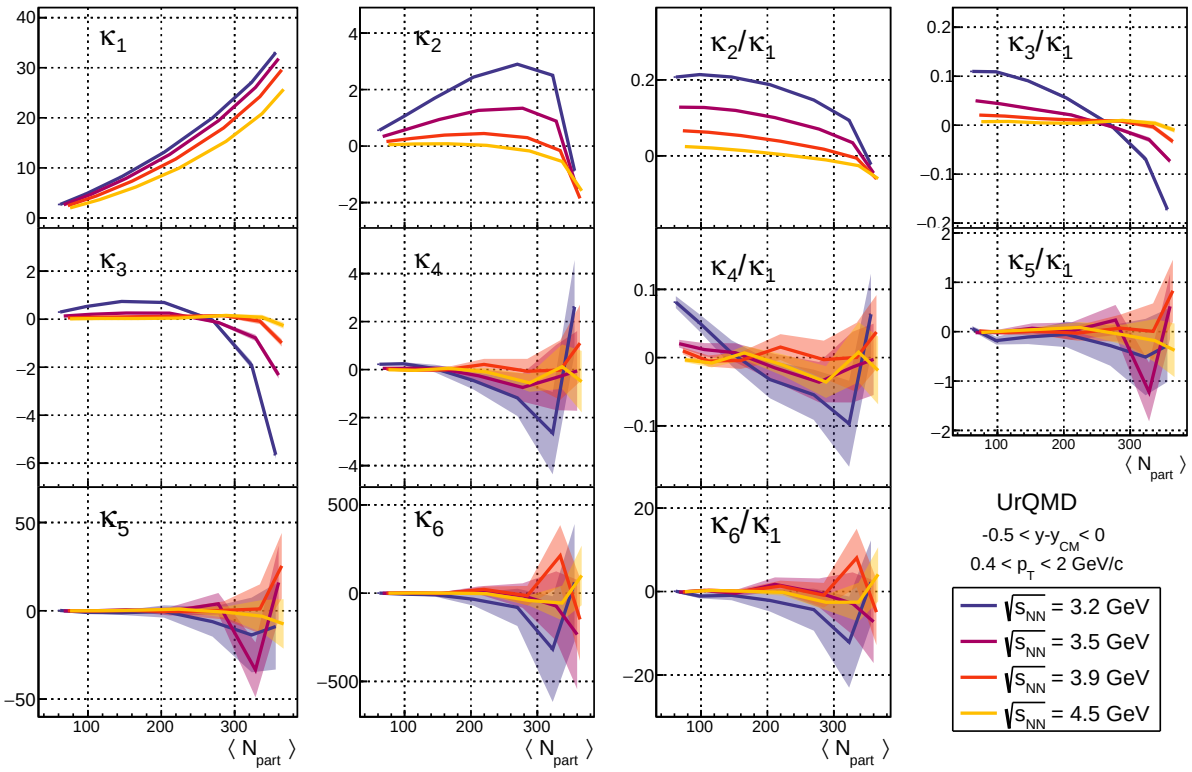

Figure 8.2: Factorial cumulants and their ratios at $\sqrt{s_{NN}} = 3.2$, 3.5, 3.9, and 4.5 GeV, as calculated in UrQMD with the same acceptance as used in the analysis.

Chapter 9

Results

This chapter contains the results of the proton-number cumulants, factorial cumulants, and their ratios at $\sqrt{s_{NN}}$ = 3.2, 3.5, 3.9, and 4.5 GeV. The results are plotted as functions of centrality and collision energy. Systematic uncertainties are displayed as gray bars behind each measurement point. Statistical uncertainties are shown as solid black lines behind each point. The values of the cumulants are tabulated in Appendix A. The contributions to the systematic uncertainties for each measurement are tabulated in Appendix B.

These results are efficiency corrected. The results at 3.2 GeV are corrected for pileup effects. The other datasets used pileup rejection and no pileup correction. The centrality-bin-width correction is also applied in order to minimize the effects of initial-volume fluctuations. It should be noted that the results shown here have non-zero contamination from pions and deuterons, resulting in a proton purity of approximately 95%. Additionally, the analysis windows at 3.5, 3.9, and 4.5 GeV have acceptance gaps which are also simulated in the UrQMD baseline. The finite purity and limited acceptance were previously discussed in Ch. 5, but it is worth mentioning again here that these are the cumulants with these limitations.

The factorial cumulant ratios are expected to have a similar energy dependence in the vicinity of a critical point as the cumulant ratios. However, the factorial cumulant ratios

have less dependence on the baseline. So if C_4/C_2 is expected to rise and then fall with increasing energy in the vicinity of a critical point, κ_4/κ_1 is expected to follow the same trend. However, the baseline for κ_4/κ_1 has less energy dependence than for C_4/C_2. Therefore a nonmonotonic energy dependence would be more visible in the factorial cumulant ratios than the cumulant ratios. According to Ref. [85], in the vicinity of a critical point, the second and third-order cumulant and factorial cumulant ratios should experience an enhancement above the baseline. The κ_4/κ_1 and C_4/C_2 should experience an enhancement at low energies and suppression at high energies.

9.1 Results at $\sqrt{s_{NN}} = 3.2$ GeV

The cumulants at $\sqrt{s_{NN}} = 3.2$ GeV as a function of the centrality are shown in Fig. 9.1. The UrQMD calculation and its statistical uncertainty are displayed as a shaded magenta band. The $\langle N_{\text{part}} \rangle$ values used to plot these were calculated in the Glauber model for both the UrQMD and data plots. The factorial cumulants are in Fig. 9.2. As shown in Fig. 9.1, UrQMD struggles to describe the low-order cumulant ratios, as well as non-central collisions at all orders. However, central collisions at fourth-order and above can be described by the model.

Both C_1 and C_2 only deviate from UrQMD at about a 1σ significance. It is interesting to note that despite this, the C_2/C_1 deviation from UrQMD is highly significant, indicating that the large systematic uncertainties on C_1 and C_2 are highly correlated and mostly cancel in the ratio. It can be seen from Eq. (6.23) how the efficiency correction is reduced (but not eliminated) by taking ratios of cumulants. The factorial cumulants in Fig. 9.2 show interesting deviations from UrQMD starting at κ_2, but the highest-order factorial cumulant κ_6 is in excellent agreement with UrQMD. It is likely that the strong agreement with UrQMD at κ_6 is simply due to the large uncertainties on both the model and the data. Central κ_5

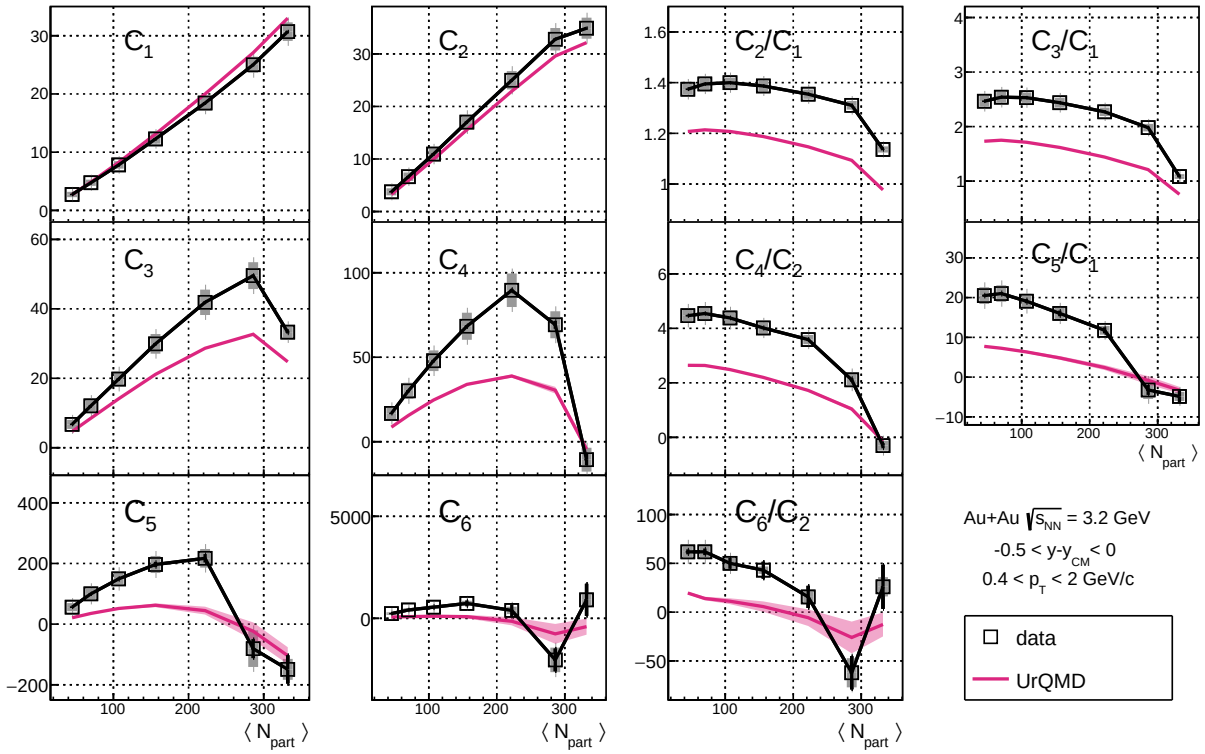

Figure 9.1: Cumulants and cumulant ratios up to sixth-order at $\sqrt{s_{NN}} = 3.2$ GeV. The UrQMD results are shown as a magenta band.

deviates from the UrQMD prediction by more than 100, but central κ_6 deviates from the UrQMD prediction by approximately 500. However, the uncertainties on the κ_6 predictions and results are much larger, so the results are statistically consistent with the predicted values. This observation underscores the need for high-statistics data in order to resolve discrepancies in high-order cumulants and factorial cumulants.

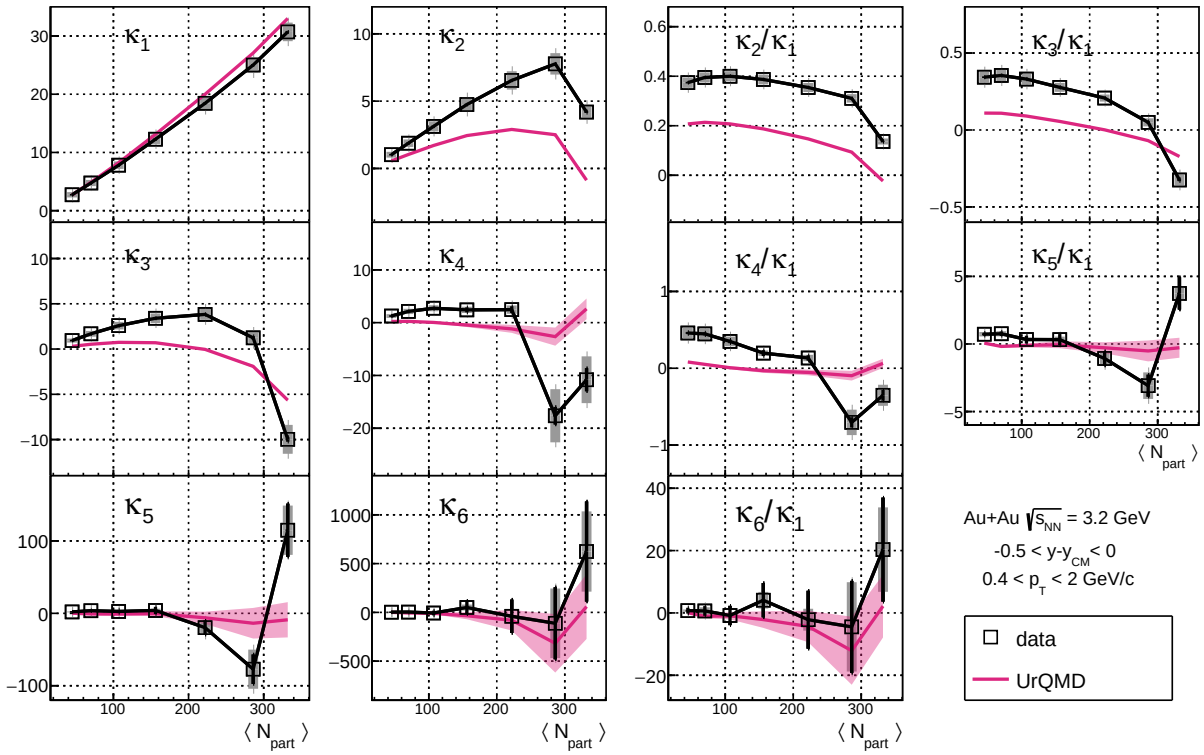

Figure 9.2: Factorial cumulants and factorial cumulant ratios up to sixth-order at $\sqrt{s_{NN}} = 3.2$ GeV. The UrQMD results are shown as a magenta band.

9.2 Results at $\sqrt{s_{NN}} = 3.5$ GeV

The cumulants at $\sqrt{s_{NN}} = 3.5$ GeV as a function of centrality are shown in Fig. 9.3. The factorial cumulants are in Fig. 9.4. A similar trend is seen at 3.5 GeV as was observed at 3.2 GeV. The best agreement with UrQMD is for high-order cumulants and central collisions.

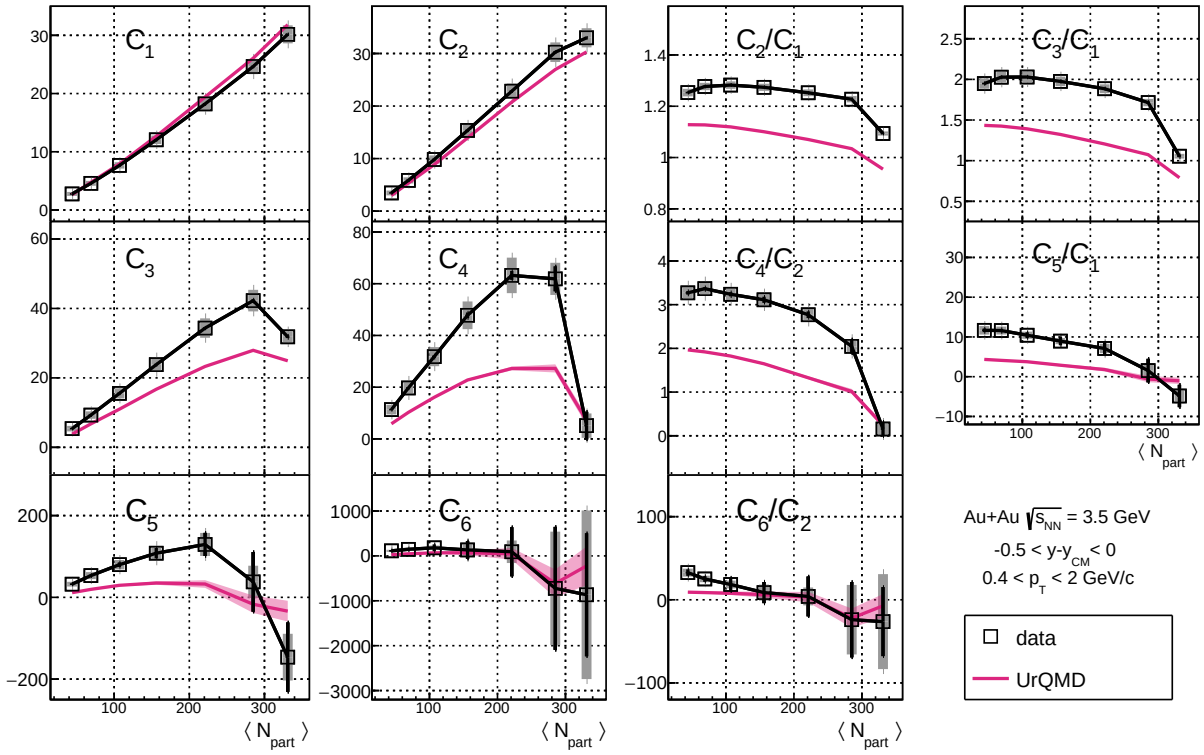

Figure 9.3: Cumulants and cumulant ratios up to sixth-order at $\sqrt{s_{NN}} = 3.5$ GeV. The UrQMD results are shown as a magenta band.

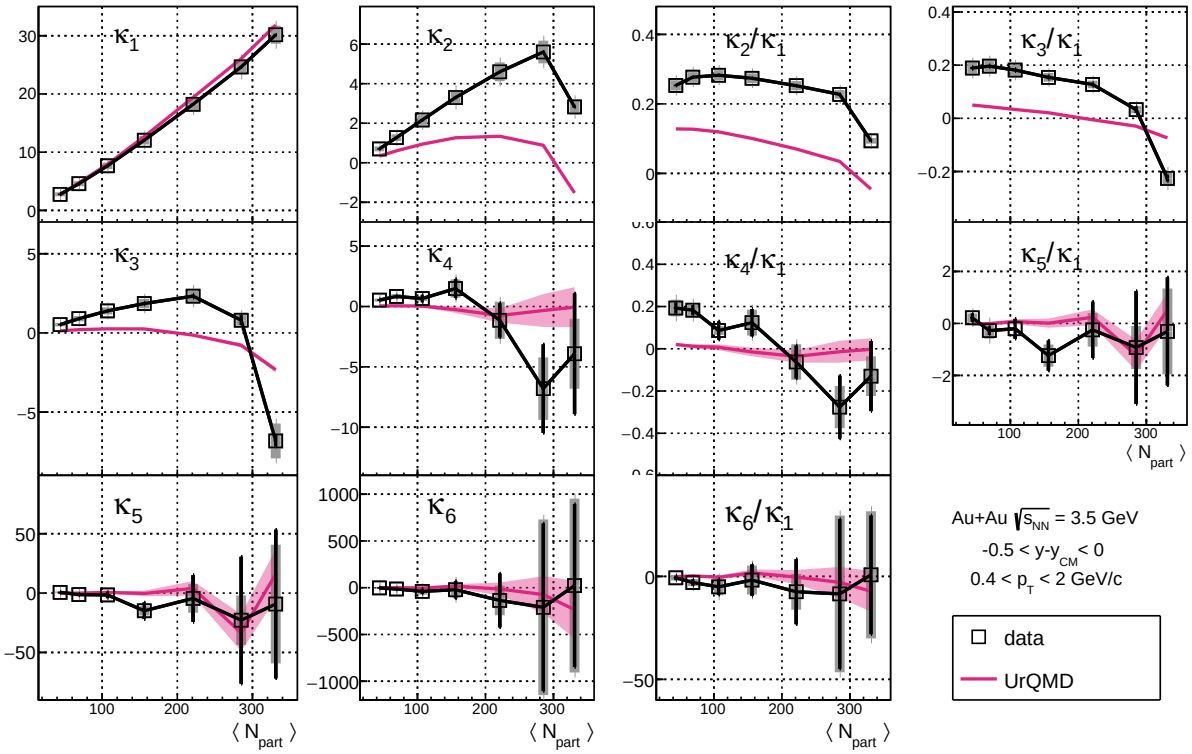

Figure 9.4: Factorial cumulants and factorial cumulant ratios up to sixth-order at $\sqrt{s_{NN}} = 3.5$ GeV. The UrQMD results are shown as a magenta band.

9.3 Results at $\sqrt{s_{NN}} = 3.9$ GeV

The cumulants at $\sqrt{s_{NN}} = 3.9$ GeV as a function of centrality are shown in Fig. 9.5. The factorial cumulants are in Fig. 9.6. The fifth-order central cumulants at 3.9 GeV deviate significantly from the baseline, which was not true at 3.2 and 3.5 GeV. However central fourth and sixth-order central cumulants are in agreement with UrQMD. Central κ_2/κ_1, κ_3/κ_1, and κ_4/κ_1 all deviate from the baseline, although κ_2/κ_1 experiences an enhancement whereas κ_3/κ_1 and κ_4/κ_1 are suppressed. It is unclear how a suppression of κ_3/κ_1 might fit into the search for critical-point signatures.

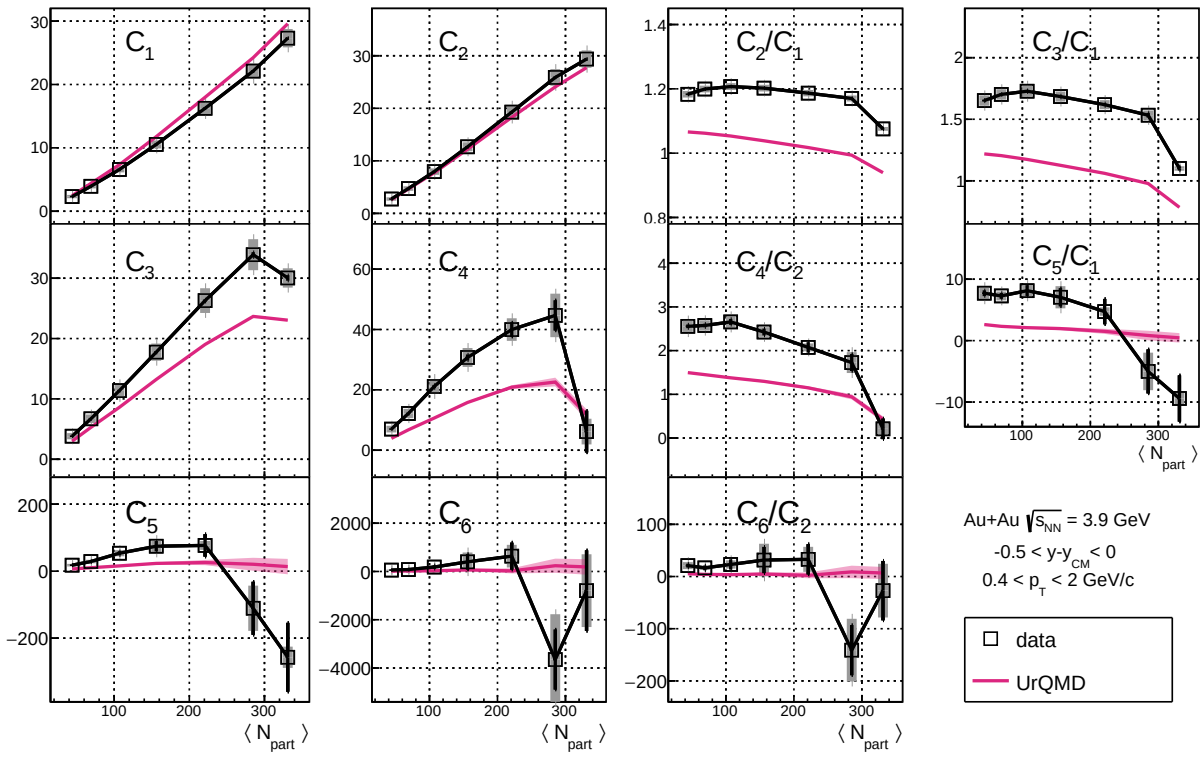

Figure 9.5: Cumulants and cumulant ratios up to sixth-order at $\sqrt{s_{NN}} = 3.9$ GeV. The UrQMD results are shown as a magenta band.

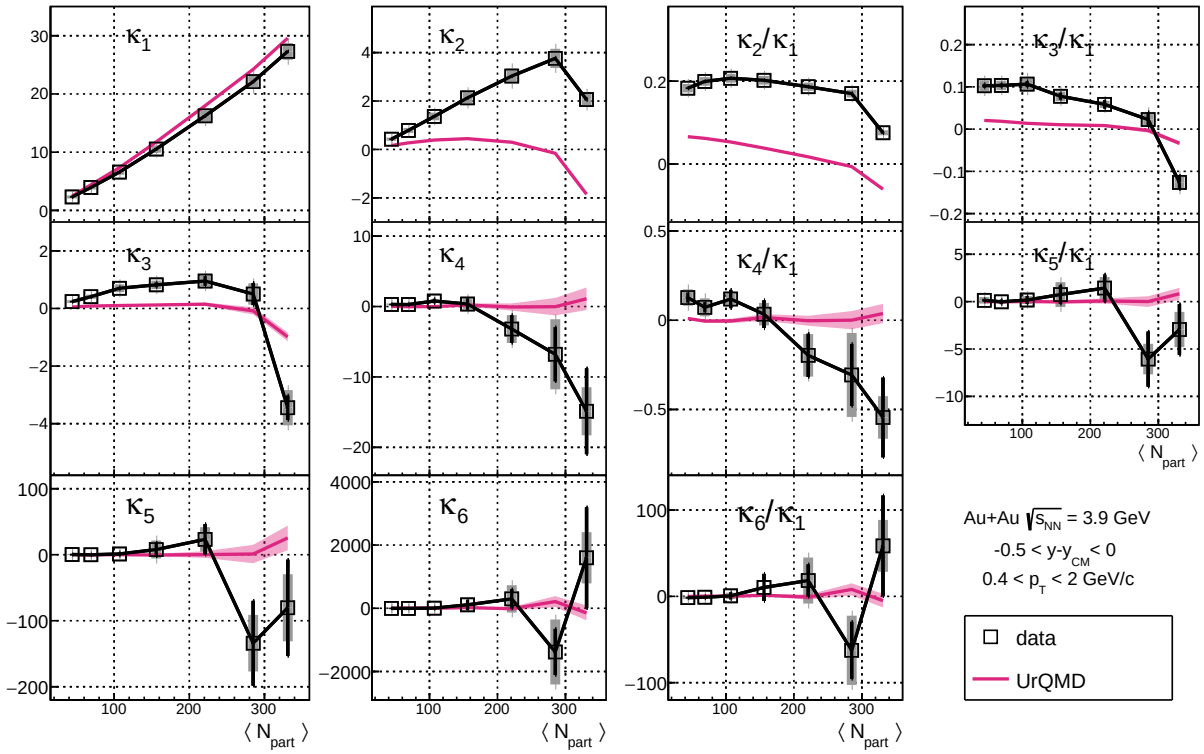

Figure 9.6: Factorial cumulants and factorial cumulant ratios up to sixth-order at $\sqrt{s_{NN}} = 3.9$ GeV. The UrQMD results are shown as a magenta band.

9.4 Results at $\sqrt{s_{NN}} = 4.5$ GeV

The cumulants at $\sqrt{s_{NN}} = 4.5$ GeV as a function of centrality are shown in Fig. 9.7. The factorial cumulants are in Fig. 9.8. Unlike 3.2, 3.5, and 3.9 GeV, the central value of C_4/C_2 does not exactly match the UrQMD prediction. This deviation is seen also in the factorial cumulant κ_4 and the ratio κ_4/κ_1. However central fifth and sixth-order cumulants at 4.5 GeV have large uncertainties and are in agreement with the baseline. Central κ_2/κ_1, κ_3/κ_1, and κ_4/κ_1 all deviate again from the baseline. Although both κ_2/κ_1 and κ_4/κ_1 now see an enhancement, whereas κ_3/κ_1 is still suppressed. The deviation in κ_4/κ_1 is of limited significance due to the large statistical and systematic uncertainties.

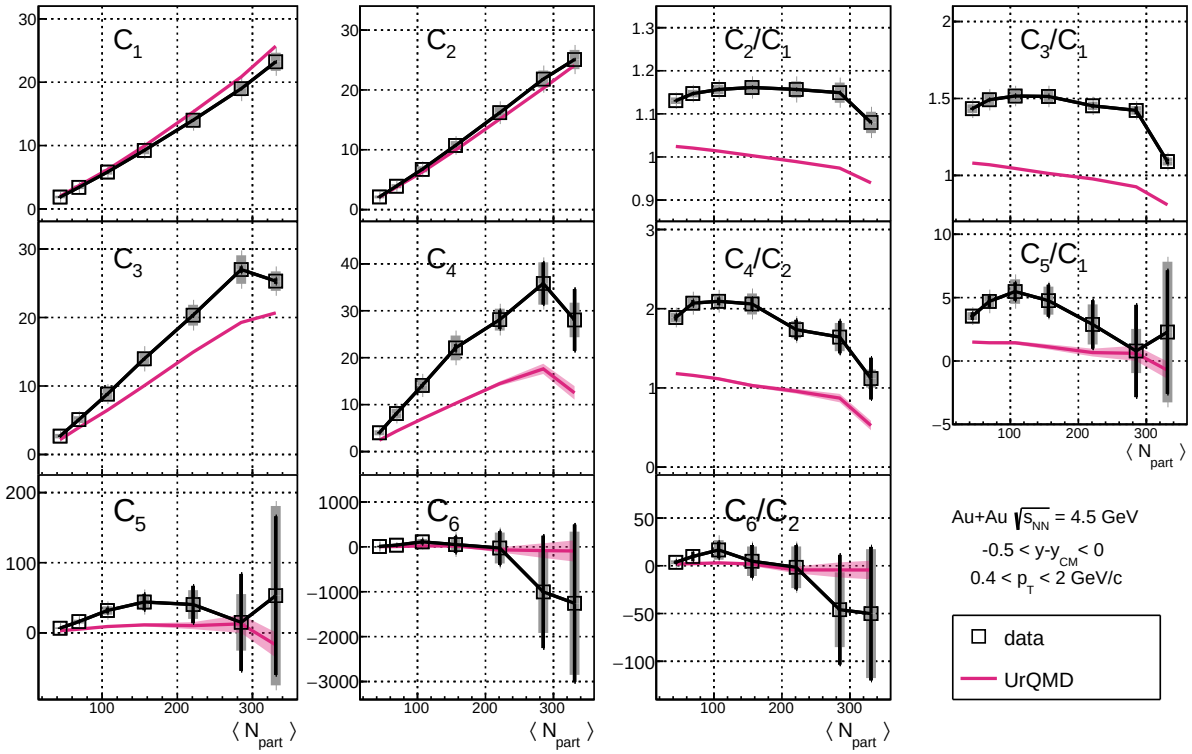

Figure 9.7: Cumulants and cumulant ratios up to sixth-order at $\sqrt{s_{NN}} = 4.5$ GeV. The UrQMD results are shown as a magenta band.

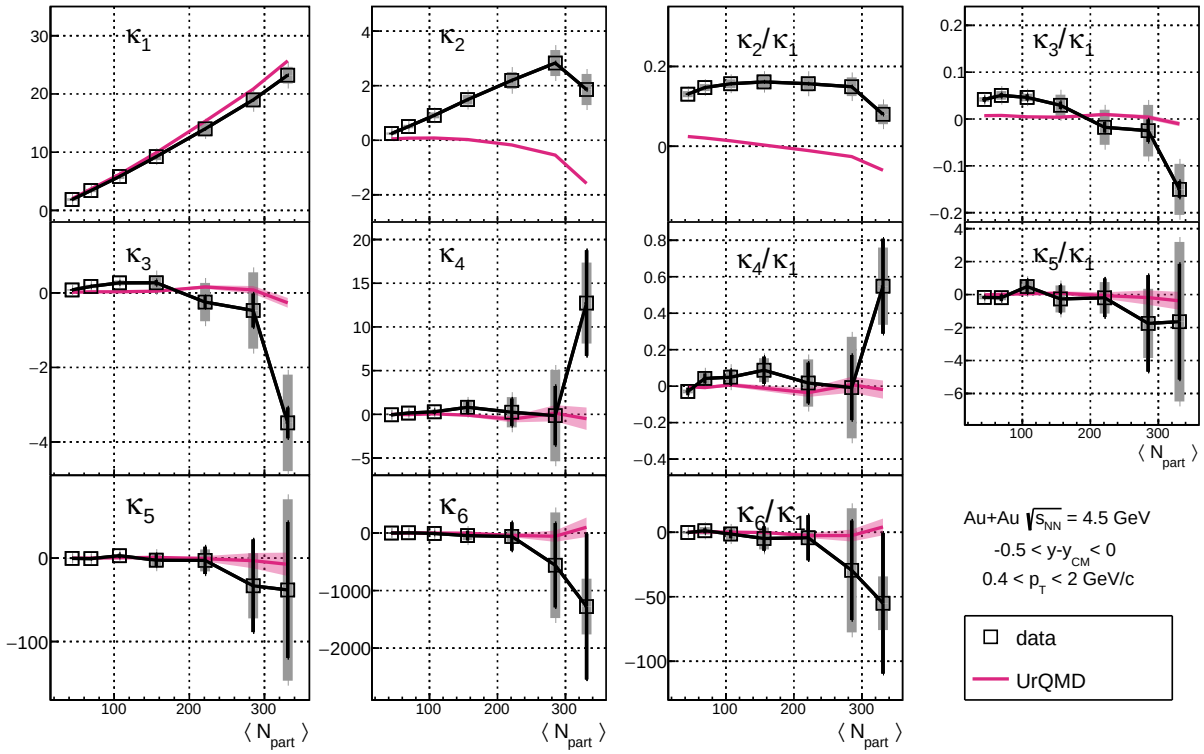

Figure 9.8: Factorial cumulants and factorial cumulant ratios up to sixth-order at $\sqrt{s_{NN}} = 4.5$ GeV. The UrQMD results are shown as a magenta band.

9.5 Energy Scans

It is helpful to view the cumulants and cumulant ratios with each energy plotted together. Figure 9.9 shows the cumulants up to sixth order where the left-most column is $\sqrt{s_{NN}} =$ 3.2 GeV, and the right-most column is $\sqrt{s_{NN}} = 4.5$ GeV. The cumulant ratios are similarly plotted in Fig. 9.10. Plotted this way, a flattening of the centrality dependence of C_2/C_1, C_3/C_1, C_4/C_2, and C_5/C_1 with increasing energy is clearly visible. This is primarily because volume fluctuations from limited centrality resolution tend to increase cumulants at low energies. At 3.2 GeV, the centrality resolution is low enough that the cumulant ratios are significantly enhanced. This is most severe for peripheral collisions. The factorial cumulants are shown in Fig. 9.11. Their ratios are in Fig. 9.12. The factorial cumulant ratios experience a similar flattening with increasing energy.

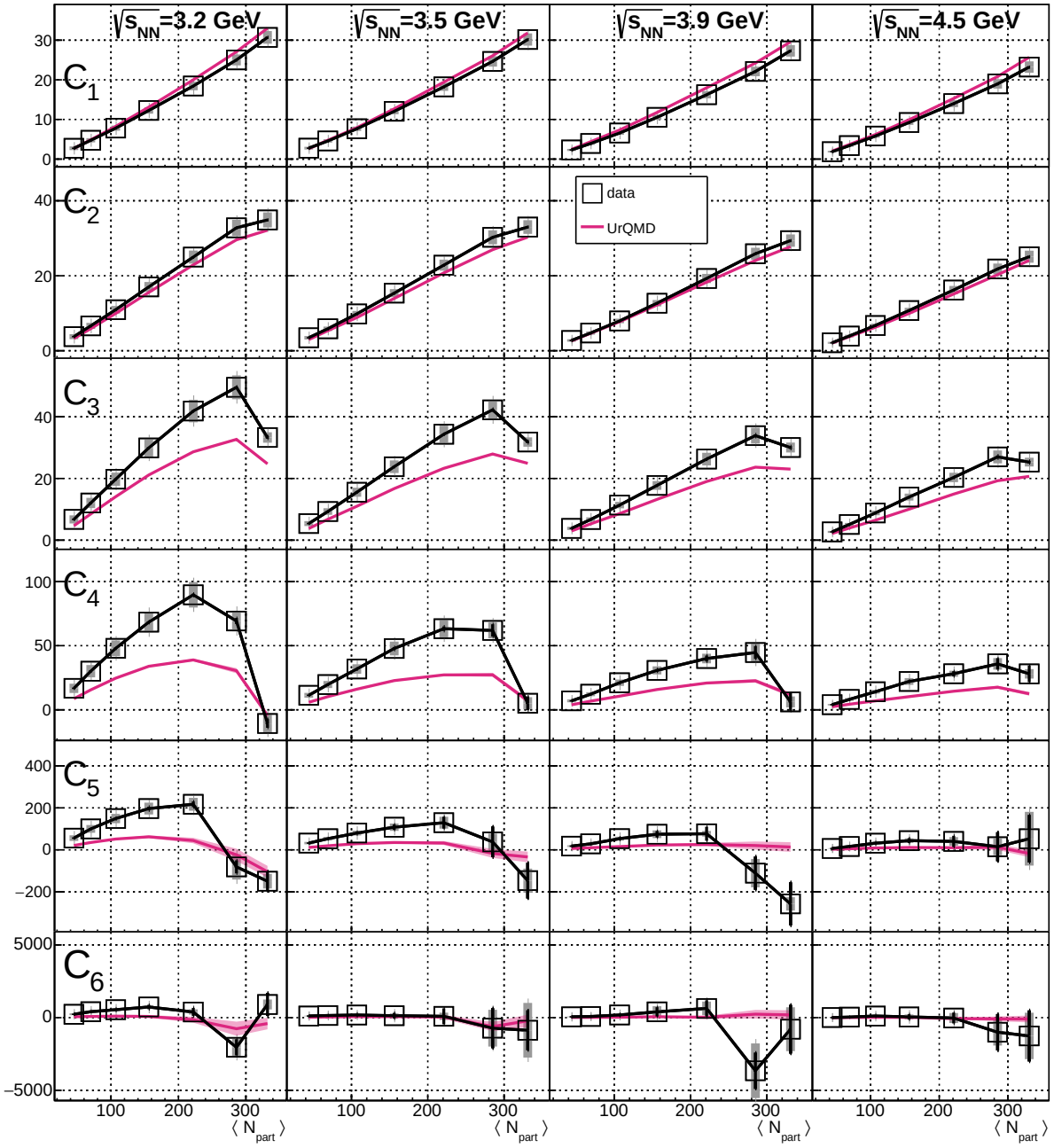

Figure 9.9: Cumulants up to sixth-order at $\sqrt{s_{NN}}$ = 3.2, 3.5, 3.9, and 4.5 GeV. The UrQMD results are shown as magenta bands.

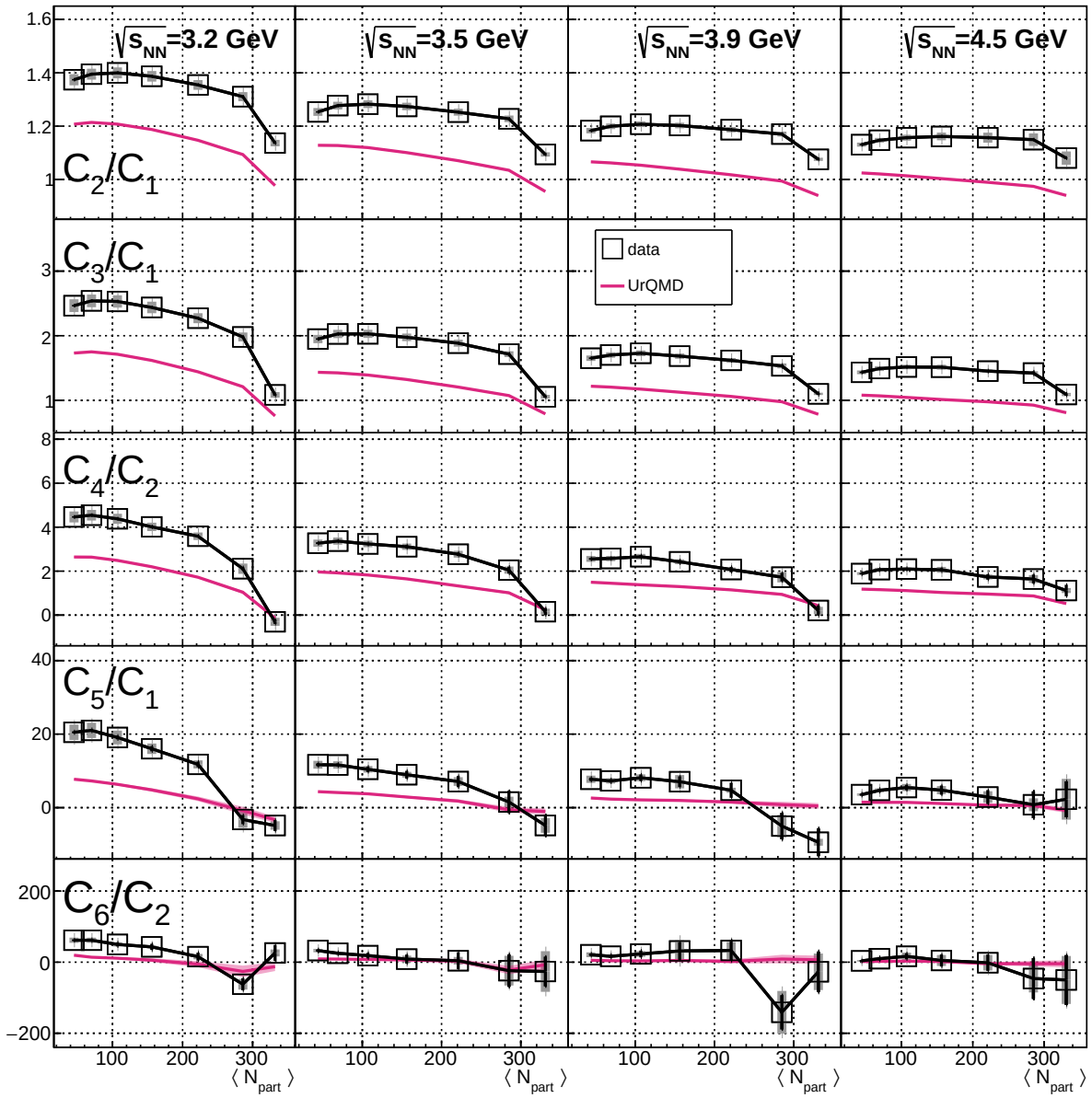

Figure 9.10: Cumulant ratios up to sixth-order at $\sqrt{s_{NN}} = 3.2$, 3.5, 3.9, and 4.5 GeV. The UrQMD results are shown as magenta bands.

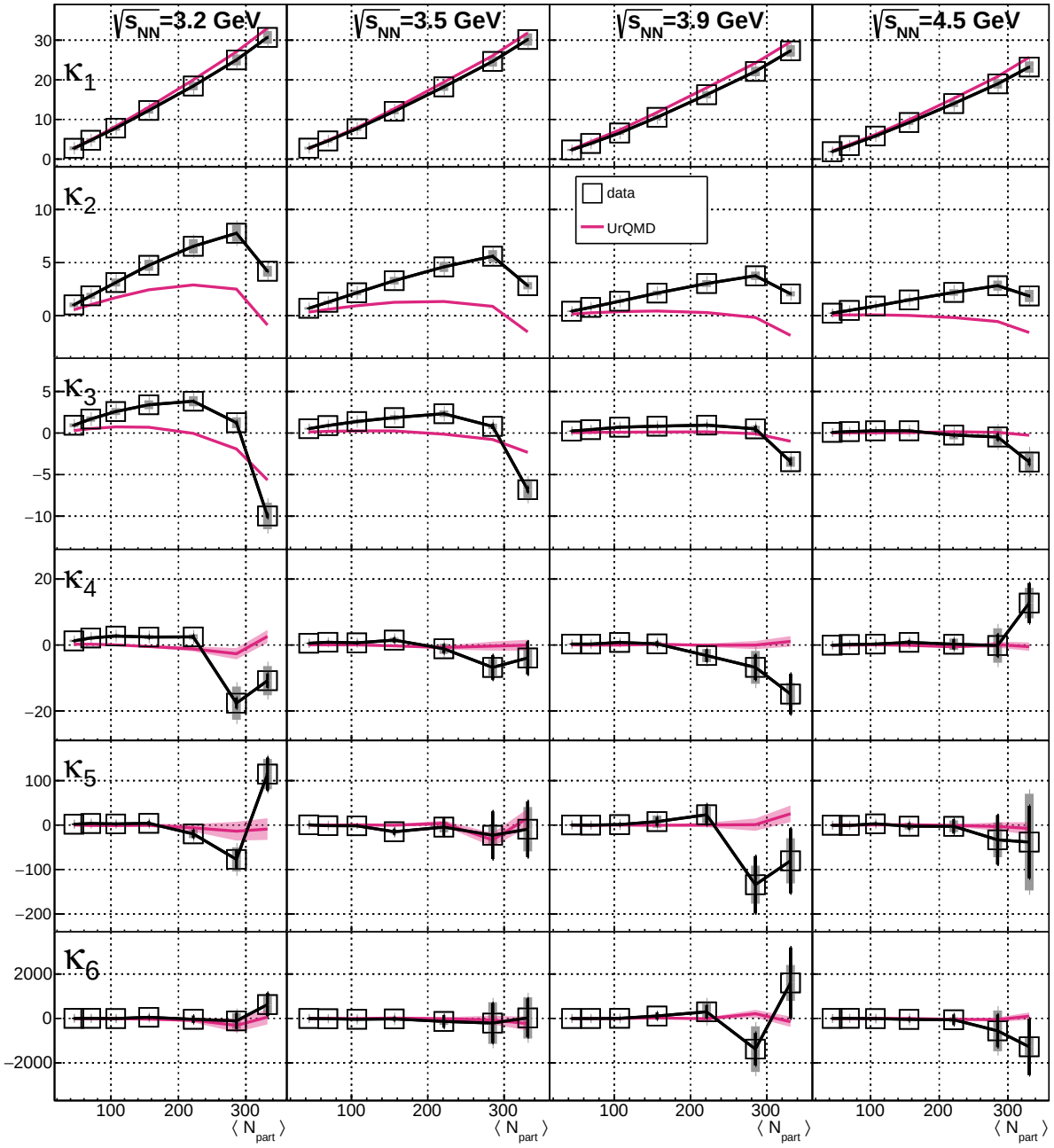

Figure 9.11: Factorial cumulants up to sixth-order at $\sqrt{s_{NN}} = 3.2$, 3.5, 3.9, and 4.5 GeV. The UrQMD results are shown as magenta bands.

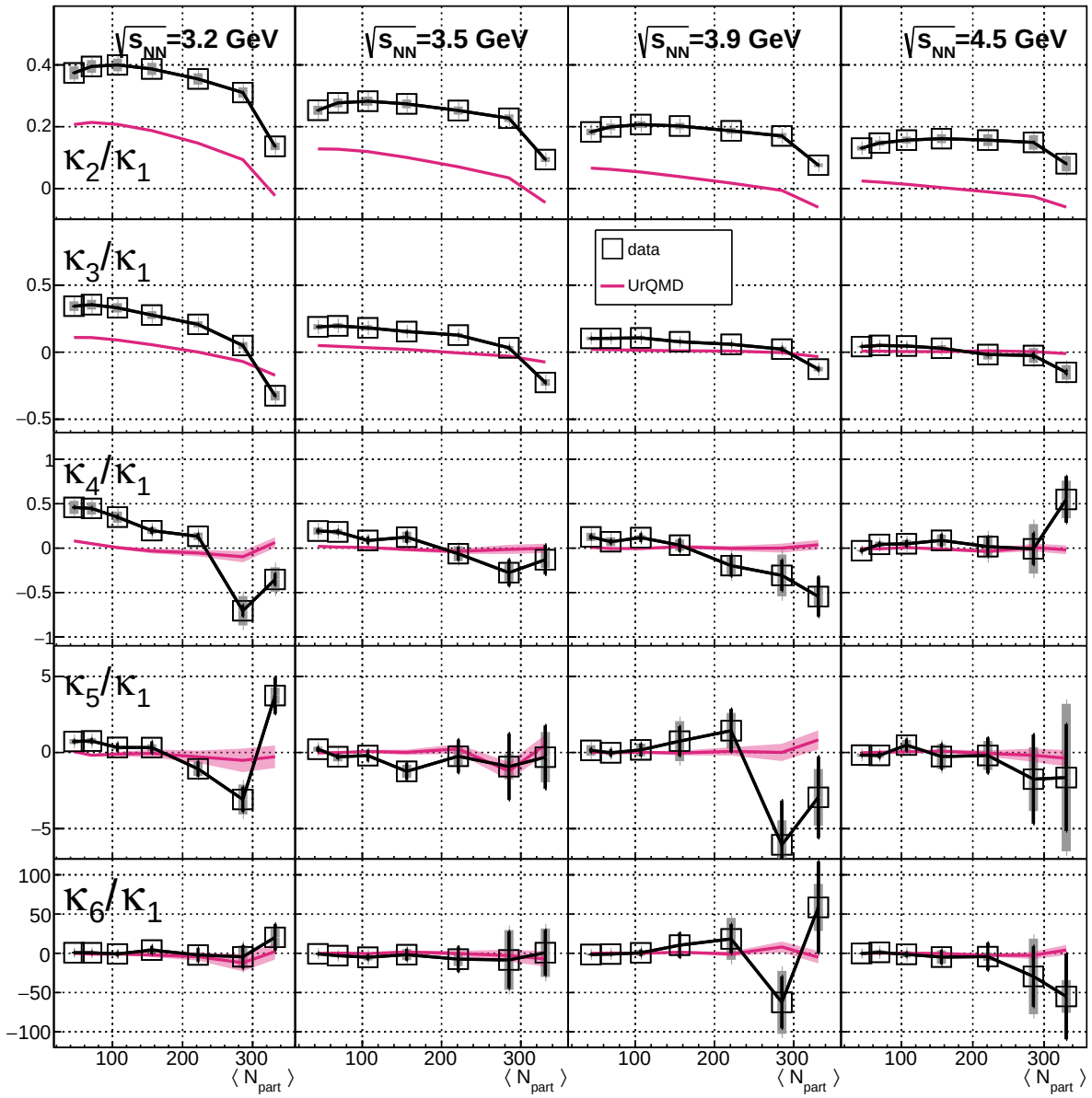

Figure 9.12: Factorial cumulant ratios up to sixth-order at $\sqrt{s_{NN}}$ = 3.2, 3.5, 3.9, and 4.5 GeV. The UrQMD results are shown as magenta bands.

9.5.1 Comparison to Collider Results

The results shown here can be compared to the recently released results from STAR's Beam Energy Scan II collider mode analyses [25]. These comparisons focus on the 0-5% most central collisions, and include cumulant and factorial cumulant ratios up to fourth order. The full midrapidity analysis window ($-0.5 < y - y_{\rm cm} < 0.5$) is simulated down to 3.0 GeV using UrQMD. This is shown as a continuation of the blue shaded band. The red shaded band represents the half midrapidity analysis window ($-0.5 < y - y_{\rm cm} < 0$) used in the fixed target analyses. The published result at $\sqrt{s_{NN}} = 3.0$ GeV [23] is displayed as a light red square.

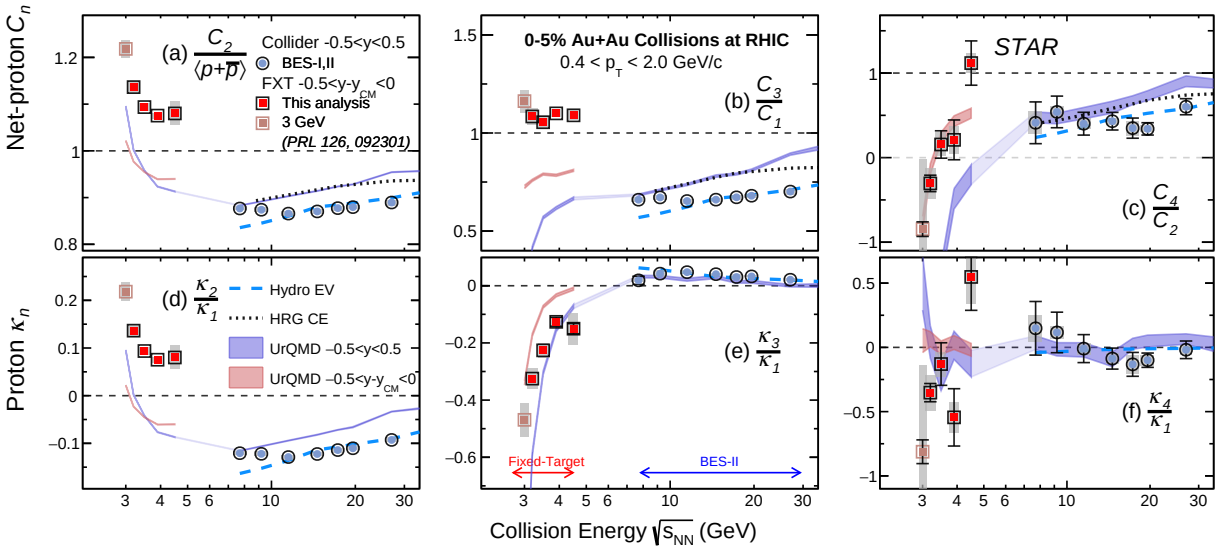

Figure 9.13: Energy dependence of cumulant ratios and factorial cumulant ratios up to fourth order for 0-5% most central collisions. The new fixed target points are shown as bright red squares. The recently released results from the collider mode analyses are shown as pale blue circles [25].

The second and third order cumulant ratios deviate significantly from the UrQMD baseline. The agreement with UrQMD is improved at fourth order. There are deviations at 4.5 GeV in C_4/C_2 and κ_4/κ_1, as well as deviations in κ_4/κ_1 at 3.2 and 3.9 GeV. However, all deviations at fourth order are below a significance of 3σ when statistical and systematic uncertainties are added in quadrature.

A recent preprint was uploaded to arXiv by Mikhail Stephanov [85] following the release of Beam Energy Scan II collider results. The preprint compares κ_2/κ_1, κ_3/κ_1, and κ_4/κ_1 to theoretical energy dependencies of these values. These comparisons are shown in Fig. 9.14. The comparisons are used to suggest that critical behavior may be causing the oscillatory behavior at κ_4/κ_1, the peak structure at κ_3/κ_1, and the rise at low energies in κ_2/κ_1. In fact the measured κ_4/κ_1 in Beam Energy Scan II is statistically indistinguishable from flat. There is absolutely no evidence for a nonmonotonic energy dependence of the Beam Energy Scan II collider κ_4/κ_1 results. The deviations from the baseline for the fixed-target results in Fig. 9.13 are much more significant, but still less than 3σ. The oscillatory behavior shown in the predictions in Fig. 9.14 is not observed. The peak structure in κ_3/κ_1 was also not observed, and instead, the measured κ_3/κ_1 in the fixed-target program goes negative in absolute terms, and also relative to the UrQMD baseline. The deviations from the baseline for κ_3/κ_1 are significant, but their interpretation is challenging. If the trajectory shown on the leftmost panel of Fig. 9.14 were to pass through the red region at low $\sqrt{s_{NN}}$, this could cause the observed energy dependence. Finally, the predicted enhancement in κ_2/κ_1 at low $\sqrt{s_{NN}}$ is observed in the STAR fixed-target measurements. However, a return to the baseline is also predicted at the lowest $\sqrt{s_{NN}}$. Instead, κ_2/κ_1 remains significantly enhanced above the baseline at all fixed-target energies.

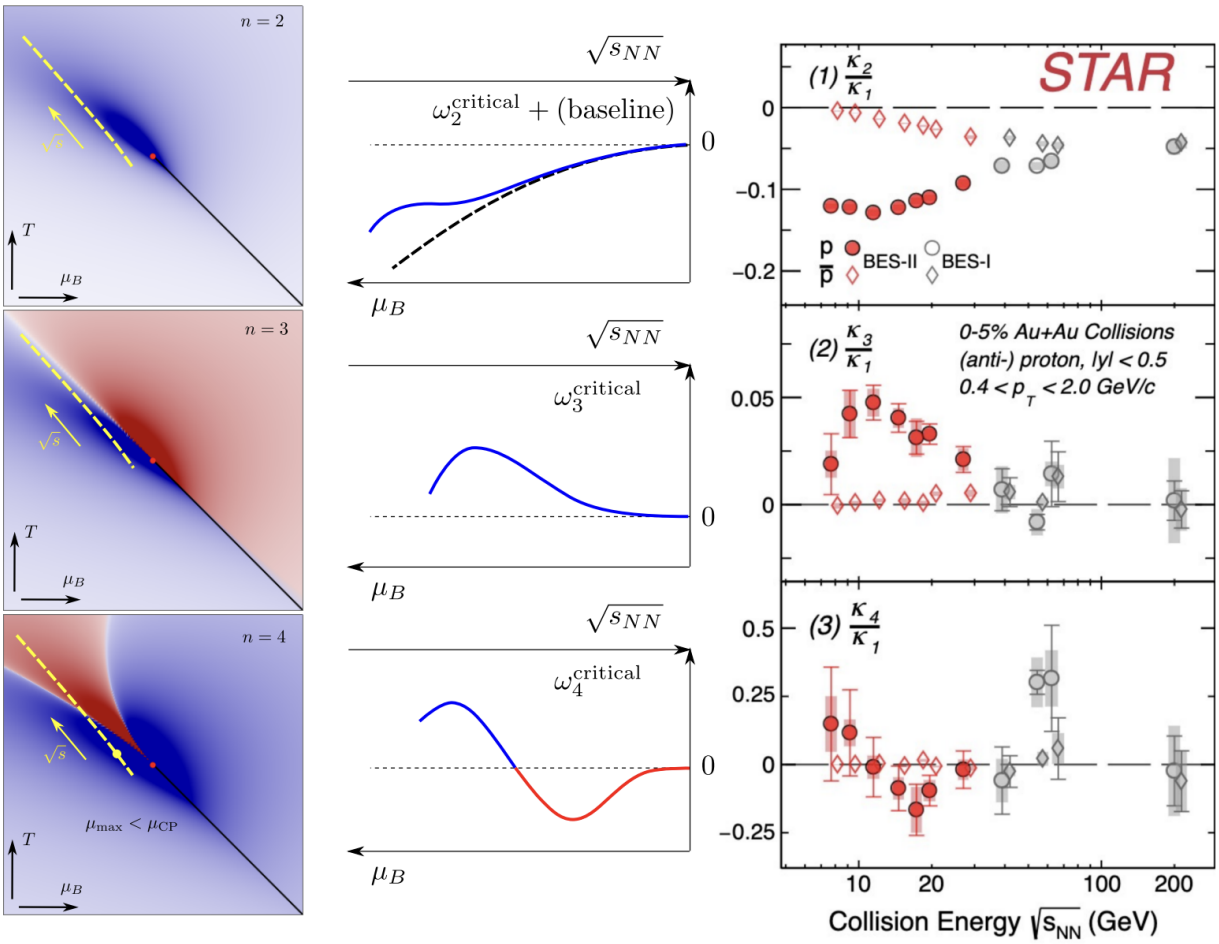

Figure 9.14: Predicted energy dependence of cumulant ratios compared with Beam Energy Scan II collider results [85]. The blue regions at left show areas of enhanced cumulants. The red are areas of suppressed cumulants.

Figure 9.15 is an enlarged version of C_4/C_2 from panel (c) of Fig. 9.13. The new fixed target points follow the UrQMD baseline, except for an interesting deviation at $\sqrt{s_{NN}} = 4.5$ GeV. However, the uncertainties on this point are too large to claim evidence of critical behavior.

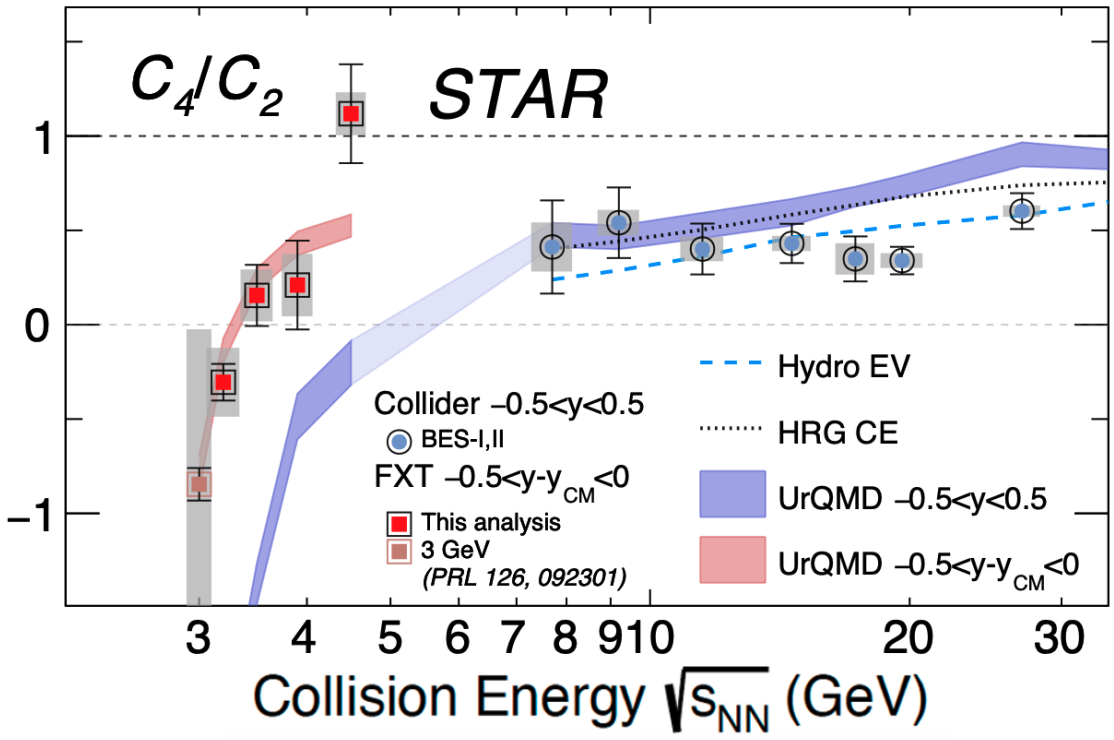

Figure 9.15: Energy dependence of C_4/C_2 for 0-5% most central collisions with new fixed target points and the recently released results from the collider mode analyses [25].

Chapter 10

Conclusions

In STAR's fixed-target program, we measured proton-number fluctuations in order to search for evidence of critical fluctuations in the range $\sqrt{s_{NN}} = 3.0-4.5$ GeV. The results have been compared with a non-critical baseline provided by UrQMD simulations. No such evidence has been observed in central measurements of C_4/C_2, although there is a hint of interesting behavior at 4.5 GeV. Central measurements of κ_4/κ_1 show deviations from the non-critical UrQMD baseline, but the significances of these deviations are each below 3σ. There is an enhancement above the baseline in C_3/C_1, and a suppression below the baseline in κ_3/κ_1. A significant deviation above the baseline is observed in C_2/C_1 and κ_2/κ_1 for central collisions. If these deviations were caused by critical phenomena, one might expect the maximal deviation at each order to occur at the same energy. Interestingly, the maximal deviation at fourth order occurs at 4.5 GeV, but that is not the case for the deviations at lower orders.

More theoretical predictions would be helpful in interpreting these results. The collider analyses [25] include comparisons to UrQMD as well as predictions using the hydrodynamic excluded volume model and the hadron resonance gas canonical ensemble models. The hydrodynamic model describes the collider data best, but deviates at low energies. Neither of these models have calculations at fixed-target energies that could serve as additional

baselines. The models provide discrepant predictions for several of these cumulant ratios, so it would be interesting to see whether they could replicate the deviations from the baselines observed in fixed-target data especially in low-order cumulants.

The cumulants measured here should be understood in the full context in which they were measured. As described in Sec. 5.2.3, the proton purity in these fixed-target measurements was maintained above 90% in each bin of rapidity and transverse momentum. Nonzero pion and deuteron contamination may affect these cumulants, and there is no known correction for this. This is an effect that could be studied in a simulation like UrQMD, and should be considered for future investigation. The limited acceptance of the fixed-target program also complicates the comparison to collider results. The UrQMD baselines account for these acceptance limitations, but more significant results could be obtained using a full acceptance window at a future facility like the future CBM experiment at Germany's GSI/FAIR [86].

We have observed no evidence of critical fluctuations in fourth-order cumulant and factorial cumulant ratios of proton number distributions in central Au+Au collisions at STAR. Interesting deviations from non-critical baselines were observed at lower orders, but more theoretical interpretation is needed to make sense of these. Although this dissertation does not detail the discovery of a QCD critical point, we have outlined the many ways that a measurement of proton-number cumulants can go wrong. We have seen that this is an incredibly sensitive measurement not only to detector failures, but also to statistical misinterpretation. With any luck, the findings discussed here will provide guidance on how to perform this measurement in a challenging experimental environment, and future experiments at J-PARC [87] or CBM [86] can measure a QCD critical point once and for all.

Appendix A

Tabulated Results

This appendix tabulates the values, statistical uncertainties, and systematic uncertainties of the cumulants, factorial cumulants, and their ratios, at $\sqrt{s_{NN}} = 3.2$, 3.5, 3.9, and 4.5 GeV in 7 centrality bins. These tabulated values are plotted and discussed in Sec. 3.4. The contributions to the systematic uncertainties for each measurement are tabulated in Appendix B.

A.1 Cumulants and Factorial Cumulants at $\sqrt{s_{NN}} = 3.2$ GeV

Table A.1: Cumulants and uncertainties at $\sqrt{s_{NN}} = 3.2$ GeV

$\sqrt{s_{NN}} = 3.2$ GeV cumulants

		0-5%	5-10%	10-20%	20-30%	30-40%	40-50%	50-60%
C_1	value	30.704	25.018	18.442	12.273	7.814	4.750	2.730
	stat.	0.034	0.008	0.013	0.003	0.021	0.026	0.035
	sys.	1.596	1.376	1.081	0.814	0.642	0.532	0.460
C_2	value	34.892	32.787	24.980	17.021	10.938	6.626	3.752
	stat.	0.032	0.017	0.019	0.008	0.030	0.037	0.050
	sys.	2.003	2.138	1.742	1.311	1.004	0.803	0.671
C_3	value	33.294	49.564	41.882	29.916	19.771	12.061	6.731
	stat.	0.400	0.204	0.068	0.054	0.060	0.070	0.095
	sys.	1.688	3.869	3.655	2.838	2.131	1.658	1.312
C_4	value	-10.639	69.209	89.627	68.321	47.919	30.108	16.752
	stat.	3.380	2.347	0.863	0.615	0.299	0.234	0.254
	sys.	7.060	7.985	9.914	8.016	6.112	4.800	3.611
C_5	value	-149.16	-80.914	217.042	196.615	149.170	99.822	55.964
	stat.	46.489	31.070	13.939	8.773	3.947	1.827	1.149
	sys.	34.520	60.324	30.673	28.105	22.135	18.468	13.331
C_6	value	905.903	-2037.6	389.240	732.015	547.076	409.503	231.652
	stat.	787.888	555.921	283.457	146.591	62.007	22.562	10.218
	sys.	342.118	601.363	180.061	128.275	89.653	87.334	60.520

Table A.2: Cumulant ratios and uncertainties at $\sqrt{s_{NN}} = 3.2$ GeV

$\sqrt{s_{NN}} = 3.2$ GeV cumulant ratios

		0-5%	5-10%	10-20%	20-30%	30-40%	40-50%	50-60%
C_2/C_1	value	1.136	1.311	1.355	1.387	1.400	1.395	1.374
	stat.	0.002	0.001	0.000	0.001	0.000	0.001	0.001
	sys.	0.012	0.017	0.018	0.020	0.020	0.020	0.021
C_3/C_1	value	1.084	1.981	2.271	2.438	2.530	2.539	2.465
	stat.	0.014	0.008	0.003	0.004	0.004	0.004	0.004
	sys.	0.043	0.069	0.077	0.089	0.095	0.098	0.099
C_4/C_2	value	-0.305	2.111	3.588	4.014	4.381	4.544	4.465
	stat.	0.097	0.072	0.035	0.035	0.026	0.023	0.020
	sys.	0.183	0.234	0.170	0.190	0.230	0.241	0.249
C_5/C_1	value	-4.858	-3.234	11.769	16.021	19.091	21.015	20.497
	stat.	1.510	1.242	0.758	0.714	0.507	0.364	0.293
	sys.	1.149	2.254	1.098	1.428	1.868	2.071	2.100
C_6/C_2	value	25.963	-62.149	15.582	43.008	50.018	61.802	61.748
	stat.	22.595	16.964	11.358	8.604	5.659	3.398	2.537
	sys.	9.893	14.948	7.534	3.767	5.809	7.231	7.306

Table A.3: Factorial cumulants and uncertainties at $\sqrt{s_{NN}} = 3.2$ GeV

$\sqrt{s_{NN}} = 3.2$ GeV factorial cumulants

		0-5%	5-10%	10-20%	20-30%	30-40%	40-50%	50-60%
κ_1	value	30.704	25.018	18.442	12.273	7.814	4.750	2.730
	stat.	0.034	0.008	0.013	0.003	0.021	0.026	0.035
	sys.	1.596	1.376	1.081	0.814	0.642	0.532	0.460
κ_2	value	4.188	7.769	6.538	4.748	3.124	1.876	1.021
	stat.	0.063	0.014	0.008	0.007	0.009	0.011	0.015
	sys.	0.506	0.796	0.682	0.516	0.376	0.279	0.214
κ_3	value	-9.974	1.241	3.826	3.399	2.585	1.684	0.937
	stat.	0.270	0.193	0.060	0.039	0.026	0.015	0.016
	sys.	1.595	0.649	0.603	0.530	0.413	0.317	0.223
κ_4	value	-10.813	-17.633	2.462	2.418	2.729	2.125	1.253
	stat.	2.184	1.660	0.643	0.473	0.184	0.093	0.044
	sys.	4.428	5.032	0.787	0.593	0.565	0.495	0.354
κ_5	value	114.802	-77.145	-19.752	3.962	2.589	3.593	1.970
	stat.	36.648	20.353	9.696	5.021	2.197	0.782	0.330
	sys.	34.055	27.036	9.388	2.463	0.603	1.317	0.681
κ_6	value	623.879	-111.80	-40.036	50.016	-6.418	3.055	1.982
	stat.	512.670	368.861	171.146	67.532	24.260	7.453	2.568
	sys.	411.244	356.358	0.000	30.317	6.058	4.423	0.999

Table A.4: Factorial cumulant ratios and uncertainties at $\sqrt{s_{NN}} = 3.2$ GeV

$\sqrt{s_{NN}} = 3.2$ GeV factorial cumulant ratios								
		0-5%	5-10%	10-20%	20-30%	30-40%	40-50%	50-60%
κ_2/κ_1	value	0.136	0.311	0.355	0.387	0.400	0.395	0.374
	±stat.	0.002	0.001	0.000	0.001	0.000	0.001	0.001
	±sys.	0.012	0.017	0.018	0.020	0.020	0.020	0.021
κ_3/κ_1	value	-0.325	0.050	0.207	0.277	0.331	0.354	0.343
	±stat.	0.008	0.008	0.003	0.003	0.003	0.003	0.003
	±sys.	0.035	0.026	0.023	0.029	0.035	0.036	0.036
κ_4/κ_1	value	-0.352	-0.705	0.134	0.197	0.349	0.447	0.459
	±stat.	0.071	0.066	0.035	0.039	0.024	0.019	0.015
	±sys.	0.137	0.166	0.042	0.035	0.063	0.070	0.073
κ_5/κ_1	value	3.739	-3.084	-1.071	0.323	0.331	0.756	0.722
	±stat.	1.193	0.814	0.526	0.409	0.280	0.164	0.119
	±sys.	0.538	0.981	0.474	0.220	0.130	0.189	0.163
κ_6/κ_1	value	20.319	-4.469	-2.171	4.075	-0.821	0.643	0.726
	±stat.	16.678	14.748	9.287	5.501	3.096	1.561	0.929
	±sys.	13.543	14.328	3.512	2.666	0.768	1.162	0.365

A.2 Cumulants and Factorial Cumulants at $\sqrt{s_{NN}} = 3.5$ GeV

Table A.5: Cumulants and uncertainties at $\sqrt{s_{NN}} = 3.5$ GeV

$\sqrt{s_{NN}} = 3.5$ GeV cumulants

		0-5%	5-10%	10-20%	20-30%	30-40%	40-50%	50-60%
C_1	value	30.167	24.642	18.224	12.056	7.659	4.582	2.762
	stat.	0.003	0.003	0.002	0.002	0.001	0.001	0.001
	sys.	1.545	1.311	1.008	0.730	0.545	0.421	0.338
C_2	value	32.992	30.246	22.824	15.357	9.823	5.851	3.462
	stat.	0.030	0.025	0.014	0.009	0.007	0.004	0.004
	sys.	1.822	1.866	1.471	1.069	0.781	0.583	0.456
C_3	value	31.825	42.256	34.346	23.814	15.540	9.289	5.382
	stat.	0.368	0.334	0.138	0.090	0.052	0.027	0.021
	sys.	1.519	3.106	2.800	2.042	1.462	1.068	0.793
C_4	value	5.123	61.881	63.218	47.787	31.807	19.697	11.323
	stat.	5.347	4.814	1.750	1.097	0.478	0.201	0.145
	sys.	4.722	6.216	6.864	5.354	3.691	2.729	1.861
C_5	value	-146.28	37.886	129.395	107.953	79.919	53.204	32.231
	stat.	84.882	72.906	28.261	12.708	5.660	1.845	1.272
	sys.	57.122	39.466	28.202	17.384	11.440	8.533	5.739
C_6	value	-865.85	-723.59	92.404	133.087	180.553	146.673	113.137
	stat.	1370.459	1369.997	546.710	194.915	77.069	20.635	13.511
	sys.	1878.021	1263.932	251.356	155.225	50.937	36.338	22.690

Table A.6: Cumulant ratios and uncertainties at $\sqrt{s_{NN}} = 3.5$ GeV

$\sqrt{s_{NN}} = 3.5$ GeV cumulant ratios								
		0-5%	5-10%	10-20%	20-30%	30-40%	40-50%	50-60%
C_2/C_1	value	1.094	1.227	1.252	1.274	1.282	1.277	1.253
	stat.	0.001	0.001	0.001	0.001	0.001	0.001	0.001
	sys.	0.008	0.012	0.013	0.014	0.014	0.014	0.015
C_3/C_1	value	1.055	1.715	1.885	1.975	2.029	2.027	1.949
	stat.	0.012	0.014	0.008	0.007	0.007	0.006	0.007
	sys.	0.029	0.045	0.054	0.058	0.063	0.064	0.064
C_4/C_2	value	0.155	2.046	2.770	3.112	3.238	3.366	3.271
	stat.	0.162	0.159	0.076	0.071	0.048	0.034	0.041
	sys.	0.138	0.163	0.154	0.142	0.149	0.162	0.164
C_5/C_1	value	-4.849	1.537	7.100	8.954	10.435	11.612	11.669
	stat.	2.814	2.959	1.551	1.054	0.739	0.403	0.460
	sys.	2.004	1.441	1.181	0.772	0.891	0.996	1.072
C_6/C_2	value	-26.244	-23.924	4.049	8.666	18.381	25.067	32.684
	stat.	41.527	45.303	23.948	12.690	7.842	3.526	3.906
	sys.	57.122	41.813	10.784	9.651	4.699	3.907	4.769

Table A.7: Factorial cumulants and uncertainties at $\sqrt{s_{NN}} = 3.5$ GeV

$\sqrt{s_{NN}} = 3.5$ GeV factorial cumulants								
		0-5%	5-10%	10-20%	20-30%	30-40%	40-50%	50-60%
κ_1	value	30.167	24.642	18.224	12.056	7.659	4.582	2.762
	stat.	0.003	0.003	0.002	0.002	0.001	0.001	0.001
	sys.	1.545	1.311	1.008	0.730	0.545	0.421	0.338
κ_2	value	2.825	5.604	4.600	3.301	2.164	1.269	0.699
	stat.	0.030	0.025	0.014	0.009	0.007	0.004	0.004
	sys.	0.340	0.574	0.476	0.354	0.245	0.168	0.121
κ_3	value	-6.818	0.803	2.322	1.856	1.390	0.899	0.522
	stat.	0.364	0.325	0.120	0.083	0.040	0.020	0.014
	sys.	1.100	0.325	0.393	0.299	0.221	0.162	0.105
κ_4	value	-3.913	-6.804	-1.138	1.490	0.662	0.837	0.533
	stat.	4.994	3.659	1.420	0.779	0.327	0.111	0.074
	sys.	2.898	2.588	1.538	0.752	0.194	0.203	0.126
κ_5	value	-9.249	-22.840	-4.502	-14.916	-1.567	-1.263	0.599
	stat.	62.572	53.422	19.685	6.942	2.911	0.771	0.490
	sys.	49.969	20.843	12.034	3.951	0.000	1.424	0.698
κ_6	value	23.122	-209.32	-135.92	-21.455	-38.811	-13.639	-1.908
	stat.	870.327	895.741	287.204	91.607	29.138	7.328	3.112
	sys.	929.256	939.061	158.320	85.024	34.096	8.467	2.840

Table A.8: Factorial cumulant ratios and uncertainties at $\sqrt{s_{NN}} = 3.5$ GeV

$\sqrt{s_{NN}} = 3.5$ GeV factorial cumulant ratios								
		0-5%	5-10%	10-20%	20-30%	30-40%	40-50%	50-60%
κ_2/κ_1	value	0.094	0.227	0.252	0.274	0.282	0.277	0.253
	±stat.	0.001	0.001	0.001	0.001	0.001	0.001	0.001
	±sys.	0.008	0.012	0.013	0.014	0.014	0.014	0.015
κ_3/κ_1	value	-0.226	0.033	0.127	0.154	0.181	0.196	0.189
	±stat.	0.012	0.013	0.007	0.007	0.005	0.004	0.005
	±sys.	0.025	0.014	0.014	0.016	0.020	0.021	0.020
κ_4/κ_1	value	-0.130	-0.276	-0.062	0.124	0.086	0.183	0.193
	±stat.	0.166	0.148	0.078	0.065	0.043	0.024	0.027
	±sys.	0.094	0.100	0.084	0.061	0.021	0.031	0.040
κ_5/κ_1	value	-0.307	-0.927	-0.247	-1.237	-0.205	-0.276	0.217
	±stat.	2.074	2.168	1.080	0.576	0.380	0.168	0.177
	±sys.	1.650	0.830	0.645	0.428	0.000	0.310	0.165
κ_6/κ_1	value	0.766	-8.495	-7.458	-1.780	-5.067	-2.977	-0.691
	±stat.	28.851	36.350	15.760	7.598	3.805	1.599	1.127
	±sys.	30.862	38.061	8.721	7.016	4.090	1.746	1.284

A.3 Cumulants and Factorial Cumulants at $\sqrt{s_{NN}} = 3.9$ GeV

Table A.9: Cumulants and uncertainties at $\sqrt{s_{NN}} = 3.9$ GeV

$\sqrt{s_{NN}} = 3.9$ GeV cumulants

		0-5%	5-10%	10-20%	20-30%	30-40%	40-50%	50-60%
C_1	value	27.310	22.113	16.243	10.538	6.582	3.939	2.312
	stat.	0.005	0.004	0.002	0.002	0.001	0.001	0.001
	sys.	1.448	1.202	0.906	0.631	0.452	0.338	0.262
C_2	value	29.370	25.874	19.274	12.669	7.945	4.725	2.735
	stat.	0.040	0.042	0.017	0.010	0.007	0.004	0.004
	sys.	1.647	1.590	1.220	0.851	0.609	0.437	0.328
C_3	value	30.043	33.896	26.288	17.750	11.373	6.703	3.819
	stat.	0.460	0.425	0.189	0.098	0.057	0.023	0.017
	sys.	1.602	2.570	2.049	1.424	1.043	0.709	0.510
C_4	value	6.170	44.665	39.976	30.728	21.112	12.167	6.991
	stat.	6.912	5.000	2.337	1.001	0.547	0.189	0.120
	sys.	4.256	7.210	3.742	3.139	2.487	1.546	1.100
C_5	value	-257.09	-110.80	76.805	74.400	53.501	28.669	17.847
	stat.	102.749	79.107	33.405	15.473	5.959	1.885	1.101
	sys.	31.773	67.525	13.359	18.346	9.161	5.183	3.828
C_6	value	-794.39	-3650.0	634.636	399.993	183.447	78.311	57.185
	stat.	1669.997	1243.975	559.279	318.616	77.575	21.902	9.986
	sys.	1507.677	1878.498	468.897	386.380	72.085	12.104	22.309

Table A.10: Cumulant ratios and uncertainties at $\sqrt{s_{NN}} = 3.9$ GeV

$\sqrt{s_{NN}} = 3.9$ GeV cumulant ratios

		0-5%	5-10%	10-20%	20-30%	30-40%	40-50%	50-60%
C_2/C_1	value	1.075	1.170	1.187	1.202	1.207	1.199	1.183
	stat.	0.001	0.002	0.001	0.001	0.001	0.001	0.001
	sys.	0.006	0.009	0.010	0.010	0.011	0.010	0.010
C_3/C_1	value	1.100	1.533	1.618	1.684	1.728	1.702	1.652
	stat.	0.017	0.019	0.012	0.009	0.009	0.006	0.007
	sys.	0.018	0.038	0.037	0.041	0.045	0.042	0.042
C_4/C_2	value	0.210	1.726	2.074	2.425	2.657	2.575	2.556
	stat.	0.235	0.193	0.121	0.079	0.068	0.039	0.042
	sys.	0.166	0.239	0.091	0.110	0.127	0.119	0.133
C_5/C_1	value	-9.414	-5.011	4.729	7.060	8.128	7.278	7.719
	stat.	3.763	3.577	2.057	1.469	0.905	0.478	0.475
	sys.	0.935	3.055	0.689	1.805	0.923	0.727	0.982
C_6/C_2	value	-27.047	-141.07	32.928	31.573	23.088	16.575	20.906
	stat.	56.846	48.047	29.019	25.149	9.764	4.635	3.645
	sys.	51.450	60.093	23.959	31.208	7.963	3.880	6.692

Table A.11: Factorial cumulants and uncertainties at $\sqrt{s_{NN}} = 3.9$ GeV

$\sqrt{s_{NN}} = 3.9$ GeV factorial cumulants								
		0-5%	5-10%	10-20%	20-30%	30-40%	40-50%	50-60%
κ_1	value	27.310	22.113	16.243	10.538	6.582	3.939	2.312
	stat.	0.005	0.004	0.002	0.002	0.001	0.001	0.001
	sys.	1.448	1.202	0.906	0.631	0.452	0.338	0.262
κ_2	value	2.060	3.761	3.031	2.131	1.363	0.785	0.423
	stat.	0.039	0.040	0.017	0.010	0.007	0.003	0.003
	sys.	0.240	0.397	0.320	0.229	0.156	0.102	0.068
κ_3	value	-3.447	0.501	0.952	0.820	0.701	0.407	0.237
	stat.	0.426	0.384	0.171	0.088	0.049	0.019	0.011
	sys.	0.612	0.370	0.183	0.147	0.136	0.073	0.049
κ_4	value	-14.876	-6.780	-3.196	0.356	0.782	0.284	0.293
	stat.	6.092	3.839	1.963	0.816	0.335	0.114	0.066
	sys.	3.415	4.977	1.985	0.691	0.192	0.198	0.129
κ_5	value	-80.352	-134.05	23.261	7.849	1.127	-0.083	0.324
	stat.	72.770	64.175	23.000	10.282	2.898	0.992	0.361
	sys.	50.814	42.842	18.514	13.659	2.775	0.663	0.825
κ_6	value	1596.935	-1382.3	297.608	108.763	3.789	-3.895	-3.515
	stat.	1594.151	729.693	303.792	165.591	28.210	5.738	1.567
	sys.	810.444	1027.330	432.319	0.000	23.650	9.440	3.392

Table A.12: Factorial cumulant ratios and uncertainties at $\sqrt{s_{NN}} = 3.9$ GeV

$\sqrt{s_{NN}} = 3.9$ GeV factorial cumulant ratios

		0-5%	5-10%	10-20%	20-30%	30-40%	40-50%	50-60%
κ_2/κ_1	value	0.075	0.170	0.187	0.202	0.207	0.199	0.183
	±stat.	0.001	0.002	0.001	0.001	0.001	0.001	0.001
	±sys.	0.006	0.009	0.010	0.010	0.011	0.010	0.010
κ_3/κ_1	value	-0.126	0.023	0.059	0.078	0.107	0.103	0.103
	±stat.	0.016	0.017	0.011	0.008	0.007	0.005	0.005
	±sys.	0.016	0.017	0.008	0.011	0.015	0.011	0.012
κ_4/κ_1	value	-0.545	-0.307	-0.197	0.034	0.119	0.072	0.127
	±stat.	0.223	0.174	0.121	0.077	0.051	0.029	0.028
	±sys.	0.119	0.235	0.119	0.063	0.029	0.050	0.046
κ_5/κ_1	value	-2.942	-6.062	1.432	0.745	0.171	-0.021	0.140
	±stat.	2.665	2.902	1.416	0.976	0.440	0.252	0.156
	±sys.	1.860	1.613	1.167	1.313	0.411	0.156	0.344
κ_6/κ_1	value	58.474	-62.511	18.323	10.321	0.576	-0.989	-1.520
	±stat.	58.376	33.001	18.702	15.714	4.286	1.457	0.678
	±sys.	30.065	40.103	26.660	0.000	3.617	1.930	1.458

A.4 Cumulants and Factorial Cumulants at $\sqrt{s_{NN}} = 4.5$ GeV

Table A.13: Cumulants and uncertainties at $\sqrt{s_{NN}} = 4.5$ GeV

$\sqrt{s_{NN}} = 4.5$ GeV cumulants

		0-5%	5-10%	10-20%	20-30%	30-40%	40-50%	50-60%
C_1	value	23.219	18.978	14.002	9.233	5.819	3.411	1.873
	stat.	0.006	0.004	0.002	0.002	0.001	0.001	0.001
	sys.	1.436	1.190	0.880	0.597	0.407	0.281	0.201
C_2	value	25.079	21.809	16.196	10.722	6.730	3.913	2.117
	stat.	0.033	0.033	0.015	0.011	0.007	0.004	0.003
	sys.	1.608	1.443	1.077	0.734	0.500	0.341	0.238
C_3	value	25.312	26.998	20.336	13.971	8.821	5.088	2.684
	stat.	0.411	0.482	0.167	0.082	0.048	0.022	0.013
	sys.	1.421	2.081	1.519	1.125	0.741	0.499	0.326
C_4	value	28.044	35.810	28.114	22.087	14.093	8.099	3.999
	stat.	6.565	4.456	1.992	0.813	0.333	0.160	0.086
	sys.	3.681	4.511	2.329	2.639	1.419	1.048	0.532
C_5	value	53.025	14.964	40.386	43.961	31.884	16.032	6.633
	stat.	113.099	69.011	26.568	11.567	4.187	1.588	0.575
	sys.	127.864	40.327	20.482	10.921	6.007	2.750	1.106
C_6	value	-1256.3	-1003.0	-25.396	50.930	111.502	38.091	7.790
	stat.	1752.298	1250.881	372.682	182.212	57.573	19.825	3.951
	sys.	1595.276	915.075	344.431	166.305	66.033	0.000	3.657

Table A.14: Cumulant ratios and uncertainties at $\sqrt{s_{NN}} = 4.5$ GeV

$\sqrt{s_{NN}} = 4.5$ GeV cumulant ratios

		0-5%	5-10%	10-20%	20-30%	30-40%	40-50%	50-60%
C_2/C_1	value	1.080	1.149	1.157	1.161	1.157	1.147	1.131
	stat.	0.001	0.002	0.001	0.001	0.001	0.001	0.001
	sys.	0.025	0.023	0.019	0.014	0.011	0.009	0.008
C_3/C_1	value	1.090	1.423	1.452	1.513	1.516	1.492	1.433
	stat.	0.018	0.025	0.012	0.009	0.008	0.006	0.007
	sys.	0.025	0.028	0.027	0.038	0.035	0.038	0.029
C_4/C_2	value	1.118	1.642	1.736	2.060	2.094	2.070	1.889
	stat.	0.262	0.204	0.123	0.076	0.049	0.040	0.040
	sys.	0.114	0.178	0.108	0.133	0.081	0.083	0.063
C_5/C_1	value	2.284	0.789	2.884	4.761	5.479	4.700	3.542
	stat.	4.871	3.636	1.897	1.253	0.719	0.466	0.307
	sys.	5.549	1.744	1.582	1.106	0.966	0.542	0.312
C_6/C_2	value	-50.093	-45.991	-1.568	4.750	16.567	9.735	3.680
	stat.	69.821	57.362	23.009	17.001	8.552	5.068	1.865
	sys.	67.496	39.190	21.819	15.435	10.229	0.000	2.042

Table A.15: Factorial cumulants and uncertainties at $\sqrt{s_{NN}} = 4.5$ GeV

$\sqrt{s_{NN}} = 4.5$ GeV factorial cumulants								
		0-5%	5-10%	10-20%	20-30%	30-40%	40-50%	50-60%
κ_1	value	23.219	18.978	14.002	9.233	5.819	3.411	1.873
	stat.	0.006	0.004	0.002	0.002	0.001	0.001	0.001
	sys.	1.436	1.190	0.880	0.597	0.407	0.281	0.201
κ_2	value	1.860	2.831	2.194	1.489	0.911	0.502	0.244
	stat.	0.033	0.032	0.015	0.011	0.007	0.004	0.003
	sys.	0.571	0.477	0.309	0.180	0.108	0.065	0.038
κ_3	value	-3.488	-0.473	-0.247	0.270	0.268	0.172	0.078
	stat.	0.413	0.454	0.162	0.074	0.040	0.016	0.010
	sys.	1.294	1.024	0.514	0.196	0.065	0.044	0.015
κ_4	value	12.731	-0.148	0.241	0.807	0.286	0.144	-0.054
	stat.	6.037	3.385	1.560	0.684	0.232	0.095	0.039
	sys.	4.633	5.226	1.731	0.616	0.244	0.108	0.018
κ_5	value	-38.208	-33.181	-2.744	-2.443	2.829	-0.648	-0.317
	stat.	81.405	55.446	16.319	7.627	2.455	0.708	0.163
	sys.	108.717	39.065	13.175	7.324	1.956	0.525	0.249
κ_6	value	-1277.7	-559.90	-59.631	-44.631	-7.751	3.983	-0.400
	stat.	1265.557	731.288	244.157	86.240	19.556	6.736	0.774
	sys.	484.106	917.505	115.230	79.264	22.272	9.502	1.230

Table A.16: Factorial cumulant ratios and uncertainties at $\sqrt{s_{NN}} = 4.5$ GeV

$\sqrt{s_{NN}} = 4.5$ GeV factorial cumulant ratios								
		0-5%	5-10%	10-20%	20-30%	30-40%	40-50%	50-60%
κ_2/κ_1	value	0.080	0.149	0.157	0.161	0.157	0.147	0.131
	±stat.	0.001	0.002	0.001	0.001	0.001	0.001	0.001
	±sys.	0.025	0.023	0.019	0.014	0.011	0.009	0.008
κ_3/κ_1	value	-0.150	-0.025	-0.018	0.029	0.046	0.050	0.042
	±stat.	0.018	0.024	0.012	0.008	0.007	0.005	0.005
	±sys.	0.055	0.055	0.037	0.023	0.008	0.009	0.005
κ_4/κ_1	value	0.548	-0.008	0.017	0.087	0.049	0.042	-0.029
	±stat.	0.260	0.178	0.111	0.074	0.040	0.028	0.021
	±sys.	0.212	0.278	0.129	0.066	0.044	0.031	0.010
κ_5/κ_1	value	-1.646	-1.748	-0.196	-0.265	0.486	-0.190	-0.170
	±stat.	3.506	2.921	1.165	0.826	0.422	0.208	0.087
	±sys.	4.839	2.099	0.955	0.819	0.333	0.152	0.116
κ_6/κ_1	value	-55.026	-29.502	-4.259	-4.834	-1.332	1.168	-0.214
	±stat.	54.507	38.537	17.437	9.341	3.361	1.975	0.413
	±sys.	20.813	48.121	5.327	8.469	3.966	2.840	0.726

Appendix B

Tabulated Systematics

This appendix tabulates the contributions to the systematic uncertainties of the cumulants, factorial cumulants, and their ratios, at $\sqrt{s_{NN}}$ = 3.2, 3.5, 3.9, and 4.5 GeV in 7 centrality bins. The tabulated values underwent the Barlow check procedure detailed in Sec. 7.2.1. Those values that were determined to be statistically significant are flagged as red in the following tables. Only those statistically significant systematic variations were included in the final systematic uncertainty. The nHitsFit cut, efficiency correction, TOF m^2 cuts, DCA cut, $n\sigma_p$ cut, nHitsDedx cut, pileup cut/correction, and centrality cuts were each varied in two ways. If neither variation was statistically significant, then the systematic contribution from that cut or correction was 0. If one variation was statistically significant, then the systematic contribution from that cut or correction was equal to the amount the value changed from the default. If both variations were statistically significant, then the systematic uncertainty contribution was the average of the absolute values of the two deviations from the default.

B.1 Systematic Contributions at $\sqrt{s_{NN}} = 3.2$ GeV

Table B.1: Systematic uncertainty contributions for C_1 at $\sqrt{s_{NN}} = 3.2$ GeV

$\sqrt{s_{NN}} = 3.2$ GeV, C_1 Systematic Uncertainties								
		0-5%	5-10%	10-20%	20-30%	30-40%	40-50%	50-60%
C_1	value	30.704	25.018	18.442	12.273	7.814	4.750	2.730
	stat.	0.034	0.008	0.013	0.003	0.021	0.026	0.035
	sys.	1.596	1.376	1.081	0.814	0.642	0.532	0.460
nHitsFit	≥ 22	-0.210	-0.176	-0.136	-0.095	-0.064	-0.041	-0.024
	≥ 25	-0.197	-0.166	-0.129	-0.091	-0.061	-0.039	-0.024
	Σ	0.203	0.171	0.132	0.093	0.063	0.040	0.024
Efficiency	–5%	-1.616	-1.317	-0.971	-0.646	-0.411	-0.250	-0.144
	+5%	1.462	1.191	0.878	0.584	0.372	0.226	0.130
	Σ	1.539	1.254	0.924	0.615	0.392	0.238	0.137
m^2 cuts (GeV^2)	[0.7,1.3]	0.000	-0.000	0.000	0.000	0.000	0.000	0.000
	[0.6,1.1]	0.000	-0.000	0.000	0.000	0.000	-0.000	0.000
	Σ	0.000	0.000	0.000	0.000	0.000	0.000	0.000
DCA (cm)	<0.9	-0.088	-0.080	-0.068	-0.053	-0.038	-0.027	-0.018
	<1.1	-0.310	-0.254	-0.191	-0.130	-0.084	-0.052	-0.030
	Σ	0.199	0.167	0.129	0.091	0.061	0.039	0.024
$\lvert n\sigma_p \rvert$	2.75	0.024	0.014	0.006	0.001	-0.001	-0.001	-0.001
	2.5	0.112	0.080	0.048	0.025	0.012	0.006	0.003
	Σ	0.068	0.047	0.027	0.013	0.007	0.004	0.003
nHitsDedx	≥ 22	-0.210	-0.183	-0.146	-0.106	-0.073	-0.048	-0.029
	≥ 25	-0.166	-0.162	-0.144	-0.114	-0.083	-0.056	-0.036
	Σ	0.188	0.172	0.145	0.110	0.078	0.052	0.032
pileup	low	0.004	-0.001	0.001	-0.002	-0.002	0.000	0.002
	high	-0.003	0.000	0.002	-0.002	-0.003	-0.004	0.000
	Σ	0.000	0.000	0.000	0.000	0.000	0.000	0.000
cent. cut	–1	0.242	0.483	0.507	0.504	0.493	0.467	0.432
	+1	-0.234	-0.480	-0.507	-0.505	-0.496	-0.471	-0.441
	Σ	0.238	0.482	0.507	0.504	0.494	0.469	0.436

Table B.2: Systematic uncertainty contributions for C_2 at $\sqrt{s_{NN}} = 3.2$ GeV

$\sqrt{s_{NN}} = 3.2$ GeV, C_2 Systematic Uncertainties								
		0-5%	5-10%	10-20%	20-30%	30-40%	40-50%	50-60%
C_2	value	34.892	32.787	24.980	17.021	10.938	6.626	3.752
	stat.	0.032	0.017	0.019	0.008	0.030	0.037	0.050
	sys.	2.003	2.138	1.742	1.311	1.004	0.803	0.671
nHitsFit	≥ 22	-0.247	-0.258	-0.211	-0.155	-0.107	-0.069	-0.041
	≥ 25	-0.229	-0.240	-0.198	-0.147	-0.102	-0.066	-0.039
	Σ	0.238	0.249	0.204	0.151	0.104	0.067	0.040
Efficiency	–5%	-2.068	-2.156	-1.677	-1.159	-0.749	-0.453	-0.254
	+5%	1.851	1.914	1.486	1.026	0.663	0.401	0.225
	Σ	1.960	2.035	1.581	1.092	0.706	0.427	0.239
m^2 cuts (GeV^2)	[0.7,1.3]	-0.000	-0.000	0.000	-0.000	-0.000	0.000	-0.000
	[0.6,1.1]	-0.000	0.000	0.000	-0.000	0.000	0.000	0.000
	Σ	0.000	0.000	0.000	0.000	0.000	0.000	0.000
DCA (cm)	<0.9	-0.079	-0.094	-0.090	-0.078	-0.060	-0.042	-0.026
	<1.1	-0.391	-0.402	-0.315	-0.220	-0.146	-0.091	-0.053
	Σ	0.235	0.248	0.202	0.149	0.103	0.067	0.039
$\lvert n\sigma_p \rvert$	2.75	0.074	0.068	0.036	0.016	0.005	0.001	0.000
	2.5	0.228	0.220	0.136	0.074	0.037	0.018	0.009
	Σ	0.151	0.144	0.086	0.045	0.021	0.010	0.009
nHitsDedx	≥ 22	-0.232	-0.250	-0.215	-0.167	-0.119	-0.078	-0.048
	≥ 25	-0.143	-0.172	-0.181	-0.162	-0.128	-0.089	-0.057
	Σ	0.187	0.211	0.198	0.164	0.123	0.084	0.052
pileup	low	-0.005	-0.002	0.001	-0.003	-0.003	0.000	0.002
	high	0.011	0.000	0.003	-0.003	-0.004	-0.005	0.000
	Σ	0.000	0.000	0.000	0.000	0.000	0.000	0.000
cent. cut	–1	-0.012	0.506	0.636	0.675	0.685	0.667	0.615
	+1	0.034	-0.476	-0.636	-0.668	-0.689	-0.669	-0.628
	Σ	0.034	0.491	0.636	0.672	0.687	0.668	0.622

Table B.3: Systematic uncertainty contributions for C_3 at $\sqrt{s_{NN}} = 3.2$ GeV

$\sqrt{s_{NN}} = 3.2$ GeV, C_3 Systematic Uncertainties								
		0-5%	5-10%	10-20%	20-30%	30-40%	40-50%	50-60%
C_3	value	33.294	49.564	41.882	29.916	19.771	12.061	6.731
	stat.	0.400	0.204	0.068	0.054	0.060	0.070	0.095
	sys.	1.688	3.869	3.655	2.838	2.131	1.658	1.312
nHitsFit	≥ 22	-0.154	-0.425	-0.414	-0.333	-0.241	-0.160	-0.094
	≥ 25	-0.145	-0.397	-0.389	-0.307	-0.227	-0.151	-0.090
	Σ	0.150	0.411	0.401	0.320	0.234	0.156	0.092
Efficiency	–5%	-1.314	-4.041	-3.726	-2.750	-1.854	-1.138	-0.631
	+5%	1.272	3.527	3.223	2.372	1.595	0.979	0.542
	Σ	1.293	3.784	3.474	2.561	1.725	1.058	0.586
m^2 cuts (GeV^2)	[0.7,1.3]	-0.000	0.000	-0.000	0.000	0.000	-0.000	0.000
	[0.6,1.1]	0.000	-0.000	-0.000	0.000	-0.000	-0.000	0.000
	Σ	0.000	0.000	0.000	0.000	0.000	0.000	0.000
DCA (cm)	<0.9	-0.003	-0.121	-0.123	-0.143	-0.121	-0.093	-0.055
	<1.1	-0.319	-0.733	-0.687	-0.501	-0.346	-0.217	-0.128
	Σ	0.319	0.427	0.405	0.322	0.233	0.155	0.092
$\lvert n\sigma_p \rvert$	2.75	0.126	0.220	0.154	0.070	0.023	0.010	0.004
	2.5	0.308	0.679	0.446	0.245	0.119	0.063	0.028
	Σ	0.217	0.450	0.300	0.157	0.071	0.037	0.028
nHitsDedx	≥ 22	-0.172	-0.370	-0.396	-0.333	-0.256	-0.174	-0.109
	≥ 25	-0.022	-0.143	-0.258	-0.264	-0.252	-0.189	-0.124
	Σ	0.097	0.256	0.327	0.299	0.254	0.182	0.116
pileup	low	-0.016	-0.002	0.001	-0.005	-0.005	0.000	0.004
	high	0.121	0.001	0.004	-0.005	-0.006	-0.010	0.001
	Σ	0.000	0.000	0.000	0.000	0.000	0.000	0.000
cent. cut	–1	-0.959	-0.027	0.888	1.108	1.164	1.246	1.152
	+1	1.037	0.174	-0.866	-1.061	-1.195	-1.241	-1.169
	Σ	0.998	0.174	0.877	1.084	1.179	1.244	1.160

Table B.4: Systematic uncertainty contributions for C_4 at $\sqrt{s_{NN}} = 3.2$ GeV

$\sqrt{s_{NN}} = 3.2$ GeV, C_4 Systematic Uncertainties								
		0-5%	5-10%	10-20%	20-30%	30-40%	40-50%	50-60%
C_4	value	-10.639	69.209	89.627	68.321	47.919	30.108	16.752
	stat.	3.380	2.347	0.863	0.615	0.299	0.234	0.254
	sys.	7.060	7.985	9.914	8.016	6.112	4.800	3.611
nHitsFit	≥ 22	0.719	-0.322	-1.037	-0.900	-0.725	-0.503	-0.300
	≥ 25	0.721	-0.521	-1.038	-0.781	-0.660	-0.464	-0.284
	Σ	0.000	0.521	1.038	0.841	0.692	0.484	0.292
Efficiency	–5%	7.635	-4.414	-10.295	-8.180	-5.975	-3.833	-2.136
	+5%	-5.878	4.134	8.696	6.880	5.001	3.199	1.782
	Σ	6.757	4.274	9.495	7.530	5.488	3.516	1.959
m^2 cuts (GeV^2)	[0.7,1.3]	0.000	-0.000	0.000	-0.000	-0.000	-0.000	-0.000
	[0.6,1.1]	-0.000	0.000	0.000	-0.000	-0.000	0.000	-0.000
	Σ	0.000	0.000	0.000	0.000	0.000	0.000	0.000
DCA (cm)	<0.9	1.271	0.114	-0.203	-0.243	-0.305	-0.276	-0.167
	<1.1	0.685	-1.196	-1.958	-1.456	-1.026	-0.690	-0.421
	Σ	1.271	1.196	1.958	0.849	0.665	0.483	0.294
$\lvert n\sigma_p \rvert$	2.75	-0.338	0.320	0.551	0.304	0.102	0.058	0.012
	2.5	-0.835	1.942	1.505	0.880	0.415	0.278	0.104
	Σ	0.835	1.131	1.028	0.592	0.258	0.168	0.104
nHitsDedx	≥ 22	0.664	0.259	-1.226	-0.842	-0.751	-0.509	-0.350
	≥ 25	2.076	-0.164	-0.293	-0.597	-0.638	-0.538	-0.373
	Σ	1.370	0.000	1.226	0.719	0.695	0.523	0.362
pileup	low	0.185	-0.007	-0.009	-0.011	-0.011	0.001	0.011
	high	1.276	0.002	0.010	-0.008	-0.014	-0.025	0.002
	Σ	0.000	0.000	0.000	0.000	0.000	0.000	0.000
cent. cut	–1	-0.615	-6.615	1.067	2.233	2.365	3.144	2.982
	+1	1.559	6.425	-0.546	-2.353	-2.437	-3.152	-2.980
	Σ	0.000	6.520	0.807	2.293	2.401	3.148	2.981

Table B.5: Systematic uncertainty contributions for C_5 at $\sqrt{s_{NN}} = 3.2$ GeV

$\sqrt{s_{NN}} = 3.2$ GeV, C_5 Systematic Uncertainties								
		0-5%	5-10%	10-20%	20-30%	30-40%	40-50%	50-60%
C_5	value	-149.16	-80.914	217.042	196.615	149.170	99.822	55.964
	stat.	46.489	31.070	13.939	8.773	3.947	1.827	1.149
	sys.	34.520	60.324	30.673	28.105	22.135	18.468	13.331
nHitsFit	≥ 22	1.218	5.130	-2.379	-2.849	-2.745	-2.017	-1.200
	≥ 25	2.944	3.103	-4.832	-1.808	-2.200	-1.741	-1.132
	Σ	0.000	0.000	4.832	2.849	2.473	1.879	1.166
Efficiency	–5%	24.141	43.646	-27.312	-29.142	-23.194	-16.182	-9.123
	+5%	-20.970	-31.715	23.111	23.922	18.926	13.119	7.390
	Σ	0.000	37.680	25.211	26.532	21.060	14.650	8.257
m^2 cuts (GeV^2)	[0.7,1.3]	0.000	0.000	-0.000	0.000	0.000	0.000	0.000
	[0.6,1.1]	0.000	0.000	-0.000	0.000	-0.000	0.000	0.000
	Σ	0.000	0.000	0.000	0.000	0.000	0.000	0.000
DCA (cm)	<0.9	16.061	10.359	-0.797	0.866	-0.283	-1.254	-0.607
	<1.1	1.911	0.049	-5.732	-4.200	-3.221	-2.852	-1.704
	Σ	0.000	10.359	5.732	4.200	3.221	2.053	1.156
$\lvert n\sigma_p \rvert$	2.75	-7.932	-6.617	-2.844	0.985	0.504	0.369	-0.082
	2.5	-17.496	-14.276	0.762	1.981	1.347	1.602	0.408
	Σ	17.496	14.276	0.000	1.981	0.925	0.985	0.408
nHitsDedx	≥ 22	2.190	11.647	-8.383	-4.300	-3.083	-1.903	-1.539
	≥ 25	16.999	10.500	-0.346	-3.884	-2.542	-2.262	-1.570
	Σ	0.000	11.074	8.383	4.092	2.813	2.082	1.554
pileup	low	6.151	-0.194	-0.117	-0.010	-0.052	0.001	0.032
	high	14.796	-0.316	-0.005	0.032	-0.050	-0.078	0.006
	Σ	0.000	0.000	0.000	0.000	0.000	0.000	0.000
cent. cut	–1	28.595	-43.812	-3.679	3.893	4.904	10.200	10.304
	+1	-30.921	40.697	13.370	-8.677	-4.300	-11.098	-10.118
	Σ	29.758	42.254	13.370	6.285	4.602	10.649	10.211

Table B.6: Systematic uncertainty contributions for C_6 at $\sqrt{s_{NN}} = 3.2$ GeV

$\sqrt{s_{NN}} = 3.2$ GeV, C_6 Systematic Uncertainties								
		0-5%	5-10%	10-20%	20-30%	30-40%	40-50%	50-60%
C_6	value	905.903	-2037.6	389.240	732.015	547.076	409.503	231.652
	stat.	787.888	555.921	283.457	146.591	62.007	22.562	10.218
	sys.	342.118	601.363	180.061	128.275	89.653	87.334	60.520
nHitsFit	≥ 22	-68.511	50.282	2.455	-13.444	-12.422	-9.617	-5.537
	≥ 25	-44.832	48.023	-52.240	3.374	-6.055	-7.566	-5.185
	Σ	0.000	0.000	0.000	0.000	0.000	8.592	5.361
Efficiency	–5%	-434.52	593.714	-15.560	-138.63	-99.007	-80.052	-45.486
	+5%	297.792	-443.30	20.694	109.351	79.277	63.196	35.889
	Σ	0.000	518.507	0.000	123.992	89.142	71.624	40.687
m^2 cuts (GeV^2)	[0.7,1.3]	-0.000	-0.000	0.000	-0.000	-0.000	-0.000	-0.000
	[0.6,1.1]	-0.000	-0.000	0.000	0.000	0.000	-0.000	-0.000
	Σ	0.000	0.000	0.000	0.000	0.000	0.000	0.000
DCA (cm)	<0.9	39.910	191.766	-32.347	15.514	12.135	-12.366	-1.980
	<1.1	-1.764	-23.956	-45.110	14.346	-6.985	-13.862	-7.510
	Σ	0.000	0.000	0.000	0.000	9.560	13.114	7.510
$\lvert n\sigma_p \rvert$	2.75	-257.02	-127.59	-105.65	7.337	4.174	1.581	-2.559
	2.5	-343.02	-426.71	-104.95	-7.470	4.625	10.680	0.694
	Σ	0.000	277.147	105.649	7.337	0.000	10.680	2.559
nHitsDedx	≥ 22	216.726	-48.968	-93.494	-37.794	-18.638	-8.690	-9.467
	≥ 25	440.119	202.299	-62.352	-32.041	-21.987	-15.414	-9.658
	Σ	328.423	0.000	0.000	32.041	0.000	12.052	9.563
pileup	low	116.780	-3.855	-3.720	-0.098	-0.399	0.012	0.076
	high	74.878	-7.098	-0.600	0.768	-0.405	-0.226	0.026
	Σ	95.829	0.000	0.000	0.000	0.000	0.000	0.000
cent. cut	–1	-54.397	126.405	-123.56	-27.736	13.145	36.736	43.471
	+1	-215.60	-71.934	168.059	-21.871	-1.484	-52.531	-41.948
	Σ	0.000	126.405	145.809	0.000	0.000	44.634	42.709

Table B.7: Systematic uncertainty contributions for C_2/C_1 at $\sqrt{s_{NN}} = 3.2$ GeV

$\sqrt{s_{NN}} = 3.2$ GeV, C_2/C_1 Systematic Uncertainties								
		0-5%	5-10%	10-20%	20-30%	30-40%	40-50%	50-60%
C_2/C_1	value	1.136	1.311	1.355	1.387	1.400	1.395	1.374
	stat.	0.002	0.001	0.000	0.001	0.000	0.001	0.001
	sys.	0.012	0.017	0.018	0.020	0.020	0.020	0.021
nHitsFit	≥ 22	-0.000	-0.001	-0.001	-0.002	-0.002	-0.002	-0.003
	≥ 25	-0.000	-0.001	-0.001	-0.002	-0.002	-0.002	-0.002
	Σ	0.000	0.001	0.001	0.002	0.002	0.002	0.002
Efficiency	–5%	-0.007	-0.016	-0.019	-0.020	-0.021	-0.021	-0.020
	+5%	0.006	0.015	0.017	0.018	0.019	0.019	0.018
	Σ	0.007	0.016	0.018	0.019	0.020	0.020	0.019
m^2 cuts (GeV^2)	[0.7,1.3]	-0.000	-0.000	0.000	-0.000	-0.000	0.000	-0.000
	[0.6,1.1]	-0.000	0.000	0.000	-0.000	0.000	0.000	0.000
	Σ	0.000	0.000	0.000	0.000	0.000	0.000	0.000
DCA (cm)	<0.9	0.001	0.000	0.000	-0.000	-0.001	-0.001	-0.001
	<1.1	-0.001	-0.003	-0.003	-0.003	-0.004	-0.004	-0.004
	Σ	0.001	0.002	0.002	0.002	0.002	0.002	0.002
$\lvert n\sigma_p \rvert$	2.75	0.002	0.002	0.002	0.001	0.001	0.001	0.000
	2.5	0.003	0.005	0.004	0.003	0.002	0.002	0.002
	Σ	0.002	0.003	0.003	0.002	0.002	0.001	0.001
nHitsDedx	≥ 22	0.000	-0.000	-0.001	-0.002	-0.002	-0.002	-0.003
	≥ 25	0.001	0.002	0.001	-0.000	-0.001	-0.002	-0.003
	Σ	0.001	0.001	0.001	0.001	0.002	0.002	0.003
pileup	low	-0.000	0.000	-0.000	-0.000	0.000	-0.000	0.000
	high	0.000	0.000	-0.000	0.000	0.000	-0.000	0.000
	Σ	0.000	0.000	0.000	0.000	0.000	0.000	0.000
cent. cut	–1	-0.009	-0.005	-0.003	-0.002	-0.001	0.004	0.009
	+1	0.010	0.006	0.003	0.003	0.001	-0.002	-0.007
	Σ	0.010	0.006	0.003	0.002	0.001	0.003	0.008

Table B.8: Systematic uncertainty contributions for C_3/C_1 at $\sqrt{s_{NN}} = 3.2$ GeV

$\sqrt{s_{NN}} = 3.2$ GeV, C_3/C_1 Systematic Uncertainties								
		0-5%	5-10%	10-20%	20-30%	30-40%	40-50%	50-60%
C_3/C_1	value	1.084	1.981	2.271	2.438	2.530	2.539	2.465
	stat.	0.014	0.008	0.003	0.004	0.004	0.004	0.004
	sys.	0.043	0.069	0.077	0.089	0.095	0.098	0.099
nHitsFit	≥ 22	0.002	-0.003	-0.006	-0.008	-0.010	-0.012	-0.012
	≥ 25	0.002	-0.003	-0.005	-0.007	-0.009	-0.011	-0.011
	Σ	0.002	0.003	0.005	0.008	0.010	0.011	0.012
Efficiency	–5%	0.014	-0.054	-0.078	-0.091	-0.099	-0.101	-0.096
	+5%	-0.011	0.049	0.070	0.081	0.088	0.089	0.085
	Σ	0.012	0.052	0.074	0.086	0.093	0.095	0.091
m^2 cuts (GeV^2)	[0.7,1.3]	-0.000	0.000	-0.000	0.000	0.000	-0.000	0.000
	[0.6,1.1]	0.000	-0.000	-0.000	0.000	-0.000	-0.000	0.000
	Σ	0.000	0.000	0.000	0.000	0.000	0.000	0.000
DCA (cm)	<0.9	0.003	0.002	0.002	-0.001	-0.003	-0.005	-0.004
	<1.1	0.001	-0.009	-0.014	-0.015	-0.017	-0.018	-0.020
	Σ	0.003	0.005	0.008	0.015	0.010	0.011	0.012
$\lvert n\sigma_p \rvert$	2.75	0.003	0.008	0.008	0.006	0.003	0.003	0.002
	2.5	0.006	0.021	0.018	0.015	0.011	0.010	0.007
	Σ	0.005	0.014	0.013	0.010	0.007	0.006	0.005
nHitsDedx	≥ 22	0.002	-0.000	-0.003	-0.006	-0.009	-0.011	-0.014
	≥ 25	0.005	0.007	0.004	0.001	-0.005	-0.009	-0.013
	Σ	0.003	0.007	0.004	0.006	0.007	0.010	0.013
pileup	low	-0.001	0.000	-0.000	-0.000	0.000	-0.000	0.000
	high	0.004	0.000	-0.000	0.000	0.000	-0.000	0.000
	Σ	0.000	0.000	0.000	0.000	0.000	0.000	0.000
cent. cut	–1	-0.040	-0.040	-0.015	-0.010	-0.011	0.014	0.038
	+1	0.042	0.044	0.015	0.013	0.007	-0.009	-0.026
	Σ	0.041	0.042	0.015	0.012	0.009	0.011	0.032

Table B.9: Systematic uncertainty contributions for C_4/C_2 at $\sqrt{s_{NN}} = 3.2$ GeV

$\sqrt{s_{NN}} = 3.2$ GeV, C_4/C_2 Systematic Uncertainties								
		0-5%	5-10%	10-20%	20-30%	30-40%	40-50%	50-60%
C_4/C_2	value	-0.305	2.111	3.588	4.014	4.381	4.544	4.465
	stat.	0.097	0.072	0.035	0.035	0.026	0.023	0.020
	sys.	0.183	0.234	0.170	0.190	0.230	0.241	0.249
nHitsFit	≥ 22	0.018	0.007	-0.011	-0.016	-0.023	-0.029	-0.031
	≥ 25	0.019	-0.000	-0.013	-0.011	-0.019	-0.025	-0.029
	Σ	0.000	0.000	0.012	0.014	0.021	0.027	0.030
Efficiency	–5%	0.190	0.004	-0.160	-0.194	-0.231	-0.251	-0.250
	+5%	-0.161	0.003	0.143	0.173	0.204	0.222	0.220
	Σ	0.175	0.000	0.152	0.183	0.217	0.236	0.235
m^2 cuts (GeV^2)	[0.7,1.3]	0.000	-0.000	0.000	-0.000	-0.000	-0.000	-0.000
	[0.6,1.1]	-0.000	0.000	0.000	-0.000	-0.000	0.000	-0.000
	Σ	0.000	0.000	0.000	0.000	0.000	0.000	0.000
DCA (cm)	<0.9	0.036	0.009	0.005	0.004	-0.004	-0.012	-0.013
	<1.1	0.016	-0.010	-0.033	-0.033	-0.035	-0.041	-0.049
	Σ	0.036	0.010	0.033	0.033	0.035	0.027	0.031
$\lvert n\sigma_p \rvert$	2.75	-0.009	0.005	0.017	0.014	0.007	0.008	0.003
	2.5	-0.022	0.045	0.041	0.034	0.023	0.029	0.018
	Σ	0.000	0.025	0.029	0.024	0.015	0.019	0.018
nHitsDedx	≥ 22	0.017	0.024	-0.018	-0.010	-0.021	-0.023	-0.036
	≥ 25	0.058	0.006	0.014	0.003	-0.007	-0.020	-0.031
	Σ	0.037	0.024	0.018	0.010	0.021	0.021	0.034
pileup	low	0.005	-0.000	-0.000	-0.000	0.000	-0.000	0.000
	high	0.037	0.000	0.000	0.000	0.000	-0.000	0.000
	Σ	0.000	0.000	0.000	0.000	0.000	0.000	0.000
cent. cut	–1	-0.018	-0.238	-0.050	-0.029	-0.062	0.019	0.075
	+1	0.045	0.223	0.068	0.019	0.050	-0.015	-0.040
	Σ	0.000	0.231	0.059	0.024	0.056	0.017	0.057

Table B.10: Systematic uncertainty contributions for C_5/C_1 at $\sqrt{s_{NN}} = 3.2$ GeV

$\sqrt{s_{NN}} = 3.2$ GeV, C_5/C_1 Systematic Uncertainties								
		0-5%	5-10%	10-20%	20-30%	30-40%	40-50%	50-60%
C_5/C_1	value	-4.858	-3.234	11.769	16.021	19.091	21.015	20.497
	stat.	1.510	1.242	0.758	0.714	0.507	0.364	0.293
	sys.	1.149	2.254	1.098	1.428	1.868	2.071	2.100
nHitsFit	≥ 22	0.006	0.181	-0.042	-0.107	-0.194	-0.242	-0.254
	≥ 25	0.064	0.102	-0.179	-0.028	-0.131	-0.191	-0.235
	Σ	0.000	0.000	0.000	0.000	0.162	0.217	0.245
Efficiency	–5%	0.504	1.496	-0.818	-1.455	-1.866	-2.185	-2.149
	+5%	-0.474	-1.169	0.727	1.246	1.589	1.849	1.817
	Σ	0.000	1.333	0.773	1.350	1.727	2.017	1.983
m^2 cuts (GeV^2)	[0.7,1.3]	0.000	0.000	-0.000	0.000	0.000	0.000	0.000
	[0.6,1.1]	0.000	0.000	-0.000	0.000	-0.000	0.000	0.000
	Σ	0.000	0.000	0.000	0.000	0.000	0.000	0.000
DCA (cm)	<0.9	0.508	0.402	0.000	0.139	0.057	-0.146	-0.089
	<1.1	0.013	-0.031	-0.187	-0.171	-0.204	-0.365	-0.394
	Σ	0.000	0.402	0.000	0.171	0.204	0.255	0.242
$\lvert n\sigma_p \rvert$	2.75	-0.255	-0.263	-0.158	0.079	0.067	0.083	-0.023
	2.5	-0.554	-0.562	0.011	0.129	0.142	0.310	0.126
	Σ	0.554	0.562	0.000	0.129	0.105	0.196	0.126
nHitsDedx	≥ 22	0.038	0.439	-0.358	-0.210	-0.214	-0.188	-0.342
	≥ 25	0.525	0.396	0.072	-0.166	-0.121	-0.224	-0.303
	Σ	0.000	0.417	0.000	0.210	0.214	0.206	0.322
pileup	low	0.201	-0.008	-0.007	0.002	-0.002	-0.000	0.000
	high	0.481	-0.013	-0.001	0.006	0.001	0.000	0.000
	Σ	0.000	0.000	0.000	0.000	0.000	0.000	0.000
cent. cut	–1	0.977	-1.722	-0.538	-0.355	-0.615	0.090	0.632
	+1	-1.036	1.535	1.021	-0.046	0.622	-0.230	-0.341
	Σ	1.007	1.629	0.779	0.355	0.619	0.160	0.486

Table B.11: Systematic uncertainty contributions for C_6/C_2 at $\sqrt{s_{NN}} = 3.2$ GeV

$\sqrt{s_{NN}} = 3.2$ GeV, C_6/C_2 Systematic Uncertainties								
		0-5%	5-10%	10-20%	20-30%	30-40%	40-50%	50-60%
C_6/C_2	value	25.963	-62.149	15.582	43.008	50.018	61.802	61.748
	stat.	22.595	16.964	11.358	8.604	5.659	3.398	2.537
	sys.	9.893	14.948	7.534	3.767	5.809	7.231	7.306
nHitsFit	≥ 22	-1.767	1.036	0.228	-0.393	-0.641	-0.802	-0.798
	≥ 25	-1.107	1.002	-1.952	0.564	-0.088	-0.525	-0.733
	Σ	0.000	0.000	0.000	0.000	0.000	0.525	0.765
Efficiency	–5%	-10.303	13.157	0.397	-4.884	-5.267	-7.357	-7.439
	+5%	7.558	-10.507	-0.105	4.078	4.490	6.174	6.238
	Σ	0.000	11.832	0.000	0.000	4.879	6.766	6.839
m^2 cuts (GeV^2)	[0.7,1.3]	-0.000	-0.000	0.000	-0.000	-0.000	-0.000	-0.000
	[0.6,1.1]	-0.000	-0.000	0.000	0.000	0.000	-0.000	-0.000
	Σ	0.000	0.000	0.000	0.000	0.000	0.000	0.000
DCA (cm)	<0.9	1.200	5.655	-1.235	1.103	1.375	-1.462	-0.098
	<1.1	0.238	-1.474	-1.590	1.381	0.029	-1.225	-1.118
	Σ	0.000	0.000	0.000	0.000	1.375	1.343	1.118
$\lvert n\sigma_p \rvert$	2.75	-7.437	-3.771	-4.258	0.391	0.361	0.226	-0.682
	2.5	-10.066	-12.683	-4.310	-0.630	0.256	1.445	0.045
	Σ	0.000	8.227	4.258	0.000	0.000	1.445	0.682
nHitsDedx	≥ 22	6.342	-1.953	-3.578	-1.782	-1.147	-0.574	-1.719
	≥ 25	12.668	5.813	-2.366	-1.460	-1.409	-1.476	-1.614
	Σ	9.505	0.000	0.000	1.460	0.000	0.000	1.666
pileup	low	3.350	-0.121	-0.149	0.001	-0.024	0.000	-0.016
	high	2.138	-0.216	-0.026	0.053	-0.019	0.016	0.001
	Σ	2.744	0.000	0.000	0.000	0.000	0.000	0.000
cent. cut	–1	-1.549	4.890	-5.483	-3.472	-2.060	-0.753	1.752
	+1	-6.210	-3.053	6.948	0.389	2.837	-1.532	-0.720
	Σ	0.000	3.971	6.215	3.472	2.837	1.532	1.236

Table B.12: Systematic uncertainty contributions for κ_1 at $\sqrt{s_{NN}} = 3.2$ GeV

$\sqrt{s_{NN}} = 3.2$ GeV, κ_1 Systematic Uncertainties								
		0-5%	5-10%	10-20%	20-30%	30-40%	40-50%	50-60%
κ_1	value	30.704	25.018	18.442	12.273	7.814	4.750	2.730
	stat.	0.034	0.008	0.013	0.003	0.021	0.026	0.035
	sys.	1.596	1.376	1.081	0.814	0.642	0.532	0.460
nHitsFit	≥ 22	-0.210	-0.176	-0.136	-0.095	-0.064	-0.041	-0.024
	≥ 25	-0.197	-0.166	-0.129	-0.091	-0.061	-0.039	-0.024
	Σ	0.203	0.171	0.132	0.093	0.063	0.040	0.024
Efficiency	–5%	-1.616	-1.317	-0.971	-0.646	-0.411	-0.250	-0.144
	+5%	1.462	1.191	0.878	0.584	0.372	0.226	0.130
	Σ	1.539	1.254	0.924	0.615	0.392	0.238	0.137
m^2 cuts (GeV^2)	[0.7,1.3]	0.000	-0.000	0.000	0.000	0.000	0.000	0.000
	[0.6,1.1]	0.000	-0.000	0.000	0.000	0.000	-0.000	0.000
	Σ	0.000	0.000	0.000	0.000	0.000	0.000	0.000
DCA (cm)	<0.9	-0.088	-0.080	-0.068	-0.053	-0.038	-0.027	-0.018
	<1.1	-0.310	-0.254	-0.191	-0.130	-0.084	-0.052	-0.030
	Σ	0.199	0.167	0.129	0.091	0.061	0.039	0.024
$\lvert n\sigma_p \rvert$	2.75	0.024	0.014	0.006	0.001	-0.001	-0.001	-0.001
	2.5	0.112	0.080	0.048	0.025	0.012	0.006	0.003
	Σ	0.068	0.047	0.027	0.013	0.007	0.004	0.003
nHitsDedx	≥ 22	-0.210	-0.183	-0.146	-0.106	-0.073	-0.048	-0.029
	≥ 25	-0.166	-0.162	-0.144	-0.114	-0.083	-0.056	-0.036
	Σ	0.188	0.172	0.145	0.110	0.078	0.052	0.032
pileup	low	0.004	-0.001	0.001	-0.002	-0.002	0.000	0.002
	high	-0.003	0.000	0.002	-0.002	-0.003	-0.004	0.000
	Σ	0.000	0.000	0.000	0.000	0.000	0.000	0.000
cent. cut	–1	0.242	0.483	0.507	0.504	0.493	0.467	0.432
	+1	-0.234	-0.480	-0.507	-0.505	-0.496	-0.471	-0.441
	Σ	0.238	0.482	0.507	0.504	0.494	0.469	0.436

Table B.13: Systematic uncertainty contributions for κ_2 at $\sqrt{s_{NN}} = 3.2$ GeV

$\sqrt{s_{NN}} = 3.2$ GeV, κ_2 Systematic Uncertainties								
		0-5%	5-10%	10-20%	20-30%	30-40%	40-50%	50-60%
κ_2	value	4.188	7.769	6.538	4.748	3.124	1.876	1.021
	stat.	0.063	0.014	0.008	0.007	0.009	0.011	0.015
	sys.	0.506	0.796	0.682	0.516	0.376	0.279	0.214
nHitsFit	≥ 22	-0.037	-0.082	-0.075	-0.060	-0.043	-0.028	-0.016
	≥ 25	-0.032	-0.074	-0.069	-0.056	-0.040	-0.026	-0.015
	Σ	0.035	0.078	0.072	0.058	0.042	0.027	0.016
Efficiency	–5%	-0.452	-0.839	-0.706	-0.513	-0.338	-0.203	-0.110
	+5%	0.389	0.722	0.608	0.441	0.290	0.174	0.095
	Σ	0.421	0.781	0.657	0.477	0.314	0.189	0.103
m^2 cuts (GeV^2)	[0.7,1.3]	-0.000	-0.000	0.000	-0.000	-0.000	0.000	-0.000
	[0.6,1.1]	-0.000	0.000	0.000	-0.000	0.000	0.000	0.000
	Σ	0.000	0.000	0.000	0.000	0.000	0.000	0.000
DCA (cm)	<0.9	0.009	-0.013	-0.021	-0.025	-0.021	-0.016	-0.008
	<1.1	-0.081	-0.148	-0.124	-0.091	-0.062	-0.039	-0.023
	Σ	0.045	0.080	0.073	0.058	0.042	0.027	0.016
$\lvert n\sigma_p \rvert$	2.75	0.050	0.053	0.031	0.015	0.006	0.003	0.001
	2.5	0.116	0.140	0.088	0.050	0.024	0.012	0.005
	Σ	0.083	0.097	0.059	0.032	0.015	0.007	0.003
nHitsDedx	≥ 22	-0.022	-0.068	-0.069	-0.060	-0.046	-0.031	-0.018
	≥ 25	0.023	-0.010	-0.037	-0.048	-0.045	-0.033	-0.021
	Σ	0.023	0.039	0.053	0.054	0.045	0.032	0.020
pileup	low	-0.010	-0.000	0.000	-0.001	-0.001	0.000	0.001
	high	0.014	0.000	0.001	-0.001	-0.001	-0.002	0.000
	Σ	0.000	0.000	0.000	0.000	0.000	0.000	0.000
cent. cut	–1	-0.254	0.023	0.129	0.171	0.192	0.200	0.183
	+1	0.268	0.004	-0.129	-0.163	-0.193	-0.198	-0.187
	Σ	0.261	0.023	0.129	0.167	0.193	0.199	0.185

Table B.14: Systematic uncertainty contributions for κ_3 at $\sqrt{s_{NN}} = 3.2$ GeV

$\sqrt{s_{NN}} = 3.2$ GeV, κ_3 Systematic Uncertainties

		0-5%	5-10%	10-20%	20-30%	30-40%	40-50%	50-60%
κ_3	value	-9.974	1.241	3.826	3.399	2.585	1.684	0.937
	stat.	0.270	0.193	0.060	0.039	0.026	0.015	0.016
	sys.	1.595	0.649	0.603	0.530	0.413	0.317	0.223
nHitsFit	≥ 22	0.167	-0.003	-0.053	-0.058	-0.049	-0.035	-0.021
	≥ 25	0.148	-0.010	-0.052	-0.049	-0.044	-0.033	-0.020
	Σ	0.157	0.000	0.053	0.053	0.047	0.034	0.021
Efficiency	–5%	1.659	-0.206	-0.637	-0.565	-0.430	-0.280	-0.156
	+5%	-1.358	0.169	0.521	0.463	0.352	0.229	0.128
	Σ	1.509	0.188	0.579	0.514	0.391	0.255	0.142
m^2 cuts (GeV^2)	[0.7,1.3]	-0.000	0.000	-0.000	0.000	0.000	-0.000	0.000
	[0.6,1.1]	0.000	-0.000	-0.000	0.000	-0.000	-0.000	0.000
	Σ	0.000	0.000	0.000	0.000	0.000	0.000	0.000
DCA (cm)	<0.9	0.058	-0.001	0.009	-0.014	-0.018	-0.019	-0.013
	<1.1	0.234	-0.036	-0.124	-0.100	-0.076	-0.048	-0.030
	Σ	0.146	0.000	0.124	0.057	0.047	0.034	0.021
$\lvert n\sigma_p \rvert$	2.75	-0.048	0.046	0.056	0.023	0.007	0.004	0.002
	2.5	-0.152	0.179	0.134	0.071	0.034	0.021	0.008
	Σ	0.100	0.113	0.095	0.047	0.021	0.021	0.008
nHitsDedx	≥ 22	0.105	0.015	-0.042	-0.046	-0.045	-0.035	-0.024
	≥ 25	0.075	0.050	-0.003	-0.007	-0.034	-0.035	-0.024
	Σ	0.090	0.000	0.042	0.046	0.040	0.035	0.024
pileup	low	0.009	-0.000	0.000	-0.001	-0.000	0.000	0.001
	high	0.083	-0.000	0.000	-0.000	-0.000	-0.002	0.000
	Σ	0.000	0.000	0.000	0.000	0.000	0.000	0.000
cent. cut	–1	-0.439	-0.579	-0.005	0.091	0.094	0.179	0.171
	+1	0.467	0.642	0.027	-0.066	-0.119	-0.176	-0.166
	Σ	0.453	0.610	0.000	0.078	0.107	0.177	0.168

Table B.15: Systematic uncertainty contributions for κ_4 at $\sqrt{s_{NN}} = 3.2$ GeV

$\sqrt{s_{NN}} = 3.2$ GeV, κ_4 Systematic Uncertainties								
		0-5%	5-10%	10-20%	20-30%	30-40%	40-50%	50-60%
κ_4	value	-10.813	-17.633	2.462	2.418	2.729	2.125	1.253
	stat.	2.184	1.660	0.643	0.473	0.184	0.093	0.044
	sys.	4.428	5.032	0.787	0.593	0.565	0.495	0.354
nHitsFit	≥ 22	0.186	0.446	-0.056	-0.038	-0.068	-0.055	-0.035
	≥ 25	0.256	0.220	-0.111	-0.008	-0.049	-0.042	-0.033
	Σ	0.000	0.446	0.000	0.000	0.059	0.049	0.034
Efficiency	–5%	2.463	4.016	-0.561	-0.551	-0.621	-0.484	-0.285
	+5%	-1.917	-3.126	0.437	0.429	0.484	0.377	0.222
	Σ	2.190	3.571	0.499	0.490	0.553	0.430	0.254
m^2 cuts (GeV^2)	[0.7,1.3]	0.000	-0.000	0.000	-0.000	-0.000	-0.000	-0.000
	[0.6,1.1]	-0.000	0.000	0.000	-0.000	-0.000	0.000	-0.000
	Σ	0.000	0.000	0.000	0.000	0.000	0.000	0.000
DCA (cm)	<0.9	0.950	0.292	-0.041	0.073	-0.007	-0.023	-0.015
	<1.1	0.160	0.308	-0.153	-0.091	-0.052	-0.077	-0.051
	Σ	0.950	0.308	0.000	0.091	0.052	0.077	0.033
$\lvert n\sigma_p \rvert$	2.75	-0.424	-0.345	-0.003	0.056	0.019	0.019	-0.004
	2.5	-0.847	-0.194	0.037	0.083	0.026	0.064	0.013
	Σ	0.636	0.000	0.000	0.083	0.019	0.041	0.000
nHitsDedx	≥ 22	0.401	0.822	-0.342	-0.040	-0.085	-0.039	-0.045
	≥ 25	1.633	-0.230	0.128	-0.105	-0.036	-0.044	-0.044
	Σ	1.633	0.822	0.342	0.000	0.085	0.039	0.045
pileup	low	0.194	-0.003	-0.010	0.000	-0.002	-0.000	0.001
	high	0.687	0.001	0.003	0.002	-0.001	-0.001	0.000
	Σ	0.687	0.000	0.000	0.000	0.000	0.000	0.000
cent. cut	–1	3.554	-3.786	-0.309	-0.015	-0.037	0.201	0.243
	+1	-2.888	3.025	0.698	-0.310	0.126	-0.240	-0.233
	Σ	3.221	3.406	0.504	0.310	0.000	0.221	0.238

Table B.16: Systematic uncertainty contributions for κ_5 at $\sqrt{s_{NN}} = 3.2$ GeV

$\sqrt{s_{NN}} = 3.2$ GeV, κ_5 Systematic Uncertainties

		0-5%	5-10%	10-20%	20-30%	30-40%	40-50%	50-60%
κ_5	value	114.802	-77.145	-19.752	3.962	2.589	3.593	1.970
	stat.	36.648	20.353	9.696	5.021	2.197	0.782	0.330
	sys.	34.055	27.036	9.388	2.463	0.603	1.317	0.681
nHitsFit	≥ 22	-4.054	2.152	0.776	-0.027	-0.140	-0.121	-0.056
	≥ 25	-2.635	2.417	-1.244	0.420	0.070	-0.062	-0.050
	Σ	0.000	0.000	0.000	0.000	0.000	0.000	0.000
Efficiency	–5%	-33.563	22.554	5.774	-1.158	-0.757	-1.050	-0.576
	+5%	24.852	-16.700	-4.276	0.858	0.560	0.778	0.426
	Σ	29.207	19.627	0.000	0.000	0.000	0.914	0.501
m^2 cuts (GeV^2)	[0.7,1.3]	0.000	0.000	-0.000	0.000	0.000	0.000	0.000
	[0.6,1.1]	0.000	-0.000	-0.000	0.000	-0.000	0.000	0.000
	Σ	0.000	0.000	0.000	0.000	0.000	0.000	0.000
DCA (cm)	<0.9	5.073	7.738	-0.230	0.929	0.603	-0.281	0.004
	<1.1	-4.003	0.336	0.959	0.704	0.212	-0.244	-0.069
	Σ	0.000	0.000	0.000	0.000	0.603	0.244	0.069
$\lvert n\sigma_p \rvert$	2.75	-3.269	-5.142	-4.670	-0.391	0.045	0.053	-0.100
	2.5	-7.078	-19.001	-4.328	-1.386	-0.150	0.262	-0.014
	Σ	0.000	12.072	4.670	1.386	0.000	0.157	0.100
nHitsDedx	≥ 22	-3.895	4.237	-2.728	-1.753	-0.342	-0.140	-0.171
	≥ 25	-1.370	11.867	-0.856	-1.822	-0.570	-0.403	-0.171
	Σ	0.000	11.867	0.000	1.787	0.000	0.271	0.171
pileup	low	4.121	-0.161	-0.019	0.017	-0.008	0.000	-0.002
	high	5.657	-0.327	-0.051	0.037	-0.010	0.000	0.000
	Σ	0.000	0.000	0.000	0.000	0.000	0.000	0.000
cent. cut	–1	7.595	7.693	-2.893	-1.305	-0.447	0.239	0.423
	+1	-17.513	-5.187	8.144	-0.975	0.814	-0.861	-0.398
	Σ	17.513	7.693	8.144	0.975	0.000	0.861	0.410

Table B.17: Systematic uncertainty contributions for κ_6 at $\sqrt{s_{NN}} = 3.2$ GeV

$\sqrt{s_{NN}} = 3.2$ GeV, κ_6 Systematic Uncertainties								
		0-5%	5-10%	10-20%	20-30%	30-40%	40-50%	50-60%
κ_6	value	623.879	-111.80	-40.036	50.016	-6.418	3.055	1.982
	stat.	512.670	368.861	171.146	67.532	24.260	7.453	2.568
	sys.	411.244	356.358	0.000	30.317	6.058	4.423	0.999
nHitsFit	≥ 22	-33.473	-7.999	1.724	-3.398	-0.122	-0.113	-0.002
	≥ 25	-34.071	0.788	-19.359	3.820	1.404	-0.090	-0.001
	Σ	0.000	0.000	0.000	0.000	0.000	0.000	0.000
Efficiency	–5%	-224.83	40.290	14.428	-18.024	2.313	-1.101	-0.714
	+5%	158.331	-28.373	-10.160	12.693	-1.629	0.775	0.503
	Σ	0.000	0.000	0.000	0.000	0.000	0.000	0.000
m^2 cuts (GeV^2)	[0.7,1.3]	-0.000	-0.000	0.000	-0.000	-0.000	-0.000	-0.000
	[0.6,1.1]	-0.000	-0.000	0.000	-0.000	0.000	-0.000	-0.000
	Σ	0.000	0.000	0.000	0.000	0.000	0.000	0.000
DCA (cm)	<0.9	-103.30	57.286	-26.337	-1.018	5.891	-4.423	0.368
	<1.1	29.686	-40.965	-34.323	21.670	2.051	0.388	0.290
	Σ	103.304	0.000	0.000	21.670	5.891	4.423	0.000
$\lvert n\sigma_p \rvert$	2.75	-177.69	-33.893	-41.364	6.983	1.414	-0.828	-0.999
	2.5	-171.82	-149.66	-57.283	0.011	1.322	0.370	-0.860
	Σ	0.000	149.655	0.000	0.000	1.414	0.000	0.999
nHitsDedx	≥ 22	240.561	-165.08	-24.288	-2.844	-2.434	0.052	-1.170
	≥ 25	347.299	35.223	-56.306	4.356	-6.547	-2.287	-1.366
	Σ	293.930	165.080	0.000	0.000	0.000	0.000	0.000
pileup	low	41.805	-1.254	-2.794	-0.289	-0.080	0.010	-0.019
	high	-62.497	-2.268	-0.067	0.149	-0.109	0.040	0.001
	Σ	0.000	0.000	0.000	0.000	0.000	0.000	0.000
cent. cut	–1	-352.19	308.007	-64.083	-21.203	7.368	-2.728	-0.157
	+1	184.667	-248.21	2.554	24.414	-4.664	-1.574	0.297
	Σ	268.430	278.107	0.000	21.203	0.000	0.000	0.000

Table B.18: Systematic uncertainty contributions for κ_2/κ_1 at $\sqrt{s_{NN}} = 3.2$ GeV

$\sqrt{s_{NN}} = 3.2$ GeV, κ_2/κ_1 Systematic Uncertainties								
		0-5%	5-10%	10-20%	20-30%	30-40%	40-50%	50-60%
κ_2/κ_1	value	0.136	0.311	0.355	0.387	0.400	0.395	0.374
	stat.	0.002	0.001	0.000	0.001	0.000	0.001	0.001
	sys.	0.012	0.017	0.018	0.020	0.020	0.020	0.021
nHitsFit	≥ 22	-0.000	-0.001	-0.001	-0.002	-0.002	-0.002	-0.003
	≥ 25	-0.000	-0.001	-0.001	-0.002	-0.002	-0.002	-0.002
	Σ	0.000	0.001	0.001	0.002	0.002	0.002	0.002
Efficiency	–5%	-0.007	-0.016	-0.019	-0.020	-0.021	-0.021	-0.020
	+5%	0.006	0.015	0.017	0.018	0.019	0.019	0.018
	Σ	0.007	0.016	0.018	0.019	0.020	0.020	0.019
m^2 cuts (GeV^2)	[0.7,1.3]	-0.000	-0.000	0.000	-0.000	-0.000	0.000	-0.000
	[0.6,1.1]	-0.000	0.000	0.000	-0.000	0.000	0.000	0.000
	Σ	0.000	0.000	0.000	0.000	0.000	0.000	0.000
DCA (cm)	<0.9	0.001	0.000	0.000	-0.000	-0.001	-0.001	-0.001
	<1.1	-0.001	-0.003	-0.003	-0.003	-0.004	-0.004	-0.004
	Σ	0.001	0.002	0.002	0.002	0.002	0.002	0.002
$\lvert n\sigma_p \rvert$	2.75	0.002	0.002	0.002	0.001	0.001	0.001	0.000
	2.5	0.003	0.005	0.004	0.003	0.002	0.002	0.002
	Σ	0.002	0.003	0.003	0.002	0.002	0.001	0.001
nHitsDedx	≥ 22	0.000	-0.000	-0.001	-0.002	-0.002	-0.002	-0.003
	≥ 25	0.001	0.002	0.001	-0.000	-0.001	-0.002	-0.003
	Σ	0.001	0.001	0.001	0.001	0.002	0.002	0.003
pileup	low	-0.000	0.000	-0.000	-0.000	0.000	-0.000	0.000
	high	0.000	0.000	-0.000	0.000	0.000	-0.000	0.000
	Σ	0.000	0.000	0.000	0.000	0.000	0.000	0.000
cent. cut	–1	-0.009	-0.005	-0.003	-0.002	-0.001	0.004	0.009
	+1	0.010	0.006	0.003	0.003	0.001	-0.002	-0.007
	Σ	0.010	0.006	0.003	0.002	0.001	0.003	0.008

Table B.19: Systematic uncertainty contributions for κ_3/κ_1 at $\sqrt{s_{NN}} = 3.2$ GeV

$\sqrt{s_{NN}} = 3.2$ GeV, κ_3/κ_1 Systematic Uncertainties								
		0-5%	5-10%	10-20%	20-30%	30-40%	40-50%	50-60%
κ_3/κ_1	value	-0.325	0.050	0.207	0.277	0.331	0.354	0.343
	stat.	0.008	0.008	0.003	0.003	0.003	0.003	0.003
	sys.	0.035	0.026	0.023	0.029	0.035	0.036	0.036
nHitsFit	≥ 22	0.003	0.000	-0.001	-0.003	-0.003	-0.004	-0.005
	≥ 25	0.003	-0.000	-0.001	-0.002	-0.003	-0.004	-0.004
	Σ	0.003	0.000	0.001	0.002	0.003	0.004	0.004
Efficiency	–5%	0.035	-0.005	-0.022	-0.030	-0.036	-0.038	-0.037
	+5%	-0.030	0.005	0.019	0.026	0.031	0.033	0.032
	Σ	0.033	0.005	0.021	0.028	0.033	0.036	0.034
m^2 cuts (GeV^2)	[0.7,1.3]	-0.000	0.000	-0.000	0.000	0.000	-0.000	0.000
	[0.6,1.1]	0.000	-0.000	-0.000	0.000	-0.000	-0.000	0.000
	Σ	0.000	0.000	0.000	0.000	0.000	0.000	0.000
DCA (cm)	<0.9	0.001	0.000	0.001	0.000	-0.001	-0.002	-0.002
	<1.1	0.004	-0.001	-0.005	-0.005	-0.006	-0.006	-0.007
	Σ	0.004	0.000	0.005	0.005	0.003	0.004	0.005
$\lvert n\sigma_p \rvert$	2.75	-0.001	0.002	0.003	0.002	0.001	0.001	0.001
	2.5	-0.004	0.007	0.007	0.005	0.004	0.004	0.003
	Σ	0.003	0.004	0.005	0.004	0.002	0.002	0.002
nHitsDedx	≥ 22	0.001	0.001	-0.001	-0.001	-0.003	-0.004	-0.005
	≥ 25	0.001	0.002	0.001	0.002	-0.001	-0.003	-0.004
	Σ	0.001	0.000	0.000	0.002	0.003	0.003	0.005
pileup	low	0.000	0.000	-0.000	-0.000	0.000	-0.000	0.000
	high	0.003	-0.000	-0.000	0.000	0.000	-0.000	-0.000
	Σ	0.000	0.000	0.000	0.000	0.000	0.000	0.000
cent. cut	–1	-0.012	-0.025	-0.006	-0.004	-0.009	0.003	0.010
	+1	0.013	0.026	0.007	0.006	0.005	-0.002	-0.005
	Σ	0.012	0.025	0.007	0.005	0.007	0.002	0.007

Table B.20: Systematic uncertainty contributions for κ_4/κ_1 at $\sqrt{s_{NN}} = 3.2$ GeV

$\sqrt{s_{NN}} = 3.2$ GeV, κ_4/κ_1 Systematic Uncertainties		0-5%	5-10%	10-20%	20-30%	30-40%	40-50%	50-60%
κ_4/κ_1	value	-0.352	-0.705	0.134	0.197	0.349	0.447	0.459
	stat.	0.071	0.066	0.035	0.039	0.024	0.019	0.015
	sys.	0.137	0.166	0.042	0.035	0.063	0.070	0.073
nHitsFit	≥ 22	0.004	0.013	-0.002	-0.002	-0.006	-0.008	-0.009
	≥ 25	0.006	0.004	-0.005	0.001	-0.004	-0.005	-0.008
	Σ	0.000	0.013	0.000	0.000	0.006	0.008	0.008
Efficiency	–5%	0.059	0.117	-0.022	-0.033	-0.058	-0.074	-0.076
	+5%	-0.048	-0.096	0.018	0.027	0.048	0.061	0.062
	Σ	0.053	0.107	0.022	0.030	0.053	0.068	0.069
m^2 cuts (GeV^2)	[0.7,1.3]	0.000	-0.000	0.000	-0.000	-0.000	-0.000	-0.000
	[0.6,1.1]	-0.000	0.000	0.000	-0.000	-0.000	0.000	-0.000
	Σ	0.000	0.000	0.000	0.000	0.000	0.000	0.000
DCA (cm)	<0.9	0.030	0.009	-0.002	0.007	0.001	-0.002	-0.003
	<1.1	0.002	0.005	-0.007	-0.005	-0.003	-0.011	-0.013
	Σ	0.030	0.000	0.000	0.005	0.000	0.011	0.013
$\lvert n\sigma_p \rvert$	2.75	-0.014	-0.013	-0.000	0.005	0.002	0.004	-0.001
	2.5	-0.026	-0.006	0.002	0.006	0.003	0.013	0.004
	Σ	0.020	0.000	0.000	0.006	0.002	0.008	0.000
nHitsDedx	≥ 22	0.011	0.028	-0.017	-0.002	-0.008	-0.004	-0.011
	≥ 25	0.051	-0.014	0.008	-0.007	-0.001	-0.004	-0.010
	Σ	0.051	0.028	0.017	0.000	0.008	0.000	0.011
pileup	low	0.006	-0.000	-0.001	0.000	-0.000	-0.000	-0.000
	high	0.022	0.000	0.000	0.000	-0.000	0.000	0.000
	Σ	0.022	0.000	0.000	0.000	0.000	0.000	0.000
cent. cut	–1	0.119	-0.140	-0.021	-0.010	-0.029	-0.002	0.020
	+1	-0.096	0.105	0.040	-0.017	0.036	-0.006	-0.010
	Σ	0.108	0.123	0.031	0.017	0.032	0.000	0.015

Table B.21: Systematic uncertainty contributions for κ_5/κ_1 at $\sqrt{s_{NN}} = 3.2$ GeV

$\sqrt{s_{NN}} = 3.2$ GeV, κ_5/κ_1 Systematic Uncertainties								
		0-5%	5-10%	10-20%	20-30%	30-40%	40-50%	50-60%
κ_5/κ_1	value	3.739	-3.084	-1.071	0.323	0.331	0.756	0.722
	stat.	1.193	0.814	0.526	0.409	0.280	0.164	0.119
	sys.	0.538	0.981	0.474	0.220	0.130	0.189	0.163
nHitsFit	≥ 22	-0.106	0.064	0.034	0.000	-0.015	-0.019	-0.014
	≥ 25	-0.061	0.076	-0.074	0.036	0.011	-0.007	-0.012
	Σ	0.000	0.000	0.000	0.000	0.000	0.000	0.000
Efficiency	–5%	-0.851	0.702	0.244	-0.074	-0.075	-0.172	-0.164
	+5%	0.663	-0.547	-0.190	0.057	0.059	0.134	0.128
	Σ	0.000	0.624	0.000	0.000	0.000	0.153	0.146
m^2 cuts (GeV^2)	[0.7,1.3]	0.000	0.000	-0.000	0.000	0.000	0.000	0.000
	[0.6,1.1]	0.000	-0.000	-0.000	0.000	-0.000	0.000	0.000
	Σ	0.000	0.000	0.000	0.000	0.000	0.000	0.000
DCA (cm)	<0.9	0.175	0.298	-0.016	0.077	0.078	-0.055	0.006
	<1.1	-0.092	-0.018	0.041	0.060	0.030	-0.043	-0.017
	Σ	0.000	0.000	0.000	0.000	0.054	0.043	0.017
$\lvert n\sigma_p \rvert$	2.75	-0.109	-0.204	-0.253	-0.032	0.006	0.011	-0.036
	2.5	-0.245	-0.752	-0.233	-0.114	-0.020	0.054	-0.006
	Σ	0.000	0.478	0.253	0.114	0.000	0.033	0.036
nHitsDedx	≥ 22	-0.101	0.146	-0.155	-0.139	-0.040	-0.022	-0.054
	≥ 25	-0.024	0.451	-0.054	-0.144	-0.069	-0.075	-0.052
	Σ	0.000	0.451	0.000	0.141	0.000	0.000	0.054
pileup	low	0.134	-0.007	-0.001	0.001	-0.001	-0.000	-0.001
	high	0.185	-0.013	-0.003	0.003	-0.001	0.001	0.000
	Σ	0.000	0.000	0.000	0.000	0.000	0.000	0.000
cent. cut	–1	0.220	0.374	-0.131	-0.125	-0.083	-0.027	0.048
	+1	-0.538	-0.262	0.401	-0.064	0.118	-0.097	-0.025
	Σ	0.538	0.374	0.401	0.125	0.118	0.097	0.025

Table B.22: Systematic uncertainty contributions for κ_6/κ_1 at $\sqrt{s_{NN}} = 3.2$ GeV

$\sqrt{s_{NN}} = 3.2$ GeV, κ_6/κ_1 Systematic Uncertainties								
		0-5%	5-10%	10-20%	20-30%	30-40%	40-50%	50-60%
κ_6/κ_1	value	20.319	-4.469	-2.171	4.075	-0.821	0.643	0.726
	stat.	16.678	14.748	9.287	5.501	3.096	1.561	0.929
	sys.	13.543	14.328	3.512	2.666	0.768	1.162	0.365
nHitsFit	≥ 22	-0.945	-0.349	0.077	-0.243	-0.022	-0.018	0.006
	≥ 25	-0.973	0.002	-1.058	0.339	0.172	-0.014	0.006
	Σ	0.000	0.000	0.000	0.000	0.000	0.000	0.000
Efficiency	–5%	-5.940	1.306	0.635	-1.191	0.240	-0.188	-0.212
	+5%	4.399	-0.967	-0.470	0.882	-0.178	0.139	0.157
	Σ	0.000	0.000	0.000	0.000	0.000	0.000	0.000
m^2 cuts (GeV^2)	[0.7,1.3]	-0.000	-0.000	0.000	-0.000	-0.000	-0.000	-0.000
	[0.6,1.1]	-0.000	-0.000	0.000	-0.000	0.000	-0.000	-0.000
	Σ	0.000	0.000	0.000	0.000	0.000	0.000	0.000
DCA (cm)	<0.9	-3.297	2.268	-1.431	-0.065	0.746	-0.922	0.139
	<1.1	1.160	-1.666	-1.864	1.790	0.251	0.088	0.113
	Σ	3.297	0.000	0.000	1.790	0.746	0.922	0.000
$\lvert n\sigma_p \rvert$	2.75	-5.807	-1.353	-2.243	0.569	0.181	-0.174	-0.365
	2.5	-5.691	-5.987	-3.109	-0.007	0.171	0.077	-0.316
	Σ	0.000	5.987	0.000	0.000	0.181	0.000	0.365
nHitsDedx	≥ 22	7.919	-6.583	-1.324	-0.195	-0.316	0.017	-0.416
	≥ 25	11.360	1.370	-3.046	0.389	-0.838	-0.468	-0.485
	Σ	9.639	6.583	0.000	0.000	0.000	0.000	0.000
pileup	low	1.359	-0.050	-0.151	-0.023	-0.010	0.002	-0.007
	high	-2.034	-0.091	-0.003	0.013	-0.014	0.009	0.000
	Σ	0.000	0.000	0.000	0.000	0.000	0.000	0.000
cent. cut	–1	-11.723	12.642	-3.512	-1.976	1.062	-0.707	-0.205
	+1	6.123	-9.818	0.077	2.072	-0.610	-0.243	0.195
	Σ	8.923	11.230	3.512	1.976	0.000	0.707	0.000

B.2 Systematic Contributions at $\sqrt{s_{NN}} = 3.5$ GeV

Table B.23: Systematic uncertainty contributions for C_1 at $\sqrt{s_{NN}} = 3.5$ GeV

$\sqrt{s_{NN}} = 3.5$ GeV, C_1 Systematic Uncertainties

		0-5%	5-10%	10-20%	20-30%	30-40%	40-50%	50-60%
C_1	value	30.167	24.642	18.224	12.056	7.659	4.582	2.762
	stat.	0.003	0.003	0.002	0.002	0.001	0.001	0.001
	sys.	1.545	1.311	1.008	0.730	0.545	0.421	0.338
nHitsFit	≥ 22	-0.185	-0.156	-0.120	-0.084	-0.056	-0.035	-0.022
	≥ 25	-0.149	-0.125	-0.096	-0.067	-0.044	-0.028	-0.017
	Σ	0.167	0.141	0.108	0.076	0.050	0.031	0.020
Efficiency	–5%	-1.588	-1.297	-0.959	-0.635	-0.403	-0.241	-0.145
	+5%	1.437	1.173	0.868	0.574	0.365	0.218	0.132
	Σ	1.512	1.235	0.913	0.604	0.384	0.230	0.138
m^2 cuts (GeV^2)	[0.7,1.3]	0.002	0.001	-0.000	-0.001	-0.001	-0.001	-0.001
	[0.6,1.1]	-0.004	-0.002	-0.001	0.000	0.000	0.000	0.000
	Σ	0.003	0.002	0.001	0.001	0.001	0.001	0.000
DCA (cm)	<0.9	-0.010	-0.017	-0.021	-0.020	-0.017	-0.013	-0.010
	<1.1	-0.314	-0.258	-0.193	-0.130	-0.084	-0.051	-0.031
	Σ	0.162	0.138	0.107	0.075	0.050	0.032	0.020
$\lvert n\sigma_p \rvert$	2.75	-0.033	-0.030	-0.026	-0.019	-0.013	-0.009	-0.005
	2.5	0.053	0.034	0.015	0.004	-0.001	-0.002	-0.002
	Σ	0.043	0.032	0.021	0.012	0.007	0.005	0.004
nHitsDedx	≥ 22	-0.125	-0.113	-0.096	-0.073	-0.051	-0.034	-0.022
	≥ 25	0.063	0.024	-0.006	-0.021	-0.022	-0.019	-0.014
	Σ	0.094	0.069	0.051	0.047	0.037	0.026	0.018
pileup	low	0.005	-0.000	-0.000	-0.000	-0.000	0.000	0.000
	high	-0.002	0.000	0.000	0.000	0.000	-0.000	0.000
	Σ	0.003	0.000	0.000	0.000	0.000	0.000	0.000
cent. cut	–1	0.195	0.385	0.394	0.393	0.378	0.345	0.300
	+1	-0.189	-0.383	-0.394	-0.393	-0.380	-0.351	-0.313
	Σ	0.192	0.384	0.394	0.393	0.379	0.348	0.306

Table B.24: Systematic uncertainty contributions for C_2 at $\sqrt{s_{NN}} = 3.5$ GeV

$\sqrt{s_{NN}} = 3.5$ GeV, C_2 Systematic Uncertainties								
		0-5%	5-10%	10-20%	20-30%	30-40%	40-50%	50-60%
C_2	value	32.992	30.246	22.824	15.357	9.823	5.851	3.462
	stat.	0.030	0.025	0.014	0.009	0.007	0.004	0.004
	sys.	1.822	1.866	1.471	1.069	0.781	0.583	0.456
nHitsFit	≥ 22	-0.204	-0.207	-0.167	-0.120	-0.082	-0.052	-0.032
	≥ 25	-0.165	-0.167	-0.133	-0.095	-0.065	-0.041	-0.025
	Σ	0.184	0.187	0.150	0.108	0.073	0.047	0.028
Efficiency	–5%	-1.893	-1.902	-1.456	-0.991	-0.637	-0.378	-0.221
	+5%	1.699	1.694	1.295	0.881	0.566	0.336	0.197
	Σ	1.796	1.798	1.376	0.936	0.601	0.357	0.209
m^2 cuts (GeV^2)	[0.7,1.3]	0.005	-0.000	0.000	-0.001	-0.001	-0.001	-0.001
	[0.6,1.1]	-0.007	-0.007	-0.002	-0.000	0.001	0.000	0.000
	Σ	0.006	0.007	0.002	0.000	0.001	0.001	0.001
DCA (cm)	<0.9	0.019	0.014	-0.014	-0.020	-0.021	-0.016	-0.013
	<1.1	-0.378	-0.375	-0.287	-0.195	-0.128	-0.078	-0.047
	Σ	0.198	0.194	0.151	0.108	0.074	0.047	0.030
$\lvert n\sigma_p \rvert$	2.75	-0.016	-0.021	-0.024	-0.020	-0.016	-0.011	-0.007
	2.5	0.121	0.110	0.066	0.031	0.011	0.003	-0.000
	Σ	0.068	0.065	0.045	0.026	0.013	0.007	0.007
nHitsDedx	≥ 22	-0.128	-0.140	-0.119	-0.100	-0.072	-0.049	-0.031
	≥ 25	0.105	0.087	0.026	-0.015	-0.026	-0.023	-0.018
	Σ	0.116	0.113	0.073	0.057	0.049	0.036	0.025
pileup	low	0.006	0.001	-0.000	-0.000	-0.000	0.000	0.000
	high	-0.006	-0.001	0.000	0.000	0.000	-0.000	-0.000
	Σ	0.000	0.000	0.000	0.000	0.000	0.000	0.000
cent. cut	–1	0.026	0.413	0.465	0.490	0.483	0.452	0.391
	+1	-0.016	-0.383	-0.468	-0.487	-0.486	-0.458	-0.415
	Σ	0.021	0.398	0.466	0.489	0.484	0.455	0.403

Table B.25: Systematic uncertainty contributions for C_3 at $\sqrt{s_{NN}} = 3.5$ GeV

$\sqrt{s_{NN}} = 3.5$ GeV, C_3 Systematic Uncertainties								
		0-5%	5-10%	10-20%	20-30%	30-40%	40-50%	50-60%
C_3	value	31.825	42.256	34.346	23.814	15.540	9.289	5.382
	stat.	0.368	0.334	0.138	0.090	0.052	0.027	0.021
	sys.	1.519	3.106	2.800	2.042	1.462	1.068	0.793
nHitsFit	≥ 22	-0.146	-0.310	-0.291	-0.224	-0.158	-0.102	-0.061
	≥ 25	-0.155	-0.245	-0.204	-0.177	-0.121	-0.083	-0.053
	Σ	0.151	0.277	0.248	0.201	0.139	0.092	0.057
Efficiency	–5%	-1.369	-3.247	-2.836	-2.013	-1.336	-0.802	-0.459
	+5%	1.296	2.846	2.467	1.747	1.157	0.695	0.398
	Σ	1.333	3.046	2.652	1.880	1.247	0.748	0.428
m^2 cuts (GeV^2)	[0.7,1.3]	0.034	-0.000	-0.003	-0.000	-0.003	-0.001	-0.000
	[0.6,1.1]	0.030	-0.006	-0.012	-0.003	-0.002	-0.000	-0.001
	Σ	0.034	0.000	0.003	0.000	0.003	0.000	0.000
DCA (cm)	<0.9	-0.049	0.124	-0.002	-0.024	-0.032	-0.025	-0.020
	<1.1	-0.340	-0.658	-0.537	-0.397	-0.263	-0.162	-0.097
	Σ	0.340	0.391	0.537	0.210	0.147	0.093	0.058
$\lvert n\sigma_p \rvert$	2.75	0.069	0.060	-0.032	-0.023	-0.021	-0.023	-0.017
	2.5	0.112	0.380	0.237	0.105	0.050	0.018	0.001
	Σ	0.091	0.220	0.134	0.064	0.035	0.020	0.017
nHitsDedx	≥ 22	-0.030	-0.219	-0.163	-0.167	-0.127	-0.097	-0.068
	≥ 25	0.132	0.150	0.216	-0.003	0.000	-0.034	-0.031
	Σ	0.000	0.184	0.190	0.167	0.127	0.066	0.049
pileup	low	0.069	-0.001	0.001	0.001	-0.001	0.000	0.000
	high	-0.047	-0.004	0.000	0.000	0.000	-0.000	0.000
	Σ	0.000	0.000	0.000	0.000	0.000	0.000	0.000
cent. cut	–1	-0.714	0.229	0.683	0.696	0.722	0.750	0.633
	+1	0.527	-0.002	-0.587	-0.742	-0.726	-0.746	-0.688
	Σ	0.620	0.229	0.635	0.719	0.724	0.748	0.660

Table B.26: Systematic uncertainty contributions for C_4 at $\sqrt{s_{NN}} = 3.5$ GeV

$\sqrt{s_{NN}} = 3.5$ GeV, C_4 Systematic Uncertainties								
		0-5%	5-10%	10-20%	20-30%	30-40%	40-50%	50-60%
C_4	value	5.123	61.881	63.218	47.787	31.807	19.697	11.323
	stat.	5.347	4.814	1.750	1.097	0.478	0.201	0.145
	sys.	4.722	6.216	6.864	5.354	3.691	2.729	1.861
nHitsFit	≥ 22	0.210	-0.610	-0.633	-0.604	-0.396	-0.277	-0.164
	≥ 25	1.159	-0.436	-0.320	-0.510	-0.382	-0.226	-0.167
	Σ	1.159	0.000	0.633	0.557	0.389	0.251	0.166
Efficiency	–5%	3.972	-4.786	-6.496	-5.322	-3.578	-2.289	-1.317
	+5%	-2.989	4.270	5.557	4.503	3.026	1.927	1.108
	Σ	3.972	4.528	6.027	4.913	3.302	2.108	1.212
m^2 cuts (GeV^2)	[0.7,1.3]	0.171	-0.250	0.124	-0.041	-0.002	0.018	0.007
	[0.6,1.1]	0.786	-0.320	-0.160	0.064	-0.004	0.015	-0.011
	Σ	0.786	0.320	0.000	0.000	0.000	0.000	0.009
DCA (cm)	<0.9	1.200	1.411	-0.113	-0.186	-0.128	-0.019	-0.030
	<1.1	1.579	-1.537	-1.745	-1.392	-0.768	-0.458	-0.303
	Σ	1.389	1.474	1.745	1.392	0.768	0.458	0.166
$\lvert n\sigma_p \rvert$	2.75	0.702	0.189	-0.239	0.049	-0.004	-0.063	-0.076
	2.5	-1.263	1.879	0.957	0.534	0.150	0.066	-0.021
	Σ	1.263	1.879	0.957	0.534	0.000	0.064	0.076
nHitsDedx	≥ 22	0.631	-1.372	-0.183	-0.429	-0.355	-0.265	-0.220
	≥ 25	0.620	-1.857	2.357	-0.586	0.223	-0.113	-0.097
	Σ	0.000	1.615	2.357	0.429	0.355	0.189	0.159
pileup	low	1.122	0.126	0.018	0.012	-0.011	0.006	0.000
	high	-0.465	-0.031	-0.007	-0.006	-0.003	0.001	-0.000
	Σ	0.000	0.000	0.000	0.000	0.000	0.000	0.000
cent. cut	–1	-1.729	-2.507	0.940	1.200	1.264	1.700	1.303
	+1	0.308	3.731	-0.346	-1.495	-1.460	-1.581	-1.459
	Σ	1.018	3.119	0.940	1.348	1.362	1.640	1.381

Table B.27: Systematic uncertainty contributions for C_5 at $\sqrt{s_{NN}} = 3.5$ GeV

$\sqrt{s_{NN}} = 3.5$ GeV, C_5 Systematic Uncertainties								
		0-5%	5-10%	10-20%	20-30%	30-40%	40-50%	50-60%
C_5	value	-146.28	37.886	129.395	107.953	79.919	53.204	32.231
	stat.	84.882	72.906	28.261	12.708	5.660	1.845	1.272
	sys.	57.122	39.466	28.202	17.384	11.440	8.533	5.739
nHitsFit	≥ 22	-0.762	-1.514	-1.900	-1.398	-1.192	-0.906	-0.586
	≥ 25	12.314	-9.458	0.908	-0.851	-2.291	-0.552	-0.723
	Σ	12.314	0.000	0.000	0.000	2.291	0.729	0.655
Efficiency	–5%	33.804	8.457	-14.163	-12.735	-10.740	-7.574	-4.838
	+5%	-26.773	-5.287	12.195	10.908	8.949	6.259	3.958
	Σ	0.000	0.000	0.000	11.822	9.844	6.917	4.398
m^2 cuts (GeV^2)	[0.7,1.3]	-5.762	-8.223	4.122	-0.171	-0.095	0.338	0.072
	[0.6,1.1]	4.187	-3.297	0.213	1.291	0.156	0.254	-0.135
	Σ	0.000	0.000	0.000	1.291	0.000	0.254	0.072
DCA (cm)	<0.9	24.585	15.080	0.962	-5.088	-1.047	0.144	0.071
	<1.1	21.296	-3.368	-12.016	-9.407	-4.005	-1.657	-1.517
	Σ	24.585	15.080	12.016	9.407	4.005	0.901	1.517
$\lvert n\sigma_p \rvert$	2.75	-0.611	9.624	-2.093	1.795	0.610	-0.084	-0.474
	2.5	-30.213	18.165	4.330	4.555	0.156	0.289	-0.314
	Σ	30.213	18.165	0.000	4.555	0.000	0.000	0.474
nHitsDedx	≥ 22	26.753	-21.790	11.384	-3.495	-1.661	-1.022	-0.893
	≥ 25	53.098	-25.060	25.514	-9.100	0.532	-1.756	-0.697
	Σ	39.925	21.790	25.514	3.495	0.000	1.389	0.795
pileup	low	13.135	1.914	0.186	0.046	-0.064	0.098	-0.001
	high	-7.068	-0.802	-0.172	-0.011	-0.063	0.011	-0.000
	Σ	0.000	0.000	0.000	0.000	0.000	0.000	0.000
cent. cut	–1	6.682	-22.921	-1.714	2.653	2.675	4.257	3.225
	+1	22.004	6.974	0.306	-6.273	-3.562	-5.045	-3.099
	Σ	0.000	22.921	0.000	6.273	3.562	4.651	3.162

Table B.28: Systematic uncertainty contributions for C_6 at $\sqrt{s_{NN}} = 3.5$ GeV

$\sqrt{s_{NN}} = 3.5$ GeV, C_6 Systematic Uncertainties								
		0-5%	5-10%	10-20%	20-30%	30-40%	40-50%	50-60%
C_6	value	-865.85	-723.59	92.404	133.087	180.553	146.673	113.137
	stat.	1370.459	1369.997	546.710	194.915	77.069	20.635	13.511
	sys.	1878.021	1263.932	251.356	155.225	50.937	36.338	22.690
nHitsFit	≥ 22	-5.958	28.191	4.291	6.028	-2.671	-2.236	-2.550
	≥ 25	-17.248	-310.84	-4.091	22.514	-13.547	3.159	-4.028
	Σ	0.000	0.000	0.000	22.514	13.547	0.000	0.000
Efficiency	–5%	181.184	244.235	34.437	11.608	-17.402	-19.891	-20.130
	+5%	-143.24	-178.54	-19.643	-3.873	16.327	16.979	16.146
	Σ	0.000	0.000	0.000	0.000	0.000	18.435	18.138
m^2 cuts (GeV^2)	[0.7,1.3]	57.560	-105.59	77.394	12.952	-4.026	3.822	0.495
	[0.6,1.1]	31.479	76.701	-2.943	24.129	0.393	2.578	-1.247
	Σ	0.000	0.000	0.000	0.000	0.000	2.578	0.000
DCA (cm)	<0.9	95.460	855.135	62.881	-134.74	-7.752	-0.711	3.141
	<1.1	-31.753	-403.04	-229.97	-102.34	-49.102	-6.617	-10.740
	Σ	0.000	855.135	229.966	118.539	49.102	6.617	10.740
$\lvert n\sigma_p \rvert$	2.75	-277.26	188.752	-48.705	8.852	7.061	0.672	-2.814
	2.5	-780.28	-62.851	-57.776	33.951	-11.525	1.464	-2.064
	Σ	780.277	0.000	0.000	33.951	0.000	0.000	2.064
nHitsDedx	≥ 22	152.176	-797.51	101.314	-30.838	3.453	-5.521	-2.705
	≥ 25	1621.359	-1064.0	232.352	-71.968	-36.530	-17.184	-7.053
	Σ	1621.359	930.736	0.000	0.000	0.000	17.184	2.705
pileup	low	196.650	2.659	0.763	-1.842	0.015	1.183	-0.017
	high	-211.59	-10.643	0.349	0.928	-0.631	0.066	-0.000
	Σ	0.000	0.000	0.000	0.000	0.000	0.000	0.000
cent. cut	–1	29.176	-152.27	29.890	-12.655	0.210	-2.381	7.676
	+1	537.889	-13.359	-101.47	-91.563	11.783	-25.197	2.662
	Σ	537.889	0.000	101.466	91.563	0.000	25.197	7.676

Table B.29: Systematic uncertainty contributions for C_2/C_1 at $\sqrt{s_{NN}} = 3.5$ GeV

$\sqrt{s_{NN}} = 3.5$ GeV, C_2/C_1 Systematic Uncertainties								
		0-5%	5-10%	10-20%	20-30%	30-40%	40-50%	50-60%
C_2/C_1	value	1.094	1.227	1.252	1.274	1.282	1.277	1.253
	stat.	0.001	0.001	0.001	0.001	0.001	0.001	0.001
	sys.	0.008	0.012	0.013	0.014	0.014	0.014	0.015
nHitsFit	≥ 22	-0.000	-0.001	-0.001	-0.001	-0.001	-0.002	-0.001
	≥ 25	-0.000	-0.001	-0.001	-0.001	-0.001	-0.001	-0.001
	Σ	0.000	0.001	0.001	0.001	0.001	0.001	0.001
Efficiency	–5%	-0.005	-0.012	-0.013	-0.014	-0.015	-0.015	-0.013
	+5%	0.004	0.011	0.012	0.013	0.013	0.013	0.012
	Σ	0.005	0.011	0.013	0.014	0.014	0.014	0.013
m^2 cuts (GeV^2)	[0.7,1.3]	0.000	-0.000	0.000	0.000	0.000	0.000	-0.000
	[0.6,1.1]	-0.000	-0.000	-0.000	-0.000	0.000	-0.000	-0.000
	Σ	0.000	0.000	0.000	0.000	0.000	0.000	0.000
DCA (cm)	<0.9	0.001	0.001	0.001	0.000	0.000	0.000	-0.000
	<1.1	-0.001	-0.002	-0.003	-0.002	-0.003	-0.003	-0.003
	Σ	0.001	0.002	0.002	0.001	0.003	0.001	0.002
$\lvert n\sigma_p \rvert$	2.75	0.001	0.001	0.000	0.000	0.000	-0.000	-0.000
	2.5	0.002	0.003	0.003	0.002	0.002	0.001	0.001
	Σ	0.001	0.002	0.002	0.001	0.001	0.001	0.000
nHitsDedx	≥ 22	0.000	-0.000	0.000	-0.001	-0.001	-0.001	-0.001
	≥ 25	0.001	0.002	0.002	0.001	0.000	0.000	-0.000
	Σ	0.001	0.002	0.002	0.001	0.001	0.001	0.001
pileup	low	0.000	0.000	-0.000	0.000	-0.000	0.000	0.000
	high	-0.000	-0.000	-0.000	0.000	0.000	0.000	-0.000
	Σ	0.000	0.000	0.000	0.000	0.000	0.000	0.000
cent. cut	–1	-0.006	-0.002	-0.002	-0.001	-0.000	0.003	0.006
	+1	0.006	0.003	0.001	0.001	0.000	-0.002	-0.007
	Σ	0.006	0.003	0.001	0.001	0.000	0.002	0.007

Table B.30: Systematic uncertainty contributions for C_3/C_1 at $\sqrt{s_{NN}} = 3.5$ GeV

$\sqrt{s_{NN}} = 3.5$ GeV, C_3/C_1 Systematic Uncertainties								
		0-5%	5-10%	10-20%	20-30%	30-40%	40-50%	50-60%
C_3/C_1	value	1.055	1.715	1.885	1.975	2.029	2.027	1.949
	stat.	0.012	0.014	0.008	0.007	0.007	0.006	0.007
	sys.	0.029	0.045	0.054	0.058	0.063	0.064	0.064
nHitsFit	≥ 22	0.002	-0.002	-0.004	-0.005	-0.006	-0.007	-0.007
	≥ 25	0.000	-0.001	-0.001	-0.004	-0.004	-0.006	-0.007
	Σ	0.000	0.000	0.002	0.004	0.005	0.006	0.007
Efficiency	–5%	0.010	-0.039	-0.054	-0.060	-0.064	-0.065	-0.060
	+5%	-0.008	0.036	0.048	0.053	0.057	0.058	0.054
	Σ	0.009	0.037	0.051	0.057	0.061	0.061	0.057
m^2 cuts (GeV^2)	[0.7,1.3]	0.001	-0.000	-0.000	0.000	-0.000	0.000	0.000
	[0.6,1.1]	0.001	-0.000	-0.001	-0.000	-0.000	-0.000	-0.001
	Σ	0.001	0.000	0.000	0.000	0.000	0.000	0.000
DCA (cm)	<0.9	-0.001	0.006	0.002	0.001	0.000	0.000	-0.000
	<1.1	-0.000	-0.009	-0.009	-0.012	-0.012	-0.013	-0.013
	Σ	0.000	0.007	0.006	0.012	0.012	0.013	0.013
$\lvert n\sigma_p \rvert$	2.75	0.003	0.005	0.001	0.001	0.001	-0.001	-0.002
	2.5	0.002	0.013	0.011	0.008	0.007	0.005	0.002
	Σ	0.003	0.009	0.011	0.005	0.007	0.003	0.002
nHitsDedx	≥ 22	0.003	-0.001	0.001	-0.002	-0.003	-0.006	-0.009
	≥ 25	0.002	0.004	0.012	0.003	0.006	0.001	-0.002
	Σ	0.003	0.004	0.012	0.002	0.004	0.003	0.009
pileup	low	0.002	-0.000	0.000	0.000	-0.000	0.000	0.000
	high	-0.001	-0.000	-0.000	0.000	0.000	0.000	0.000
	Σ	0.000	0.000	0.000	0.000	0.000	0.000	0.000
cent. cut	–1	-0.031	-0.018	-0.003	-0.007	-0.006	0.012	0.020
	+1	0.024	0.026	0.008	0.003	0.006	-0.007	-0.026
	Σ	0.027	0.022	0.006	0.005	0.006	0.009	0.023

Table B.31: Systematic uncertainty contributions for C_4/C_2 at $\sqrt{s_{NN}} = 3.5$ GeV

$\sqrt{s_{NN}} = 3.5$ GeV, C_4/C_2 Systematic Uncertainties								
		0-5%	5-10%	10-20%	20-30%	30-40%	40-50%	50-60%
C_4/C_2	value	0.155	2.046	2.770	3.112	3.238	3.366	3.271
	stat.	0.162	0.159	0.076	0.071	0.048	0.034	0.041
	sys.	0.138	0.163	0.154	0.142	0.149	0.162	0.164
nHitsFit	≥ 22	0.007	-0.006	-0.007	-0.015	-0.013	-0.017	-0.017
	≥ 25	0.036	-0.003	0.002	-0.014	-0.017	-0.015	-0.024
	Σ	0.036	0.000	0.000	0.015	0.015	0.016	0.021
Efficiency	–5%	0.122	-0.028	-0.101	-0.137	-0.145	-0.163	-0.161
	+5%	-0.104	0.028	0.091	0.122	0.129	0.144	0.142
	Σ	0.113	0.000	0.096	0.129	0.137	0.154	0.152
m^2 cuts (GeV^2)	[0.7,1.3]	0.005	-0.008	0.005	-0.003	0.000	0.004	0.003
	[0.6,1.1]	0.024	-0.010	-0.007	0.004	-0.001	0.002	-0.003
	Σ	0.024	0.010	0.000	0.000	0.000	0.000	0.003
DCA (cm)	<0.9	0.036	0.046	-0.003	-0.008	-0.006	0.006	0.004
	<1.1	0.049	-0.025	-0.041	-0.050	-0.036	-0.033	-0.043
	Σ	0.043	0.046	0.041	0.050	0.036	0.033	0.043
$\lvert n\sigma_p \rvert$	2.75	0.021	0.008	-0.008	0.007	0.005	-0.004	-0.015
	2.5	-0.039	0.055	0.034	0.029	0.012	0.009	-0.006
	Σ	0.039	0.055	0.034	0.029	0.000	0.007	0.015
nHitsDedx	≥ 22	0.020	-0.036	0.006	-0.008	-0.012	-0.017	-0.034
	≥ 25	0.018	-0.067	0.100	-0.035	0.031	-0.006	-0.011
	Σ	0.000	0.067	0.100	0.000	0.031	0.017	0.022
pileup	low	0.034	0.004	0.001	0.001	-0.001	0.001	0.000
	high	-0.014	-0.001	-0.000	-0.000	-0.000	0.000	-0.000
	Σ	0.000	0.000	0.000	0.000	0.000	0.000	0.000
cent. cut	–1	-0.053	-0.112	-0.016	-0.022	-0.032	0.033	0.008
	+1	0.009	0.147	0.041	0.001	0.011	-0.006	-0.026
	Σ	0.031	0.130	0.041	0.000	0.032	0.033	0.026

Table B.32: Systematic uncertainty contributions for C_5/C_1 at $\sqrt{s_{NN}} = 3.5$ GeV

$\sqrt{s_{NN}} = 3.5$ GeV, C_5/C_1 Systematic Uncertainties								
		0-5%	5-10%	10-20%	20-30%	30-40%	40-50%	50-60%
C_5/C_1	value	-4.849	1.537	7.100	8.954	10.435	11.612	11.669
	stat.	2.814	2.959	1.551	1.054	0.739	0.403	0.460
	sys.	2.004	1.441	1.181	0.772	0.891	0.996	1.072
nHitsFit	≥ 22	-0.055	-0.051	-0.057	-0.053	-0.078	-0.108	-0.118
	≥ 25	0.382	-0.374	0.087	-0.021	-0.237	-0.050	-0.187
	Σ	0.382	0.000	0.000	0.000	0.237	0.079	0.153
Efficiency	–5%	0.822	0.403	-0.383	-0.556	-0.810	-0.990	-1.081
	+5%	-0.689	-0.302	0.348	0.502	0.705	0.854	0.921
	Σ	0.000	0.000	0.000	0.000	0.758	0.922	1.001
m^2 cuts (GeV^2)	[0.7,1.3]	-0.191	-0.334	0.226	-0.013	-0.011	0.076	0.028
	[0.6,1.1]	0.138	-0.134	0.012	0.107	0.020	0.054	-0.051
	Σ	0.000	0.000	0.000	0.107	0.000	0.054	0.028
DCA (cm)	<0.9	0.813	0.613	0.061	-0.406	-0.113	0.064	0.066
	<1.1	0.649	-0.119	-0.578	-0.677	-0.404	-0.229	-0.415
	Σ	0.813	0.613	0.578	0.677	0.404	0.147	0.240
$\lvert n\sigma_p \rvert$	2.75	-0.025	0.392	-0.105	0.163	0.098	0.003	-0.149
	2.5	-0.995	0.736	0.232	0.375	0.022	0.068	-0.106
	Σ	0.995	0.000	0.000	0.269	0.000	0.000	0.149
nHitsDedx	≥ 22	0.863	-0.873	0.659	-0.234	-0.146	-0.137	-0.229
	≥ 25	1.774	-1.019	1.402	-0.738	0.099	-0.335	-0.193
	Σ	1.318	0.873	1.030	0.234	0.000	0.335	0.211
pileup	low	0.436	0.078	0.010	0.004	-0.008	0.021	-0.000
	high	-0.235	-0.033	-0.009	-0.001	-0.008	0.003	-0.000
	Σ	0.000	0.000	0.000	0.000	0.000	0.000	0.000
cent. cut	–1	0.254	-0.969	-0.253	-0.074	-0.174	0.058	-0.111
	+1	0.695	0.302	0.167	-0.221	0.051	-0.196	0.179
	Σ	0.695	0.969	0.000	0.000	0.000	0.000	0.000

Table B.33: Systematic uncertainty contributions for C_6/C_2 at $\sqrt{s_{NN}} = 3.5$ GeV

$\sqrt{s_{NN}} = 3.5$ GeV, C_6/C_2 Systematic Uncertainties								
		0-5%	5-10%	10-20%	20-30%	30-40%	40-50%	50-60%
C_6/C_2	value	-26.244	-23.924	4.049	8.666	18.381	25.067	32.684
	stat.	41.527	45.303	23.948	12.690	7.842	3.526	3.906
	sys.	57.122	41.813	10.784	9.651	4.699	3.907	4.769
nHitsFit	≥ 22	-0.341	0.763	0.216	0.457	-0.117	-0.158	-0.434
	≥ 25	-0.651	-10.352	-0.155	1.510	-1.250	0.712	-0.918
	Σ	0.000	0.000	0.000	0.000	0.000	0.000	0.000
Efficiency	–5%	3.770	6.182	1.661	1.235	-0.545	-1.671	-3.506
	+5%	-3.152	-4.834	-1.156	-0.795	0.640	1.551	2.978
	Σ	0.000	0.000	0.000	0.000	0.000	0.000	3.242
m^2 cuts (GeV^2)	[0.7,1.3]	1.749	-3.491	3.391	0.844	-0.408	0.657	0.150
	[0.6,1.1]	0.948	2.530	-0.129	1.571	0.039	0.439	-0.363
	Σ	0.000	0.000	0.000	0.000	0.000	0.439	0.000
DCA (cm)	<0.9	2.910	28.297	2.756	-8.751	-0.749	-0.054	1.024
	<1.1	-1.249	-13.455	-9.900	-6.472	-4.699	-0.787	-2.626
	Σ	0.000	28.297	9.900	7.611	4.699	0.787	1.825
$\lvert n\sigma_p \rvert$	2.75	-8.413	6.220	-2.127	0.587	0.747	0.163	-0.743
	2.5	-23.641	-1.999	-2.550	2.198	-1.195	0.237	-0.593
	Σ	23.641	0.000	0.000	2.198	0.000	0.000	0.593
nHitsDedx	≥ 22	4.494	-26.356	4.437	-1.939	0.483	-0.728	-0.482
	≥ 25	49.385	-35.210	10.187	-4.674	-3.662	-2.828	-1.859
	Σ	49.385	30.783	0.000	0.000	0.000	2.828	0.000
pileup	low	5.967	0.088	0.033	-0.120	0.002	0.201	-0.005
	high	-6.417	-0.352	0.015	0.060	-0.064	0.011	-0.000
	Σ	0.000	0.000	0.000	0.000	0.000	0.000	0.000
cent. cut	–1	0.906	-4.773	1.253	-1.137	-0.928	-2.540	-1.666
	+1	16.282	-0.736	-4.275	-5.512	2.009	-2.175	4.183
	Σ	16.282	0.000	4.275	5.512	0.000	2.540	2.924

Table B.34: Systematic uncertainty contributions for κ_1 at $\sqrt{s_{NN}} = 3.5$ GeV

$\sqrt{s_{NN}} = 3.5$ GeV, κ_1 Systematic Uncertainties								
		0-5%	5-10%	10-20%	20-30%	30-40%	40-50%	50-60%
κ_1	value	30.167	24.642	18.224	12.056	7.659	4.582	2.762
	stat.	0.003	0.003	0.002	0.002	0.001	0.001	0.001
	sys.	1.545	1.311	1.008	0.730	0.545	0.421	0.338
nHitsFit	≥ 22	-0.185	-0.156	-0.120	-0.084	-0.056	-0.035	-0.022
	≥ 25	-0.149	-0.125	-0.096	-0.067	-0.044	-0.028	-0.017
	Σ	0.167	0.141	0.108	0.076	0.050	0.031	0.020
Efficiency	–5%	-1.588	-1.297	-0.959	-0.635	-0.403	-0.241	-0.145
	+5%	1.437	1.173	0.868	0.574	0.365	0.218	0.132
	Σ	1.512	1.235	0.913	0.604	0.384	0.230	0.138
m^2 cuts (GeV^2)	[0.7,1.3]	0.002	0.001	-0.000	-0.001	-0.001	-0.001	-0.001
	[0.6,1.1]	-0.004	-0.002	-0.001	0.000	0.000	0.000	0.000
	Σ	0.003	0.002	0.001	0.001	0.001	0.001	0.000
DCA (cm)	<0.9	-0.010	-0.017	-0.021	-0.020	-0.017	-0.013	-0.010
	<1.1	-0.314	-0.258	-0.193	-0.130	-0.084	-0.051	-0.031
	Σ	0.162	0.138	0.107	0.075	0.050	0.032	0.020
$\lvert n\sigma_p \rvert$	2.75	-0.033	-0.030	-0.026	-0.019	-0.013	-0.009	-0.005
	2.5	0.053	0.034	0.015	0.004	-0.001	-0.002	-0.002
	Σ	0.043	0.032	0.021	0.012	0.007	0.005	0.004
nHitsDedx	≥ 22	-0.125	-0.113	-0.096	-0.073	-0.051	-0.034	-0.022
	≥ 25	0.063	0.024	-0.006	-0.021	-0.022	-0.019	-0.014
	Σ	0.094	0.069	0.051	0.047	0.037	0.026	0.018
pileup	low	0.005	-0.000	-0.000	-0.000	-0.000	0.000	0.000
	high	-0.002	0.000	0.000	0.000	0.000	-0.000	0.000
	Σ	0.003	0.000	0.000	0.000	0.000	0.000	0.000
cent. cut	–1	0.195	0.385	0.394	0.393	0.378	0.345	0.300
	+1	-0.189	-0.383	-0.394	-0.393	-0.380	-0.351	-0.313
	Σ	0.192	0.384	0.394	0.393	0.379	0.348	0.306

Table B.35: Systematic uncertainty contributions for κ_2 at $\sqrt{s_{NN}} = 3.5$ GeV

$\sqrt{s_{NN}} = 3.5$ GeV, κ_2 Systematic Uncertainties								
		0-5%	5-10%	10-20%	20-30%	30-40%	40-50%	50-60%
κ_2	value	2.825	5.604	4.600	3.301	2.164	1.269	0.699
	stat.	0.030	0.025	0.014	0.009	0.007	0.004	0.004
	sys.	0.340	0.574	0.476	0.354	0.245	0.168	0.121
nHitsFit	≥ 22	-0.019	-0.051	-0.046	-0.036	-0.026	-0.017	-0.010
	≥ 25	-0.016	-0.042	-0.036	-0.028	-0.020	-0.014	-0.008
	Σ	0.017	0.046	0.041	0.032	0.023	0.015	0.009
Efficiency	–5%	-0.305	-0.605	-0.497	-0.357	-0.234	-0.137	-0.076
	+5%	0.263	0.521	0.428	0.307	0.201	0.118	0.065
	Σ	0.284	0.563	0.462	0.332	0.217	0.128	0.070
m^2 cuts (GeV^2)	[0.7,1.3]	0.003	-0.001	0.001	0.000	-0.000	-0.000	-0.000
	[0.6,1.1]	-0.003	-0.005	-0.001	-0.000	0.000	-0.000	-0.000
	Σ	0.003	0.000	0.001	0.000	0.000	0.000	0.000
DCA (cm)	<0.9	0.029	0.031	0.007	0.000	-0.004	-0.003	-0.003
	<1.1	-0.063	-0.117	-0.095	-0.066	-0.044	-0.027	-0.016
	Σ	0.046	0.074	0.051	0.066	0.024	0.015	0.010
$\lvert n\sigma_p \rvert$	2.75	0.017	0.009	0.002	-0.001	-0.002	-0.003	-0.002
	2.5	0.068	0.076	0.051	0.027	0.012	0.005	0.001
	Σ	0.042	0.042	0.051	0.027	0.007	0.004	0.002
nHitsDedx	≥ 22	-0.002	-0.027	-0.023	-0.027	-0.021	-0.015	-0.009
	≥ 25	0.043	0.063	0.032	0.007	-0.003	-0.004	-0.004
	Σ	0.043	0.045	0.028	0.017	0.021	0.010	0.007
pileup	low	0.001	0.001	-0.000	-0.000	-0.000	0.000	0.000
	high	-0.004	-0.001	-0.000	0.000	0.000	-0.000	-0.000
	Σ	0.000	0.000	0.000	0.000	0.000	0.000	0.000
cent. cut	–1	-0.168	0.028	0.071	0.097	0.105	0.107	0.092
	+1	0.172	-0.001	-0.074	-0.094	-0.105	-0.106	-0.102
	Σ	0.170	0.028	0.072	0.096	0.105	0.107	0.097

Table B.36: Systematic uncertainty contributions for κ_3 at $\sqrt{s_{NN}} = 3.5$ GeV

$\sqrt{s_{NN}} = 3.5$ GeV, κ_3 Systematic Uncertainties

		0-5%	5-10%	10-20%	20-30%	30-40%	40-50%	50-60%
κ_3	value	-6.818	0.803	2.322	1.856	1.390	0.899	0.522
	stat.	0.364	0.325	0.120	0.083	0.040	0.020	0.014
	sys.	1.100	0.325	0.393	0.299	0.221	0.162	0.105
nHitsFit	≥ 22	0.096	-0.001	-0.032	-0.032	-0.025	-0.016	-0.010
	≥ 25	0.041	0.006	0.002	-0.025	-0.016	-0.014	-0.012
	Σ	0.096	0.000	0.032	0.028	0.020	0.015	0.011
Efficiency	–5%	1.134	-0.134	-0.386	-0.309	-0.231	-0.150	-0.087
	+5%	-0.928	0.109	0.316	0.253	0.189	0.122	0.071
	Σ	1.031	0.000	0.351	0.281	0.210	0.136	0.079
m^2 cuts (GeV^2)	[0.7,1.3]	0.023	0.001	-0.005	-0.000	-0.001	0.000	0.001
	[0.6,1.1]	0.044	0.010	-0.007	-0.001	-0.003	-0.001	-0.001
	Σ	0.000	0.000	0.000	0.000	0.000	0.000	0.000
DCA (cm)	<0.9	-0.126	0.048	-0.002	-0.004	-0.004	-0.003	-0.000
	<1.1	0.165	-0.050	-0.060	-0.070	-0.048	-0.031	-0.018
	Σ	0.165	0.000	0.060	0.070	0.048	0.031	0.018
$\lvert n\sigma_p \rvert$	2.75	0.052	0.063	-0.012	-0.001	-0.000	-0.006	-0.005
	2.5	-0.143	0.119	0.070	0.019	0.016	0.005	-0.002
	Σ	0.098	0.091	0.070	0.019	0.016	0.006	0.005
nHitsDedx	≥ 22	0.102	-0.025	0.002	-0.013	-0.013	-0.018	-0.018
	≥ 25	-0.058	-0.063	0.125	-0.001	0.033	-0.003	-0.005
	Σ	0.102	0.000	0.125	0.000	0.033	0.018	0.012
pileup	low	0.061	-0.003	0.001	0.001	-0.000	0.000	0.000
	high	-0.033	-0.002	0.000	-0.000	-0.000	0.000	0.000
	Σ	0.000	0.000	0.000	0.000	0.000	0.000	0.000
cent. cut	–1	-0.403	-0.240	0.076	0.011	0.029	0.084	0.058
	+1	0.198	0.383	0.028	-0.067	-0.030	-0.075	-0.069
	Σ	0.301	0.312	0.076	0.067	0.029	0.080	0.064

Table B.37: Systematic uncertainty contributions for κ_4 at $\sqrt{s_{NN}} = 3.5$ GeV

$\sqrt{s_{NN}} = 3.5$ GeV, κ_4 Systematic Uncertainties

		0-5%	5-10%	10-20%	20-30%	30-40%	40-50%	50-60%
κ_4	value	-3.913	-6.804	-1.138	1.490	0.662	0.837	0.533
	stat.	4.994	3.659	1.420	0.779	0.327	0.111	0.074
	sys.	2.898	2.588	1.538	0.752	0.194	0.203	0.126
nHitsFit	≥ 22	-0.049	-0.092	0.005	-0.077	-0.012	-0.026	-0.014
	≥ 25	1.172	-0.053	0.021	-0.094	-0.103	-0.018	-0.022
	Σ	1.172	0.000	0.000	0.000	0.103	0.000	0.000
Efficiency	–5%	0.891	1.550	0.259	-0.339	-0.151	-0.191	-0.121
	+5%	-0.694	-1.206	-0.202	0.264	0.117	0.148	0.094
	Σ	0.000	0.000	0.000	0.000	0.000	0.170	0.108
m^2 cuts (GeV^2)	[0.7,1.3]	0.009	-0.251	0.151	-0.040	0.008	0.019	0.004
	[0.6,1.1]	0.550	-0.347	-0.107	0.075	0.011	0.018	-0.007
	Σ	0.550	0.347	0.107	0.075	0.000	0.018	0.004
DCA (cm)	<0.9	1.764	0.924	-0.129	-0.140	-0.062	0.034	0.005
	<1.1	1.346	-0.165	-0.529	-0.382	-0.092	-0.033	-0.054
	Σ	1.764	0.924	0.529	0.382	0.000	0.034	0.054
$\lvert n\sigma_p \rvert$	2.75	0.306	-0.222	-0.154	0.079	0.028	-0.000	-0.024
	2.5	-0.928	0.599	0.170	0.223	-0.026	0.003	-0.019
	Σ	0.000	0.599	0.000	0.223	0.000	0.000	0.024
nHitsDedx	≥ 22	0.158	-0.918	0.063	-0.090	-0.080	-0.018	-0.027
	≥ 25	0.609	-1.944	1.385	-0.604	0.072	-0.049	-0.022
	Σ	0.000	1.431	1.385	0.604	0.000	0.000	0.027
pileup	low	0.745	0.138	0.013	0.006	-0.006	0.005	-0.000
	high	-0.235	-0.013	-0.007	-0.006	-0.003	0.001	-0.000
	Σ	0.000	0.000	0.000	0.000	0.000	0.000	0.000
cent. cut	–1	1.675	-1.648	-0.406	0.059	-0.024	0.104	0.011
	+1	-1.900	1.821	0.396	-0.042	-0.164	-0.032	-0.016
	Σ	1.900	1.821	0.396	0.000	0.164	0.104	0.000

Table B.38: Systematic uncertainty contributions for κ_5 at $\sqrt{s_{NN}} = 3.5$ GeV

$\sqrt{s_{NN}} = 3.5$ GeV, κ_5 Systematic Uncertainties								
		0-5%	5-10%	10-20%	20-30%	30-40%	40-50%	50-60%
κ_5	value	-9.249	-22.840	-4.502	-14.916	-1.567	-1.263	0.599
	stat.	62.572	53.422	19.685	6.942	2.911	0.771	0.490
	sys.	49.969	20.843	12.034	3.951	0.000	1.424	0.698
nHitsFit	≥ 22	-2.205	0.348	-0.327	0.789	-0.018	0.053	-0.030
	≥ 25	-0.049	-8.320	1.299	1.211	-0.526	0.213	-0.067
	Σ	0.000	0.000	0.000	1.211	0.000	0.213	0.000
Efficiency	–5%	2.704	6.677	1.316	4.361	0.458	0.369	-0.175
	+5%	-2.002	-4.944	-0.975	-3.229	-0.339	-0.273	0.130
	Σ	0.000	0.000	0.000	0.000	0.000	0.000	0.000
m^2 cuts (GeV^2)	[0.7,1.3]	-6.478	-5.725	2.736	0.233	-0.136	0.150	0.012
	[0.6,1.1]	-2.355	-0.009	1.484	0.582	0.112	0.085	-0.050
	Σ	0.000	0.000	2.736	0.582	0.000	0.000	0.000
DCA (cm)	<0.9	9.672	4.198	2.222	-3.562	-0.261	-0.057	0.091
	<1.1	4.969	1.529	-3.613	-2.718	-1.155	-0.091	-0.264
	Σ	9.672	4.198	3.613	3.562	0.000	0.000	0.264
$\lvert n\sigma_p \rvert$	2.75	-5.187	10.160	-0.252	1.055	0.384	0.116	-0.063
	2.5	-18.414	8.020	0.116	1.424	-0.154	0.064	-0.096
	Σ	5.187	0.000	0.000	1.055	0.000	0.000	0.096
nHitsDedx	≥ 22	22.776	-11.457	11.149	-1.793	-0.175	-0.136	-0.018
	≥ 25	47.766	-5.012	8.052	-3.112	-0.935	-1.117	-0.263
	Σ	35.271	0.000	11.149	0.000	0.000	1.117	0.000
pileup	low	4.145	0.597	0.033	-0.036	0.014	0.042	-0.001
	high	-3.823	-0.610	-0.100	0.048	-0.035	0.001	0.000
	Σ	0.000	0.000	0.000	0.000	0.000	0.000	0.000
cent. cut	–1	2.347	-1.245	-1.005	-0.073	0.234	-0.823	-0.023
	+1	33.651	-20.416	-2.849	-2.369	0.781	-0.891	0.639
	Σ	33.651	20.416	0.000	0.000	0.000	0.857	0.639

Table B.39: Systematic uncertainty contributions for κ_6 at $\sqrt{s_{NN}} = 3.5$ GeV

$\sqrt{s_{NN}} = 3.5$ GeV, κ_6 Systematic Uncertainties								
		0-5%	5-10%	10-20%	20-30%	30-40%	40-50%	50-60%
κ_6	value	23.122	-209.32	-135.92	-21.455	-38.811	-13.639	-1.908
	stat.	870.327	895.741	287.204	91.607	29.138	7.328	3.112
	sys.	929.256	939.061	158.320	85.024	34.096	8.467	2.840
nHitsFit	≥ 22	22.429	30.755	13.337	3.245	1.422	0.710	0.013
	≥ 25	-95.757	-181.69	-23.856	13.672	3.095	2.852	-0.260
	Σ	0.000	0.000	0.000	0.000	0.000	2.852	0.000
Efficiency	–5%	-8.333	75.433	48.981	7.732	13.987	4.915	0.687
	+5%	5.868	-53.122	-34.494	-5.445	-9.850	-3.461	-0.484
	Σ	0.000	0.000	0.000	0.000	0.000	0.000	0.000
m^2 cuts (GeV^2)	[0.7,1.3]	151.960	-3.450	27.011	12.067	-2.364	0.345	-0.029
	[0.6,1.1]	27.218	98.631	-17.561	10.663	-1.765	0.165	-0.001
	Σ	0.000	0.000	17.561	0.000	1.765	0.000	0.000
DCA (cm)	<0.9	-153.83	726.873	37.949	-71.803	0.652	-1.672	1.616
	<1.1	-206.40	-406.91	-132.87	-28.244	-20.082	0.616	-1.161
	Σ	0.000	566.892	132.865	71.803	20.082	0.000	1.389
$\lvert n\sigma_p \rvert$	2.75	-224.50	44.840	-33.840	-12.008	-0.427	-0.421	0.251
	2.5	-432.99	-235.23	-78.414	-4.526	-9.320	-0.283	0.758
	Σ	328.743	235.228	0.000	12.008	0.000	0.000	0.000
nHitsDedx	≥ 22	-208.73	-562.75	-69.373	3.988	13.128	-0.208	1.234
	≥ 25	869.163	-858.72	9.273	13.871	-30.019	3.146	-1.018
	Σ	869.163	710.730	0.000	0.000	21.574	0.000	0.000
pileup	low	80.536	-15.014	-0.666	-1.763	0.267	0.201	-0.000
	high	-135.84	-0.443	2.320	0.583	0.076	-0.017	-0.000
	Σ	0.000	0.000	0.000	0.000	0.000	0.000	0.000
cent. cut	–1	-73.567	-6.114	61.965	-19.835	-7.999	-7.972	-1.104
	+1	133.640	140.463	-84.283	-43.922	17.050	0.699	3.851
	Σ	0.000	0.000	84.283	43.922	17.050	7.972	2.477

Table B.40: Systematic uncertainty contributions for κ_2/κ_1 at $\sqrt{s_{NN}} = 3.5$ GeV

$\sqrt{s_{NN}} = 3.5$ GeV, κ_2/κ_1 Systematic Uncertainties		0-5%	5-10%	10-20%	20-30%	30-40%	40-50%	50-60%
κ_2/κ_1	value	0.094	0.227	0.252	0.274	0.282	0.277	0.253
	stat.	0.001	0.001	0.001	0.001	0.001	0.001	0.001
	sys.	0.008	0.012	0.013	0.014	0.014	0.014	0.015
nHitsFit	≥ 22	-0.000	-0.001	-0.001	-0.001	-0.001	-0.002	-0.001
	≥ 25	-0.000	-0.001	-0.001	-0.001	-0.001	-0.001	-0.001
	Σ	0.000	0.001	0.001	0.001	0.001	0.001	0.001
Efficiency	–5%	-0.005	-0.012	-0.013	-0.014	-0.015	-0.015	-0.013
	+5%	0.004	0.011	0.012	0.013	0.013	0.013	0.012
	Σ	0.005	0.011	0.013	0.014	0.014	0.014	0.013
m^2 cuts (GeV^2)	[0.7,1.3]	0.000	-0.000	0.000	0.000	0.000	0.000	-0.000
	[0.6,1.1]	-0.000	-0.000	-0.000	-0.000	0.000	-0.000	-0.000
	Σ	0.000	0.000	0.000	0.000	0.000	0.000	0.000
DCA (cm)	<0.9	0.001	0.001	0.001	0.000	0.000	0.000	-0.000
	<1.1	-0.001	-0.002	-0.003	-0.002	-0.003	-0.003	-0.003
	Σ	0.001	0.002	0.002	0.001	0.003	0.001	0.002
$\lvert n\sigma_p \rvert$	2.75	0.001	0.001	0.000	0.000	0.000	-0.000	-0.000
	2.5	0.002	0.003	0.003	0.002	0.002	0.001	0.001
	Σ	0.001	0.002	0.002	0.001	0.001	0.001	0.000
nHitsDedx	≥ 22	0.000	-0.000	0.000	-0.001	-0.001	-0.001	-0.001
	≥ 25	0.001	0.002	0.002	0.001	0.000	0.000	-0.000
	Σ	0.001	0.002	0.002	0.001	0.001	0.001	0.001
pileup	low	0.000	0.000	-0.000	0.000	-0.000	0.000	0.000
	high	-0.000	-0.000	-0.000	0.000	0.000	0.000	-0.000
	Σ	0.000	0.000	0.000	0.000	0.000	0.000	0.000
cent. cut	–1	-0.006	-0.002	-0.002	-0.001	-0.000	0.003	0.006
	+1	0.006	0.003	0.001	0.001	0.000	-0.002	-0.007
	Σ	0.006	0.003	0.001	0.001	0.000	0.002	0.007

Table B.41: Systematic uncertainty contributions for κ_3/κ_1 at $\sqrt{s_{NN}} = 3.5$ GeV

$\sqrt{s_{NN}} = 3.5$ GeV, κ_3/κ_1 Systematic Uncertainties								
		0-5%	5-10%	10-20%	20-30%	30-40%	40-50%	50-60%
κ_3/κ_1	value	-0.226	0.033	0.127	0.154	0.181	0.196	0.189
	stat.	0.012	0.013	0.007	0.007	0.005	0.004	0.005
	sys.	0.025	0.014	0.014	0.016	0.020	0.021	0.020
nHitsFit	≥ 22	0.002	0.000	-0.001	-0.002	-0.002	-0.002	-0.002
	≥ 25	0.000	0.000	0.001	-0.001	-0.001	-0.002	-0.003
	Σ	0.002	0.000	0.000	0.002	0.002	0.002	0.003
Efficiency	–5%	0.024	-0.004	-0.014	-0.017	-0.020	-0.021	-0.020
	+5%	-0.021	0.003	0.012	0.014	0.017	0.018	0.018
	Σ	0.023	0.000	0.013	0.015	0.018	0.020	0.019
m^2 cuts (GeV^2)	[0.7,1.3]	0.001	0.000	-0.000	-0.000	-0.000	0.000	0.000
	[0.6,1.1]	0.001	0.000	-0.000	-0.000	-0.000	-0.000	-0.000
	Σ	0.000	0.000	0.000	0.000	0.000	0.000	0.000
DCA (cm)	<0.9	-0.004	0.002	0.000	-0.000	-0.000	-0.000	0.001
	<1.1	0.003	-0.002	-0.002	-0.004	-0.004	-0.005	-0.004
	Σ	0.003	0.000	0.002	0.004	0.004	0.005	0.004
$\lvert n\sigma_p \rvert$	2.75	0.001	0.003	-0.000	0.000	0.000	-0.001	-0.002
	2.5	-0.004	0.005	0.004	0.002	0.002	0.001	-0.001
	Σ	0.003	0.004	0.004	0.002	0.002	0.001	0.002
nHitsDedx	≥ 22	0.002	-0.001	0.001	-0.000	-0.000	-0.002	-0.005
	≥ 25	-0.001	-0.003	0.007	0.000	0.005	0.000	-0.001
	Σ	0.002	0.000	0.004	0.000	0.005	0.002	0.003
pileup	low	0.002	-0.000	0.000	0.000	-0.000	0.000	0.000
	high	-0.001	-0.000	0.000	-0.000	-0.000	0.000	0.000
	Σ	0.000	0.000	0.000	0.000	0.000	0.000	0.000
cent. cut	–1	-0.012	-0.010	0.001	-0.004	-0.005	0.004	0.001
	+1	0.005	0.016	0.004	-0.001	0.005	-0.001	-0.003
	Σ	0.009	0.013	0.003	0.002	0.005	0.004	0.002

Table B.42: Systematic uncertainty contributions for κ_4/κ_1 at $\sqrt{s_{NN}} = 3.5$ GeV

$\sqrt{s_{NN}} = 3.5$ GeV, κ_4/κ_1 Systematic Uncertainties								
		0-5%	5-10%	10-20%	20-30%	30-40%	40-50%	50-60%
κ_4/κ_1	value	-0.130	-0.276	-0.062	0.124	0.086	0.183	0.193
	stat.	0.166	0.148	0.078	0.065	0.043	0.024	0.027
	sys.	0.094	0.100	0.084	0.061	0.021	0.031	0.040
nHitsFit	≥ 22	-0.002	-0.005	-0.000	-0.005	-0.001	-0.004	-0.003
	≥ 25	0.038	-0.004	0.001	-0.007	-0.013	-0.003	-0.007
	Σ	0.038	0.000	0.000	0.000	0.013	0.000	0.000
Efficiency	–5%	0.022	0.046	0.010	-0.021	-0.014	-0.030	-0.032
	+5%	-0.018	-0.038	-0.009	0.017	0.012	0.025	0.026
	Σ	0.000	0.000	0.000	0.000	0.000	0.028	0.029
m^2 cuts (GeV^2)	[0.7,1.3]	0.000	-0.010	0.008	-0.003	0.001	0.004	0.002
	[0.6,1.1]	0.018	-0.014	-0.006	0.006	0.001	0.004	-0.002
	Σ	0.018	0.014	0.006	0.006	0.000	0.004	0.002
DCA (cm)	<0.9	0.058	0.037	-0.007	-0.011	-0.008	0.008	0.002
	<1.1	0.043	-0.009	-0.029	-0.030	-0.011	-0.005	-0.017
	Σ	0.058	0.037	0.029	0.030	0.000	0.008	0.017
$\lvert n\sigma_p \rvert$	2.75	0.010	-0.009	-0.009	0.007	0.004	0.000	-0.008
	2.5	-0.031	0.025	0.009	0.018	-0.003	0.001	-0.007
	Σ	0.000	0.025	0.000	0.018	0.000	0.000	0.008
nHitsDedx	≥ 22	0.005	-0.038	0.003	-0.007	-0.010	-0.003	-0.008
	≥ 25	0.020	-0.079	0.076	-0.050	0.010	-0.010	-0.007
	Σ	0.000	0.059	0.076	0.050	0.000	0.000	0.000
pileup	low	0.025	0.006	0.001	0.000	-0.001	0.001	-0.000
	high	-0.008	-0.001	-0.000	-0.000	-0.000	0.000	-0.000
	Σ	0.000	0.000	0.000	0.000	0.000	0.000	0.000
cent. cut	–1	0.057	-0.064	-0.021	0.001	-0.008	0.010	-0.019
	+1	-0.063	0.069	0.020	0.001	-0.016	0.006	0.014
	Σ	0.060	0.066	0.020	0.000	0.016	0.010	0.019

Table B.43: Systematic uncertainty contributions for κ_5/κ_1 at $\sqrt{s_{NN}} = 3.5$ GeV

$\sqrt{s_{NN}} = 3.5$ GeV, κ_5/κ_1 Systematic Uncertainties								
		0-5%	5-10%	10-20%	20-30%	30-40%	40-50%	50-60%
κ_5/κ_1	value	-0.307	-0.927	-0.247	-1.237	-0.205	-0.276	0.217
	stat.	2.074	2.168	1.080	0.576	0.380	0.168	0.177
	sys.	1.650	0.830	0.645	0.428	0.000	0.310	0.165
nHitsFit	≥ 22	-0.075	0.008	-0.019	0.056	-0.004	0.009	-0.009
	≥ 25	-0.003	-0.341	0.070	0.093	-0.069	0.045	-0.023
	Σ	0.000	0.000	0.000	0.093	0.000	0.045	0.000
Efficiency	–5%	0.070	0.211	0.056	0.282	0.047	0.063	-0.049
	+5%	-0.054	-0.164	-0.044	-0.219	-0.036	-0.049	0.038
	Σ	0.000	0.000	0.000	0.000	0.000	0.000	0.000
m^2 cuts (GeV^2)	[0.7,1.3]	-0.215	-0.232	0.150	0.019	-0.018	0.033	0.004
	[0.6,1.1]	-0.078	-0.000	0.081	0.048	0.015	0.019	-0.018
	Σ	0.000	0.000	0.150	0.048	0.000	0.000	0.000
DCA (cm)	<0.9	0.320	0.170	0.121	-0.297	-0.034	-0.013	0.033
	<1.1	0.160	0.052	-0.199	-0.236	-0.151	-0.023	-0.092
	Σ	0.320	0.000	0.000	0.297	0.000	0.000	0.092
$\lvert n\sigma_p \rvert$	2.75	-0.172	0.411	-0.014	0.085	0.050	0.025	-0.022
	2.5	-0.611	0.327	0.007	0.119	-0.020	0.014	-0.035
	Σ	0.172	0.000	0.000	0.085	0.000	0.000	0.035
nHitsDedx	≥ 22	0.751	-0.467	0.607	-0.155	-0.024	-0.032	-0.005
	≥ 25	1.587	-0.203	0.442	-0.260	-0.122	-0.244	-0.094
	Σ	1.169	0.000	0.607	0.155	0.000	0.244	0.000
pileup	low	0.137	0.024	0.002	-0.003	0.002	0.009	-0.000
	high	-0.127	-0.025	-0.005	0.004	-0.005	0.000	0.000
	Σ	0.000	0.000	0.000	0.000	0.000	0.000	0.000
cent. cut	–1	0.080	-0.037	-0.051	0.035	0.043	-0.172	-0.036
	+1	1.107	-0.830	-0.158	-0.229	0.087	-0.200	0.230
	Σ	1.107	0.830	0.158	0.229	0.000	0.186	0.133

Table B.44: Systematic uncertainty contributions for κ_6/κ_1 at $\sqrt{s_{NN}} = 3.5$ GeV

$\sqrt{s_{NN}} = 3.5$ GeV, κ_6/κ_1 Systematic Uncertainties								
		0-5%	5-10%	10-20%	20-30%	30-40%	40-50%	50-60%
κ_6/κ_1	value	0.766	-8.495	-7.458	-1.780	-5.067	-2.977	-0.691
	stat.	28.851	36.350	15.760	7.598	3.805	1.599	1.127
	sys.	30.862	38.061	8.721	7.016	4.090	1.746	1.284
nHitsFit	≥ 22	0.744	1.187	0.678	0.255	0.147	0.131	-0.001
	≥ 25	-3.155	-7.379	-1.341	1.118	0.373	0.601	-0.098
	Σ	0.000	0.000	0.000	0.000	0.000	0.601	0.000
Efficiency	–5%	-0.224	2.483	2.180	0.520	1.481	0.870	0.202
	+5%	0.166	-1.839	-1.614	-0.385	-1.097	-0.644	-0.150
	Σ	0.000	0.000	0.000	0.000	0.000	0.000	0.000
m^2 cuts (GeV^2)	[0.7,1.3]	5.038	-0.140	1.482	1.001	-0.309	0.075	-0.011
	[0.6,1.1]	0.902	4.001	-0.964	0.884	-0.230	0.036	-0.000
	Σ	0.000	0.000	0.964	0.000	0.230	0.000	0.000
DCA (cm)	<0.9	-5.097	29.471	2.071	-5.949	0.074	-0.372	0.581
	<1.1	-6.763	-16.430	-7.292	-2.337	-2.648	0.100	-0.423
	Σ	0.000	22.951	7.292	5.949	2.648	0.000	0.502
$\lvert n\sigma_p \rvert$	2.75	-7.433	1.807	-1.865	-0.997	-0.065	-0.097	0.089
	2.5	-14.380	-9.547	-4.300	-0.375	-1.217	-0.063	0.274
	Σ	10.906	9.547	0.000	0.997	0.000	0.000	0.000
nHitsDedx	≥ 22	-6.887	-22.772	-3.826	0.318	1.669	-0.067	0.438
	≥ 25	28.870	-34.874	0.506	1.145	-3.923	0.672	-0.370
	Σ	28.870	28.823	0.000	0.000	2.796	0.000	0.000
pileup	low	2.670	-0.609	-0.037	-0.146	0.035	0.044	-0.000
	high	-4.503	-0.018	0.127	0.048	0.010	-0.004	-0.000
	Σ	0.000	0.000	0.000	0.000	0.000	0.000	0.000
cent. cut	–1	-2.460	-0.117	3.640	-1.641	-0.836	-1.639	-0.364
	+1	4.407	5.483	-4.685	-3.584	1.881	-0.070	1.182
	Σ	0.000	0.000	4.685	3.584	1.358	1.639	1.182

B.3 Systematic Contributions at $\sqrt{s_{NN}} = 3.9$ GeV

Table B.45: Systematic uncertainty contributions for C_1 at $\sqrt{s_{NN}} = 3.9$ GeV

$\sqrt{s_{NN}} = 3.9$ GeV, C_1 Systematic Uncertainties								
		0-5%	5-10%	10-20%	20-30%	30-40%	40-50%	50-60%
C_1	value	27.310	22.113	16.243	10.538	6.582	3.939	2.312
	stat.	0.005	0.004	0.002	0.002	0.001	0.001	0.001
	sys.	1.448	1.202	0.906	0.631	0.452	0.338	0.262
nHitsFit	≥ 22	-0.145	-0.121	-0.093	-0.064	-0.042	-0.027	-0.016
	≥ 25	-0.070	-0.056	-0.040	-0.025	-0.015	-0.008	-0.004
	Σ	0.108	0.088	0.067	0.044	0.029	0.017	0.010
Efficiency	–5%	-1.437	-1.164	-0.855	-0.555	-0.346	-0.207	-0.122
	+5%	1.300	1.053	0.773	0.502	0.313	0.188	0.110
	Σ	1.369	1.108	0.814	0.528	0.330	0.197	0.116
m^2 cuts (GeV^2)	[0.7,1.3]	0.006	0.003	0.000	-0.001	-0.001	-0.001	-0.001
	[0.6,1.1]	-0.010	-0.005	-0.003	-0.000	0.000	0.001	0.001
	Σ	0.008	0.004	0.003	0.001	0.001	0.001	0.001
DCA (cm)	<0.9	0.250	0.202	0.146	0.093	0.058	0.035	0.019
	<1.1	-0.429	-0.355	-0.266	-0.179	-0.116	-0.072	-0.043
	Σ	0.339	0.279	0.206	0.136	0.087	0.053	0.031
$\lvert n\sigma_p \rvert$	2.75	0.010	0.004	-0.000	-0.003	-0.003	-0.003	-0.002
	2.5	0.087	0.062	0.037	0.018	0.008	0.003	0.001
	Σ	0.048	0.033	0.019	0.010	0.005	0.003	0.001
nHitsDedx	≥ 22	0.054	0.033	0.015	0.003	-0.001	-0.002	-0.002
	≥ 25	0.462	0.346	0.233	0.138	0.083	0.048	0.028
	Σ	0.258	0.190	0.124	0.071	0.042	0.025	0.015
pileup	low	0.004	-0.002	-0.001	-0.001	-0.000	0.000	0.000
	high	-0.000	0.001	0.000	0.001	0.000	-0.000	-0.000
	Σ	0.004	0.000	0.000	0.001	0.000	0.000	0.000
cent. cut	–1	0.163	0.306	0.310	0.306	0.292	0.266	0.228
	+1	-0.160	-0.304	-0.310	-0.305	-0.293	-0.270	-0.237
	Σ	0.162	0.305	0.310	0.306	0.293	0.268	0.233

Table B.46: Systematic uncertainty contributions for C_2 at $\sqrt{s_{NN}} = 3.9$ GeV

$\sqrt{s_{NN}} = 3.9$ GeV, C_2 Systematic Uncertainties								
		0-5%	5-10%	10-20%	20-30%	30-40%	40-50%	50-60%
C_2	value	29.370	25.874	19.274	12.669	7.945	4.725	2.735
	stat.	0.040	0.042	0.017	0.010	0.007	0.004	0.004
	sys.	1.647	1.590	1.220	0.851	0.609	0.437	0.328
nHitsFit	≥ 22	-0.159	-0.150	-0.118	-0.084	-0.056	-0.035	-0.021
	≥ 25	-0.083	-0.073	-0.062	-0.039	-0.022	-0.012	-0.007
	Σ	0.121	0.112	0.090	0.061	0.039	0.024	0.014
Efficiency	–5%	-1.660	-1.570	-1.182	-0.785	-0.494	-0.292	-0.167
	+5%	1.492	1.403	1.055	0.700	0.440	0.261	0.149
	Σ	1.576	1.486	1.119	0.742	0.467	0.276	0.158
m^2 cuts (GeV^2)	[0.7,1.3]	0.014	0.006	0.005	0.000	-0.001	-0.001	-0.001
	[0.6,1.1]	-0.020	-0.010	-0.006	-0.001	-0.001	0.000	0.000
	Σ	0.017	0.006	0.006	0.000	0.000	0.001	0.001
DCA (cm)	<0.9	0.244	0.238	0.174	0.115	0.075	0.046	0.025
	<1.1	-0.476	-0.465	-0.349	-0.243	-0.156	-0.095	-0.058
	Σ	0.360	0.352	0.261	0.179	0.116	0.070	0.042
$\lvert n\sigma_p \rvert$	2.75	0.015	0.021	0.012	0.004	-0.001	-0.002	-0.001
	2.5	0.123	0.126	0.078	0.040	0.019	0.009	0.004
	Σ	0.069	0.074	0.045	0.022	0.010	0.005	0.002
nHitsDedx	≥ 22	0.060	0.053	0.028	0.005	0.001	-0.002	-0.002
	≥ 25	0.491	0.480	0.324	0.178	0.110	0.064	0.035
	Σ	0.275	0.266	0.176	0.091	0.110	0.033	0.018
pileup	low	0.000	0.000	-0.000	0.000	-0.001	-0.000	0.000
	high	-0.003	0.001	0.001	0.001	0.001	-0.001	-0.000
	Σ	0.000	0.000	0.000	0.000	0.000	0.000	0.000
cent. cut	–1	0.064	0.319	0.359	0.361	0.353	0.326	0.278
	+1	-0.046	-0.335	-0.356	-0.354	-0.357	-0.330	-0.289
	Σ	0.055	0.327	0.358	0.358	0.355	0.328	0.283

Table B.47: Systematic uncertainty contributions for C_3 at $\sqrt{s_{NN}} = 3.9$ GeV

$\sqrt{s_{NN}} = 3.9$ GeV, C_3 Systematic Uncertainties								
		0-5%	5-10%	10-20%	20-30%	30-40%	40-50%	50-60%
C_3	value	30.043	33.896	26.288	17.750	11.373	6.703	3.819
	stat.	0.460	0.425	0.189	0.098	0.057	0.023	0.017
	sys.	1.602	2.570	2.049	1.424	1.043	0.709	0.510
nHitsFit	≥ 22	-0.119	-0.174	-0.167	-0.137	-0.091	-0.061	-0.034
	≥ 25	0.057	-0.224	-0.139	-0.081	-0.041	-0.021	-0.018
	Σ	0.119	0.199	0.153	0.109	0.066	0.041	0.026
Efficiency	–5%	-1.532	-2.466	-1.996	-1.382	-0.905	-0.530	-0.298
	+5%	1.406	2.170	1.748	1.208	0.789	0.462	0.260
	Σ	1.469	2.318	1.872	1.295	0.847	0.496	0.279
m^2 cuts (GeV^2)	[0.7,1.3]	0.064	0.035	0.007	0.012	-0.002	-0.003	-0.002
	[0.6,1.1]	-0.050	-0.040	-0.035	-0.003	-0.000	0.001	-0.000
	Σ	0.000	0.035	0.000	0.000	0.000	0.000	0.000
DCA (cm)	<0.9	-0.016	0.435	0.207	0.179	0.132	0.074	0.044
	<1.1	-0.359	-0.895	-0.587	-0.392	-0.250	-0.155	-0.102
	Σ	0.359	0.665	0.397	0.285	0.191	0.115	0.073
$\lvert n\sigma_p \rvert$	2.75	0.010	0.098	0.048	0.006	-0.001	-0.000	-0.002
	2.5	0.045	0.410	0.210	0.080	0.040	0.022	0.007
	Σ	0.000	0.254	0.129	0.080	0.040	0.022	0.005
nHitsDedx	≥ 22	0.127	0.049	0.054	0.072	0.012	0.005	0.003
	≥ 25	0.463	0.813	0.519	0.339	0.237	0.115	0.060
	Σ	0.463	0.813	0.519	0.206	0.237	0.115	0.060
pileup	low	0.031	0.007	0.010	0.003	-0.006	0.001	0.001
	high	-0.051	-0.016	0.003	-0.007	-0.001	-0.000	-0.001
	Σ	0.000	0.000	0.000	0.000	0.000	0.000	0.000
cent. cut	–1	-0.227	0.033	0.545	0.446	0.520	0.469	0.411
	+1	0.167	-0.156	-0.406	-0.469	-0.522	-0.487	-0.419
	Σ	0.227	0.156	0.476	0.458	0.521	0.478	0.415

Table B.48: Systematic uncertainty contributions for C_4 at $\sqrt{s_{NN}} = 3.9$ GeV

$\sqrt{s_{NN}} = 3.9$ GeV, C_4 Systematic Uncertainties								
		0-5%	5-10%	10-20%	20-30%	30-40%	40-50%	50-60%
C_4	value	6.170	44.665	39.976	30.728	21.112	12.167	6.991
	stat.	6.912	5.000	2.337	1.001	0.547	0.189	0.120
	sys.	4.256	7.210	3.742	3.139	2.487	1.546	1.100
nHitsFit	≥ 22	0.073	0.291	-0.101	-0.280	-0.197	-0.147	-0.078
	≥ 25	-0.733	0.149	-0.527	-0.205	-0.098	-0.076	-0.050
	Σ	0.000	0.000	0.527	0.280	0.197	0.111	0.064
Efficiency	–5%	3.833	-2.964	-3.369	-3.065	-2.255	-1.273	-0.745
	+5%	-2.813	2.708	2.957	2.621	1.912	1.082	0.631
	Σ	0.000	2.708	3.163	2.843	2.084	1.177	0.688
m^2 cuts (GeV^2)	[0.7,1.3]	1.557	-0.734	-0.142	0.035	-0.035	-0.007	-0.006
	[0.6,1.1]	0.145	0.423	-0.204	0.045	0.048	0.011	-0.002
	Σ	1.557	0.000	0.204	0.000	0.000	0.000	0.000
DCA (cm)	<0.9	-0.813	1.900	0.023	0.181	0.117	0.095	0.159
	<1.1	-0.767	-4.256	-0.142	-0.713	-0.637	-0.355	-0.252
	Σ	0.000	3.078	0.000	0.447	0.377	0.225	0.205
$\lvert n\sigma_p \rvert$	2.75	0.205	1.262	-0.039	0.006	-0.074	0.006	-0.024
	2.5	-0.259	2.666	0.388	0.315	-0.012	0.043	-0.019
	Σ	0.000	1.964	0.000	0.315	0.074	0.043	0.021
nHitsDedx	≥ 22	-0.960	4.432	-1.918	0.924	0.138	0.046	0.076
	≥ 25	-2.779	6.484	-0.283	0.762	0.820	0.401	0.232
	Σ	2.779	5.458	1.918	0.843	0.820	0.401	0.154
pileup	low	0.926	0.262	0.028	-0.023	-0.021	0.007	0.002
	high	0.111	-0.529	0.012	-0.032	-0.028	0.004	-0.003
	Σ	0.000	0.000	0.000	0.000	0.000	0.000	0.000
cent. cut	–1	-2.822	-1.312	0.901	0.948	1.018	0.701	0.862
	+1	1.023	1.167	0.016	-0.700	-0.966	-1.063	-0.770
	Σ	2.822	1.239	0.000	0.824	0.992	0.882	0.816

Table B.49: Systematic uncertainty contributions for C_5 at $\sqrt{s_{NN}} = 3.9$ GeV

$\sqrt{s_{NN}} = 3.9$ GeV, C_5 Systematic Uncertainties								
		0-5%	5-10%	10-20%	20-30%	30-40%	40-50%	50-60%
C_5	value	-257.09	-110.80	76.805	74.400	53.501	28.669	17.847
	stat.	102.749	79.107	33.405	15.473	5.959	1.885	1.101
	sys.	31.773	67.525	13.359	18.346	9.161	5.183	3.828
nHitsFit	≥ 22	2.560	12.538	0.296	-1.598	-0.693	-0.383	-0.262
	≥ 25	-6.114	19.578	2.050	-5.589	0.297	-0.276	-0.031
	Σ	0.000	19.578	0.000	5.589	0.000	0.000	0.000
Efficiency	–5%	66.931	45.290	-9.247	-10.522	-7.581	-3.798	-2.556
	+5%	-51.331	-33.037	7.609	8.594	6.231	3.156	2.098
	Σ	0.000	0.000	0.000	0.000	6.906	3.477	2.327
m^2 cuts (GeV^2)	[0.7,1.3]	21.196	-11.736	-3.600	-0.333	-0.592	-0.016	-0.029
	[0.6,1.1]	-13.750	21.653	1.046	0.303	1.624	0.081	0.020
	Σ	13.750	16.695	0.000	0.000	0.592	0.000	0.000
DCA (cm)	<0.9	-22.369	-0.295	-6.263	-6.560	-1.700	-0.173	1.298
	<1.1	-1.281	-17.101	12.676	-0.626	-3.775	-1.532	-0.892
	Σ	0.000	0.000	12.676	6.560	2.737	1.532	1.095
$\lvert n\sigma_p \rvert$	2.75	16.260	8.559	-4.216	0.713	-0.984	0.215	-0.207
	2.5	-13.267	25.852	-3.677	1.873	-1.652	0.015	-0.381
	Σ	0.000	25.852	4.216	0.000	1.318	0.000	0.294
nHitsDedx	≥ 22	28.644	53.952	-2.514	0.455	2.006	0.673	0.966
	≥ 25	-17.825	30.996	-6.330	-15.073	5.224	2.365	1.987
	Σ	28.644	42.474	0.000	15.073	3.615	1.519	1.477
pileup	low	2.256	2.876	-0.259	-0.232	0.034	-0.023	0.000
	high	-4.383	-6.834	-0.944	0.103	-0.140	-0.006	-0.014
	Σ	0.000	0.000	0.000	0.000	0.000	0.000	0.000
cent. cut	–1	-8.923	-39.253	6.737	5.926	2.325	0.205	2.571
	+1	2.296	36.252	-1.092	-1.368	-3.686	-3.180	-2.234
	Σ	0.000	37.753	0.000	5.926	3.686	3.180	2.403

Table B.50: Systematic uncertainty contributions for C_6 at $\sqrt{s_{NN}} = 3.9$ GeV

$\sqrt{s_{NN}} = 3.9$ GeV, C_6 Systematic Uncertainties								
		0-5%	5-10%	10-20%	20-30%	30-40%	40-50%	50-60%
C_6	value	-794.39	-3650.0	634.636	399.993	183.447	78.311	57.185
	stat.	1669.997	1243.975	559.279	318.616	77.575	21.902	9.986
	sys.	1507.677	1878.498	468.897	386.380	72.085	12.104	22.309
nHitsFit	≥ 22	-6.604	243.379	-14.413	-17.210	-5.434	-0.823	-1.113
	≥ 25	141.716	107.724	76.532	-86.577	15.961	0.251	1.564
	Σ	0.000	0.000	0.000	86.577	0.000	0.000	0.000
Efficiency	–5%	40.365	1165.116	-187.20	-98.846	-33.288	-11.382	-9.585
	+5%	-62.082	-846.19	135.397	73.878	26.464	9.465	7.776
	Σ	0.000	1005.655	0.000	0.000	0.000	0.000	8.681
m^2 cuts (GeV^2)	[0.7,1.3]	265.841	-42.208	-49.950	22.973	-2.792	0.330	-0.074
	[0.6,1.1]	-239.16	506.212	-39.182	7.802	30.791	-0.090	0.327
	Σ	252.501	506.212	49.950	0.000	30.791	0.000	0.000
DCA (cm)	<0.9	-807.40	-920.47	310.446	-103.64	-13.465	2.155	13.728
	<1.1	586.877	-449.88	55.257	59.334	-30.582	-14.433	-4.301
	Σ	807.399	920.467	310.446	103.64	30.582	0.000	9.014
$\lvert n\sigma_p \rvert$	2.75	441.001	165.716	-63.327	25.519	-3.206	3.523	-1.306
	2.5	67.020	277.169	-93.662	24.449	-11.575	0.900	-3.220
	Σ	441.001	0.000	0.000	0.000	11.575	3.523	3.220
nHitsDedx	≥ 22	1167.458	886.248	306.824	-41.909	22.486	3.679	10.267
	≥ 25	393.826	64.865	-58.859	-353.51	60.675	13.268	18.367
	Σ	1167.458	886.248	306.824	353.505	41.580	3.679	14.317
pileup	low	47.825	110.777	24.954	-0.183	0.026	-0.498	-0.057
	high	-5.628	-68.922	-17.257	2.287	1.380	-0.318	0.010
	Σ	0.000	0.000	0.000	0.000	0.000	0.000	0.000
cent. cut	–1	391.973	-905.85	99.974	78.020	-0.510	-10.980	7.891
	+1	-84.276	679.672	-163.87	8.582	-38.080	-1.575	-14.535
	Σ	0.000	792.760	163.865	78.020	38.080	10.980	11.213

Table B.51: Systematic uncertainty contributions for C_2/C_1 at $\sqrt{s_{NN}} = 3.9$ GeV

$\sqrt{s_{NN}} = 3.9$ GeV, C_2/C_1 Systematic Uncertainties								
		0-5%	5-10%	10-20%	20-30%	30-40%	40-50%	50-60%
C_2/C_1	value	1.075	1.170	1.187	1.202	1.207	1.199	1.183
	stat.	0.001	0.002	0.001	0.001	0.001	0.001	0.001
	sys.	0.006	0.009	0.010	0.010	0.011	0.010	0.010
nHitsFit	≥ 22	-0.000	-0.000	-0.001	-0.001	-0.001	-0.001	-0.001
	≥ 25	-0.000	-0.000	-0.001	-0.001	-0.001	-0.000	-0.001
	Σ	0.000	0.000	0.001	0.001	0.001	0.001	0.001
Efficiency	–5%	-0.004	-0.009	-0.010	-0.011	-0.011	-0.010	-0.010
	+5%	0.004	0.008	0.009	0.010	0.010	0.009	0.009
	Σ	0.004	0.009	0.009	0.010	0.010	0.010	0.009
m^2 cuts (GeV^2)	[0.7,1.3]	0.000	0.000	0.000	0.000	0.000	0.000	-0.000
	[0.6,1.1]	-0.000	-0.000	-0.000	-0.000	-0.000	-0.000	-0.000
	Σ	0.000	0.000	0.000	0.000	0.000	0.000	0.000
DCA (cm)	<0.9	-0.001	0.000	0.000	0.000	0.001	0.001	0.001
	<1.1	-0.001	-0.002	-0.002	-0.003	-0.002	-0.002	-0.003
	Σ	0.001	0.002	0.002	0.001	0.002	0.002	0.002
$\lvert n\sigma_p \rvert$	2.75	0.000	0.001	0.001	0.001	0.000	0.000	0.000
	2.5	0.001	0.002	0.002	0.002	0.001	0.001	0.001
	Σ	0.001	0.002	0.001	0.001	0.001	0.001	0.001
nHitsDedx	≥ 22	0.000	0.001	0.001	0.000	0.000	0.000	-0.000
	≥ 25	-0.000	0.003	0.003	0.001	0.002	0.002	0.001
	Σ	0.000	0.002	0.002	0.001	0.002	0.002	0.000
pileup	low	-0.000	0.000	0.000	0.000	-0.000	-0.000	0.000
	high	-0.000	-0.000	0.000	-0.000	0.000	-0.000	-0.000
	Σ	0.000	0.000	0.000	0.000	0.000	0.000	0.000
cent. cut	–1	-0.004	-0.002	-0.001	-0.001	0.000	0.002	0.004
	+1	0.005	0.001	0.001	0.001	-0.000	-0.001	-0.003
	Σ	0.004	0.001	0.001	0.001	0.000	0.002	0.004

Table B.52: Systematic uncertainty contributions for C_3/C_1 at $\sqrt{s_{NN}} = 3.9$ GeV

$\sqrt{s_{NN}} = 3.9$ GeV, C_3/C_1 Systematic Uncertainties								
		0-5%	5-10%	10-20%	20-30%	30-40%	40-50%	50-60%
C_3/C_1	value	1.100	1.533	1.618	1.684	1.728	1.702	1.652
	stat.	0.017	0.019	0.012	0.009	0.009	0.006	0.007
	sys.	0.018	0.038	0.037	0.041	0.045	0.042	0.042
nHitsFit	≥ 22	0.001	0.000	-0.001	-0.003	-0.003	-0.004	-0.003
	≥ 25	0.005	-0.006	-0.005	-0.004	-0.002	-0.002	-0.005
	Σ	0.005	0.006	0.005	0.003	0.003	0.003	0.004
Efficiency	–5%	0.002	-0.029	-0.036	-0.040	-0.044	-0.043	-0.040
	+5%	-0.001	0.026	0.032	0.036	0.039	0.038	0.036
	Σ	0.000	0.028	0.034	0.038	0.042	0.040	0.038
m^2 cuts (GeV^2)	[0.7,1.3]	0.002	0.001	0.000	0.001	0.000	-0.000	-0.000
	[0.6,1.1]	-0.001	-0.001	-0.002	-0.000	-0.000	0.000	-0.001
	Σ	0.000	0.001	0.000	0.000	0.000	0.000	0.000
DCA (cm)	<0.9	-0.011	0.006	-0.002	0.002	0.005	0.004	0.005
	<1.1	0.004	-0.016	-0.010	-0.008	-0.007	-0.008	-0.013
	Σ	0.011	0.011	0.006	0.008	0.006	0.006	0.009
$\lvert n\sigma_p \rvert$	2.75	-0.000	0.004	0.003	0.001	0.001	0.001	0.000
	2.5	-0.002	0.014	0.009	0.005	0.004	0.004	0.003
	Σ	0.000	0.009	0.006	0.005	0.004	0.003	0.003
nHitsDedx	≥ 22	0.002	-0.000	0.002	0.006	0.002	0.002	0.002
	≥ 25	-0.002	0.013	0.009	0.010	0.014	0.008	0.006
	Σ	0.000	0.013	0.009	0.008	0.014	0.008	0.006
pileup	low	0.001	0.000	0.001	0.000	-0.001	0.000	0.000
	high	-0.002	-0.001	0.000	-0.001	-0.000	0.000	-0.000
	Σ	0.000	0.000	0.000	0.000	0.000	0.000	0.000
cent. cut	–1	-0.015	-0.020	0.003	-0.007	0.003	0.005	0.016
	+1	0.012	0.014	0.006	0.004	-0.002	-0.006	-0.011
	Σ	0.014	0.017	0.006	0.005	0.003	0.005	0.013

Table B.53: Systematic uncertainty contributions for C_4/C_2 at $\sqrt{s_{NN}} = 3.9$ GeV

$\sqrt{s_{NN}} = 3.9$ GeV, C_4/C_2 Systematic Uncertainties								
		0-5%	5-10%	10-20%	20-30%	30-40%	40-50%	50-60%
C_4/C_2	value	0.210	1.726	2.074	2.425	2.657	2.575	2.556
	stat.	0.235	0.193	0.121	0.079	0.068	0.039	0.042
	sys.	0.166	0.239	0.091	0.110	0.127	0.119	0.133
nHitsFit	≥ 22	0.004	0.021	0.007	-0.006	-0.006	-0.012	-0.009
	≥ 25	-0.024	0.011	-0.021	-0.009	-0.005	-0.010	-0.011
	Σ	0.000	0.000	0.000	0.006	0.000	0.011	0.010
Efficiency	–5%	0.135	-0.009	-0.045	-0.086	-0.112	-0.104	-0.109
	+5%	-0.112	0.012	0.042	0.077	0.099	0.092	0.096
	Σ	0.123	0.000	0.000	0.082	0.105	0.098	0.103
m^2 cuts (GeV^2)	[0.7,1.3]	0.053	-0.029	-0.008	0.003	-0.004	-0.001	-0.001
	[0.6,1.1]	0.005	0.017	-0.010	0.004	0.006	0.002	-0.001
	Σ	0.053	0.000	0.000	0.000	0.000	0.000	0.000
DCA (cm)	<0.9	-0.030	0.058	-0.018	-0.008	-0.011	-0.005	0.035
	<1.1	-0.022	-0.131	0.030	-0.010	-0.028	-0.023	-0.037
	Σ	0.000	0.095	0.030	0.000	0.019	0.023	0.036
$\lvert n\sigma_p \rvert$	2.75	0.007	0.047	-0.003	-0.000	-0.009	0.002	-0.008
	2.5	-0.010	0.095	0.012	0.017	-0.008	0.004	-0.010
	Σ	0.000	0.071	0.000	0.017	0.009	0.000	0.009
nHitsDedx	≥ 22	-0.033	0.168	-0.103	0.072	0.017	0.011	0.030
	≥ 25	-0.100	0.223	-0.050	0.026	0.067	0.050	0.053
	Σ	0.000	0.195	0.077	0.072	0.067	0.050	0.042
pileup	low	0.032	0.010	0.001	-0.002	-0.002	0.002	0.000
	high	0.004	-0.020	0.000	-0.003	-0.004	0.001	-0.001
	Σ	0.000	0.000	0.000	0.000	0.000	0.000	0.000
cent. cut	–1	-0.097	-0.073	0.008	0.006	0.010	-0.031	0.062
	+1	0.035	0.067	0.038	0.012	-0.002	-0.042	-0.010
	Σ	0.097	0.070	0.038	0.000	0.000	0.037	0.062

Table B.54: Systematic uncertainty contributions for C_5/C_1 at $\sqrt{s_{NN}} = 3.9$ GeV

$\sqrt{s_{NN}} = 3.9$ GeV, C_5/C_1 Systematic Uncertainties								
		0-5%	5-10%	10-20%	20-30%	30-40%	40-50%	50-60%
C_5/C_1	value	-9.414	-5.011	4.729	7.060	8.128	7.278	7.719
	stat.	3.763	3.577	2.057	1.469	0.905	0.478	0.475
	sys.	0.935	3.055	0.689	1.805	0.923	0.727	0.982
nHitsFit	≥ 22	0.044	0.537	0.045	-0.108	-0.053	-0.048	-0.059
	≥ 25	-0.248	0.871	0.138	-0.513	0.063	-0.054	0.001
	Σ	0.000	0.871	0.000	0.513	0.000	0.000	0.000
Efficiency	–5%	1.858	1.695	-0.304	-0.596	-0.688	-0.552	-0.664
	+5%	-1.503	-1.318	0.255	0.503	0.588	0.477	0.567
	Σ	0.000	0.000	0.000	0.000	0.638	0.515	0.616
m^2 cuts (GeV^2)	[0.7,1.3]	0.778	-0.530	-0.222	-0.031	-0.088	-0.002	-0.010
	[0.6,1.1]	-0.507	0.978	0.065	0.029	0.246	0.020	0.006
	Σ	0.507	0.754	0.000	0.000	0.088	0.000	0.000
DCA (cm)	<0.9	-0.740	0.033	-0.432	-0.691	-0.332	-0.109	0.501
	<1.1	-0.192	-0.840	0.844	0.059	-0.423	-0.252	-0.238
	Σ	0.000	0.000	0.638	0.691	0.378	0.000	0.370
$\lvert n\sigma_p \rvert$	2.75	0.599	0.388	-0.259	0.069	-0.145	0.059	-0.083
	2.5	-0.457	1.187	-0.238	0.166	-0.261	-0.001	-0.168
	Σ	0.000	1.187	0.259	0.000	0.203	0.000	0.126
nHitsDedx	≥ 22	1.070	2.451	-0.159	0.041	0.306	0.174	0.423
	≥ 25	-0.502	1.504	-0.464	-1.543	0.701	0.518	0.775
	Σ	0.786	1.977	0.000	1.543	0.503	0.346	0.599
pileup	low	0.084	0.130	-0.016	-0.022	0.005	-0.006	-0.001
	high	-0.161	-0.309	-0.058	0.009	-0.022	-0.001	-0.006
	Σ	0.000	0.000	0.000	0.000	0.000	0.000	0.000
cent. cut	–1	-0.272	-1.730	0.331	0.368	-0.007	-0.470	0.389
	+1	0.029	1.549	0.023	0.073	-0.189	-0.288	-0.158
	Σ	0.000	1.640	0.000	0.368	0.000	0.379	0.273

Table B.55: Systematic uncertainty contributions for C_6/C_2 at $\sqrt{s_{NN}} = 3.9$ GeV

$\sqrt{s_{NN}} = 3.9$ GeV, C_6/C_2 Systematic Uncertainties								
		0-5%	5-10%	10-20%	20-30%	30-40%	40-50%	50-60%
C_6/C_2	value	-27.047	-141.07	32.928	31.573	23.088	16.575	20.906
	stat.	56.846	48.047	29.019	25.149	9.764	4.635	3.645
	sys.	51.450	60.093	23.959	31.208	7.963	3.880	6.692
nHitsFit	≥ 22	-0.370	8.538	-0.542	-1.141	-0.519	-0.049	-0.243
	≥ 25	4.736	3.756	4.063	-6.716	2.066	0.093	0.625
	Σ	0.000	0.000	0.000	6.716	0.000	0.000	0.000
Efficiency	–5%	-0.146	34.384	-7.248	-5.505	-2.594	-1.303	-2.096
	+5%	-0.779	-26.494	5.525	4.326	2.172	1.153	1.799
	Σ	0.000	0.000	0.000	0.000	0.000	0.000	0.000
m^2 cuts (GeV^2)	[0.7,1.3]	9.069	-1.601	-2.600	1.812	-0.348	0.074	-0.020
	[0.6,1.1]	-8.156	19.505	-2.021	0.619	3.876	-0.020	0.117
	Σ	8.612	19.505	2.600	0.000	3.876	0.000	0.000
DCA (cm)	<0.9	-27.494	-34.596	15.954	-8.543	-1.932	0.297	4.870
	<1.1	19.232	-19.572	3.402	5.189	-3.331	-2.669	-1.106
	Σ	27.494	34.596	15.954	8.543	2.632	0.000	2.988
$\lvert n\sigma_p \rvert$	2.75	15.037	6.526	-3.308	2.006	-0.401	0.753	-0.467
	2.5	2.405	11.457	-5.012	1.835	-1.516	0.161	-1.206
	Σ	15.037	0.000	0.000	0.000	1.516	0.753	1.206
nHitsDedx	≥ 22	39.886	34.614	15.895	-3.322	2.826	0.785	3.768
	≥ 25	14.096	5.219	-3.668	-28.749	7.420	2.619	6.533
	Σ	39.886	34.614	15.895	28.749	5.123	0.785	5.151
pileup	low	1.628	4.283	1.295	-0.015	0.005	-0.105	-0.023
	high	-0.194	-2.661	-0.897	0.179	0.172	-0.065	0.005
	Σ	0.000	0.000	0.000	0.000	0.000	0.000	0.000
cent. cut	–1	13.434	-33.688	4.660	5.414	-1.142	-3.725	0.849
	+1	-2.907	24.127	-7.751	1.518	-3.594	0.771	-2.806
	Σ	0.000	28.908	7.751	5.414	3.594	3.725	2.806

Table B.56: Systematic uncertainty contributions for κ_1 at $\sqrt{s_{NN}} = 3.9$ GeV

$\sqrt{s_{NN}} = 3.9$ GeV, κ_1 Systematic Uncertainties								
		0-5%	5-10%	10-20%	20-30%	30-40%	40-50%	50-60%
κ_1	value	27.310	22.113	16.243	10.538	6.582	3.939	2.312
	stat.	0.005	0.004	0.002	0.002	0.001	0.001	0.001
	sys.	1.448	1.202	0.906	0.631	0.452	0.338	0.262
nHitsFit	≥ 22	-0.145	-0.121	-0.093	-0.064	-0.042	-0.027	-0.016
	≥ 25	-0.070	-0.056	-0.040	-0.025	-0.015	-0.008	-0.004
	Σ	0.108	0.088	0.067	0.044	0.029	0.017	0.010
Efficiency	–5%	-1.437	-1.164	-0.855	-0.555	-0.346	-0.207	-0.122
	+5%	1.300	1.053	0.773	0.502	0.313	0.188	0.110
	Σ	1.369	1.108	0.814	0.528	0.330	0.197	0.116
m^2 cuts (GeV^2)	[0.7,1.3]	0.006	0.003	0.000	-0.001	-0.001	-0.001	-0.001
	[0.6,1.1]	-0.010	-0.005	-0.003	-0.000	0.000	0.001	0.001
	Σ	0.008	0.004	0.003	0.001	0.001	0.001	0.001
DCA (cm)	<0.9	0.250	0.202	0.146	0.093	0.058	0.035	0.019
	<1.1	-0.429	-0.355	-0.266	-0.179	-0.116	-0.072	-0.043
	Σ	0.339	0.279	0.206	0.136	0.087	0.053	0.031
$\lvert n\sigma_p \rvert$	2.75	0.010	0.004	-0.000	-0.003	-0.003	-0.003	-0.002
	2.5	0.087	0.062	0.037	0.018	0.008	0.003	0.001
	Σ	0.048	0.033	0.019	0.010	0.005	0.003	0.001
nHitsDedx	≥ 22	0.054	0.033	0.015	0.003	-0.001	-0.002	-0.002
	≥ 25	0.462	0.346	0.233	0.138	0.083	0.048	0.028
	Σ	0.258	0.190	0.124	0.071	0.042	0.025	0.015
pileup	low	0.004	-0.002	-0.001	-0.001	-0.000	0.000	0.000
	high	-0.000	0.001	0.000	0.001	0.000	-0.000	-0.000
	Σ	0.004	0.000	0.000	0.001	0.000	0.000	0.000
cent. cut	–1	0.163	0.306	0.310	0.306	0.292	0.266	0.228
	+1	-0.160	-0.304	-0.310	-0.305	-0.293	-0.270	-0.237
	Σ	0.162	0.305	0.310	0.306	0.293	0.268	0.233

Table B.57: Systematic uncertainty contributions for κ_2 at $\sqrt{s_{NN}} = 3.9$ GeV

$\sqrt{s_{NN}} = 3.9$ GeV, κ_2 Systematic Uncertainties								
		0-5%	5-10%	10-20%	20-30%	30-40%	40-50%	50-60%
κ_2	value	2.060	3.761	3.031	2.131	1.363	0.785	0.423
	stat.	0.039	0.040	0.017	0.010	0.007	0.003	0.003
	sys.	0.240	0.397	0.320	0.229	0.156	0.102	0.068
nHitsFit	≥ 22	-0.015	-0.030	-0.026	-0.020	-0.014	-0.009	-0.005
	≥ 25	-0.012	-0.017	-0.022	-0.014	-0.007	-0.003	-0.003
	Σ	0.015	0.023	0.024	0.017	0.010	0.006	0.004
Efficiency	–5%	-0.223	-0.406	-0.327	-0.230	-0.147	-0.085	-0.046
	+5%	0.192	0.350	0.282	0.198	0.127	0.073	0.039
	Σ	0.207	0.378	0.305	0.214	0.137	0.079	0.043
m^2 cuts (GeV^2)	[0.7,1.3]	0.008	0.003	0.004	0.001	0.000	-0.000	-0.000
	[0.6,1.1]	-0.010	-0.004	-0.004	-0.001	-0.001	-0.000	-0.000
	Σ	0.009	0.000	0.004	0.001	0.000	0.000	0.000
DCA (cm)	<0.9	-0.006	0.036	0.027	0.022	0.018	0.011	0.006
	<1.1	-0.048	-0.110	-0.083	-0.064	-0.040	-0.023	-0.015
	Σ	0.027	0.073	0.055	0.043	0.029	0.017	0.011
$\lvert n\sigma_p \rvert$	2.75	0.006	0.017	0.012	0.006	0.002	0.001	0.000
	2.5	0.036	0.064	0.041	0.022	0.011	0.006	0.003
	Σ	0.036	0.041	0.027	0.014	0.007	0.003	0.003
nHitsDedx	≥ 22	0.006	0.020	0.013	0.002	0.002	-0.000	-0.001
	≥ 25	0.029	0.134	0.090	0.039	0.027	0.016	0.006
	Σ	0.029	0.077	0.052	0.039	0.027	0.016	0.006
pileup	low	-0.004	0.002	0.001	0.001	-0.000	-0.000	0.000
	high	-0.002	-0.000	0.001	0.000	0.000	-0.000	-0.000
	Σ	0.000	0.000	0.000	0.000	0.000	0.000	0.000
cent. cut	–1	-0.100	0.013	0.050	0.055	0.062	0.060	0.050
	+1	0.114	-0.031	-0.046	-0.049	-0.064	-0.060	-0.052
	Σ	0.107	0.031	0.048	0.052	0.063	0.060	0.051

Table B.58: Systematic uncertainty contributions for κ_3 at $\sqrt{s_{NN}} = 3.9$ GeV

$\sqrt{s_{NN}} = 3.9$ GeV, κ_3 Systematic Uncertainties								
		0-5%	5-10%	10-20%	20-30%	30-40%	40-50%	50-60%
κ_3	value	-3.447	0.501	0.952	0.820	0.701	0.407	0.237
	stat.	0.426	0.384	0.171	0.088	0.049	0.019	0.011
	sys.	0.612	0.370	0.183	0.147	0.136	0.073	0.049
nHitsFit	≥ 22	0.070	0.035	0.002	-0.012	-0.008	-0.008	-0.003
	≥ 25	0.164	-0.117	-0.034	-0.013	-0.006	-0.003	-0.006
	Σ	0.164	0.076	0.034	0.013	0.008	0.008	0.004
Efficiency	–5%	0.573	-0.083	-0.158	-0.136	-0.117	-0.068	-0.039
	+5%	-0.469	0.068	0.130	0.112	0.095	0.055	0.032
	Σ	0.521	0.000	0.144	0.124	0.106	0.062	0.036
m^2 cuts (GeV^2)	[0.7,1.3]	0.033	0.024	-0.006	0.009	-0.001	-0.001	-0.000
	[0.6,1.1]	-0.010	-0.022	-0.020	0.001	0.002	0.001	-0.000
	Σ	0.000	0.000	0.000	0.000	0.000	0.000	0.000
DCA (cm)	<0.9	-0.248	0.126	-0.021	0.021	0.021	0.005	0.007
	<1.1	0.213	-0.210	-0.071	-0.021	-0.015	-0.014	-0.014
	Σ	0.230	0.168	0.071	0.021	0.018	0.014	0.011
$\lvert n\sigma_p \rvert$	2.75	-0.016	0.042	0.011	-0.010	-0.005	0.001	-0.002
	2.5	-0.151	0.155	0.051	-0.005	-0.002	0.002	-0.002
	Σ	0.151	0.155	0.051	0.000	0.000	0.000	0.002
nHitsDedx	≥ 22	0.056	-0.045	-0.001	0.063	0.006	0.008	0.006
	≥ 25	-0.085	0.066	0.014	0.083	0.072	0.018	0.012
	Σ	0.000	0.045	0.000	0.073	0.072	0.018	0.009
pileup	low	0.039	0.002	0.009	0.001	-0.004	0.002	0.000
	high	-0.044	-0.015	0.000	-0.008	-0.002	0.001	-0.000
	Σ	0.000	0.000	0.000	0.000	0.000	0.000	0.000
cent. cut	–1	-0.091	-0.311	0.086	-0.024	0.043	0.023	0.034
	+1	-0.017	0.242	0.041	-0.016	-0.038	-0.037	-0.026
	Σ	0.000	0.277	0.064	0.016	0.041	0.030	0.030

Table B.59: Systematic uncertainty contributions for κ_4 at $\sqrt{s_{NN}} = 3.9$ GeV

$\sqrt{s_{NN}} = 3.9$ GeV, κ_4 Systematic Uncertainties

		0-5%	5-10%	10-20%	20-30%	30-40%	40-50%	50-60%
κ_4	value	-14.876	-6.780	-3.196	0.356	0.782	0.284	0.293
	stat.	6.092	3.839	1.963	0.816	0.335	0.114	0.066
	sys.	3.415	4.977	1.985	0.691	0.192	0.198	0.129
nHitsFit	≥ 22	-0.098	0.409	0.157	-0.002	-0.012	-0.010	-0.007
	≥ 25	-1.562	1.028	-0.131	-0.002	-0.000	-0.027	0.008
	Σ	1.562	1.028	0.000	0.000	0.000	0.027	0.000
Efficiency	–5%	3.388	1.544	0.728	-0.081	-0.178	-0.065	-0.067
	+5%	-2.638	-1.202	-0.567	0.063	0.139	0.050	0.052
	Σ	0.000	0.000	0.000	0.000	0.000	0.000	0.059
m^2 cuts (GeV^2)	[0.7,1.3]	1.295	-0.898	-0.136	-0.029	-0.028	0.004	-0.002
	[0.6,1.1]	0.286	0.592	-0.051	0.049	0.041	0.005	0.000
	Σ	0.790	0.592	0.000	0.000	0.000	0.000	0.000
DCA (cm)	<0.9	0.469	0.692	-0.190	-0.191	-0.191	-0.051	0.056
	<1.1	-1.281	-1.871	1.135	0.041	-0.153	-0.036	-0.018
	Σ	0.000	0.692	1.135	0.191	0.172	0.051	0.037
$\lvert n\sigma_p \rvert$	2.75	0.251	0.885	-0.190	0.025	-0.056	0.001	-0.015
	2.5	0.304	1.222	-0.241	0.170	-0.086	-0.011	-0.029
	Σ	0.000	1.054	0.000	0.000	0.086	0.000	0.022
nHitsDedx	≥ 22	-1.388	4.526	-2.022	0.528	0.086	0.003	0.045
	≥ 25	-2.932	4.808	-1.235	-0.148	0.112	0.130	0.085
	Σ	2.932	4.667	1.628	0.528	0.000	0.130	0.065
pileup	low	0.716	0.234	-0.029	-0.035	0.008	-0.002	-0.000
	high	0.390	-0.435	0.006	0.012	-0.019	0.001	-0.001
	Σ	0.000	0.000	0.000	0.000	0.000	0.000	0.000
cent. cut	–1	-1.741	0.159	-0.274	0.403	0.034	-0.123	0.083
	+1	0.481	0.236	0.399	0.047	0.001	-0.154	-0.016
	Σ	0.000	0.000	0.000	0.403	0.000	0.138	0.083

Table B.60: Systematic uncertainty contributions for κ_5 at $\sqrt{s_{NN}} = 3.9$ GeV

$\sqrt{s_{NN}} = 3.9$ GeV, κ_5 Systematic Uncertainties								
		0-5%	5-10%	10-20%	20-30%	30-40%	40-50%	50-60%
κ_5	value	-80.352	-134.05	23.261	7.849	1.127	-0.083	0.324
	stat.	72.770	64.175	23.000	10.282	2.898	0.992	0.361
	sys.	50.814	42.842	18.514	13.659	2.775	0.663	0.825
nHitsFit	≥ 22	2.161	8.138	-0.857	-0.908	-0.130	0.077	-0.017
	≥ 25	5.658	12.541	4.581	-5.000	0.563	0.127	0.079
	Σ	0.000	12.541	0.000	5.000	0.000	0.000	0.000
Efficiency	–5%	23.491	39.191	-6.800	-2.295	-0.330	0.024	-0.095
	+5%	-17.394	-29.019	5.035	1.699	0.244	-0.018	0.070
	Σ	0.000	0.000	0.000	0.000	0.000	0.000	0.000
m^2 cuts (GeV^2)	[0.7,1.3]	7.298	-3.394	-2.148	-0.295	-0.284	-0.018	0.001
	[0.6,1.1]	-16.196	16.359	2.129	-0.182	1.175	0.008	0.026
	Σ	16.196	16.359	0.000	0.000	1.175	0.000	0.000
DCA (cm)	<0.9	-21.014	-11.101	-4.400	-5.601	-0.638	-0.003	0.454
	<1.1	7.357	8.866	4.625	0.637	-1.160	-0.397	-0.088
	Σ	21.014	0.000	0.000	5.601	1.160	0.000	0.454
$\lvert n\sigma_p \rvert$	2.75	14.050	-1.608	-2.773	0.624	-0.327	0.186	-0.018
	2.5	-13.171	8.720	-3.188	-0.058	-0.916	-0.006	-0.094
	Σ	14.050	0.000	3.188	0.000	0.916	0.186	0.094
nHitsDedx	≥ 22	40.997	9.476	17.506	-6.434	0.957	0.457	0.372
	≥ 25	12.730	-21.077	4.072	-16.386	1.799	0.319	0.704
	Σ	40.997	21.077	17.506	11.410	1.378	0.457	0.538
pileup	low	-5.824	0.447	-0.202	0.078	0.065	-0.045	-0.004
	high	-7.151	-2.097	-1.016	0.170	0.092	-0.034	0.005
	Σ	0.000	0.000	0.000	0.000	0.000	0.000	0.000
cent. cut	–1	12.094	-33.567	6.261	1.367	-0.314	-0.303	-0.080
	+1	-3.655	28.604	-5.113	-0.395	-1.496	0.443	-0.420
	Σ	0.000	31.085	5.113	0.000	1.496	0.443	0.420

Table B.61: Systematic uncertainty contributions for κ_6 at $\sqrt{s_{NN}} = 3.9$ GeV

$\sqrt{s_{NN}} = 3.9$ GeV, κ_6 Systematic Uncertainties								
		0-5%	5-10%	10-20%	20-30%	30-40%	40-50%	50-60%
κ_6	value	1596.935	-1382.3	297.608	108.763	3.789	-3.895	-3.515
	stat.	1594.151	729.693	303.792	165.591	28.210	5.738	1.567
	sys.	810.444	1027.330	432.319	0.000	23.650	9.440	3.392
nHitsFit	≥ 22	-38.315	92.610	-11.109	-1.679	-1.538	-0.296	0.072
	≥ 25	144.060	-136.07	20.144	-9.785	8.288	0.482	0.486
	Σ	0.000	136.071	0.000	0.000	0.000	0.000	0.000
Efficiency	–5%	-575.49	498.145	-107.25	-39.196	-1.366	1.404	1.267
	+5%	405.277	-350.81	75.528	27.602	0.962	-0.989	-0.892
	Σ	0.000	0.000	0.000	0.000	0.000	0.000	0.000
m^2 cuts (GeV^2)	[0.7,1.3]	69.005	64.836	-8.446	28.399	3.399	0.465	0.066
	[0.6,1.1]	-13.569	224.492	-65.840	7.354	10.341	-0.615	-0.051
	Σ	0.000	0.000	65.840	0.000	10.341	0.000	0.000
DCA (cm)	<0.9	-500.40	-811.58	389.665	-9.896	6.016	4.636	2.436
	<1.1	542.568	-438.59	-78.619	51.217	-0.557	-4.061	-0.026
	Σ	500.398	811.575	389.665	0.000	6.016	4.348	2.436
$\lvert n\sigma_p \rvert$	2.75	215.163	127.967	-10.744	15.261	5.734	0.607	0.079
	2.5	257.182	50.882	-36.041	14.005	7.580	1.383	0.128
	Σ	0.000	127.967	0.000	0.000	7.580	1.383	0.000
nHitsDedx	≥ 22	637.511	453.299	175.287	14.550	1.895	-4.040	1.227
	≥ 25	399.775	58.109	-43.988	-106.87	18.940	-2.150	0.933
	Σ	637.511	453.299	175.287	0.000	18.940	4.040	1.080
pileup	low	85.245	88.597	29.028	0.798	-1.089	0.145	0.004
	high	80.314	-7.823	-2.426	-0.376	1.389	0.041	0.028
	Σ	0.000	88.597	0.000	0.000	0.000	0.000	0.000
cent. cut	–1	334.842	-385.40	14.226	31.455	-4.097	-2.613	-1.136
	+1	-62.601	214.712	-115.07	14.708	-10.002	7.208	-3.063
	Σ	0.000	385.400	0.000	0.000	0.000	7.208	2.100

Table B.62: Systematic uncertainty contributions for κ_2/κ_1 at $\sqrt{s_{NN}} = 3.9$ GeV

$\sqrt{s_{NN}} = 3.9$ GeV, κ_2/κ_1 Systematic Uncertainties								
		0-5%	5-10%	10-20%	20-30%	30-40%	40-50%	50-60%
κ_2/κ_1	value	0.075	0.170	0.187	0.202	0.207	0.199	0.183
	stat.	0.001	0.002	0.001	0.001	0.001	0.001	0.001
	sys.	0.006	0.009	0.010	0.010	0.011	0.010	0.010
nHitsFit	≥ 22	-0.000	-0.000	-0.001	-0.001	-0.001	-0.001	-0.001
	≥ 25	-0.000	-0.000	-0.001	-0.001	-0.001	-0.000	-0.001
	Σ	0.000	0.000	0.001	0.001	0.001	0.001	0.001
Efficiency	–5%	-0.004	-0.009	-0.010	-0.011	-0.011	-0.010	-0.010
	+5%	0.004	0.008	0.009	0.010	0.010	0.009	0.009
	Σ	0.004	0.009	0.009	0.010	0.010	0.010	0.009
m^2 cuts (GeV^2)	[0.7,1.3]	0.000	0.000	0.000	0.000	0.000	0.000	-0.000
	[0.6,1.1]	-0.000	-0.000	-0.000	-0.000	-0.000	-0.000	-0.000
	Σ	0.000	0.000	0.000	0.000	0.000	0.000	0.000
DCA (cm)	<0.9	-0.001	0.000	0.000	0.000	0.001	0.001	0.001
	<1.1	-0.001	-0.002	-0.002	-0.003	-0.002	-0.002	-0.003
	Σ	0.001	0.002	0.002	0.001	0.002	0.002	0.002
$\lvert n\sigma_p \rvert$	2.75	0.000	0.001	0.001	0.001	0.000	0.000	0.000
	2.5	0.001	0.002	0.002	0.002	0.001	0.001	0.001
	Σ	0.001	0.002	0.001	0.001	0.001	0.001	0.001
nHitsDedx	≥ 22	0.000	0.001	0.001	0.000	0.000	0.000	-0.000
	≥ 25	-0.000	0.003	0.003	0.001	0.002	0.002	0.001
	Σ	0.000	0.002	0.002	0.001	0.002	0.002	0.000
pileup	low	-0.000	0.000	0.000	0.000	-0.000	-0.000	0.000
	high	-0.000	-0.000	0.000	-0.000	0.000	-0.000	-0.000
	Σ	0.000	0.000	0.000	0.000	0.000	0.000	0.000
cent. cut	–1	-0.004	-0.002	-0.001	-0.001	0.000	0.002	0.004
	+1	0.005	0.001	0.001	0.001	-0.000	-0.001	-0.003
	Σ	0.004	0.001	0.001	0.001	0.000	0.002	0.004

Table B.63: Systematic uncertainty contributions for κ_3/κ_1 at $\sqrt{s_{NN}} = 3.9$ GeV

$\sqrt{s_{NN}} = 3.9$ GeV, κ_3/κ_1 Systematic Uncertainties								
		0-5%	5-10%	10-20%	20-30%	30-40%	40-50%	50-60%
κ_3/κ_1	value	-0.126	0.023	0.059	0.078	0.107	0.103	0.103
	stat.	0.016	0.017	0.011	0.008	0.007	0.005	0.005
	sys.	0.016	0.017	0.008	0.011	0.015	0.011	0.012
nHitsFit	≥ 22	0.002	0.002	0.000	-0.001	-0.001	-0.001	-0.001
	≥ 25	0.006	-0.005	-0.002	-0.001	-0.001	-0.001	-0.002
	Σ	0.006	0.005	0.002	0.001	0.000	0.001	0.001
Efficiency	–5%	0.014	-0.002	-0.006	-0.008	-0.012	-0.011	-0.011
	+5%	-0.012	0.002	0.005	0.007	0.010	0.010	0.010
	Σ	0.013	0.000	0.006	0.008	0.011	0.010	0.010
m^2 cuts (GeV^2)	[0.7,1.3]	0.001	0.001	-0.000	0.001	-0.000	-0.000	-0.000
	[0.6,1.1]	-0.000	-0.001	-0.001	0.000	0.000	0.000	-0.000
	Σ	0.000	0.000	0.000	0.000	0.000	0.000	0.000
DCA (cm)	<0.9	-0.008	0.006	-0.002	0.001	0.002	0.000	0.002
	<1.1	0.006	-0.009	-0.003	-0.001	-0.000	-0.002	-0.004
	Σ	0.007	0.007	0.003	0.000	0.002	0.002	0.003
$\lvert n\sigma_p \rvert$	2.75	-0.001	0.002	0.001	-0.001	-0.001	0.000	-0.001
	2.5	-0.005	0.007	0.003	-0.001	-0.000	0.000	-0.001
	Σ	0.005	0.007	0.003	0.000	0.000	0.000	0.001
nHitsDedx	≥ 22	0.002	-0.002	-0.000	0.006	0.001	0.002	0.003
	≥ 25	-0.001	0.003	0.000	0.007	0.010	0.003	0.004
	Σ	0.000	0.002	0.000	0.006	0.010	0.003	0.003
pileup	low	0.001	0.000	0.001	0.000	-0.001	0.000	0.000
	high	-0.002	-0.001	0.000	-0.001	-0.000	0.000	-0.000
	Σ	0.000	0.000	0.000	0.000	0.000	0.000	0.000
cent. cut	–1	-0.003	-0.015	0.004	-0.005	0.002	-0.001	0.005
	+1	-0.001	0.011	0.004	0.001	-0.001	-0.002	-0.000
	Σ	0.000	0.013	0.004	0.005	0.000	0.001	0.005

Table B.64: Systematic uncertainty contributions for κ_4/κ_1 at $\sqrt{s_{NN}} = 3.9$ GeV

$\sqrt{s_{NN}} = 3.9$ GeV, κ_4/κ_1 Systematic Uncertainties								
		0-5%	5-10%	10-20%	20-30%	30-40%	40-50%	50-60%
κ_4/κ_1	value	-0.545	-0.307	-0.197	0.034	0.119	0.072	0.127
	stat.	0.223	0.174	0.121	0.077	0.051	0.029	0.028
	sys.	0.119	0.235	0.119	0.063	0.029	0.050	0.046
nHitsFit	≥ 22	-0.006	0.017	0.009	0.000	-0.001	-0.002	-0.002
	≥ 25	-0.058	0.046	-0.009	-0.000	0.000	-0.007	0.004
	Σ	0.058	0.046	0.000	0.000	0.000	0.007	0.000
Efficiency	–5%	0.091	0.051	0.033	-0.006	-0.020	-0.012	-0.021
	+5%	-0.074	-0.042	-0.027	0.005	0.016	0.010	0.017
	Σ	0.000	0.000	0.000	0.000	0.000	0.000	0.019
m^2 cuts (GeV^2)	[0.7,1.3]	0.048	-0.041	-0.008	-0.003	-0.004	0.001	-0.001
	[0.6,1.1]	0.010	0.027	-0.003	0.005	0.006	0.001	-0.000
	Σ	0.029	0.027	0.000	0.000	0.000	0.000	0.000
DCA (cm)	<0.9	0.022	0.034	-0.010	-0.019	-0.030	-0.014	0.023
	<1.1	-0.055	-0.088	0.066	0.004	-0.021	-0.008	-0.005
	Σ	0.000	0.061	0.066	0.000	0.026	0.014	0.014
$\lvert n\sigma_p \rvert$	2.75	0.009	0.040	-0.012	0.002	-0.008	0.000	-0.006
	2.5	0.013	0.056	-0.014	0.016	-0.013	-0.003	-0.013
	Σ	0.000	0.048	0.000	0.000	0.013	0.000	0.009
nHitsDedx	≥ 22	-0.050	0.205	-0.124	0.050	0.013	0.001	0.019
	≥ 25	-0.100	0.226	-0.074	-0.015	0.016	0.032	0.036
	Σ	0.100	0.216	0.099	0.050	0.000	0.032	0.028
pileup	low	0.026	0.011	-0.002	-0.003	0.001	-0.000	-0.000
	high	0.014	-0.020	0.000	0.001	-0.003	0.000	-0.000
	Σ	0.000	0.000	0.000	0.000	0.000	0.000	0.000
cent. cut	–1	-0.061	0.012	-0.013	0.038	-0.000	-0.039	0.026
	+1	0.014	0.006	0.020	0.005	0.005	-0.032	0.006
	Σ	0.000	0.000	0.000	0.038	0.000	0.035	0.026

Table B.65: Systematic uncertainty contributions for κ_5/κ_1 at $\sqrt{s_{NN}} = 3.9$ GeV

$\sqrt{s_{NN}} = 3.9$ GeV, κ_5/κ_1 Systematic Uncertainties		0-5%	5-10%	10-20%	20-30%	30-40%	40-50%	50-60%
κ_5/κ_1	value	-2.942	-6.062	1.432	0.745	0.171	-0.021	0.140
	stat.	2.665	2.902	1.416	0.976	0.440	0.252	0.156
	sys.	1.860	1.613	1.167	1.313	0.411	0.156	0.344
nHitsFit	≥ 22	0.063	0.333	-0.044	-0.081	-0.019	0.019	-0.006
	≥ 25	0.199	0.550	0.285	-0.472	0.086	0.032	0.034
	Σ	0.000	0.550	0.000	0.472	0.000	0.000	0.000
Efficiency	–5%	0.670	1.381	-0.326	-0.170	-0.039	0.005	-0.032
	+5%	-0.522	-1.075	0.254	0.132	0.030	-0.004	0.025
	Σ	0.000	0.000	0.000	0.000	0.000	0.000	0.000
m^2 cuts (GeV^2)	[0.7,1.3]	0.268	-0.153	-0.132	-0.028	-0.043	-0.005	0.000
	[0.6,1.1]	-0.594	0.738	0.131	-0.017	0.178	0.002	0.011
	Σ	0.594	0.738	0.000	0.000	0.178	0.000	0.000
DCA (cm)	<0.9	-0.749	-0.451	-0.286	-0.543	-0.099	-0.001	0.197
	<1.1	0.220	0.299	0.303	0.072	-0.170	-0.099	-0.035
	Σ	0.749	0.000	0.286	0.543	0.170	0.000	0.197
$\lvert n\sigma_p \rvert$	2.75	0.516	-0.072	-0.171	0.059	-0.050	0.047	-0.008
	2.5	-0.474	0.413	-0.200	-0.007	-0.140	-0.001	-0.041
	Σ	0.516	0.000	0.200	0.000	0.140	0.047	0.041
nHitsDedx	≥ 22	1.510	0.438	1.077	-0.611	0.145	0.116	0.161
	≥ 25	0.525	-0.872	0.234	-1.586	0.275	0.082	0.307
	Σ	1.510	0.000	1.077	1.098	0.210	0.116	0.234
pileup	low	-0.213	0.020	-0.012	0.007	0.010	-0.011	-0.002
	high	-0.262	-0.095	-0.063	0.016	0.014	-0.009	0.002
	Σ	0.000	0.000	0.000	0.000	0.000	0.000	0.000
cent. cut	–1	0.463	-1.454	0.365	0.111	-0.058	-0.081	-0.054
	+1	-0.150	1.194	-0.282	-0.016	-0.210	0.104	-0.152
	Σ	0.000	1.324	0.282	0.000	0.210	0.092	0.152

Table B.66: Systematic uncertainty contributions for κ_6/κ_1 at $\sqrt{s_{NN}} = 3.9$ GeV

$\sqrt{s_{NN}} = 3.9$ GeV, κ_6/κ_1 Systematic Uncertainties								
		0-5%	5-10%	10-20%	20-30%	30-40%	40-50%	50-60%
κ_6/κ_1	value	58.474	-62.511	18.323	10.321	0.576	-0.989	-1.520
	stat.	58.376	33.001	18.702	15.714	4.286	1.457	0.678
	sys.	30.065	40.103	26.660	0.000	3.617	1.930	1.458
nHitsFit	≥ 22	-1.088	3.826	-0.576	-0.096	-0.229	-0.081	0.020
	≥ 25	5.412	-6.296	1.282	-0.902	1.258	0.120	0.207
	Σ	0.000	6.296	0.000	0.000	0.000	0.000	0.000
Efficiency	–5%	-17.095	18.276	-5.357	-3.017	-0.168	0.289	0.445
	+5%	12.658	-13.532	3.966	2.234	0.125	-0.214	-0.329
	Σ	0.000	0.000	0.000	0.000	0.000	0.000	0.000
m^2 cuts (GeV^2)	[0.7,1.3]	2.515	2.941	-0.520	2.696	0.516	0.118	0.028
	[0.6,1.1]	-0.476	10.134	-4.050	0.698	1.571	-0.156	-0.022
	Σ	0.000	0.000	4.050	0.000	1.571	0.000	0.000
DCA (cm)	<0.9	-19.033	-36.464	24.042	-1.039	0.917	1.196	1.075
	<1.1	20.463	-20.509	-4.468	4.951	-0.073	-1.030	-0.039
	Σ	19.033	28.486	24.042	0.000	0.917	1.113	1.075
$\lvert n\sigma_p \rvert$	2.75	7.861	5.801	-0.661	1.450	0.871	0.153	0.033
	2.5	9.261	2.484	-2.265	1.314	1.152	0.352	0.056
	Σ	0.000	5.801	0.000	0.000	1.152	0.352	0.000
nHitsDedx	≥ 22	23.273	20.624	10.785	1.378	0.288	-1.026	0.529
	≥ 25	13.884	3.664	-3.014	-10.414	2.907	-0.540	0.427
	Σ	23.273	20.624	10.785	0.000	2.907	1.026	0.478
pileup	low	3.113	4.000	1.788	0.076	-0.165	0.037	0.002
	high	2.942	-0.351	-0.150	-0.036	0.211	0.010	0.012
	Σ	0.000	4.000	0.000	0.000	0.000	0.000	0.000
cent. cut	–1	11.983	-16.797	0.537	2.766	-0.678	-0.640	-0.379
	+1	-1.938	8.730	-6.609	1.647	-1.430	1.649	-1.343
	Σ	0.000	16.797	0.000	0.000	0.000	1.144	0.861

B.4 Systematic Contributions at $\sqrt{s_{NN}} = 4.5$ GeV

Table B.67: Systematic uncertainty contributions for C_1 at $\sqrt{s_{NN}} = 4.5$ GeV

$\sqrt{s_{NN}} = 4.5$ GeV, C_1 Systematic Uncertainties								
		0-5%	5-10%	10-20%	20-30%	30-40%	40-50%	50-60%
C_1	value	23.219	18.978	14.002	9.233	5.819	3.411	1.873
	stat.	0.006	0.004	0.002	0.002	0.001	0.001	0.001
	sys.	1.436	1.190	0.880	0.597	0.407	0.281	0.201
nHitsFit	≥ 22	-0.092	-0.077	-0.059	-0.041	-0.028	-0.017	-0.010
	≥ 25	0.035	0.032	0.029	0.024	0.019	0.013	0.008
	Σ	0.063	0.054	0.044	0.033	0.023	0.015	0.009
Efficiency	–5%	-1.222	-0.999	-0.737	-0.486	-0.306	-0.180	-0.099
	+5%	1.106	0.904	0.667	0.440	0.277	0.162	0.089
	Σ	1.164	0.951	0.702	0.463	0.292	0.171	0.094
m^2 cuts (GeV^2)	[0.7,1.3]	0.015	0.009	0.004	0.001	-0.001	-0.001	-0.001
	[0.6,1.1]	-0.011	-0.005	-0.002	0.000	0.001	0.001	0.001
	Σ	0.013	0.007	0.003	0.001	0.001	0.001	0.001
DCA (cm)	<0.9	0.519	0.467	0.341	0.218	0.135	0.078	0.042
	<1.1	-0.551	-0.491	-0.366	-0.244	-0.157	-0.093	-0.052
	Σ	0.535	0.479	0.353	0.231	0.146	0.086	0.047
$\lvert n\sigma_p \rvert$	2.75	-0.002	-0.003	-0.005	-0.005	-0.004	-0.003	-0.002
	2.5	0.066	0.050	0.031	0.016	0.007	0.003	0.001
	Σ	0.034	0.026	0.018	0.010	0.006	0.003	0.001
nHitsDedx	≥ 22	0.273	0.203	0.135	0.080	0.047	0.026	0.013
	≥ 25	0.993	0.752	0.514	0.314	0.190	0.109	0.058
	Σ	0.633	0.478	0.325	0.197	0.118	0.067	0.036
pileup	low	0.002	-0.001	-0.001	-0.001	-0.000	0.000	0.000
	high	0.000	0.001	0.000	0.000	0.000	-0.000	-0.000
	Σ	0.000	0.000	0.000	0.000	0.000	0.000	0.000
cent. cut	–1	0.126	0.223	0.224	0.221	0.211	0.193	0.164
	+1	-0.125	-0.220	-0.224	-0.220	-0.213	-0.195	-0.170
	Σ	0.125	0.221	0.224	0.221	0.212	0.194	0.167

Table B.68: Systematic uncertainty contributions for C_2 at $\sqrt{s_{NN}} = 4.5$ GeV

$\sqrt{s_{NN}} = 4.5$ GeV, C_2 Systematic Uncertainties								
		0-5%	5-10%	10-20%	20-30%	30-40%	40-50%	50-60%
C_2	value	25.079	21.809	16.196	10.722	6.730	3.913	2.117
	stat.	0.033	0.033	0.015	0.011	0.007	0.004	0.003
	sys.	1.608	1.443	1.077	0.734	0.500	0.341	0.238
nHitsFit	≥ 22	-0.104	-0.101	-0.077	-0.053	-0.035	-0.021	-0.012
	≥ 25	0.083	0.060	0.052	0.039	0.026	0.017	0.010
	Σ	0.094	0.081	0.064	0.046	0.031	0.019	0.011
Efficiency	–5%	-1.423	-1.305	-0.974	-0.647	-0.405	-0.234	-0.125
	+5%	1.279	1.167	0.871	0.578	0.362	0.209	0.112
	Σ	1.351	1.236	0.922	0.612	0.383	0.221	0.118
m^2 cuts (GeV^2)	[0.7,1.3]	0.032	0.017	0.010	0.005	-0.001	0.000	-0.000
	[0.6,1.1]	-0.027	-0.018	-0.009	-0.003	-0.000	0.002	0.001
	Σ	0.029	0.017	0.010	0.004	0.000	0.002	0.001
DCA (cm)	<0.9	-0.153	-0.024	0.074	0.106	0.097	0.070	0.044
	<1.1	-0.237	-0.331	-0.294	-0.225	-0.161	-0.102	-0.061
	Σ	0.195	0.178	0.184	0.166	0.129	0.086	0.053
$\lvert n\sigma_p \rvert$	2.75	-0.002	-0.004	-0.005	-0.007	-0.004	-0.002	-0.002
	2.5	0.068	0.068	0.041	0.020	0.013	0.006	0.002
	Σ	0.068	0.036	0.023	0.014	0.009	0.004	0.002
nHitsDedx	≥ 22	0.403	0.301	0.193	0.108	0.063	0.032	0.016
	≥ 25	1.276	1.045	0.711	0.418	0.250	0.138	0.072
	Σ	0.839	0.673	0.452	0.263	0.157	0.085	0.044
pileup	low	0.007	0.003	-0.000	-0.000	0.000	0.000	0.000
	high	-0.003	-0.001	-0.001	0.000	0.000	-0.000	-0.000
	Σ	0.000	0.000	0.000	0.000	0.000	0.000	0.000
cent. cut	–1	0.065	0.256	0.256	0.254	0.244	0.228	0.190
	+1	-0.057	-0.238	-0.260	-0.251	-0.248	-0.231	-0.198
	Σ	0.061	0.247	0.258	0.253	0.246	0.229	0.194

Table B.69: Systematic uncertainty contributions for C_3 at $\sqrt{s_{NN}} = 4.5$ GeV

$\sqrt{s_{NN}} = 4.5$ GeV, C_3 Systematic Uncertainties								
		0-5%	5-10%	10-20%	20-30%	30-40%	40-50%	50-60%
C_3	value	25.312	26.998	20.336	13.971	8.821	5.088	2.684
	stat.	0.411	0.482	0.167	0.082	0.048	0.022	0.013
	sys.	1.421	2.081	1.519	1.125	0.741	0.499	0.326
nHitsFit	≥ 22	-0.043	-0.173	-0.084	-0.085	-0.050	-0.028	-0.017
	≥ 25	0.016	0.092	0.023	0.061	0.038	0.022	0.016
	Σ	0.000	0.173	0.084	0.073	0.044	0.025	0.016
Efficiency	–5%	-1.245	-1.838	-1.407	-1.014	-0.646	-0.371	-0.191
	+5%	1.150	1.629	1.245	0.892	0.568	0.326	0.168
	Σ	1.197	1.733	1.326	0.953	0.607	0.348	0.179
m^2 cuts (GeV^2)	[0.7,1.3]	0.047	0.045	-0.001	0.030	0.001	0.001	0.000
	[0.6,1.1]	0.048	0.025	-0.008	-0.015	-0.001	0.004	0.001
	Σ	0.000	0.045	0.000	0.023	0.000	0.004	0.000
DCA (cm)	<0.9	0.129	0.423	0.219	0.062	0.055	0.063	0.053
	<1.1	-0.042	-0.557	-0.454	-0.349	-0.214	-0.137	-0.084
	Σ	0.129	0.490	0.337	0.205	0.135	0.100	0.068
$\lvert n\sigma_p \rvert$	2.75	0.073	-0.030	-0.028	-0.011	-0.007	0.003	-0.002
	2.5	0.173	0.135	0.027	0.058	0.039	0.016	0.008
	Σ	0.123	0.135	0.028	0.034	0.023	0.016	0.005
nHitsDedx	≥ 22	0.350	0.569	0.267	0.187	0.093	0.046	0.022
	≥ 25	1.101	1.365	0.913	0.754	0.398	0.224	0.104
	Σ	0.726	0.967	0.590	0.471	0.246	0.135	0.063
pileup	low	0.016	0.019	-0.000	-0.002	-0.002	-0.000	0.000
	high	0.025	-0.000	-0.004	-0.000	0.001	0.000	-0.000
	Σ	0.000	0.000	0.000	0.000	0.000	0.000	0.000
cent. cut	–1	-0.221	0.382	0.276	0.312	0.308	0.311	0.250
	+1	0.115	-0.258	-0.290	-0.282	-0.325	-0.318	-0.260
	Σ	0.168	0.320	0.283	0.297	0.316	0.315	0.255

Table B.70: Systematic uncertainty contributions for C_4 at $\sqrt{s_{NN}} = 4.5$ GeV

$\sqrt{s_{NN}} = 4.5$ GeV, C_4 Systematic Uncertainties								
		0-5%	5-10%	10-20%	20-30%	30-40%	40-50%	50-60%
C_4	value	28.044	35.810	28.114	22.087	14.093	8.099	3.999
	stat.	6.565	4.456	1.992	0.813	0.333	0.160	0.086
	sys.	3.681	4.511	2.329	2.639	1.419	1.048	0.532
nHitsFit	≥ 22	0.643	-0.708	-0.112	-0.271	-0.109	-0.047	-0.027
	≥ 25	-0.094	1.946	-0.163	0.036	-0.050	0.015	0.028
	Σ	0.000	1.946	0.000	0.271	0.109	0.047	0.027
Efficiency	–5%	-2.047	-2.634	-2.204	-2.066	-1.328	-0.763	-0.349
	+5%	1.724	2.334	1.935	1.773	1.140	0.655	0.303
	Σ	0.000	0.000	2.069	1.919	1.234	0.709	0.326
m^2 cuts (GeV^2)	[0.7,1.3]	-1.336	-0.252	-0.267	0.241	-0.070	-0.010	-0.001
	[0.6,1.1]	1.847	-0.295	-0.150	0.015	0.088	0.017	-0.004
	Σ	1.592	0.000	0.267	0.000	0.000	0.017	0.000
DCA (cm)	<0.9	0.974	2.685	0.326	0.326	-0.110	0.037	0.085
	<1.1	3.319	-0.247	-1.035	-1.340	-0.538	-0.238	-0.131
	Σ	3.319	2.685	1.035	0.833	0.324	0.238	0.108
$\lvert n\sigma_p \rvert$	2.75	0.162	0.061	-0.258	-0.041	-0.047	0.034	0.006
	2.5	-0.374	0.278	-0.140	0.274	0.186	0.047	0.031
	Σ	0.000	0.000	0.000	0.274	0.116	0.047	0.031
nHitsDedx	≥ 22	-0.444	-2.776	0.015	0.846	0.267	-0.025	0.042
	≥ 25	-0.268	0.936	-0.232	1.867	0.669	0.421	0.206
	Σ	0.000	2.776	0.000	1.356	0.468	0.421	0.124
pileup	low	-0.415	0.175	-0.025	-0.027	-0.016	0.000	-0.000
	high	0.120	0.025	-0.004	0.005	-0.002	0.000	0.000
	Σ	0.000	0.175	0.000	0.000	0.000	0.000	0.000
cent. cut	–1	-0.866	1.271	-0.163	0.772	0.287	0.577	0.388
	+1	-0.347	-0.266	-0.175	-0.231	-0.461	-0.617	-0.383
	Σ	0.000	1.271	0.000	0.772	0.374	0.597	0.386

Table B.71: Systematic uncertainty contributions for C_5 at $\sqrt{s_{NN}} = 4.5$ GeV

$\sqrt{s_{NN}} = 4.5$ GeV, C_5 Systematic Uncertainties								
		0-5%	5-10%	10-20%	20-30%	30-40%	40-50%	50-60%
C_5	value	53.025	14.964	40.386	43.961	31.884	16.032	6.633
	stat.	113.099	69.011	26.568	11.567	4.187	1.588	0.575
	sys.	127.864	40.327	20.482	10.921	6.007	2.750	1.106
nHitsFit	≥ 22	7.488	-4.389	-3.070	-0.521	-0.539	-0.136	-0.053
	≥ 25	-13.228	13.274	-0.107	0.537	-1.988	-0.308	-0.062
	Σ	0.000	0.000	0.000	0.000	1.988	0.308	0.000
Efficiency	–5%	-7.554	6.417	-3.009	-5.148	-4.377	-1.847	-0.603
	+5%	6.127	-4.202	2.717	4.339	3.581	1.563	0.531
	Σ	0.000	0.000	0.000	0.000	3.979	1.705	0.567
m^2 cuts (GeV^2)	[0.7,1.3]	12.399	8.894	-2.258	2.458	-0.686	-0.416	-0.052
	[0.6,1.1]	33.612	-14.452	-3.867	0.962	1.250	-0.004	-0.032
	Σ	33.612	14.452	0.000	2.458	1.250	0.416	0.000
DCA (cm)	<0.9	37.174	0.614	-4.954	4.353	-2.139	-0.117	0.183
	<1.1	81.099	-23.544	1.927	-4.844	-2.560	-0.591	-0.080
	Σ	81.099	23.544	0.000	4.598	2.349	0.000	0.000
$\lvert n\sigma_p \rvert$	2.75	-13.463	2.931	-3.522	-0.788	-0.364	0.282	0.092
	2.5	1.062	-19.007	1.998	0.547	1.291	0.293	0.115
	Σ	0.000	0.000	0.000	0.000	1.291	0.293	0.115
nHitsDedx	≥ 22	47.251	-26.538	-13.760	6.907	3.570	-1.167	0.056
	≥ 25	138.679	9.644	-22.370	-3.481	1.926	0.204	0.761
	Σ	92.965	26.538	18.065	5.194	2.748	1.167	0.761
pileup	low	-8.447	-2.901	-0.093	-0.140	-0.083	-0.004	-0.005
	high	2.904	1.301	-0.428	-0.076	-0.033	-0.011	0.000
	Σ	0.000	0.000	0.000	0.000	0.000	0.000	0.000
cent. cut	–1	-7.305	12.603	-9.653	8.069	-0.830	1.848	0.507
	+1	-19.608	2.712	5.056	0.375	-0.612	-1.581	-0.605
	Σ	0.000	12.603	9.653	8.069	0.000	1.715	0.556

Table B.72: Systematic uncertainty contributions for C_6 at $\sqrt{s_{NN}} = 4.5$ GeV

$\sqrt{s_{NN}} = 4.5$ GeV, C_6 Systematic Uncertainties								
		0-5%	5-10%	10-20%	20-30%	30-40%	40-50%	50-60%
C_6	value	-1256.3	-1003.0	-25.396	50.930	111.502	38.091	7.790
	stat.	1752.298	1250.881	372.682	182.212	57.573	19.825	3.951
	sys.	1595.276	915.075	344.431	166.305	66.033	0.000	3.657
nHitsFit	≥ 22	19.899	-75.214	-31.049	5.932	-1.763	-1.254	-0.101
	≥ 25	-503.08	81.476	-23.161	-17.186	-24.839	-2.880	-1.352
	Σ	503.077	0.000	0.000	0.000	24.839	0.000	1.352
Efficiency	–5%	484.301	346.067	25.578	5.326	-21.225	-5.166	0.254
	+5%	-337.88	-248.27	-17.311	-1.911	16.709	4.287	-0.008
	Σ	0.000	0.000	0.000	0.000	0.000	0.000	0.000
m^2 cuts (GeV^2)	[0.7,1.3]	-90.262	74.420	-17.984	14.098	-6.404	-7.000	-0.563
	[0.6,1.1]	198.559	-501.86	-42.474	16.519	12.935	-1.089	-0.024
	Σ	0.000	501.859	0.000	0.000	9.669	0.000	0.000
DCA (cm)	<0.9	439.858	-398.90	27.952	66.781	-35.184	0.841	0.374
	<1.1	438.446	-300.33	66.139	41.282	-21.430	-9.612	0.930
	Σ	0.000	349.615	0.000	41.282	35.184	0.000	0.000
$\lvert n\sigma_p \rvert$	2.75	-312.47	-106.11	-31.870	-15.248	-1.284	1.676	0.756
	2.5	10.330	-228.63	58.369	-1.703	12.409	2.389	0.438
	Σ	0.000	0.000	0.000	0.000	0.000	0.000	0.000
nHitsDedx	≥ 22	779.796	211.129	-266.30	99.349	43.580	-11.541	-0.935
	≥ 25	2128.114	-486.00	-351.80	-165.70	33.475	-0.383	3.398
	Σ	1453.955	485.998	309.050	132.525	43.580	0.000	3.398
pileup	low	-25.405	-49.245	-1.310	0.218	0.098	-0.145	-0.031
	high	-55.881	-6.225	-1.352	-1.125	0.067	-0.071	0.001
	Σ	0.000	0.000	0.000	0.000	0.000	0.000	0.000
cent. cut	–1	-221.45	274.028	-152.06	91.599	-22.644	16.261	-1.572
	+1	-621.96	476.524	96.920	-40.470	0.825	-2.642	-1.680
	Σ	421.705	476.524	152.057	91.599	22.644	0.000	0.000

Table B.73: Systematic uncertainty contributions for C_2/C_1 at $\sqrt{s_{NN}} = 4.5$ GeV

$\sqrt{s_{NN}} = 4.5$ GeV, C_2/C_1 Systematic Uncertainties								
		0-5%	5-10%	10-20%	20-30%	30-40%	40-50%	50-60%
C_2/C_1	value	1.080	1.149	1.157	1.161	1.157	1.147	1.131
	stat.	0.001	0.002	0.001	0.001	0.001	0.001	0.001
	sys.	0.025	0.023	0.019	0.014	0.011	0.009	0.008
nHitsFit	≥ 22	-0.000	-0.001	-0.001	-0.001	-0.001	-0.000	-0.001
	≥ 25	0.002	0.001	0.001	0.001	0.001	0.000	0.000
	Σ	0.001	0.001	0.001	0.001	0.001	0.000	0.001
Efficiency	–5%	-0.004	-0.008	-0.008	-0.008	-0.008	-0.008	-0.007
	+5%	0.004	0.007	0.007	0.008	0.007	0.007	0.006
	Σ	0.004	0.007	0.008	0.008	0.008	0.007	0.007
m^2 cuts (GeV^2)	[0.7,1.3]	0.001	0.000	0.000	0.000	-0.000	0.000	0.000
	[0.6,1.1]	-0.001	-0.001	-0.000	-0.000	-0.000	0.000	-0.000
	Σ	0.001	0.000	0.000	0.000	0.000	0.000	0.000
DCA (cm)	<0.9	-0.031	-0.030	-0.023	-0.016	-0.011	-0.006	-0.002
	<1.1	0.015	0.012	0.009	0.006	0.003	0.002	-0.001
	Σ	0.023	0.021	0.016	0.011	0.007	0.004	0.001
$\lvert n\sigma_p \rvert$	2.75	0.000	-0.000	-0.000	-0.000	0.000	0.000	0.000
	2.5	-0.000	0.001	0.000	0.000	0.001	0.001	0.001
	Σ	0.000	0.001	0.000	0.000	0.001	0.001	0.001
nHitsDedx	≥ 22	0.005	0.004	0.003	0.002	0.002	0.001	0.001
	≥ 25	0.009	0.010	0.009	0.006	0.005	0.004	0.004
	Σ	0.007	0.007	0.006	0.004	0.004	0.002	0.002
pileup	low	0.000	0.000	0.000	0.000	0.000	-0.000	0.000
	high	-0.000	-0.000	-0.000	-0.000	0.000	-0.000	0.000
	Σ	0.000	0.000	0.000	0.000	0.000	0.000	0.000
cent. cut	–1	-0.003	0.000	-0.000	-0.000	0.000	0.002	0.003
	+1	0.003	0.001	-0.000	0.000	-0.000	-0.002	-0.003
	Σ	0.003	0.001	0.000	0.000	0.000	0.002	0.003

Table B.74: Systematic uncertainty contributions for C_3/C_1 at $\sqrt{s_{NN}} = 4.5$ GeV

$\sqrt{s_{NN}} = 4.5$ GeV, C_3/C_1 Systematic Uncertainties								
		0-5%	5-10%	10-20%	20-30%	30-40%	40-50%	50-60%
C_3/C_1	value	1.090	1.423	1.452	1.513	1.516	1.492	1.433
	stat.	0.018	0.025	0.012	0.009	0.008	0.006	0.007
	sys.	0.025	0.028	0.027	0.038	0.035	0.038	0.029
nHitsFit	≥ 22	0.002	-0.003	0.000	-0.002	-0.001	-0.001	-0.002
	≥ 25	-0.001	0.003	-0.001	0.003	0.002	0.001	0.002
	Σ	0.000	0.003	0.000	0.003	0.001	0.001	0.002
Efficiency	–5%	0.004	-0.021	-0.023	-0.029	-0.030	-0.029	-0.025
	+5%	-0.003	0.019	0.021	0.026	0.027	0.026	0.023
	Σ	0.000	0.020	0.022	0.027	0.028	0.027	0.024
m^2 cuts (GeV^2)	[0.7,1.3]	0.001	0.002	-0.000	0.003	0.000	0.001	0.001
	[0.6,1.1]	0.003	0.002	-0.000	-0.002	-0.000	0.000	-0.000
	Σ	0.000	0.002	0.000	0.002	0.000	0.000	0.001
DCA (cm)	<0.9	-0.019	-0.013	-0.020	-0.030	-0.026	-0.016	-0.004
	<1.1	0.024	0.007	0.005	0.002	0.004	0.001	-0.005
	Σ	0.021	0.010	0.013	0.016	0.015	0.016	0.004
$\lvert n\sigma_p \rvert$	2.75	0.003	-0.001	-0.002	-0.000	-0.000	0.002	0.000
	2.5	0.004	0.003	-0.001	0.004	0.005	0.003	0.003
	Σ	0.004	0.003	0.001	0.004	0.005	0.003	0.003
nHitsDedx	≥ 22	0.002	0.015	0.005	0.007	0.004	0.002	0.001
	≥ 25	0.001	0.016	0.012	0.031	0.020	0.019	0.012
	Σ	0.000	0.016	0.009	0.019	0.012	0.019	0.012
pileup	low	0.001	0.001	0.000	-0.000	-0.000	-0.000	0.000
	high	0.001	-0.000	-0.000	-0.000	0.000	0.000	0.000
	Σ	0.000	0.000	0.000	0.000	0.000	0.000	0.000
cent. cut	–1	-0.016	0.003	-0.004	-0.002	-0.002	0.007	0.009
	+1	0.011	0.003	0.002	0.005	-0.000	-0.008	-0.008
	Σ	0.013	0.000	0.003	0.005	0.002	0.007	0.008

Table B.75: Systematic uncertainty contributions for C_4/C_2 at $\sqrt{s_{NN}} = 4.5$ GeV

$\sqrt{s_{NN}} = 4.5$ GeV, C_4/C_2 Systematic Uncertainties								
		0-5%	5-10%	10-20%	20-30%	30-40%	40-50%	50-60%
C_4/C_2	value	1.118	1.642	1.736	2.060	2.094	2.070	1.889
	stat.	0.262	0.204	0.123	0.076	0.049	0.040	0.040
	sys.	0.114	0.178	0.108	0.133	0.081	0.083	0.063
nHitsFit	≥ 22	0.030	-0.025	0.001	-0.015	-0.005	-0.001	-0.002
	≥ 25	-0.007	0.085	-0.016	-0.004	-0.016	-0.005	0.004
	Σ	0.000	0.085	0.000	0.015	0.000	0.000	0.000
Efficiency	–5%	-0.017	-0.021	-0.030	-0.065	-0.067	-0.067	-0.050
	+5%	0.012	0.020	0.028	0.057	0.060	0.060	0.045
	Σ	0.000	0.000	0.000	0.061	0.064	0.064	0.048
m^2 cuts (GeV^2)	[0.7,1.3]	-0.055	-0.013	-0.018	0.021	-0.010	-0.003	-0.000
	[0.6,1.1]	0.075	-0.012	-0.008	0.002	0.013	0.003	-0.003
	Σ	0.065	0.000	0.018	0.000	0.000	0.003	0.000
DCA (cm)	<0.9	0.045	0.125	0.012	0.010	-0.047	-0.028	0.001
	<1.1	0.142	0.013	-0.032	-0.080	-0.029	-0.007	-0.008
	Σ	0.093	0.125	0.032	0.080	0.038	0.028	0.008
$\lvert n\sigma_p \rvert$	2.75	0.007	0.003	-0.015	-0.003	-0.006	0.010	0.005
	2.5	-0.018	0.008	-0.013	0.022	0.023	0.009	0.013
	Σ	0.000	0.000	0.000	0.022	0.015	0.010	0.013
nHitsDedx	≥ 22	-0.036	-0.152	-0.020	0.059	0.020	-0.023	0.005
	≥ 25	-0.071	-0.038	-0.095	0.098	0.023	0.036	0.034
	Σ	0.000	0.095	0.095	0.078	0.020	0.030	0.034
pileup	low	-0.017	0.008	-0.001	-0.002	-0.002	0.000	-0.000
	high	0.005	0.001	-0.000	0.000	-0.000	0.000	0.000
	Σ	0.000	0.000	0.000	0.000	0.000	0.000	0.000
cent. cut	–1	-0.038	0.039	-0.038	0.024	-0.034	0.028	0.016
	+1	-0.011	0.006	0.017	0.026	0.008	-0.034	-0.003
	Σ	0.000	0.000	0.038	0.026	0.021	0.031	0.016

Table B.76: Systematic uncertainty contributions for C_5/C_1 at $\sqrt{s_{NN}} = 4.5$ GeV

$\sqrt{s_{NN}} = 4.5$ GeV, C_5/C_1 Systematic Uncertainties								
		0-5%	5-10%	10-20%	20-30%	30-40%	40-50%	50-60%
C_5/C_1	value	2.284	0.789	2.884	4.761	5.479	4.700	3.542
	stat.	4.871	3.636	1.897	1.253	0.719	0.466	0.307
	sys.	5.549	1.744	1.582	1.106	0.966	0.542	0.312
nHitsFit	≥ 22	0.330	-0.227	-0.206	-0.035	-0.066	-0.016	-0.009
	≥ 25	-0.574	0.699	-0.014	0.046	-0.361	-0.109	-0.048
	Σ	0.000	0.000	0.000	0.000	0.361	0.109	0.000
Efficiency	–5%	-0.195	0.361	-0.060	-0.292	-0.441	-0.279	-0.129
	+5%	0.163	-0.272	0.060	0.255	0.372	0.246	0.121
	Σ	0.000	0.000	0.000	0.000	0.000	0.246	0.000
m^2 cuts (GeV^2)	[0.7,1.3]	0.533	0.469	-0.162	0.266	-0.117	-0.121	-0.026
	[0.6,1.1]	1.448	-0.761	-0.276	0.104	0.214	-0.003	-0.019
	Σ	1.448	0.761	0.000	0.266	0.214	0.121	0.000
DCA (cm)	<0.9	1.585	0.013	-0.435	0.368	-0.507	-0.145	0.019
	<1.1	3.465	-1.189	0.208	-0.389	-0.285	-0.044	0.054
	Σ	3.465	0.000	0.000	0.378	0.507	0.145	0.000
$\lvert n\sigma_p \rvert$	2.75	-0.580	0.155	-0.251	-0.083	-0.059	0.087	0.053
	2.5	0.039	-1.006	0.137	0.051	0.215	0.082	0.060
	Σ	0.000	0.000	0.000	0.000	0.215	0.082	0.060
nHitsDedx	≥ 22	2.032	-1.422	-1.020	0.713	0.574	-0.381	0.005
	≥ 25	6.138	0.497	-1.769	-0.558	0.158	-0.093	0.306
	Σ	4.085	1.422	1.394	0.636	0.574	0.381	0.306
pileup	low	-0.364	-0.153	-0.006	-0.015	-0.014	-0.001	-0.003
	high	0.125	0.069	-0.031	-0.008	-0.006	-0.003	0.000
	Σ	0.000	0.000	0.000	0.000	0.000	0.000	0.000
cent. cut	–1	-0.329	0.663	-0.747	0.779	-0.354	0.292	-0.043
	+1	-0.828	0.150	0.401	0.151	0.092	-0.184	-0.001
	Σ	0.000	0.663	0.747	0.779	0.354	0.184	0.000

Table B.77: Systematic uncertainty contributions for C_6/C_2 at $\sqrt{s_{NN}} = 4.5$ GeV

$\sqrt{s_{NN}} = 4.5$ GeV, C_6/C_2 Systematic Uncertainties								
		0-5%	5-10%	10-20%	20-30%	30-40%	40-50%	50-60%
C_6/C_2	value	-50.093	-45.991	-1.568	4.750	16.567	9.735	3.680
	stat.	69.821	57.362	23.009	17.001	8.552	5.068	1.865
	sys.	67.496	39.190	21.819	15.435	10.229	0.000	2.042
nHitsFit	≥ 22	0.583	-3.645	-1.915	0.574	-0.174	-0.267	-0.026
	≥ 25	-19.960	3.873	-1.430	-1.626	-3.770	-0.781	-0.659
	Σ	19.960	0.000	0.000	0.000	3.770	0.000	0.659
Efficiency	–5%	15.584	12.376	1.401	0.739	-2.035	-0.697	0.318
	+5%	-11.505	-9.427	-1.040	-0.459	1.683	0.608	-0.209
	Σ	0.000	0.000	0.000	0.000	0.000	0.000	0.000
m^2 cuts (GeV^2)	[0.7,1.3]	-3.539	3.451	-1.110	1.313	-0.949	-1.790	-0.265
	[0.6,1.1]	7.856	-23.030	-2.622	1.542	1.923	-0.283	-0.014
	Σ	0.000	23.030	0.000	0.000	1.436	0.000	0.000
DCA (cm)	<0.9	17.128	-18.321	1.741	6.243	-5.545	0.041	0.102
	<1.1	16.849	-14.252	3.983	3.869	-2.722	-2.148	0.530
	Σ	0.000	16.287	0.000	0.000	5.545	0.000	0.000
$\lvert n\sigma_p \rvert$	2.75	-12.462	-4.874	-1.968	-1.418	-0.180	0.434	0.361
	2.5	0.550	-10.372	3.617	-0.168	1.815	0.596	0.203
	Σ	0.000	0.000	0.000	0.000	0.000	0.000	0.000
nHitsDedx	≥ 22	32.418	10.461	-16.622	9.312	6.379	-3.053	-0.474
	≥ 25	92.087	-21.090	-22.648	-16.275	4.527	-0.456	1.532
	Σ	62.253	21.090	19.635	12.793	6.379	0.000	1.532
pileup	low	-0.999	-2.253	-0.081	0.021	0.015	-0.037	-0.015
	high	-2.234	-0.288	-0.084	-0.105	0.009	-0.018	0.000
	Σ	0.000	0.000	0.000	0.000	0.000	0.000	0.000
cent. cut	–1	-8.722	13.261	-9.514	8.635	-4.114	3.811	-1.178
	+1	-24.858	21.116	5.865	-3.579	0.707	-0.096	-0.410
	Σ	16.790	17.188	9.514	8.635	4.114	0.000	1.178

Table B.78: Systematic uncertainty contributions for κ_1 at $\sqrt{s_{NN}} = 4.5$ GeV

$\sqrt{s_{NN}} = 4.5$ GeV, κ_1 Systematic Uncertainties

		0-5%	5-10%	10-20%	20-30%	30-40%	40-50%	50-60%
κ_1	value	23.219	18.978	14.002	9.233	5.819	3.411	1.873
	stat.	0.006	0.004	0.002	0.002	0.001	0.001	0.001
	sys.	1.436	1.190	0.880	0.597	0.407	0.281	0.201
nHitsFit	≥ 22	-0.092	-0.077	-0.059	-0.041	-0.028	-0.017	-0.010
	≥ 25	0.035	0.032	0.029	0.024	0.019	0.013	0.008
	Σ	0.063	0.054	0.044	0.033	0.023	0.015	0.009
Efficiency	–5%	-1.222	-0.999	-0.737	-0.486	-0.306	-0.180	-0.099
	+5%	1.106	0.904	0.667	0.440	0.277	0.162	0.089
	Σ	1.164	0.951	0.702	0.463	0.292	0.171	0.094
m^2 cuts (GeV^2)	[0.7,1.3]	0.015	0.009	0.004	0.001	-0.001	-0.001	-0.001
	[0.6,1.1]	-0.011	-0.005	-0.002	0.000	0.001	0.001	0.001
	Σ	0.013	0.007	0.003	0.001	0.001	0.001	0.001
DCA (cm)	<0.9	0.519	0.467	0.341	0.218	0.135	0.078	0.042
	<1.1	-0.551	-0.491	-0.366	-0.244	-0.157	-0.093	-0.052
	Σ	0.535	0.479	0.353	0.231	0.146	0.086	0.047
$\lvert n\sigma_p \rvert$	2.75	-0.002	-0.003	-0.005	-0.005	-0.004	-0.003	-0.002
	2.5	0.066	0.050	0.031	0.016	0.007	0.003	0.001
	Σ	0.034	0.026	0.018	0.010	0.006	0.003	0.001
nHitsDedx	≥ 22	0.273	0.203	0.135	0.080	0.047	0.026	0.013
	≥ 25	0.993	0.752	0.514	0.314	0.190	0.109	0.058
	Σ	0.633	0.478	0.325	0.197	0.118	0.067	0.036
pileup	low	0.002	-0.001	-0.001	-0.001	-0.000	0.000	0.000
	high	0.000	0.001	0.000	0.000	0.000	-0.000	-0.000
	Σ	0.000	0.000	0.000	0.000	0.000	0.000	0.000
cent. cut	–1	0.126	0.223	0.224	0.221	0.211	0.193	0.164
	+1	-0.125	-0.220	-0.224	-0.220	-0.213	-0.195	-0.170
	Σ	0.125	0.221	0.224	0.221	0.212	0.194	0.167

Table B.79: Systematic uncertainty contributions for κ_2 at $\sqrt{s_{NN}} = 4.5$ GeV

$\sqrt{s_{NN}} = 4.5$ GeV, κ_2 Systematic Uncertainties

		0-5%	5-10%	10-20%	20-30%	30-40%	40-50%	50-60%
κ_2	value	1.860	2.831	2.194	1.489	0.911	0.502	0.244
	stat.	0.033	0.032	0.015	0.011	0.007	0.004	0.003
	sys.	0.571	0.477	0.309	0.180	0.108	0.065	0.038
nHitsFit	≥ 22	-0.012	-0.024	-0.017	-0.012	-0.007	-0.004	-0.002
	≥ 25	0.048	0.028	0.022	0.015	0.007	0.004	0.002
	Σ	0.030	0.026	0.020	0.013	0.007	0.004	0.002
Efficiency	–5%	-0.201	-0.306	-0.237	-0.161	-0.098	-0.054	-0.026
	+5%	0.173	0.263	0.204	0.138	0.085	0.047	0.023
	Σ	0.187	0.285	0.220	0.150	0.092	0.050	0.025
m^2 cuts (GeV^2)	[0.7,1.3]	0.017	0.008	0.006	0.004	-0.001	0.001	0.000
	[0.6,1.1]	-0.015	-0.012	-0.007	-0.003	-0.002	0.000	-0.000
	Σ	0.016	0.010	0.007	0.004	0.002	0.001	0.000
DCA (cm)	<0.9	-0.672	-0.492	-0.266	-0.112	-0.039	-0.008	0.002
	<1.1	0.314	0.160	0.072	0.019	-0.004	-0.008	-0.009
	Σ	0.493	0.326	0.169	0.065	0.021	0.008	0.006
$\lvert n\sigma_p \rvert$	2.75	0.000	-0.002	-0.001	-0.002	-0.000	0.001	-0.000
	2.5	0.002	0.018	0.010	0.004	0.006	0.003	0.001
	Σ	0.000	0.018	0.010	0.003	0.006	0.003	0.001
nHitsDedx	≥ 22	0.129	0.098	0.059	0.028	0.017	0.006	0.003
	≥ 25	0.282	0.293	0.197	0.104	0.060	0.029	0.014
	Σ	0.206	0.196	0.128	0.066	0.038	0.017	0.009
pileup	low	0.005	0.004	0.001	0.000	0.000	-0.000	0.000
	high	-0.003	-0.002	-0.001	-0.000	0.000	-0.000	0.000
	Σ	0.000	0.000	0.000	0.000	0.000	0.000	0.000
cent. cut	–1	-0.061	0.033	0.032	0.033	0.033	0.035	0.026
	+1	0.067	-0.019	-0.036	-0.031	-0.035	-0.036	-0.028
	Σ	0.064	0.026	0.034	0.032	0.034	0.035	0.027

Table B.80: Systematic uncertainty contributions for κ_3 at $\sqrt{s_{NN}} = 4.5$ GeV

$\sqrt{s_{NN}} = 4.5$ GeV, κ_3 Systematic Uncertainties

		0-5%	5-10%	10-20%	20-30%	30-40%	40-50%	50-60%
κ_3	value	-3.488	-0.473	-0.247	0.270	0.268	0.172	0.078
	stat.	0.413	0.454	0.162	0.074	0.040	0.016	0.010
	sys.	1.294	1.024	0.514	0.196	0.065	0.044	0.015
nHitsFit	≥ 22	0.086	-0.023	0.027	-0.009	-0.000	0.000	0.000
	≥ 25	-0.163	-0.024	-0.073	-0.008	-0.003	-0.002	0.002
	Σ	0.125	0.000	0.073	0.000	0.000	0.000	0.000
Efficiency	–5%	0.580	0.079	0.041	-0.045	-0.045	-0.029	-0.013
	+5%	-0.475	-0.064	-0.034	0.037	0.037	0.023	0.011
	Σ	0.528	0.000	0.000	0.045	0.041	0.026	0.012
m^2 cuts (GeV^2)	[0.7,1.3]	-0.019	0.012	-0.023	0.016	0.003	-0.001	-0.000
	[0.6,1.1]	0.104	0.068	0.015	-0.006	0.003	0.002	-0.000
	Σ	0.104	0.000	0.023	0.000	0.000	0.002	0.000
DCA (cm)	<0.9	1.627	1.431	0.677	0.179	0.036	0.008	0.004
	<1.1	-0.432	-0.547	-0.305	-0.161	-0.044	-0.019	-0.005
	Σ	1.030	0.989	0.491	0.170	0.040	0.013	0.005
$\lvert n\sigma_p \rvert$	2.75	0.074	-0.022	-0.022	0.001	-0.001	0.004	0.001
	2.5	0.101	0.031	-0.034	0.029	0.014	0.003	0.003
	Σ	0.087	0.000	0.034	0.029	0.014	0.004	0.003
nHitsDedx	≥ 22	-0.311	0.071	-0.043	0.023	-0.004	0.003	-0.001
	≥ 25	-0.739	-0.267	-0.193	0.127	0.028	0.029	0.004
	Σ	0.525	0.267	0.118	0.075	0.028	0.029	0.004
pileup	low	-0.002	0.009	-0.001	-0.002	-0.002	-0.000	0.000
	high	0.034	0.005	-0.001	0.000	0.000	0.000	0.000
	Σ	0.000	0.000	0.000	0.000	0.000	0.000	0.000
cent. cut	–1	-0.165	0.059	-0.044	-0.008	-0.002	0.014	0.009
	+1	0.038	0.018	0.042	0.032	-0.007	-0.017	-0.005
	Σ	0.165	0.000	0.044	0.032	0.000	0.015	0.007

Table B.81: Systematic uncertainty contributions for κ_4 at $\sqrt{s_{NN}} = 4.5$ GeV

$\sqrt{s_{NN}} = 4.5$ GeV, κ_4 Systematic Uncertainties

		0-5%	5-10%	10-20%	20-30%	30-40%	40-50%	50-60%
κ_4	value	12.731	-0.148	0.241	0.807	0.286	0.144	-0.054
	stat.	6.037	3.385	1.560	0.684	0.232	0.095	0.039
	sys.	4.633	5.226	1.731	0.616	0.244	0.108	0.018
nHitsFit	≥ 22	0.305	-0.319	-0.094	-0.097	-0.028	-0.007	-0.001
	≥ 25	0.512	1.861	0.091	-0.047	-0.103	-0.012	-0.006
	Σ	0.000	1.861	0.000	0.097	0.000	0.000	0.000
Efficiency	–5%	-2.899	0.034	-0.055	-0.184	-0.065	-0.033	0.012
	+5%	2.257	-0.026	0.043	0.143	0.051	0.026	-0.010
	Σ	0.000	0.000	0.000	0.000	0.000	0.000	0.000
m^2 cuts (GeV^2)	[0.7,1.3]	-1.354	-0.390	-0.176	0.112	-0.084	-0.011	-0.002
	[0.6,1.1]	1.338	-0.610	-0.189	0.073	0.078	0.004	-0.003
	Σ	1.346	0.000	0.000	0.000	0.081	0.011	0.000
DCA (cm)	<0.9	-4.602	-2.926	-2.215	-0.186	-0.188	-0.036	0.003
	<1.1	4.265	2.403	0.655	-0.261	-0.085	0.025	0.014
	Σ	4.434	2.665	1.435	0.223	0.136	0.000	0.000
$\lvert n\sigma_p \rvert$	2.75	-0.280	0.209	-0.118	-0.025	-0.033	0.009	0.006
	2.5	-1.058	-0.085	-0.038	0.053	0.052	0.005	0.003
	Σ	0.000	0.000	0.000	0.000	0.000	0.000	0.000
nHitsDedx	≥ 22	0.242	-4.092	-0.270	0.430	0.127	-0.107	0.011
	≥ 25	1.196	-0.268	-0.968	0.062	-0.111	-0.063	0.025
	Σ	0.000	4.092	0.968	0.430	0.119	0.085	0.018
pileup	low	-0.444	0.094	-0.019	-0.016	-0.004	0.001	-0.001
	high	-0.061	0.010	0.008	0.003	-0.005	-0.001	0.000
	Σ	0.000	0.000	0.000	0.000	0.000	0.000	0.000
cent. cut	–1	0.424	0.459	-0.347	0.368	-0.142	0.059	-0.010
	+1	-0.921	-0.023	0.048	0.018	0.038	-0.073	0.017
	Σ	0.000	0.000	0.000	0.368	0.142	0.066	0.000

Table B.82: Systematic uncertainty contributions for κ_5 at $\sqrt{s_{NN}} = 4.5$ GeV

$\sqrt{s_{NN}} = 4.5$ GeV, κ_5 Systematic Uncertainties								
		0-5%	5-10%	10-20%	20-30%	30-40%	40-50%	50-60%
κ_5	value	-38.208	-33.181	-2.744	-2.443	2.829	-0.648	-0.317
	stat.	81.405	55.446	16.319	7.627	2.455	0.708	0.163
	sys.	108.717	39.065	13.175	7.324	1.956	0.525	0.249
nHitsFit	≥ 22	2.566	-0.165	-2.490	0.877	-0.116	-0.007	-0.001
	≥ 25	-15.031	-5.189	0.448	0.951	-1.017	-0.210	-0.089
	Σ	0.000	0.000	2.490	0.000	1.017	0.000	0.089
Efficiency	–5%	11.170	9.701	0.802	0.714	-0.827	0.189	0.093
	+5%	-8.271	-7.183	-0.594	-0.529	0.612	-0.140	-0.069
	Σ	0.000	0.000	0.000	0.000	0.000	0.000	0.000
m^2 cuts (GeV^2)	[0.7,1.3]	26.153	12.360	-0.022	0.865	0.084	-0.298	-0.030
	[0.6,1.1]	17.861	-9.854	-2.250	0.432	0.406	-0.090	0.006
	Σ	17.861	11.107	0.000	0.000	0.000	0.298	0.030
DCA (cm)	<0.9	52.076	1.011	3.911	3.186	-0.704	0.076	-0.025
	<1.1	45.092	-35.821	2.284	1.755	-0.381	-0.161	0.092
	Σ	48.584	35.821	0.000	3.186	0.000	0.000	0.058
$\lvert n\sigma_p \rvert$	2.75	-12.506	1.427	-1.785	-0.514	0.005	0.090	0.023
	2.5	9.029	-19.249	3.043	-0.798	0.324	0.127	-0.012
	Σ	9.029	0.000	3.043	0.000	0.000	0.000	0.012
nHitsDedx	≥ 22	50.387	10.936	-10.993	1.526	2.102	-0.280	-0.097
	≥ 25	139.964	13.838	-11.340	-9.147	1.238	-0.431	0.144
	Σ	95.176	10.936	11.166	5.336	1.670	0.431	0.144
pileup	low	-4.052	-4.133	0.128	0.066	0.011	-0.012	-0.000
	high	2.717	1.113	-0.468	-0.118	0.007	-0.007	-0.000
	Σ	0.000	0.000	0.000	0.000	0.000	0.000	0.000
cent. cut	–1	-6.631	5.810	-5.783	3.875	-0.062	0.205	-0.169
	+1	-12.236	2.987	4.280	0.097	-0.083	0.292	-0.049
	Σ	0.000	0.000	5.783	3.875	0.000	0.000	0.169

Table B.83: Systematic uncertainty contributions for κ_6 at $\sqrt{s_{NN}} = 4.5$ GeV

$\sqrt{s_{NN}} = 4.5$ GeV, κ_6 Systematic Uncertainties

		0-5%	5-10%	10-20%	20-30%	30-40%	40-50%	50-60%
κ_6	value	-1277.7	-559.90	-59.631	-44.631	-7.751	3.983	-0.400
	stat.	1265.557	731.288	244.157	86.240	19.556	6.736	0.774
	sys.	484.106	917.505	115.230	79.264	22.272	9.502	1.230
nHitsFit	≥ 22	-45.676	-49.033	10.570	0.245	2.062	-0.615	0.033
	≥ 25	-297.76	39.601	-29.945	-28.184	-2.888	1.082	0.132
	Σ	0.000	0.000	0.000	0.000	0.000	0.000	0.000
Efficiency	–5%	460.432	201.772	21.490	16.084	2.793	-1.435	0.144
	+5%	-324.25	-142.09	-15.134	-11.327	-1.967	1.011	-0.102
	Σ	0.000	0.000	0.000	0.000	0.000	0.000	0.000
m^2 cuts (GeV^2)	[0.7,1.3]	-393.35	-86.989	-4.343	-7.755	-2.477	-1.760	0.042
	[0.6,1.1]	-165.24	-320.10	2.400	5.954	1.494	-0.149	0.120
	Σ	393.352	320.100	0.000	0.000	2.477	0.000	0.120
DCA (cm)	<0.9	-168.30	-337.87	60.184	18.177	-14.542	1.462	0.067
	<1.1	-485.46	125.498	14.881	46.071	-5.918	-6.824	-0.593
	Σ	0.000	337.870	0.000	46.071	0.000	0.000	0.000
$\lvert n\sigma_p \rvert$	2.75	-113.31	-139.02	4.546	-5.878	0.899	-0.618	-0.007
	2.5	-65.527	62.261	17.890	4.017	2.727	-0.159	0.100
	Σ	113.308	0.000	0.000	0.000	0.000	0.000	0.000
nHitsDedx	≥ 22	31.948	303.465	-81.923	45.476	3.594	-0.860	-0.244
	≥ 25	7.668	-662.02	-108.07	-47.479	17.524	6.570	-1.224
	Σ	0.000	662.017	108.068	46.478	17.524	6.570	1.224
pileup	low	64.187	5.659	-1.863	0.424	0.399	-0.031	0.012
	high	-95.610	-23.924	5.271	0.384	0.251	0.065	-0.000
	Σ	0.000	0.000	0.000	0.000	0.000	0.000	0.000
cent. cut	–1	-132.93	150.451	-39.989	9.046	-13.521	6.864	-0.168
	+1	-383.96	432.353	27.117	-44.723	1.525	0.505	-0.530
	Σ	258.445	432.353	39.989	44.723	13.521	6.864	0.000

Table B.84: Systematic uncertainty contributions for κ_2/κ_1 at $\sqrt{s_{NN}} = 4.5$ GeV

$\sqrt{s_{NN}} = 4.5$ GeV, κ_2/κ_1 Systematic Uncertainties								
		0-5%	5-10%	10-20%	20-30%	30-40%	40-50%	50-60%
κ_2/κ_1	value	0.080	0.149	0.157	0.161	0.157	0.147	0.131
	stat.	0.001	0.002	0.001	0.001	0.001	0.001	0.001
	sys.	0.025	0.023	0.019	0.014	0.011	0.009	0.008
nHitsFit	≥ 22	-0.000	-0.001	-0.001	-0.001	-0.001	-0.000	-0.001
	≥ 25	0.002	0.001	0.001	0.001	0.001	0.000	0.000
	Σ	0.001	0.001	0.001	0.001	0.001	0.000	0.001
Efficiency	–5%	-0.004	-0.008	-0.008	-0.008	-0.008	-0.008	-0.007
	+5%	0.004	0.007	0.007	0.008	0.007	0.007	0.006
	Σ	0.004	0.007	0.008	0.008	0.008	0.007	0.007
m^2 cuts (GeV^2)	[0.7,1.3]	0.001	0.000	0.000	0.000	-0.000	0.000	0.000
	[0.6,1.1]	-0.001	-0.001	-0.000	-0.000	-0.000	0.000	-0.000
	Σ	0.001	0.000	0.000	0.000	0.000	0.000	0.000
DCA (cm)	<0.9	-0.031	-0.030	-0.023	-0.016	-0.011	-0.006	-0.002
	<1.1	0.015	0.012	0.009	0.006	0.003	0.002	-0.001
	Σ	0.023	0.021	0.016	0.011	0.007	0.004	0.001
$\lvert n\sigma_p \rvert$	2.75	0.000	-0.000	-0.000	-0.000	0.000	0.000	0.000
	2.5	-0.000	0.001	0.000	0.000	0.001	0.001	0.001
	Σ	0.000	0.001	0.000	0.000	0.001	0.001	0.001
nHitsDedx	≥ 22	0.005	0.004	0.003	0.002	0.002	0.001	0.001
	≥ 25	0.009	0.010	0.009	0.006	0.005	0.004	0.004
	Σ	0.007	0.007	0.006	0.004	0.004	0.002	0.002
pileup	low	0.000	0.000	0.000	0.000	0.000	-0.000	0.000
	high	-0.000	-0.000	-0.000	-0.000	0.000	-0.000	0.000
	Σ	0.000	0.000	0.000	0.000	0.000	0.000	0.000
cent. cut	–1	-0.003	0.000	-0.000	-0.000	0.000	0.002	0.003
	+1	0.003	0.001	-0.000	0.000	-0.000	-0.002	-0.003
	Σ	0.003	0.001	0.000	0.000	0.000	0.002	0.003

Table B.85: Systematic uncertainty contributions for κ_3/κ_1 at $\sqrt{s_{NN}} = 4.5$ GeV

$\sqrt{s_{NN}} = 4.5$ GeV, κ_3/κ_1 Systematic Uncertainties								
		0-5%	5-10%	10-20%	20-30%	30-40%	40-50%	50-60%
κ_3/κ_1	value	-0.150	-0.025	-0.018	0.029	0.046	0.050	0.042
	stat.	0.018	0.024	0.012	0.008	0.007	0.005	0.005
	sys.	0.055	0.055	0.037	0.023	0.008	0.009	0.005
nHitsFit	≥ 22	0.003	-0.001	0.002	-0.001	0.000	0.000	0.000
	≥ 25	-0.007	-0.001	-0.005	-0.001	-0.001	-0.001	0.001
	Σ	0.000	0.000	0.005	0.000	0.000	0.000	0.000
Efficiency	–5%	0.016	0.003	0.002	-0.003	-0.005	-0.005	-0.005
	+5%	-0.014	-0.002	-0.002	0.003	0.004	0.005	0.004
	Σ	0.015	0.000	0.000	0.000	0.005	0.005	0.004
m^2 cuts (GeV^2)	[0.7,1.3]	-0.001	0.001	-0.002	0.002	0.001	-0.000	-0.000
	[0.6,1.1]	0.004	0.004	0.001	-0.001	0.001	0.000	-0.000
	Σ	0.004	0.000	0.002	0.000	0.000	0.000	0.000
DCA (cm)	<0.9	0.075	0.078	0.050	0.019	0.005	0.001	0.001
	<1.1	-0.022	-0.029	-0.022	-0.016	-0.006	-0.004	-0.002
	Σ	0.048	0.053	0.036	0.018	0.006	0.003	0.001
$\lvert n\sigma_p \rvert$	2.75	0.003	-0.001	-0.002	0.000	-0.000	0.001	0.000
	2.5	0.005	0.002	-0.002	0.003	0.002	0.001	0.002
	Σ	0.004	0.000	0.002	0.003	0.002	0.001	0.002
nHitsDedx	≥ 22	-0.012	0.004	-0.003	0.002	-0.001	0.000	-0.001
	≥ 25	-0.027	-0.014	-0.014	0.013	0.003	0.007	0.001
	Σ	0.019	0.014	0.008	0.013	0.000	0.007	0.000
pileup	low	-0.000	0.000	-0.000	-0.000	-0.000	-0.000	0.000
	high	0.001	0.000	-0.000	0.000	0.000	0.000	0.000
	Σ	0.000	0.000	0.000	0.000	0.000	0.000	0.000
cent. cut	–1	-0.006	0.003	-0.003	-0.002	-0.002	0.001	0.001
	+1	0.001	0.001	0.003	0.004	0.001	-0.002	0.001
	Σ	0.000	0.000	0.003	0.004	0.002	0.001	0.000

Table B.86: Systematic uncertainty contributions for κ_4/κ_1 at $\sqrt{s_{NN}} = 4.5$ GeV

$\sqrt{s_{NN}} = 4.5$ GeV, κ_4/κ_1 Systematic Uncertainties								
		0-5%	5-10%	10-20%	20-30%	30-40%	40-50%	50-60%
κ_4/κ_1	value	0.548	-0.008	0.017	0.087	0.049	0.042	-0.029
	stat.	0.260	0.178	0.111	0.074	0.040	0.028	0.021
	sys.	0.212	0.278	0.129	0.066	0.044	0.031	0.010
nHitsFit	≥ 22	0.015	-0.017	-0.007	-0.010	-0.005	-0.002	-0.000
	≥ 25	0.021	0.098	0.006	-0.005	-0.018	-0.004	-0.003
	Σ	0.000	0.098	0.000	0.010	0.000	0.000	0.000
Efficiency	–5%	-0.091	0.001	-0.003	-0.015	-0.008	-0.007	0.005
	+5%	0.075	-0.001	0.002	0.012	0.007	0.006	-0.004
	Σ	0.000	0.000	0.000	0.000	0.000	0.000	0.000
m^2 cuts (GeV^2)	[0.7,1.3]	-0.059	-0.021	-0.013	0.012	-0.014	-0.003	-0.001
	[0.6,1.1]	0.058	-0.032	-0.013	0.008	0.013	0.001	-0.002
	Σ	0.058	0.000	0.000	0.000	0.014	0.003	0.000
DCA (cm)	<0.9	-0.215	-0.158	-0.163	-0.023	-0.034	-0.012	0.002
	<1.1	0.192	0.123	0.046	-0.025	-0.013	0.008	0.007
	Σ	0.204	0.141	0.104	0.024	0.024	0.000	0.000
$\lvert n\sigma_p \rvert$	2.75	-0.012	0.011	-0.008	-0.003	-0.006	0.003	0.003
	2.5	-0.047	-0.004	-0.003	0.006	0.009	0.001	0.002
	Σ	0.000	0.000	0.000	0.000	0.000	0.000	0.000
nHitsDedx	≥ 22	0.004	-0.218	-0.020	0.046	0.022	-0.032	0.006
	≥ 25	0.029	-0.014	-0.072	0.004	-0.021	-0.020	0.014
	Σ	0.000	0.218	0.072	0.046	0.021	0.026	0.010
pileup	low	-0.019	0.005	-0.001	-0.002	-0.001	0.000	-0.000
	high	-0.003	0.001	0.001	0.000	-0.001	-0.000	0.000
	Σ	0.000	0.000	0.000	0.000	0.000	0.000	0.000
cent. cut	–1	0.015	0.025	-0.025	0.039	-0.027	0.016	-0.003
	+1	-0.037	-0.001	0.004	0.004	0.008	-0.018	0.006
	Σ	0.000	0.025	0.025	0.039	0.027	0.017	0.000

Table B.87: Systematic uncertainty contributions for κ_5/κ_1 at $\sqrt{s_{NN}} = 4.5$ GeV

$\sqrt{s_{NN}} = 4.5$ GeV, κ_5/κ_1 Systematic Uncertainties								
		0-5%	5-10%	10-20%	20-30%	30-40%	40-50%	50-60%
κ_5/κ_1	value	-1.646	-1.748	-0.196	-0.265	0.486	-0.190	-0.170
	stat.	3.506	2.921	1.165	0.826	0.422	0.208	0.087
	sys.	4.839	2.099	0.955	0.819	0.333	0.152	0.116
nHitsFit	≥ 22	0.104	-0.016	-0.178	0.093	-0.017	-0.003	-0.001
	≥ 25	-0.646	-0.271	0.033	0.104	-0.177	-0.061	-0.047
	Σ	0.000	0.000	0.178	0.000	0.177	0.000	0.047
Efficiency	–5%	0.375	0.398	0.045	0.060	-0.111	0.043	0.039
	+5%	-0.292	-0.310	-0.035	-0.047	0.086	-0.034	-0.030
	Σ	0.000	0.000	0.000	0.000	0.000	0.000	0.000
m^2 cuts (GeV^2)	[0.7,1.3]	1.128	0.652	-0.002	0.094	0.014	-0.087	-0.016
	[0.6,1.1]	0.768	-0.520	-0.161	0.047	0.070	-0.026	0.003
	Σ	0.768	0.586	0.000	0.000	0.000	0.087	0.016
DCA (cm)	<0.9	2.332	0.099	0.291	0.360	-0.136	0.027	-0.010
	<1.1	1.859	-1.884	0.154	0.178	-0.051	-0.051	0.043
	Σ	2.095	1.884	0.000	0.360	0.000	0.000	0.000
$\lvert n\sigma_p \rvert$	2.75	-0.539	0.075	-0.128	-0.056	0.001	0.026	0.012
	2.5	0.395	-1.012	0.218	-0.086	0.055	0.037	-0.007
	Σ	0.000	0.000	0.218	0.000	0.000	0.000	0.007
nHitsDedx	≥ 22	2.216	0.601	-0.791	0.169	0.360	-0.081	-0.051
	≥ 25	6.371	0.831	-0.833	-1.016	0.204	-0.124	0.085
	Σ	4.293	0.716	0.812	0.593	0.282	0.124	0.085
pileup	low	-0.174	-0.218	0.009	0.007	0.002	-0.003	-0.000
	high	0.117	0.059	-0.033	-0.013	0.001	-0.002	-0.000
	Σ	0.000	0.000	0.000	0.000	0.000	0.000	0.000
cent. cut	–1	-0.278	0.331	-0.417	0.436	-0.029	0.075	-0.083
	+1	-0.533	0.136	0.298	0.004	0.003	0.071	-0.038
	Σ	0.000	0.000	0.417	0.436	0.000	0.000	0.060

Table B.88: Systematic uncertainty contributions for κ_6/κ_1 at $\sqrt{s_{NN}} = 4.5$ GeV

$\sqrt{s_{NN}} = 4.5$ GeV, κ_6/κ_1 Systematic Uncertainties								
		0-5%	5-10%	10-20%	20-30%	30-40%	40-50%	50-60%
κ_6/κ_1	value	-55.026	-29.502	-4.259	-4.834	-1.332	1.168	-0.214
	stat.	54.507	38.537	17.437	9.341	3.361	1.975	0.413
	sys.	20.813	48.121	5.327	8.469	3.966	2.840	0.726
nHitsFit	≥ 22	-2.176	-2.692	0.734	0.005	0.346	-0.173	0.016
	≥ 25	-12.760	2.140	-2.134	-3.048	-0.494	0.314	0.072
	Σ	0.000	0.000	0.000	0.000	0.000	0.000	0.000
Efficiency	–5%	16.087	8.625	1.245	1.413	0.389	-0.341	0.062
	+5%	-11.912	-6.386	-0.922	-1.046	-0.288	0.253	-0.046
	Σ	0.000	0.000	0.000	0.000	0.000	0.000	0.000
m^2 cuts (GeV^2)	[0.7,1.3]	-16.916	-4.572	-0.309	-0.840	-0.426	-0.516	0.022
	[0.6,1.1]	-7.140	-16.870	0.171	0.645	0.257	-0.044	0.064
	Σ	16.916	16.870	0.000	0.000	0.426	0.000	0.064
DCA (cm)	<0.9	-6.155	-17.508	4.512	2.133	-2.527	0.411	0.042
	<1.1	-21.699	5.702	0.927	4.737	-1.025	-1.916	-0.314
	Σ	0.000	17.508	4.512	4.737	0.000	0.000	0.000
$\lvert n\sigma_p \rvert$	2.75	-4.884	-7.328	0.323	-0.639	0.154	-0.180	-0.004
	2.5	-2.673	3.367	1.290	0.444	0.471	-0.048	0.054
	Σ	4.884	0.000	0.000	0.000	0.000	0.000	0.000
nHitsDedx	≥ 22	2.048	16.483	-5.866	5.010	0.633	-0.263	-0.130
	≥ 25	2.804	-35.105	-7.850	-5.153	3.158	1.951	-0.668
	Σ	0.000	35.105	0.000	5.082	3.158	1.951	0.668
pileup	low	2.769	0.296	-0.133	0.046	0.069	-0.009	0.006
	high	-4.118	-1.260	0.377	0.042	0.043	0.019	-0.000
	Σ	0.000	0.000	0.000	0.000	0.000	0.000	0.000
cent. cut	–1	-5.456	8.372	-2.833	1.122	-2.361	2.063	-0.078
	+1	-16.742	22.184	1.839	-4.844	0.206	0.203	-0.277
	Σ	11.099	22.184	2.833	4.844	2.361	2.063	0.277

Bibliography

[1] Yasuo Koizumi, Shoji Mori, and Tomio Okawa. *Fundamentals of Thermal and Nuclear Power Generation, Volume 1*. 1st ed. Elsevier, 2021. DOI: https://doi.org/10.1016/C2018-0-04630-7.

[2] Samuel Glasstone and Phillip J. Dolan. *The Effects of Nuclear Weapons*. 3rd ed. United States Department of Defense, the Energy Research, and Development Administration, 1977. DOI: https://doi.org/10.2172/6852629.

[3] *Color Charge*. 2025. URL: https://en.wikipedia.org/wiki/Color_charge.

[4] N. Cabibbo and G. Parisi. "Exponential hadronic spectrum and quark liberation." In: *Physics Letters B* 59.1 (1975), pp. 67–69. ISSN: 0370-2693. DOI: https://doi.org/10.1016/0370-2693(75)90158-6. URL: https://www.sciencedirect.com/science/article/pii/0370269375901586.

[5] Bertram M. Schwarzschild. "NSAC recommends a relativistic heavy-ion collider." In: *Physics Today* 37.1 (1984), pp. 20–22. DOI: 10.1063/1.2916040. eprint: https://doi.org/10.1063/1.2916040. URL: https://doi.org/10.1063/1.2916040.

[6] Ulrich Heinz and Maurice Jacob. *Evidence for a New State of Matter: An Assessment of the Results from the CERN Lead Beam Programme*. 2000. arXiv: nucl-th/0002042 [nucl-th].

[7] J. Adams et al. "Evidence fromd+AuMeasurements for Final-State Suppression of High-pTHadrons inAu+AuCollisions at RHIC." In: *Physical Review Letters* 91.7 (Aug. 2003). ISSN: 1079-7114. DOI: 10.1103/physrevlett.91.072304. URL: http://dx.doi.org/10.1103/PhysRevLett.91.072304.

[8] The STAR Collaboration and The CBM Collaboration eTOF Group. *Physics Program for the STAR/CBM eTOF Upgrade*. 2016. arXiv: 1609.05102 [nucl-ex]. URL: https://arxiv.org/abs/1609.05102.

[9] Xiaofeng Luo and Nu Xu. "Search for the QCD critical point with fluctuations of conserved quantities in relativistic heavy-ion collisions at RHIC: an overview." In: *Nuclear Science and Techniques* 28.8 (July 2017). ISSN: 2210-3147. DOI: 10.1007/s41365-017-0257-0. URL: http://dx.doi.org/10.1007/s41365-017-0257-0.

[10] F. Karsch. "Lattice results on QCD thermodynamics." In: *Nuclear Physics A* 698.1-4 (Feb. 2002), pp. 199–208. ISSN: 0375-9474. DOI: 10.1016/s0375-9474(01)01365-3. URL: http://dx.doi.org/10.1016/S0375-9474(01)01365-3.

[11] S. Aoki et al. "Bulk first-order phase transition in three-flavor lattice QCD with $O(a)$-improved Wilson fermion action at zero temperature." In: *Physical Review D* 72.5 (Sept. 2005). ISSN: 1550-2368. DOI: 10.1103/physrevd.72.054510. URL: http://dx.doi.org/10.1103/PhysRevD.72.054510.

[12] Bo Ling and Mikhail A. Stephanov. "Acceptance dependence of fluctuation measures near the QCD critical point." In: *Phys. Rev. C* 93 (3 Mar. 2016), p. 034915. DOI: 10.1103/PhysRevC.93.034915. URL: https://link.aps.org/doi/10.1103/PhysRevC.93.034915.

[13] Adam Bzdak, Volker Koch, and Nils Strodthoff. "Cumulants and correlation functions versus the QCD phase diagram." In: *Phys. Rev. C* 95 (5 May 2017), p. 054906. DOI:

10.1103/PhysRevC.95.054906. URL: https://link.aps.org/doi/10.1103/PhysRevC.95.054906.

[14] Masakiyo Kitazawa and Xiaofeng Luo. "Properties and uses of factorial cumulants in relativistic heavy-ion collisions." In: *Phys. Rev. C* 96 (2 Aug. 2017), p. 024910. DOI: 10.1103/PhysRevC.96.024910. URL: https://link.aps.org/doi/10.1103/PhysRevC.96.024910.

[15] M. J. Klein and L. Tisza. "Theory of Critical Fluctuations." In: *Phys. Rev.* 76 (12 Dec. 1949), pp. 1861–1868. DOI: 10.1103/PhysRev.76.1861. URL: https://link.aps.org/doi/10.1103/PhysRev.76.1861.

[16] Moupriya Das and Jason R. Green. "Critical fluctuations and slowing down of chaos." In: *Nature Communications* 10.1 (May 2019). ISSN: 2041-1723. DOI: 10.1038/s41467-019-10040-3. URL: http://dx.doi.org/10.1038/s41467-019-10040-3.

[17] Ryo Hanai and Peter B. Littlewood. "Critical fluctuations at a many-body exceptional point." In: *Phys. Rev. Res.* 2 (3 July 2020), p. 033018. DOI: 10.1103/PhysRevResearch.2.033018. URL: https://link.aps.org/doi/10.1103/PhysRevResearch.2.033018.

[18] Hassan Alnatah et al. "Critical fluctuations in a confined driven-dissipative quantum condensate." In: *Science Advances* 10.12 (2024), eadi6762. DOI: 10.1126/sciadv.adi6762. eprint: https://www.science.org/doi/pdf/10.1126/sciadv.adi6762. URL: https://www.science.org/doi/abs/10.1126/sciadv.adi6762.

[19] Masakiyo Kitazawa and Masayuki Asakawa. "Relation between baryon number fluctuations and experimentally observed proton number fluctuations in relativistic heavy ion collisions." In: *Phys. Rev. C* 86 (2 Aug. 2012), p. 024904. DOI: 10.1103/PhysRevC.86.024904. URL: https://link.aps.org/doi/10.1103/PhysRevC.86.024904.

[20] M. A. Stephanov. "Non-Gaussian Fluctuations near the QCD Critical Point." In: *Physical Review Letters* 102.3 (Jan. 2009). ISSN: 1079-7114. DOI: 10.1103/physrevlett.102.032301. URL: http://dx.doi.org/10.1103/PhysRevLett.102.032301.

[21] M A Stephanov. "QCD critical point and event-by-event fluctuations." In: *Journal of Physics G: Nuclear and Particle Physics* 38.12 (Nov. 2011), p. 124147. DOI: 10.1088/0954-3899/38/12/124147. URL: https://dx.doi.org/10.1088/0954-3899/38/12/124147.

[22] Jiunn-Wei Chen et al. "Robust characteristics of non-Gaussian fluctuations from the NJL model." In: *Phys. Rev. D* 93 (3 Feb. 2016), p. 034037. DOI: 10.1103/PhysRevD.93.034037. URL: https://link.aps.org/doi/10.1103/PhysRevD.93.034037.

[23] M. S. Abdallah et al. "Measurements of Proton High-Order Cumulants in $\sqrt{s_{NN}} = 3$ GeV Au + Au Collisions and Implications for the QCD Critical Point." In: *Phys. Rev. Lett.* 128 (20 May 2022), p. 202303. DOI: 10.1103/PhysRevLett.128.202303. URL: https://link.aps.org/doi/10.1103/PhysRevLett.128.202303.

[24] J. Adamczewski-Musch et al. "Proton-number fluctuations in $\sqrt{s_{NN}} = 2.4$GeVAu+Au collisions studied with the High-Acceptance DiElectron Spectrometer (HADES)." In: *Phys. Rev. C* 102 (2 Aug. 2020), p. 024914. DOI: 10.1103/PhysRevC.102.024914. URL: https://link.aps.org/doi/10.1103/PhysRevC.102.024914.

[25] The STAR Collaboration. *Precision Measurement of (Net-)proton Number Fluctuations in Au+Au Collisions at RHIC*. 2025. arXiv: 2504.00817 [nucl-ex]. URL: https://arxiv.org/abs/2504.00817.

[26] Volodymyr Vovchenko, Volker Koch, and Chun Shen. "Proton number cumulants and correlation functions in Au-Au collisions at $\sqrt{s_{NN}} = 7.7$–200 GeV from hydrodynamics." In: *Phys. Rev. C* 105 (1 Jan. 2022), p. 014904. DOI: 10.1103/PhysRevC.105.014904. URL: https://link.aps.org/doi/10.1103/PhysRevC.105.014904.

[27] P. Braun-Munzinger et al. "Relativistic nuclear collisions: Establishing a non-critical baseline for fluctuation measurements." In: *Nuclear Physics A* 1008 (Apr. 2021), p. 122141. ISSN: 0375-9474. DOI: 10.1016/j.nuclphysa.2021.122141. URL: http://dx.doi.org/10.1016/j.nuclphysa.2021.122141.

[28] A. Bazavov et al. "Skewness, kurtosis, and the fifth and sixth order cumulants of net baryon-number distributions from lattice QCD confront high-statistics STAR data." In: *Phys. Rev. D* 101 (7 Apr. 2020), p. 074502. DOI: 10.1103/PhysRevD.101.074502. URL: https://link.aps.org/doi/10.1103/PhysRevD.101.074502.

[29] H. Hahn et al. "The RHIC design overview." In: *Nuclear Instruments and Methods in Physics Research Section A: Accelerators, Spectrometers, Detectors and Associated Equipment* 499.2 (2003). The Relativistic Heavy Ion Collider Project: RHIC and its Detectors, pp. 245–263. ISSN: 0168-9002. DOI: https://doi.org/10.1016/S0168-9002(02)01938-1. URL: https://www.sciencedirect.com/science/article/pii/S0168900202019381.

[30] J. Alessi et al. "High performance EBIS for RHIC." In: *2007 IEEE Particle Accelerator Conference (PAC)*. 2007, pp. 3782–3785. DOI: 10.1109/PAC.2007.4440116.

[31] M.J. Rhoades-Brown. *The Heavy Ion Stripping Foil Requirements between AGS and RHIC*. 1990. URL: https://www.agsrhichome.bnl.gov/RHIC/RAP/rhic_notes/AD-RHIC-1-142/RHIC-68.pdf.

[32] M. Anderson et al. "The STAR time projection chamber: a unique tool for studying high multiplicity events at RHIC." In: *Nuclear Instruments and Methods in Physics Research Section A: Accelerators, Spectrometers, Detectors and Associated Equipment* 499.2 (2003). The Relativistic Heavy Ion Collider Project: RHIC and its Detectors, pp. 659–678. ISSN: 0168-9002. DOI: https://doi.org/10.1016/S0168-9002(02)

01964-2. URL: https://www.sciencedirect.com/science/article/pii/S0168900202019642.

[33] Jim Thomas. *Choosing the Gas*. 1998. URL: https://www.star.bnl.gov/public/tpc/hard/tpcrings/page3.html.

[34] K. H. Ackermann et al. "STAR detector overview." In: *Nucl. Instrum. Meth. A* 499 (2003), pp. 624–632. DOI: 10.1016/S0168-9002(02)01960-5.

[35] The STAR TOF Collaboration. *Proposal for a Large Area Time of Flight System for STAR*. 2004. URL: https://www.star.bnl.gov/public/tof/publications/TOF_20040524.pdf.

[36] I. Deppner and N. Herrmann. "The CBM Time-of-Flight system." In: *Journal of Instrumentation* 14.09 (Sept. 2019), p. C09020. DOI: 10.1088/1748-0221/14/09/C09020. URL: https://dx.doi.org/10.1088/1748-0221/14/09/C09020.

[37] D. Cebra. *Insights from the STAR Fixed-Target Program*. 2021. URL: https://drupal.star.bnl.gov/STAR/files/APS_April_17_2021_Cebra_v3.pdf.

[38] J. Cleymans et al. "Comparison of chemical freeze-out criteria in heavy-ion collisions." In: *Phys. Rev. C* 73 (3 Mar. 2006), p. 034905. DOI: 10.1103/PhysRevC.73.034905. URL: https://link.aps.org/doi/10.1103/PhysRevC.73.034905.

[39] P. Braun-Munzinger, A. Rustamov, and J. Stachel. In: *Nuclear Physics A* 960 (2017), pp. 114–130. ISSN: 0375-9474. DOI: https://doi.org/10.1016/j.nuclphysa.2017.01.011. URL: https://www.sciencedirect.com/science/article/pii/S0375947417300258.

[40] V. Skokov, B. Friman, and K. Redlich. In: *Phys. Rev. C* 88 (3 Sept. 2013), p. 034911. DOI: 10.1103/PhysRevC.88.034911. URL: https://link.aps.org/doi/10.1103/PhysRevC.88.034911.

[41] Toshihiro Nonaka, Masakiyo Kitazawa, and ShinIchi Esumi. "More efficient formulas for efficiency correction of cumulants and effect of using averaged efficiency." In: *Phys. Rev. C* 95 (6 June 2017), p. 064912. DOI: 10.1103/PhysRevC.95.064912. URL: https://link.aps.org/doi/10.1103/PhysRevC.95.064912.

[42] C. Liu et al. "Gold-gold luminosity increase in RHIC for a beam energy scan with colliding beam energies extending below the nominal injection energy." In: *Phys. Rev. Accel. Beams* 25 (5 May 2022), p. 051001. DOI: 10.1103/PhysRevAccelBeams.25.051001. URL: https://link.aps.org/doi/10.1103/PhysRevAccelBeams.25.051001.

[43] Chuyu Liu et al. "Fixed Target Operation at RHIC in 2019." In: *3rd North American Particle Accelerator Conference (NAPAC2019)*. 2019, TUPLO05. DOI: 10.18429/JACoW-NAPAC2019-TUPLO05.

[44] M. S. Abdallah et al. In: *Phys. Rev. C* 107 (2 Feb. 2023), p. 024908. DOI: 10.1103/PhysRevC.107.024908. URL: https://link.aps.org/doi/10.1103/PhysRevC.107.024908.

[45] M. S. Abdallah et al. In: *Phys. Rev. Lett.* 128 (20 May 2022), p. 202303. DOI: 10.1103/PhysRevLett.128.202303. URL: https://link.aps.org/doi/10.1103/PhysRevLett.128.202303.

[46] Toshihiro Nonaka, Masakiyo Kitazawa, and ShinIchi Esumi. In: *Nucl. Instrum. Meth. A* 984 (2020), p. 164632. ISSN: 0168-9002. DOI: https://doi.org/10.1016/j.nima.2020.164632. URL: https://www.sciencedirect.com/science/article/pii/S0168900220310299.

[47] Yu Zhang et al. In: *Nucl. Instrum. Meth. A* 1026 (2022), p. 166246. ISSN: 0168-9002. DOI: https://doi.org/10.1016/j.nima.2021.166246. URL: https://www.sciencedirect.com/science/article/pii/S0168900221010871.

[48] B. E. Aboona et al. In: *Phys. Rev. Lett.* 130 (8 Feb. 2023), p. 082301. DOI: 10.1103/PhysRevLett.130.082301. URL: https://link.aps.org/doi/10.1103/PhysRevLett.130.082301.

[49] M. S. Abdallah et al. "Measurement of the Sixth-Order Cumulant of Net-Proton Multiplicity Distributions in Au+Au Collisions at $\sqrt{s_{NN}} = 27$, 54.4, and 200 GeV at RHIC." In: *Phys. Rev. Lett.* 127 (26 Dec. 2021), p. 262301. DOI: 10.1103/PhysRevLett.127.262301. URL: https://link.aps.org/doi/10.1103/PhysRevLett.127.262301.

[50] J. Adam et al. In: *Phys. Rev. Lett.* 126 (9 Mar. 2021), p. 092301. DOI: 10.1103/PhysRevLett.126.092301. URL: https://link.aps.org/doi/10.1103/PhysRevLett.126.092301.

[51] M. S. Abdallah et al. In: *Phys. Rev. C* 104 (2 Aug. 2021), p. 024902. DOI: 10.1103/PhysRevC.104.024902. URL: https://link.aps.org/doi/10.1103/PhysRevC.104.024902.

[52] M.I. Abdulhamid et al. In: *Physics Letters B* 855 (2024), p. 138560. ISSN: 0370-2693. DOI: https://doi.org/10.1016/j.physletb.2024.138560. URL: https://www.sciencedirect.com/science/article/pii/S0370269324001187.

[53] J. Adamczewski-Musch et al. In: *Phys. Rev. C* 102 (2 Aug. 2020), p. 024914. DOI: 10.1103/PhysRevC.102.024914. URL: https://link.aps.org/doi/10.1103/PhysRevC.102.024914.

[54] S. Acharya et al. In: *Physics Letters B* 844 (2023), p. 137545. ISSN: 0370-2693. DOI: https://doi.org/10.1016/j.physletb.2022.137545. URL: https://www.sciencedirect.com/science/article/pii/S0370269322006797.

[55] S. Acharya et al. In: *Phys. Rev. Lett.* 131 (4 July 2023), p. 041901. DOI: 10.1103/PhysRevLett.131.041901. URL: https://link.aps.org/doi/10.1103/PhysRevLett.131.041901.

[56] J. Adam et al. "Erratum: Nonmonotonic Energy Dependence of Net-Proton Number Fluctuations [Phys. Rev. Lett. 126, 092301 (2021)]." In: *Phys. Rev. Lett.* 134 (13 Mar. 2025), p. 139902. DOI: 10.1103/PhysRevLett.134.139902. URL: https://link.aps.org/doi/10.1103/PhysRevLett.134.139902.

[57] B. E. Aboona and Anonymous. "Erratum: Beam Energy Dependence of Fifth- and Sixth-Order Net-Proton Number Fluctuations in Au + Au Collisions at RHIC [Phys. Rev. Lett. 130, 082301 (2023)]." In: *Phys. Rev. Lett.* 134 (13 Apr. 2025), p. 139901. DOI: 10.1103/PhysRevLett.134.139901. URL: https://link.aps.org/doi/10.1103/PhysRevLett.134.139901.

[58] M. S. Abdallah et al. "Erratum: Measurement of the Sixth-Order Cumulant of Net-Proton Multiplicity Distributions in Au + Au Collisions at $\sqrt{s_{\mathrm{NN}}} = 27$, 54.4, and 200 GeV at RHIC [Phys. Rev. Lett. 127, 262301 (2021)]." In: *Phys. Rev. Lett.* 134 (13 Apr. 2025), p. 139903. DOI: 10.1103/PhysRevLett.134.139903. URL: https://link.aps.org/doi/10.1103/PhysRevLett.134.139903.

[59] M. A. Stephanov. "Sign of Kurtosis near the QCD Critical Point." In: *Phys. Rev. Lett.* 107 (5 July 2011), p. 052301. DOI: 10.1103/PhysRevLett.107.052301. URL: https://link.aps.org/doi/10.1103/PhysRevLett.107.052301.

[60] Wei-jie Fu, Jan M. Pawlowski, and Fabian Rennecke. In: *Phys. Rev. D* 101 (5 Mar. 2020), p. 054032. DOI: 10.1103/PhysRevD.101.054032. URL: https://link.aps.org/doi/10.1103/PhysRevD.101.054032.

[61] Fei Gao and Jan M. Pawlowski. In: *Physics Letters B* 820 (2021), p. 136584. ISSN: 0370-2693. DOI: https://doi.org/10.1016/j.physletb.2021.136584. URL: https://www.sciencedirect.com/science/article/pii/S0370269321005244.

[62] Pascal J. Gunkel and Christian S. Fischer. "Locating the critical endpoint of QCD: Mesonic backcoupling effects." In: *Phys. Rev. D* 104 (5 Sept. 2021), p. 054022. DOI: 10.1103/PhysRevD.104.054022. URL: https://link.aps.org/doi/10.1103/PhysRevD.104.054022.

[63] Goswami, Jishnu et al. "Exploring the critical points in QCD with multi-point Padé and machine learning techniques in (2+1)-flavor QCD." In: *EPJ Web Conf.* 296 (2024), p. 06007. DOI: 10.1051/epjconf/202429606007. URL: https://doi.org/10.1051/epjconf/202429606007.

[64] Agnieszka Sorensen and Paul Sorensen. 2024. arXiv: 2405.10278 [nucl-th]. URL: https://arxiv.org/abs/2405.10278.

[65] Mauricio Hippert et al. 2023. arXiv: 2309.00579 [nucl-th]. URL: https://arxiv.org/abs/2309.00579.

[66] M. Stephanov, K. Rajagopal, and E. Shuryak. "Event-by-event fluctuations in heavy ion collisions and the QCD critical point." In: *Phys. Rev. D* 60 (11 Nov. 1999), p. 114028. DOI: 10.1103/PhysRevD.60.114028. URL: https://link.aps.org/doi/10.1103/PhysRevD.60.114028.

[67] Sourendu Gupta et al. "Scale for the Phase Diagram of Quantum Chromodynamics." In: *Science* 332.6037 (2011), pp. 1525–1528. DOI: 10.1126/science.1204621. eprint: https://www.science.org/doi/pdf/10.1126/science.1204621. URL: https://www.science.org/doi/abs/10.1126/science.1204621.

[68] Ashik Ikbal. *FXT datasets*. 2024. URL: https://drupal.star.bnl.gov/STAR/pwg/common/bes-ii-run-qa/FXT-datasets.

[69] Yannick Söhngen. "EToF Status Update." ETOF Workshop. 2024. URL: https://drupal.star.bnl.gov/STAR/system/files/EToFWorkshop24.pdf.

[70] S. Navas et al. "Review of Particle Physics." In: *Phys. Rev. D* 110 (3 Aug. 2024), p. 030001. DOI: 10.1103/PhysRevD.110.030001. URL: https://link.aps.org/doi/10.1103/PhysRevD.110.030001.

[71] Hans Bichsel. In: *Nuclear Instruments and Methods in Physics Research Section A: Accelerators, Spectrometers, Detectors and Associated Equipment* 562.1 (2006), pp. 154–197. ISSN: 0168-9002. DOI: https://doi.org/10.1016/j.nima.2006.03.009. URL: https://www.sciencedirect.com/science/article/pii/S0168900206005353.

[72] Zachary Sweger, Daniel Cebra, and Xin Dong. "Effects of pileup and detector decorrelations on high-order cumulants in heavy-ion collisions." In: *Phys. Rev. C* 111 (3 Mar. 2025), p. 034902. DOI: 10.1103/PhysRevC.111.034902. URL: https://link.aps.org/doi/10.1103/PhysRevC.111.034902.

[73] Yannick Söhngen. "EToF Status Update." ETOF and BES-II Workshop. 2024. URL: https://drupal.star.bnl.gov/STAR/system/files/STAR_ETOF_BESII_Workshop24.pdf.

[74] Michael L. Miller et al. "Glauber Modeling in High-Energy Nuclear Collisions." In: *Annual Review of Nuclear and Particle Science* 57.Volume 57, 2007 (2007), pp. 205–243. ISSN: 1545-4134. DOI: https://doi.org/10.1146/annurev.nucl.57.090506.123020. URL: https://www.annualreviews.org/content/journals/10.1146/annurev.nucl.57.090506.123020.

[75] H. De Vries, C.W. De Jager, and C. De Vries. "Nuclear charge-density-distribution parameters from elastic electron scattering." In: *Atomic Data and Nuclear Data Tables* 36.3 (1987), pp. 495–536. ISSN: 0092-640X. DOI: https://doi.org/10.1016/0092-640X(87)90013-1. URL: https://www.sciencedirect.com/science/article/pii/0092640X87900131.

[76] Particle Data Group. "Review of Particle Physics." In: *Progress of Theoretical and Experimental Physics* 2022.8 (Aug. 2022), p. 083C01. ISSN: 2050-3911. DOI: 10.1093/ptep/ptac097. eprint: https://academic.oup.com/ptep/article-pdf/2022/8/083C01/49175539/ptac097.pdf. URL: https://doi.org/10.1093/ptep/ptac097.

[77] Christopher Flores. 2017. URL: https://drupal.star.bnl.gov/STAR/system/files/CEF_Thesis_Final.pdf.

[78] Tetsuro Sugiura, Toshihiro Nonaka, and ShinIchi Esumi. "Volume fluctuation and multiplicity correlation in higher-order cumulants." In: *Phys. Rev. C* 100 (4 Oct. 2019), p. 044904. DOI: 10.1103/PhysRevC.100.044904. URL: https://link.aps.org/doi/10.1103/PhysRevC.100.044904.

[79] Roger Barlow. *Systematic Errors: facts and fictions*. 2002. arXiv: hep-ex/0207026 [hep-ex]. URL: https://arxiv.org/abs/hep-ex/0207026.

[80] Ashish Pandav, Debasish Mallick, and Bedangadas Mohanty. "Effect of limited statistics on higher order cumulants measurement in heavy-ion collision experiments." In: *Nuclear Physics A* 991 (2019), p. 121608. ISSN: 0375-9474. DOI: https://doi.org/10.1016/j.nuclphysa.2019.08.002. URL: https://www.sciencedirect.com/science/article/pii/S0375947419301769.

[81] Xiaofeng Luo. "Error estimation for moment analysis in heavy-ion collision experiment." In: *Journal of Physics G: Nuclear and Particle Physics* 39.2 (Jan. 2012),

p. 025008. DOI: 10.1088/0954-3899/39/2/025008. URL: https://dx.doi.org/10.1088/0954-3899/39/2/025008.

[82] Xiaofeng Luo. "Unified description of efficiency correction and error estimation for moments of conserved quantities in heavy-ion collisions." In: *Phys. Rev. C* 91 (3 Mar. 2015), p. 034907. DOI: 10.1103/PhysRevC.91.034907. URL: https://link.aps.org/doi/10.1103/PhysRevC.91.034907.

[83] S. Acharya et al. In: *The European Physical Journal C* 79.3 (2019). ISSN: 1434-6052. DOI: 10.1140/epjc/s10052-019-6711-x. URL: http://dx.doi.org/10.1140/epjc/s10052-019-6711-x.

[84] L. Adamczyk et al. "Energy dependence of $K\pi$, $p\pi$, and Kp fluctuations in Au + Au collisions from $\sqrt{s_{NN}} = 7.7$ to 200 GeV." In: *Phys. Rev. C* 92 (2 Aug. 2015), p. 021901. DOI: 10.1103/PhysRevC.92.021901. URL: https://link.aps.org/doi/10.1103/PhysRevC.92.021901.

[85] Mikhail Stephanov. *QCD critical point: recent developments*. 2024. arXiv: 2410.02861 [nucl-th]. URL: https://arxiv.org/abs/2410.02861.

[86] V. Friese. "The CBM experiment at GSI/FAIR." In: *Nuclear Physics A* 774 (2006). QUARK MATTER 2005, pp. 377–386. ISSN: 0375-9474. DOI: https://doi.org/10.1016/j.nuclphysa.2006.06.018. URL: https://www.sciencedirect.com/science/article/pii/S0375947406002776.

[87] H. Sako et al. "Towards the heavy-ion program at J-PARC." In: *Nuclear Physics A* 931 (2014). QUARK MATTER 2014, pp. 1158–1162. ISSN: 0375-9474. DOI: https://doi.org/10.1016/j.nuclphysa.2014.08.065. URL: https://www.sciencedirect.com/science/article/pii/S0375947414003248.